QUASICLASSICAL AND SEMICLASSICAL FORMULATION OF THE ELECTRON NUCLEAR DYNAMICS THEORY: A METHOD FOR MOLECULAR DYNAMICAL PROCESSES

By

JORGE ALBERTO MORALES

A DISSERTATION PRESENTED TO THE GRADUATE SCHOOL
OF THE UNIVERSITY OF FLORIDA IN PARTIAL FULFILLMENT
OF THE REQUIREMENTS FOR THE DEGREE OF
DOCTOR OF PHILOSOPHY

UNIVERSITY OF FLORIDA

1997

To my mother, Martha B. L. Samperio de Morales.

ACKNOWLEDGMENTS

I would like to thank Dr. Yngve Öhrn and Dr. Erik Deumens for their wise guidance, warm encouragement, and adamant support during these exhilarating years in their group. Both have created a fertile and friendly atmosphere to develop my professional skills and to sustain my interests in science.

This gratitude is also extended to the other members of my advisory committee.

I would like to thank Dr. John Klauder for his thoughtful comments about coherent state theory.

I would like to thank Dr. David A. Micha and Dr. Keith Runge for their support and hospitality during the year and half I spent in their group.

I would like to thank past and present members of Dr. Ohrn's group for their help and friendship: Dr. Agustín Diz, Mr. Juan Oreiro, Mr. Denis Jacquemin and Mr. Magnus Hedström. In this regard, I would specially like to thank my dear fellow Dr. Benny Mogensen for his cordial friendship during all these years and for making it possible for me to visit his beautiful country, Denmark. I would also like to thank Mr. Mauricio Coutinho-Neto for the many good moments we spent together auditing courses and attending conferences.

The completion of this thesis work inexorably called for the help and support from many people in the Quantum Theory Project and outside. Unlike some of my ungrateful colleges, I do not fear to acknowledge all the invaluable assistance from my different benefactors. I would like to thank for so diverse reasons Dr. Dario Beksic, Dr. Herbet

Dacosta, Professor Joaquim Delphino Da Motta-Neto, Mr. Piotr Rozyczko and his wife Ewa ("Piotra"), Dr. Marcel Nooijen, Ms. Lynn Salemi, Dr. Richard Johannes Alphonse von Mathar, Dr. Henk Monkhorst, Ms. Judy Parker and her family, Dr. Jeff Krause, Dr. Rod Bartlett, Dr. Frank Harris, Dr. James Deyrup, Dr. James Horvath, Mr. Karl Zachary, Dr. Fabio Zuluaga, Dr. Pedro Ruesta, Ms. Norma Barahona, Ms. Gerry Sams, Ms. Cecilia Coletti, Mr. Sergio Cabado and his wife Monika, Ms. Gloria Atkins and Mr. Larry Monroe.

My most special gratitude is to my two dearest friends in the Quantum Theory Project: Dr. S. Ajith Perera and Dr. Raymond "The Pig" Sadeghi. What could have been of my harsh life if the other two musketeers had not been around here? I would like to thank both of them for their loyal friendship and their continuous help in all aspects of life.

I would like to thank all the people in Argentina who also made this thesis possible: my mother, my sister María Martha, my recently deceased grandmother Angela, and my friends Fernando Marcer, Roberto Marcer, Dr. Jorge Zobenica, Dr. Carlos Díaz, Lic. Marcelo Radicioni, and Dr. Marcelo Fernández.

Finally, I would like to thank my dearest Ana Rosa Segarra for all the love, caring, encouragement and support she gave me this year. Gracias, linda!

May the reader forgive me for whom I am unconsciously forgetting and agree with me for whom I am consciously omitting. "El olvido es el mejor perdón y la peor venganza."

TABLE OF CONTENTS

LIST OF TABLES

LIST OF FIGURES

Figures Page

Abstract of Dissertation Presented to the Graduate School
of the University of Florida in Partial Fulfillment of the
Requirements for the Degree of Doctor of Philosophy

QUASICLASSICAL AND SEMICLASSICAL FORMULATION OF THE ELECTRON NUCLEAR DYNAMICS THEORY: A METHOD FOR MOLECULAR DYNAMICS PROCESSES

By

Jorge Alberto Morales

December, 1997

Chairman: N. Yngve Öhrn
Major Department: Chemistry

A quasi-classical and semiclassical formulation of the nuclear degrees of freedom for the Electron Nuclear Dynamics theory is presented. The level of the theory being used describes the nuclei by frozen Gaussian wave packets and the electrons by a Thouless single-determinant wave function. The coherent state theory is employed for the treatment of the internal degrees of freedom as an unifying concept. In the case of the vibrational and the rotational motions, the use of quasi-classical coherent states makes the connection between the quantum and the classical theories. A novel application of a nearly quasi-classical rotational coherent state is proposed in that context. A further improvement of the Electron Nuclear Dynamics theory in terms of a double nuclear configuration is also analyzed.

Different scattering properties such as transition probabilities, the scattering matrix, and cross sections are formulated within this theoretical frame. The derived scattering matrix contains quasi-classical amplitudes for both the vibrational and the rotational motions. The final treatment of differential and integral cross sections is in the spirit of the semiclassical theory. The present formalism is applied to the reaction systems: $H^+ + H_2$, $H^+ + CH_4$, and $H^+ + H_2O$, for both transfer and nontransfer channels. The obtained numerical results show an excellent agreement with available experimental data. Future developments of the present theory are finally discussed.

CHAPTER 1
INTRODUCTION

Quantum chemists have neglected time-dependent processes for a very long time. For many, the main concern of quantum chemistry is the solution of the time-independent Schrödinger equation of a given system and the subsequent evaluation of its stationary properties. A great deal of thought, efforts, and resources have been conjured to accurately solve that time-independent problem. The calculation of energy eigenvalues, potential energy surfaces, time-independent wave functions and densities, dipole moments and other stationary properties has been and still is the routine task of a quantum chemist. However, there is no need for too much speculation in order to discover that chemistry is highly concerned with time-dependent phenomena. Is a chemical reaction the transformation of some reagents into some products in time? Is chemical kinetics concerned in the time variation of the reagents' concentrations? Is it not important to predict into what species a given mixture of substances will evolve, and how fast? It is well known that the most satisfactory answer to such questions can only be given by the time-dependent Schrödinger equation. Nonetheless, the systematic employment of this fundamental equation has been far scantier than that of its time-independent counterpart. The main reason for this restricted use is that the computational problems posed by the time-dependent Schrödinger equation are much more difficult than those posed by the time-independent one. In fact, time-independent approaches to treat dynamic processes do exist even though the high detail of information given by a time-dependent treatment is lost in it. Only after the advent of the modern computers in the 1970s, the solution of

the time-dependent Schrödinger have become feasible in systems of chemical concern. Since then the interest in studying dynamical processes time-dependently has steadily increased and disseminated amid quantum chemists.

The Electron Nuclear Dynamics (END) theory, formulated by Yngve Öhrn and Erik Deumens by mid 1980s [1], is attuned to this *zeitgeist* of time-dependent quantum chemistry. This novel theory provides an approximate but still accurate solution to the time-dependent Schrödinger equation by means of the time-dependent variational principle (TDVP). The most remarkable feature of this method is the simultaneous calculation of both the nuclear and the electronic dynamics without employing any predetermined potential energy surface (PES). This very general theory admits a progression of realizations in increasing order of complexity and accuracy. At the pedestal of this hierarchy is the END realization in which the nuclei are treated classically and the electrons are described by a single-determinant wave function. This model will be called the Quasi-Classical-Single-Determinant (QCSD) END theory throughout this thesis for reasons better explained in chapter 3. This is the "minimal" END version capable of describing many time-dependent phenomena accurately. This QCSD END version has been coded into the Endyne program package [2] which has been systematically applied to many reaction systems.

It might be fascinating to develop and apply the more advanced realizations of the END theory. However, the QCSD END version can still describe a great deal of chemistry and physics and has obvious computational advantages with respect to its more sophisticated relatives. Bearing in mind these ideas, the present thesis work originally started as a further application of the QCSD END theory to more complex systems not explored before. A series of accurate beam experiments on gas phase scattering processes were judged appropriate for an END study. The description of these reactive systems and the theoretical reproduction of their measured properties were the original goals of

this work. Nonetheless, it became clear from the very beginning that these applications would not be fully achieved unless further theoretical and computational developments were undertaken. In that sense, this thesis also aims to answer the following questions: what is the relationship between the classical dynamics in the QCSD END theory and the real quantum dynamics? Is it possible to recover some nuclear quantum effects obviously manifest in the experiments. What is the relationship between the QCSD END theory and the traditional semiclassical methods? What is the role played by the Coherent State Theory in the classical description of the nuclei? How does the formulation of some scattering properties, such as cross sections, appears in the END theory? What computational tools must be developed to calculate those properties?

This dissertation is organized in the following way. In chapter 2, the type of scattering processes to be studied will be carefully defined and the current methods to describe them will be reviewed in detail. Both the time-independent and time-dependent quantum methods will be discussed. The traditional semiclassical methods will be also explained because of their relationship, by either coincidence or contrast, with the END theory. In chapter 3, the QCSD END theory will be introduced as a time-dependent scattering method. Unlike some previous presentation of the same subject, a special emphasis will be given to the classical limiting process involved in this formulation. In chapter 4, a review of the coherent state theory will be presented as well. The relationship between the CS theory and the END theory, specially in its quasi-classical aspects will be discussed. Furthermore, a novel rotational coherent state for scattering processes will be proposed. In chapter 5, a review of the quantum, semiclassical and classical methods to calculate cross sections and other scattering properties will be discussed. In chapter 6, the explicit derivation of the END scattering properties will be presented. Finally, in chapter 7, numerical applications of the mentioned theoretical developments will be presented.

CHAPTER 2
AN OVERVIEW OF THE SCATTERING THEORY METHODS

Experiments and Theory for Scattering Processes

Scattering Beam Experiments

In the most basic approach, a scattering beam experiment can be described as the collision between a primary beam of particles A with a secondary (slower) beam of particles B to produce the final species C and D.

$$A_{(g)} + B_{(g)} \rightarrow C_{(g)} + D_{(g)} \tag{1}$$

A and B are called the incoming projectile and the initial target, respectively. One of the new particles, say C, will abandon the collision chamber to be detected and analyzed, and it is therefore called the outgoing projectile. The remaining particle D is called the final target. In some cases, B is stationary (or almost stationary) with respect to A. A, B, C, and D can be atoms, molecules, ions, or clusters. The level of difficulty to prepare beams and targets with these species varies considerably (*e.g.* it is easier to prepare charged atomic projectile beams and neutral targets). The scattering process is said to be reactive if the species C and D are different from A and B (*i.e.* a chemical reaction) and non reactive otherwise (*i.e.* a pure scattering process). In the former case, A and B are called the reactants, and C and D the products. The formation of a third or even more final products will not modify our discussion since most of the beam experiments detect only one final projectile from which the states of the others final products are inferred.

As previously presented, a scattering experiment is an inextricable, dynamical, many-body phenomenon whose experimental interpretation is difficult and whose theoretical description is nearly impossible. Only if a precise control on the experimental variables is introduced, then the measurements become meaningful and the theoretical studies feasible. This control aims to obtain information about the above microscopical process as accurately as possible disregarding any effect of the macroscopical setting. The theoretical studies of these measurements can therefore focus on that elementary, few-body process. In general, a good scattering beam experiment satisfies the following requirements [3–5] :

1. The projectiles are prepared in beams of perfectly parallel and non-interactive particles, all with the same initial momentum. The beam intensity I_0 (number of projectile particles per unit time and per unit area) is constant on a beam sectional area. The initial collisional energy ranges from about 1 eV to 1 keV in experiments of interest for chemistry and molecular physics. The energy selected and the dimensions of the experimental setup should allow a nearly classical description of translational motion of the projectile as non-spreading wave packets (See Ref. [3], chapter 3).
2. In the case of stationary targets, these particles are in thermal equilibrium at hundredths of Kelvin; therefore, they can be considered at rest with respect to the fast projectiles. By controlling the pressure, the target particles become non interactive as well.
3. Also by controlling the pressure, the possibility of multiple scattering (a projectiles sequentially colliding many targets before going to detection) or many-body scattering (one projectile simultaneously colliding with two or more targets) are totally ruled out. In the reactive scattering, possible secondary reactions are not allowed to occur by selecting appropriate conditions.
4. Because of the previous requirements, the full experiment is an ensemble of inde-

pendent, noninteractive elementary scattering processes. The detection procedure averages a measured property over the ensemble members.

5. The beam is prepared to be very narrow (ideally, of microscopic width) and the detector is placed very far away from the collision chamber (ideally, at infinity). Therefore, it is possible to discern, up to some tolerance, the nonscattered projectiles form the scattered ones. The remoteness of the detector also guaranties that particles originally scattered in parallel direction will encounter each other on the detection device at final time (a Fraunhofer condition for scattering).
6. A continuous inflow of projectiles and a continuous outflow of scattered particle are created; therefore, the signal on the detector in a given direction is constant during the experiment (a stationary detection).

All the experiments theoretically simulated or referred to in this work will comply with these specifications.

Observables in Scattering Beam Processes: Cross Sections

In a beam experiment, two important quantities are usually measured: the differential cross section (DCS) $\frac{d\sigma_{i\to f}}{d\Omega}(\theta,\varphi)$, and the integral cross section (ICS) $\sigma_{i\to f}$. Both have dimensions of area as their names suggest. The DCS is defined as [6]

$$\frac{d\sigma_{i\to f}}{d\Omega}(\theta,\varphi) = \frac{d\dot{N}_{i\to f}(\theta,\varphi)}{I_0 d\Omega(\theta,\varphi)} \tag{2}$$

i.e. the number of final projectile particles per unit time $d\dot{N}_{i\to f}$ and per initial projectile intensity I_0 being scattered into the solid angle $d\Omega(\theta,\varphi) = \sin\theta d\theta d\varphi$. The labels "i" and "f" refer to a particular initial and final state of the target and the projectile before and after the collision. The angles θ and ϕ are the polar and the azimuthal scattering angles in the laboratory frame (Lab a nonrotating space-fixed frame) The z-axis of that frame, which defines the angle θ, is usually taken parallel to the initial direction of the

incoming projectile and positive in its momentum direction. The angle ϕ usually occurs in theoretical treatments but it is not manifest in the measurements. In some theoretical contexts, these two angles are defined in the center-of-mass frame (CM, a nonrotating frame travelling with the CM of the scattering system) giving rise to the erroneous term CM DCS. However, it must be borne in mind that the actual experimentally determined value is the Lab DCS. The relationship between these two properties in different frames will be discussed in chapter 5.

The ICS is defined as [6]

$$\sigma_{i\to f} = \int \left(\frac{d\sigma_{i\to f}}{d\Omega}\right) d\Omega = \frac{\dot{N}_{i\to f}}{I_0} \tag{3}$$

i.e. the total number of particles per unit time and per initial projectile intensity integrated over all the directions. Obviously, an ICS is not a function of the scattering angles and it is a less detailed property than a DCS.

In the measurement of a DCS, a small (ideally, point-like) detector is placed very far away (ideally, at infinity) from the collision chamber forming an angle θ with the projectile beam. The detector count during a given time is proportional to the differential cross sections at that scattering angle. By varying the position θ of the detector, the different values of the DCS $\frac{d\sigma_{i\to f}}{d\Omega}(\theta)$ are obtained. However, a variation in the angle ϕ does not cause a change in the detection, as previously mentioned. This is a consequence of the axial symmetry of the incoming beam and of the random nature of the collision. In the measurement of an ICS, the detector covers a big area so that it can capture all the scattered particles without detecting the nonscattered ones (for instance, a cylindrical metallic mesh around the beam leaving the collision chamber).

For a given scattering process, there exist other properties of interest which can be more, equally, or less, detailed than the defined cross sections. Among the more detailed

properties is the transition scattering (or reaction) probability, which is a theoretical quantity not accessible to any experiment. Among the less detailed properties is the kinetic rate constant which relates to the ICSs $\sigma_{i\to f}$ according to [6]

$$k(T) = \langle k_{i\to f}(T)\rangle = \langle \int_0^\infty v\sigma_{i\to f}(v)P(v;T)v^2 dv\rangle \tag{4}$$

where $k_{i\to f}(T)$ is the state-to-state kinetic rate constant, v the relative velocity of the scattering partners and $P(v;T)$ an statistical distribution of the relative velocities at temperature T (usually, a Maxwell-Boltzmann distribution); the brackets denote an averaging over the initial states on the said distribution. This rate constant is usually measured in bulk experiments. The given definition of rate constants is clearly connected to the ICS definition. However, an algorithm directly implemented from this definition could be extremely demanding. For a more practical definition in the END context see Ref. 7.

Finally, among the equally detailed properties is the projectile average energy loss [8]

$$\begin{aligned}\langle \Delta E\rangle &= \sum_b \Delta E_{a\to b} P_{a\to b} \\ &= \frac{\sum_b \Delta E_{a\to b}\left(\frac{d\sigma_{a\to b}}{d\Omega}\right)}{\sum_{b'}\frac{d\sigma_{a\to b'}}{d\Omega}}\end{aligned} \tag{5}$$

where $\Delta E_{a\to b}$ is the target energy difference corresponding to the target transition from state a to b. The weights $P_{a\to b}$ are defined as

$$P_{a\to b} = \frac{\frac{d\sigma_{a\to b}}{d\Omega}}{\sum_{a'}\frac{d\sigma_{a\to b'}}{d\Omega}} \tag{6}$$

From the DCS definition, it is easy to see that these weights are

$$P_{a\to b} = \frac{d\dot{N}_{a\to b}}{\sum_{f'} d\dot{N}_{a\to b'}} = \frac{\dot{N}_{a\to b}}{\sum_{f'}\dot{N}_{a\to b'}} \tag{7}$$

i.e. the ratio of the number of scattered projectile by exciting the targets from state a to b at a given time to the total number of scattered projectiles at the same time. This property is an average of projectile kinetic energy transferred to the target during the scattering process.

The present END work will be devoted to the theoretical description and numerical determination of all these experimental properties with the exception of the rate constants.

The Theory for Scattering Processes

It is noteworthy that the previous definitions of the scattering properties have been done in terms of experimental observables, *i.e.* in complete absence of any theoretical description of the scattering process itself. It is the mission of a theory to accurately describe the dynamics and calculate the observables of a given scattering process. At present, only a full quantum mechanical treatment one can provide that exact description. Therefore, this review chapter will amply exemplify full quantum methods for scattering systems. However, it should be borne in mind that almost all the quantum methods henceforth presented are approximate. Any realistic scattering process constitutes a theoretical problem so complicated that it can only be solved if some approximations are introduced into the formalism. However, the resulting approximate quantum methods are still so cumbersome that real departures from the exact quantum theory are usually employed. This is the case of the semiclassical (SC) theory. This theory can be loosely defined as the $\hbar \to 0$ limit of the exact quantum theory obtained by using some mathematical techniques. If properly used in the above limit, the SC theory is nothing but the exact quantum theory in a more tractable form without any loss of accuracy. However, the real benefit of the SC is to use it in situations somewhat far from the original $\hbar \to 0$ limit. In those cases, it is still possible to obtain quite acceptable results by using a less

intricate procedure. Other interesting facet of the SC theory, although more theoretical, is that its resulting expressions are almost those of the classical mechanics theory plus some additional terms such as oscillatory phases. These terms are real vestiges of the original quantum theory which still account for important quantum effects. These terms are totally absent in a pure classical treatment of the problem. In other words, the quantum theory does not totally go to the classical theory when $\hbar \rightarrow 0$: some quantum effects still survive. In that respect, the SC theory is "halfway" (semi = half) between the quantum and the classical theories. If the cited terms are discarded in the SC theory then the full classical theory will rise.

The relationship between quantum and classical theory is a fascinating subject still under intense investigation [9]. In fact, the quantum theory depends upon the classical one since the former can be constructed in the Schrödinger picture by promoting some classical variables (position and momentum) to the rank of operators. Even the Feyman path formulation of the quantum mechanics invokes the classical Lagrangian. Nonetheless, the kind of relationship considered here is under what circumstances the quantum results coincide with their classical counterparts. This problem has been traditionally addressed by means of the SC theory even though other option exists. This is the case of the henceforth called the quasi-classical theory[1]. In that approach, the aim is to construct quantum states whose position and momentum averages evolve in time exactly the same way as their classical analogues do. This type of construction is far from trivial to accomplish as the developments of this thesis will convincingly show. Intimately related to the quasi-classical theory, although exceeding its aims, is the coherent state theory [11], the definition of which is postponed to a later chapter. The

1. The quasi-classical theory definition adopted throughout this thesis work must not be confused with that of other authors as, for instance, in Ref. 10. In that case, the term quasi-classical theory denotes some simplified version of the previously mentioned SC theory.

present version of the END theory is strongly related to both the quasi-classical and the coherent state theory as will be seen during this thesis work.

All the traditional methods thus far developed to study scattering processes have been formulated within the framework of either the quantum or SC or classical theory. Quantum and SC methods will be explicitly presented in the next sections. Nonetheless, the classical methods will be indirectly presented as a simplification of the SC approach. Special emphasis will be given to those treatments exhibiting some analogies with the END theory. Methods theoretically less related to the END theory but to be used for numerical comparison will be discussed as well. In this chapter, only the way in which these methods describe the full dynamics will be considered. The connection of each type of dynamics with the scattering observables will be carefully discussed in chapter 5.

Quantum Mechanical Scattering Theory

Formal Scattering Theory

A scattering process is a real time-dependent phenomenon which can only be described in full detail by the time-dependent scattering theory. This implies the solution of the time-dependent Schrödinger equation of the whole system

$$H\Psi(t) = i\hbar\frac{\partial\Psi(t)}{\partial t} \tag{8}$$

when the Schrödinger picture is adopted. At initial time, both the projectile and the target are described by the wave function $\Psi(t = -\infty)$. In the usual case of a state-to-state scattering problem, the initial wave function is a stationary eigenfunction of the whole Hamiltonian with a trivial time dependency through a phase. However, it is usual in some type of simulations not to employ a single state but some linear combination of states forming a wave packet. In either case, at a remote final time, the evolved wave function $\Psi(t = \infty)$ can be decomposed into a linear combination of the stationary

eigenfunction of the products. Then, the coefficients of that combination ought to have a trivial time-dependency through their phases again. At any time of the evolution $-\infty \leq t \leq \infty$, all the properties of the scattering system, including final time properties such as cross sections, can be calculated from the wave function $\Psi(t)$. The probability of the system to yield by reaction some type of products at final time can be obtained by projecting the final wave function against the product states. As shown, the scattering problem also demands the previous solution of the time-independent eigenvalue problem of both reactants and products. For a time-independent Hamiltonian, the totally formal solution of this problem for an evolution between the times t_1 and t_2 $t_2 \geq t_1$ is

$$\begin{aligned} \psi(t_2) &= U(t_2 - t_1)\psi(t_1) \\ &= \exp\left[\frac{-iH(t_2 - t_1)}{\hbar}\right]\psi(t_1) \end{aligned} \tag{9}$$

where the central unitary operator $U(t_2 - t_1)$ is called the time-evolution operator or propagator.

The formal scattering theory was developed since the origin of the quantum mechanics until the 1950s (see Ref. 3, chapters 3–5, and 12, chapters 5–6). The main concern of that discipline is to rigorously define a scattering process in mathematical terms, to attempt a formal, exact solution of the time-dependent and the time-independent Schrödinger equations, and to define the formal tools to treat a scattering process (*e.g.* the wave and the S-operators, the S- and the T- matrices, etc.). The analysis of the scattering problem given in the previous paragraphs and the careful definition of scattering processes at the beginning of this chapter are in the spirit of the formal theory. The purely formal solutions are usually obtained from an integral equation reformulation of the original Schrödinger equation in both the time-dependent and the time-independent cases. These developments are of high theoretical value but of little practical consequences since no definite algorithm to solve the scattering problem can be devised in this way. Therefore,

a systematic presentation of the formal scattering theory will not be attempted here. Instead, the main concepts of the formal theory will be revealed during the presentation of the practical methods. A case of note is that of the S-matrix which will be introduced in the following sections and will be fully developed in the next chapters in the context of the END theory.

Time-Independent Scattering Theory

Time-Independent vs. Time Dependent Schemes

The most detailed description of a given scattering process or a chemical reaction can only be achieved by the time-dependent formulation of the problem. However, the solution of a realistic scattering problem is far more difficult to find in the time-dependent scheme than in the time-independent one. The difficulties posed by the time-dependent methods had favored the adoption of the time-independent approach until the 1970s. The justification of how essentially time-dependent phenomena such as scattering processes and chemical reactions can be treated time-independently is rigorously explained in the more advanced literature on the subject [3, 12]. Here, it can be loosely stated that the eigenfunctions ψ_n of the time-independent Schrödinger equation for a scattering problem

$$H\psi_n = E_n\psi_n \tag{10}$$

contain in the asymptotic region an incoming component describing the reactants and different outgoing components describing the products. Most of the relevant properties of the scattering process can be calculated from those outgoing components. However, all the intermediate details of a scattering processes or a chemical reaction can not be obtained in this way. This approach is an extension of the most traditional methods to calculate bound states in isolated molecules to the case of several colliding molecules involving some unbound translational states. This connection to the methods in electronic

structure theory has also favored the bias to the time-independent schemes. Because of its historical precedence, the time-independent methods will be presented first. Furthermore, the time-independent approach directly refers to the stationary description of reactants and products, a problem which must be necessarily addressed before attempting a time-dependent solution. It is also important to remember that some of the techniques further developed within END theory have their remote origins in the time-independent theory.

Adiabatic and diabatic representations

In the time-independent approach, a solution of the time-independent Schrödinger equation for the whole system is attempted

$$H(\mathbf{x}, \mathbf{X})\psi_n(\mathbf{x}, \mathbf{X}) = E_n\psi_n(\mathbf{x}, \mathbf{X}) \tag{11}$$

where $\mathbf{X}$ and $\mathbf{x}$ are the nuclear and the electronic coordinates, respectively, and $\psi_n(\mathbf{x}, \mathbf{X})$ are the total wave function of the system with total energy eigenvalue E_n. In the asymptotic regions, these wave functions describe the incoming reactants and the different outgoing products into which the system can be divided. Exact solutions of such a complex problem only exist for very simple systems. Therefore, some expansion of the $\psi_n(\mathbf{x}, \mathbf{X})$ functions in a suitable basis set is necessarily introduced. The type of basis set selected constitutes a representation, and two of them, named adiabatic and diabatic, respectively, are the most widely used (for other possibilities see citations in Ref. 13, chapter 6). The representation problem has a very long story [14] and has been reviewed many times from different standpoints. A recent review by Yarkony [15] mostly adopts a nondynamical, electronic structure point of view, whereas the reviews by Baer [16, 17] and the work by Child [13, 18] strongly emphasizes the dynamical aspects. These diverse views on the same subject will be unified in the discussion below.

In the adiabatic representation, the total Hamiltonian is partitioned into two terms

$$H(\mathbf{x}, \mathbf{X}) = T_n + H_{el}(\mathbf{x}; \mathbf{X}) \tag{12}$$

where the first one is the total nuclear kinetic energy

$$T_n = -\sum_{k}^{Nucl} \frac{1}{2M_k} \nabla_k^2 \tag{13}$$

and the second one is the electronic Hamiltonian $H_{el}(\mathbf{x}; \mathbf{X})$ which includes the nuclear repulsion and depends parametrically on the nuclear coordinates $\mathbf{X}$. This electronic Hamiltonian can be further divided into [15]

$$H_{el}(\mathbf{x}; \mathbf{X}) = H_a(\mathbf{x}; \mathbf{X}) + H_{BP}(\mathbf{x}; \mathbf{X}) \tag{14}$$

where $H_a(\mathbf{x}; \mathbf{X})$ is the traditional nonrelativistic electronic Hamiltonian and $H_{BP}(\mathbf{x}; \mathbf{X})$ is the relativistic correction within the Breit-Pauli approximation (it is usually approximated to the spin-orbit interaction term, $H_{so}(\mathbf{x}; \mathbf{X})$, only). Thus, the total wave function $\psi_n(\mathbf{x}, \mathbf{X})$ can be expanded as

$$\psi_n(\mathbf{x}, \mathbf{X}) = \sum_i F_i^n(\mathbf{X}) \psi_i^a(\mathbf{x}, \mathbf{X}) \tag{15}$$

The basis function $\psi_i^a(\mathbf{x}, \mathbf{X})$ are the eigenfunctions of the nonrelativistic Hamiltonian

$$H_0(\mathbf{x}; \mathbf{X}) \psi_i^a(\mathbf{x}; \mathbf{X}) = E_i^a(\mathbf{X}) \psi_i^a(\mathbf{x}; \mathbf{X}) \tag{16}$$

and are termed the adiabatic (Born-Oppenheimer) electronic states. Their energy eigenvalues $E_i^a(\mathbf{X})$ also depend parametrically on $\mathbf{X}$ and are termed the adiabatic potential energy surfaces (PES). The energy matrix $\mathrm{E}^a(\mathbf{X})$

$$\mathrm{E}_{ij}^a(\mathbf{X}) = \langle \psi_i^a(\mathbf{x}, \mathbf{X}) | H_0 | \psi_j^a(\mathbf{x}, \mathbf{X}) \rangle_{\mathbf{x}} \tag{17}$$

is diagonal in this basis set, with eigenvalues $E_i^a(\mathbf{X})$. The expansion coefficients $F_i^n(\mathbf{X})$ are the adiabatic nuclear wave functions. The preceding expansion is exact provided

that the infinite basis set of functions $\psi_i^a(\mathbf{x},\mathbf{X})$ is used in full. If the above electronic eigenvalue problem has been solved *a priori* then the nuclear wave functions can be successively obtained by inserting the previous expansion into the total Hamiltonian, and by projecting the resulting equation into the electronic states $\psi_i^a(\mathbf{x},\mathbf{X})$. Thus, an intricate system of coupled differential equations for the functions $F_i^n(\mathbf{X})$ is obtained (cf. Ref. 15, its notation has been changed to facilitate the comparison with other references)

$$[T_n + E_i^a(\mathbf{X}) - H_{ii}^a(\mathbf{X}) - E_n]F_i^n(\mathbf{X}) = \\ -\sum_{J\neq I}\left[H_{ij}^a(\mathbf{X}) + H_{ij}^{BP,a}(\mathbf{X}) + \sum_{k=1}^{Nucl}\left(\frac{-1}{M_k}\mathbf{f}_{\mathbf{k}}^{\mathbf{ij}}(\mathbf{X})\cdot\nabla_{\mathbf{k}}\right)\right]F_j^n(\mathbf{X}) \tag{18}$$

where the so-called coupling terms $\mathbf{f}_{\mathbf{k}}^{\mathbf{ij}}(\mathbf{X}) = \left[f_{X_k}^{ij}(\mathbf{X}), f_{Y_k}^{ij}(\mathbf{X}), f_{Z_k}^{ij}(\mathbf{X})\right]$, $H_{ij}^a(\mathbf{X})$ and $H_{ij}^{BP,a}(\mathbf{X})$ are

$$f_{W_k}^{ij}(\mathbf{X}) = \langle\psi_i^a(\mathbf{x};\mathbf{X})|\frac{\partial}{\partial W_k}\psi_j^a(\mathbf{x};\mathbf{X})\rangle_{\mathbf{x}} \tag{19}$$

$$H_{ij}^a(\mathbf{X}) = \sum_{W,k}\frac{-1}{2M_k}\langle\psi_i^a(\mathbf{x};\mathbf{X})|\frac{\partial^2}{\partial W_k\partial W_l}\psi_j^a(\mathbf{r};\mathbf{R})\rangle_{\mathbf{x}} \tag{20}$$

and

$$H_{ij}^{BP,a}(\mathbf{X}) = \sum_{W,k}\frac{-1}{2M_k}\langle\psi_i^a(\mathbf{x};\mathbf{X})|H^{BP}|\psi_i^a(\mathbf{x};\mathbf{X})\rangle_{\mathbf{x}} \tag{21}$$

Notice that the integrals above are evaluated in the electronic variables only. The coupling terms $H_{ij}^a(\mathbf{X})$ and $H_{ij}^{BP,a}(\mathbf{X})$ are of "potential energy" type whereas the remaining $\mathbf{f}_{\mathbf{k}}^{\mathbf{ij}}(\mathbf{X})\cdot\nabla_{\mathbf{k}}$ are of (nuclear) "kinetic energy" type. Due to this latter type of coupling terms, the adiabatic representation is thought of as a kinetic energy coupling scheme.

The complete solution of the previous problem has then two stages: 1) solve the electronic eigenvalue problem for the $\psi_i^a(\mathbf{x},\mathbf{X})$ and then 2) solve the coupled system of equations for $F_i^n(\mathbf{X})$. The second stage of this problem will be discussed first whereas the first one is postponed to the next section. It is assumed in what follows that at least some relevant adiabatic states are known with some level of accuracy.

The set of equations for the nuclear functions couples a given function $F_i^n(\mathbf{X})$ with all the others $F_j^n(\mathbf{X})$ belonging to other adiabatic states. From a dynamical point of view, these coupling terms induce nonadiabatic transitions between different states. The solution of these coupled equations is extremely difficult even when a truncated basis set is employed. Therefore, it is important to know under what conditions it is possible to introduce uncouplings. It can be shown [15] that if the energy difference $\Delta E_{ij}(\mathbf{X}) = \Delta E_{ij}^a(\mathbf{X}) + \Delta E_{ij}^{BP}(\mathbf{X}) + \Delta H_{ij}(\mathbf{X})$, with $\Delta E_{ij}^a(\mathbf{X}) = E_i^a(\mathbf{X}) - E_j^a(\mathbf{X})$, $\Delta E_{ij}^{BP}(\mathbf{X}) = E_i^{BP}(\mathbf{X}) - E_j^{BP}(\mathbf{X})$ and $\Delta H_{ij}^a(\mathbf{X}) = H_{ii}^a(\mathbf{X}) - H_{jj}^a(\mathbf{X})$ is large at some values of $\mathbf{X}$ then the coupling between the states i and j may be neglected [15]. If the right hand side of the coupling equations, which have the nondiagonal terms, is neglected then the problem becomes uncoupled. This is the adiabatic approximation. In that case, the term $H_{ii}(\mathbf{X})$ (the adiabatic correction) makes a usually small refinement to the adiabatic energy $E_i^a(\mathbf{X})$. If this term is also neglected, the famous (or infamous) Born-Oppenheimer approximation is obtained. Molecular nuclear functions within the Born-Oppenheimer approximation are very well-known in electronic structure theory and spectroscopy [19]. In fact, the adiabatic representation and its approximations are the only representations in use for nonscattering problems. As implied before, the adiabatic and the Born-Oppenheimer approximations are valid in all regions of the nuclear coordinates $\mathbf{X}$ where the $\Delta E_{ij}(\mathbf{X})$ are not small. In practice, the leading term in that difference is the adiabatic energy difference $\Delta E_{ij}^a(\mathbf{X})$. Thus, these approximations break where at the least two adiabatic energy surfaces actually or nearly intersect. Extensive studies have been devoted to the different types of surface intersections or near-intersections (conical allowed, conical actual, or avoided crossings [15]) and to some effects associated with them (as the change of sign of the geometric phase around conical intersections). Those topics will not be discussed here.

In the diabaic representation, a different expansion is proposed for the same total wave function

$$\psi_n(\mathbf{x}, \mathbf{X}) = \sum_I G_i^n(\mathbf{X}) \psi_i^d(\mathbf{x}) \tag{22}$$

where the diabatic states $\psi_i^d(\mathbf{x})$ do not depend on the nuclear coordinates $\mathbf{X}$. More precisely, the diabatic states are the eigenfunctions of the above electronic Hamiltonian $H_a(\mathbf{x}; \mathbf{X})$ with the nuclear translational separation of the collision partners at the asymptotic limit of $\mathbf{X_{trans}} \to \infty$ and with the remaining nuclear internal coordinates fixed at the equilibrium values $\mathbf{X_{int}} = \mathbf{X_{eq}}$ [18]

$$H_a(\mathbf{x}; \mathbf{X}) \psi_i^d(\mathbf{x}) = E_i^d \psi_i^d(\mathbf{x}); \ \mathbf{X_{trans}} \to \infty, \ \mathbf{X_{int}} = \mathbf{X_{eq}} \tag{23}$$

The diabatic energies E_i^d are therefore independent of the coordinates $\mathbf{X}$. From the definition, it immediately holds that

$$\lim_{\mathbf{X_{trans}} \to \infty} \psi_i^a(\mathbf{x}; \mathbf{X}) = \psi_i^d(\mathbf{x}); \ \mathbf{X_{int}} = \mathbf{X_{eq}} \tag{24}$$

At an arbitrary position $\mathbf{X}$, there exists a unitary matrix $\mathcal{A}(\mathbf{X})$ so that

$$\psi_{\mathbf{i}}^{\mathbf{d}}(\mathbf{x}) = \mathcal{A}(\mathbf{X}) \psi_{\mathbf{i}}^{\mathbf{a}}(\mathbf{x}; \mathbf{X}) \tag{25}$$

This matrix is unique [16, 17] and it can be constructed by solving a vectorial equation [16, 17]. Simple examples of that equation and its matrix solution can be found in the literature for the model cases of two [16–18] and of three [16, 17] PES. The energy matrix $\mathrm{E}^d(\mathbf{X})$

$$\mathrm{E}_{ij}^d(\mathbf{X}) = \langle \psi_i^d(\mathbf{x}) | H_a(\mathbf{X}) | \psi_j^d(\mathbf{x}) \rangle_{\mathbf{x}} \tag{26}$$

is not diagonal, except in the asymptotic region, but it can be diagonalized to its adiabatic counterpart according to $\mathrm{E}^a(\mathbf{X}) = A^\dagger(\mathbf{X}) \mathrm{E}^d(\mathbf{X}) A(\mathbf{X})$. The diabatic nuclear

wave functions $G_i^n(\mathbf{X})$ can be obtained by repeating the same procedure as that to find their adiabatic counterparts $F_i^n(\mathbf{X})$ [18]

$$\left[T_{nucl} + H_{ii}^d(\mathbf{X}) + E_n\right] G_i^n(\mathbf{X}) = -\sum_{j \neq i} H_{ij}^d(\mathbf{X}) G_i^n(\mathbf{X}) \tag{27}$$

where the diabatic coupling terms are

$$H_{ij}^d(\mathbf{X}) = \langle \psi_i^d(\mathbf{x}) | H_a | \psi_j^d(\mathbf{x}) \rangle \tag{28}$$

Noticeable in these equations is the absence of the gradient couplings terms $\mathbf{f}_\mathbf{k}^{\mathbf{ij}}(\mathbf{X}) \cdot \nabla_\mathbf{k}$ present in the adiabatic case. All the coupling terms $H_{ij}^d(\mathbf{X})$ are of "potential energy" type. Therefore, the diabatic representation is thought of as a potential energy scheme. In fact, the change of basis set has "transferred" the adiabatic gradient coupling terms into the "energy potential" diabatic terms. The real possibility to obtain exact diabatic states or only approximate ones (quasi-diabatic) has been debated in the literature [15] but this subtle aspect of this matter will not be addressed here.

The selection of one or the other representation depends on different theoretical and computational factors [16–18] . There is no simple answer to this question and they are too case-dependent to allow a generalization. The adiabatic representation has the advantage of keeping a direct relationship to the electronic structure PESs. The diabatic representation blurs that connection but omits the bothersome gradient coupling terms. Numerically, the adiabatic representation runs into serious problems when two adiabatic states becomes closer in value (avoided crossings) or directly cross. There, the coupling terms $\mathbf{f}_\mathbf{k}^{\mathbf{ij}}(\mathbf{X})$ usually develop a near singularity. In those cases, the diabatic representation is preferred unless those coupling terms are really smooth functions. This problem can occur even in the case of simple unidimensional dynamics models with only two PESs. Additional complications can happen in the tridimensional case. For instance, it has been found [17] that the coupling terms $\mathbf{f}_\mathbf{k}^{\mathbf{ij}}(\mathbf{X})$ may diverge in the asymptotic region as well.

This again favors the diabatic representation. Further discussion on this subject along with specific examples can be seen in the cited literature.

Potential energy surface calculation

The calculation of the adiabatic PESs totally belongs to the field of the electronic structure theory. Massive efforts have been devoted to this problem since the advent of the quantum chemistry in the 1930s up to now. The main goal of these undertakings was and is to construct very accurate PESs, *i.e.* surfaces with exact numerical values ("energetics"), correct spin description, and right asymptotic behavior toward reagents and products. In the *ab initio* approach to this problem, the calculation of the PESs is accomplished in a rigorous way starting from the time-independent Schrödinger equation. These calculations usually begin with either a noncorrelated single-reference self-consisted field (SCF) or a partially correlated multi-reference self-consistent field (MCSCF) wave function according to the spin symmetry and asymptotic considerations. From these reference states, increasing levels of correlation can be achieved by performing variational (configuration of interactions, CI) or perturbational (many-body perturbation theory, MBPT, or coupled-cluster theory, CC) techniques on them. The multi-reference CI approach is the preferred one since it is the one to better satisfy the above requisites of a good PES [15] . Obviously, the PESs calculation by these means is not an easy task to perform, especially for excited states.

In view of the theoretical and numerical difficulties found during the *ab initio* PES calculations, less rigorous but still accurate methods are in some instances employed. An example is the case of the semiempirical methods. Some of them are the more familiar Hartree-Fock based semiempirical methods, relying on the complete neglect of differential overlap (CNDO), intermediate neglect of differential overlap (INDO), or

neglect of diatomic differential overlap (NDDO) approximations *inter alia* [20], whose use for dynamical problems are rather recently being explored [21, 7]. Among the nonHartree-Fock based semiempirical methods, the diatomic-in-molecule (DIM) method [22, 23] has been extensively used for dynamical purposes. More recently, density functional theory (DFT) [24] PESs have been employed for that type of problems. Finally, and as the most drastic approximation, the PES determination can be totally abandoned and some model potentials can be introduced. These potentials are relatively simple functions bearing some parameters. These parameters can be numerically determined by fitting them using scattering experimental data. Some of these model potentials will be briefly discussed in chapter 5.

The calculation of a PES by any of the mentioned methods, except for the model potentials, renders a collection of energy values on a grid of points. To solve dynamical problems, the PES must be adequately known at any point required by the dynamical equations. Therefore, the PES on the grid must either be fitted to a function or interpolated. The fitting and/or interpolation procedures to finally construct a PES for dynamical use are cumbersome and vexatious. Many techniques have been employed but still the Holy Grail of a universal, cost effective, master procedure, adequate for any region of the potential has not been found.

In spite of the mentioned difficulties, the use of PES standpoint is commonplace in dynamics theory. The topological features of the PESs (surface crossings, energy minima, transitions state saddle points, minimum energy paths, etc.) allow very pictorial explanations of some dynamical effects. It is perhaps because of this tangible representation of the dynamics that the PESs are so popularly acclaimed.

Exact time-independent method: The close-coupling Formalism

After some set of PESs is made available, the time-independent solution of a scattering problem can be undertaken. This involves the solution of the above set of nuclear coupled equations in a selected representation. The first step in solving this problem is to transform the Hamiltonian to the CM frame to eliminate the trivial CM dynamics. In this way, three degrees of freedom are eliminated by appealing to three constants of the motion: the three components of the CM linear momentum. After this transformation is effected, the exact way to solve the remaining problem consists in expanding each nuclear wave function in terms of the angular momentum eigenfunctions of the whole system. This is the partial wave expansion. The expansion coefficients are functions of radial coordinates only and are termed the radial components. By setting these new expansions into the previous set of equations, an equivalent, new set of coupled equations for the radial component only is obtained. This resulting set is the one to be solved. In this process, two angular degrees of freedom have been eliminated. This is not a surprise since by expanding in terms of the angular momentum eigenfunctions of the whole system, the constants of motion associated with the total angular momentum and one of its components are eliminated. However, the use of these angular functions introduces the intricate problem of the angular momentum couplings. This way to solve the time-independent scattering problem is called the close-coupling or coupled-channel (CC) formalism.

The CC formalism will be first exemplified for systems not undergoing reactive processes (*i.e.* rearrangements or combinations). The case of an atom-atom collision (where atom means both a neutral atom and an atomic ion) will be examined first. The diabatic representation is more concise and will be used in the example. The formal

extension to the adiabatic representation is straightforward. In the CM frame, the diabatic equations for an atom-atom collision can be now written [13] (cf. the previous section)

$$\left[-\frac{\hbar^2}{2\mu}\nabla^2_{\mathbf{X}} + E\right] G^n_i(\mathbf{X}) = -\sum_i H^d_{ij}(\mathbf{X}) G^n_j(\mathbf{X}) \tag{29}$$

where only one nuclear coordinate $\mathbf{X}$ describes the separation between the two atoms. The incoming projectile is supposed to be initially travelling in the $\mathbf{z}$ direction here and in all the subsequent theoretical discussion in this work. Each of the nuclear diabatic functions $G^n_i(\mathbf{X})$ is termed a channel since each one "leads" the reactants to different types of products. In the asymptotic region $\mathbf{X} \to \infty$, the nuclear wave function must satisfy the following scattering boundary conditions

$$\lim_{\mathbf{X}\to\infty} G^n_j(\mathbf{X}) = \delta_{ij} e^{ik_j z} + f_{ij}(\theta)\frac{e^{ik_j r}}{r} \tag{30}$$

where the wave vectors $\mathbf{k_j}$ have the fixed value

$$k^2_j = \frac{2\mu(E - E_j)}{\hbar^2} \tag{31}$$

with E_i the electronic energy for the channel j. The wave vectors contain the outgoing nuclear kinetic energy per channel. The first component of the above asymptotic functions is an incoming plane wave travelling in the z direction. It describes the relative motion of the reactants in the incoming situation. The Kronecker delta makes only one channel, the "entrance" channel i, to be the incoming component in accordance with the experimental initial conditions. The second component describes the outgoing scattered products by a spherical wave modified by the angular function $f_{ij}(\theta)$ termed the scattering amplitude. There is also an outgoing component in the entrance channel to describe the elastic scattering. All the other outgoing components in the "exit" channels correspond to inelastic scatterings. Notice that because of the spherical symmetry of the interaction potential, the azimuthal angle ϕ plays no role in the atom-atom scattering problem. The

scattering process distorts the cylindrically symmetric incoming plane wave into outgoing spherical waves with an angularly modified amplitude.

It remains now to integrate the set of coupled equations to fully solve the dynamical problem at hand. The CC formalism applied to the atom-atom problem implies the expansion of each nuclear function in terms of the angular momentum eigenfunctions of the whole system. In this case, the total angular momentum is due solely to the relative orbital motion of one reactant with respect to the other. The bothersome problem of the coupling of this angular momentum to other "internal" ones is not present in this simple situation. Furthermore, the interaction potential is spherical so that the orbital (total) angular momentum is conserved. The incoming plane wave has a zero angular component in the **z** direction which will be conserved during the scattering process. Therefore, it suffices for the atom-atom collision to make the expansions in terms of the zero L_z eigenfunctions $Y_l^0(\theta,\phi)$ [25]

$$Y_l^0(\theta,\phi) = \left[\frac{2l+1}{4\pi}\right]^{\frac{1}{2}} P_l(\cos\theta) \tag{32}$$

Therefore, the wave expansions are [13]

$$G_j^n(\mathbf{X}) = \frac{1}{r}\sum_{l=0}^{\infty} A_l \psi_{jl}(r) P_l[\cos\theta] \tag{33}$$

where the A_l are the fixed part of the coefficients and the $\psi_{jl}(r)$ are the radial components. The $\frac{1}{r}$ factor has been introduced to cancel out the first derivative terms in r during further manipulations. By setting these expansions into the nuclear diabatic equations, the CC set of equations is obtained [13]

$$\left[\frac{d^2}{dr^2} + k_i^2 - \frac{l(l+1)}{r^2}\right]\psi_{il}(r) = \sum_j H_{jl}(r)\psi_{lj}(r) \tag{34}$$

It can be demonstrated that for rapidly decreasing atom-atom potential satisfying $\lim_{r\to\infty} rU(r) = 0$ [26, 13] the previous scattering boundary conditions applied to radial

component render

$$\lim_{r\to\infty}\psi_{jl}(r)\sim\delta_{ij}\sin\left[k_j r-l\frac{\pi}{2}+\delta(l)\right]-\frac{1}{2}\left(\frac{k_i}{k_j}\right)^{1/2}T^l_{ij}e^{\left(ik_j r-il\frac{\pi}{2}\right)} \tag{35}$$

where $\delta(l)$ is a real phase related strongly dependent on potential energy function and T^l_{ij} are the elements of the transition matrix (T-matrix) [13]. The special case posed by the Coulomb potential, which does not satisfy the above decreasing condition, is not more difficult to be solved and can be seen in Ref. 26. It is not difficult to see that each element of the T-matrix is related to the probability to find the system exiting through the channel j after entering through the channel i. The solution of the previous set of equations under the mentioned asymptotic conditions will determine the radial components $\psi_{jl}(r)$ and therefore the total nuclear wave function. From the radial components in the asymptotic region, the values of T^l_{ij} can be determined. In turn, the determination of the A_l coefficients is simple and analytical. The first step to find them is to introduce a wave expansion for the incoming plane wave. This expansion is analytical having the radial components in term of spherical Bessel functions [27]. By setting both wave expansions into the entrance channel function in the asymptotic region

$$\lim_{\mathbf{X}\to\infty}G^n_i(\mathbf{X})=e^{ik_i z}+f_{ii}(\theta)\frac{e^{ik_i r}}{r} \tag{36}$$

it can be easily determined that

$$A_l=(2l+1)\frac{i^l}{k_i} \tag{37}$$

(where the i in i^l is the imaginary unit not the entrance label i. By repeating the same procedure in other channels, it can be concluded that

$$\begin{aligned} f_{ij}(\theta) &= -\frac{1}{2[k_i k_j]^{\frac{1}{2}}}\sum_{l=0}^{\infty}(2l+1)T^l_{ij}P_l(\cos\theta) \\ &= -\frac{1}{2[k_i k_j]^{\frac{1}{2}}}\sum_{l=0}^{\infty}(2l+1)\left(S^l_{ij}-\delta_{ij}\right)P_l(\cos\theta) \end{aligned} \tag{38}$$

In the second line, the scattering or S-matrix has been defined by $T_{ij}^{l} = S_{ij}^{l} - \delta_{ij}$. In the case of elastic scattering, $i = j$, the amplitude has two contributions: one coming from the sum in S_{ii}^{l}, which represents a scattered (distorted) wave, and other form the sum in $\delta_{ii} = 1$, which represents the nonscattered (formerly incoming) plane wave. Since the latter contribution is only strong near $\theta = 0$, it is customary to simply write

$$f_{ij}(\theta) = -\frac{1}{2[k_i k_j]^{\frac{1}{2}}} \sum_{l=0}^{\infty} (2l+1) S_{ij}^{l} P_l(\cos\theta): \ \theta \neq 0 \tag{39}$$

for the practically accessible values of the scattered wave at $\theta \neq 0$. This is the expression to be used henceforth in this thesis work. After the scattering amplitudes have been determined, the scattering properties can be calculated form the asymptotic wave functions.

The type of scattering hitherto presented contains as a special case the simplest type of atom-atom scattering processes: the elastic scattering. That situation occurs in noble gas systems at relatively low collision energies. There, the scattering process will undergo neither electronic excitations nor charge transfer. Therefore, the process can be perfectly described by only one PES. The elastic atom-atom scattering is discussed in full detail in Ref. 13, chapter 3 through 5. The formation of a bound state by part of the colliding atoms (combination) constitute a departure from the relatively simple description shown thus far. This complication will be addressed in the following paragraphs in the broader context of atom-molecule scattering processes. Other complications not discussed here are the formation of quasi-bound states (resonances) and the problems posed by identical particles (*e.g.* $He + He$ scattering). These situations are treated in some detail in Ref. 13.

The scattering processes involving more than two atoms are far more difficult to treat by the CC formalism. The case of an atom (or atomic ion) colliding with a diatomic molecule (or molecular ion) has been extensively studied [13, 28] and will

be discussed in some detail below. Present efforts in the time-independent scattering theory are focused on four-atom systems (*e.g.* two colliding diatomic molecules [29, 30]). The simplest case to study is when electron excitations or electron transfers do not occur. In most of these cases, only one PES is actually employed [13, 28], *i.e.* the Born-Oppenheimer approximation is adopted. The Hamiltonian is transformed into the CM frame, and relative, internal coordinates are then used. However, different types of internal coordinates have been prescribed for the three-atom system. A simple type of internal coordinate are the Jacobi coordinates: $\mathbf{r}$, the separation between the two atoms in the diatomic molecule, and $\mathbf{R}$, the separation between CM of the diatomic molecule (target) and the atom (projectile). In principle, there exist three different ways or arrangements in which these coordinates can be defined according to what atoms form the diatomic molecule. In the case of a non reactive scattering, the selection is unique since the initial diatomic target and the projectile retain their identities throughout the processes. If the scattering system does undergo rearrangements, three, or at the least two, different selections of the Jacobi coordinates ought to be considered. One arrangement describes both the entrance channel and the non reactive exit channel, whereas the others arrangements describe the reactive exit channels. This swapping of coordinates in different asymptotic regions is obviously motivated by the ease of convergency at each channel. However, it introduces the complication of smoothly turning from one type of Jacobi coordinates to another in the intermediate regions. Other types of coordinates not presenting this difficulty have been proposed. The most conspicuous of them are the natural [13] and the hyperspherical [31, 32] coordinates. They will not be discussed here. Using the adiabatic representation with only one PES, the Schrödinger equation

for the arrangement λ is now [28]

$$\left[-\frac{\hbar^2}{2\mu_R^\lambda}\nabla^2_{\mathbf{R}'_\lambda} - \frac{\hbar^2}{2\mu_r^\lambda}\nabla^2_{\mathbf{r}'_\lambda} + V\left(R'_\lambda, r'_\lambda, \gamma_\lambda\right)\right]\Phi^\lambda\left(\mathbf{R}'_\lambda, \mathbf{r}'_\lambda\right) = E\Phi^\lambda\left(\mathbf{R}'_\lambda, \mathbf{r}'_\lambda\right) \tag{40}$$

where $\mathbf{R}'_\lambda$ and $\mathbf{r}'_\lambda$ are the Jacobi coordinates in that arrangement, γ_λ is the orientation angle between the two previous vectors

$$\gamma_\lambda = \cos^{-1}\left(\frac{\mathbf{R}'_\lambda \cdot \mathbf{r}'_\lambda}{R'_\lambda r'_\lambda}\right) \tag{41}$$

and μ_R^λ and μ_r^λ are the translational and the vibrational reduced masses

$$\mu_R^\lambda = \frac{\left(m_1^\lambda + m_2^\lambda\right)m_3^\lambda}{\left(m_1^\lambda + m_2^\lambda + m_3^\lambda\right)} \tag{42}$$

$$\mu_r^\lambda = \frac{m_1^\lambda m_2^\lambda}{\left(m_1^\lambda + m_2^\lambda\right)} \tag{43}$$

with indices 1 and 2 denoting the atoms in the diatomic and 3 the projectile. This equation can be set in a more symmetric form if the transformations

$$\mathbf{R}_\lambda^{'} = \left(\frac{\mu_R^\lambda}{\mu_r^\lambda}\right)^{1/4}\mathbf{R}_\lambda \tag{44}$$

$$\mathbf{r}_\lambda^{'} = \left(\frac{\mu_r^\lambda}{\mu_R^\lambda}\right)^{1/4}\mathbf{r}_\lambda \tag{45}$$

are introduced

$$\left[-\frac{\hbar^2}{2\mu}\left(\nabla^2_{\mathbf{R}_\lambda} + \nabla^2_{\mathbf{r}_\lambda}\right) + V(R_\lambda, r_\lambda, \gamma_\lambda)\right]\Phi^\lambda(\mathbf{R}_\lambda, \mathbf{r}_\lambda) = E\Phi^\lambda(\mathbf{R}_\lambda, \mathbf{r}_\lambda) \tag{46}$$

Note that the transformation does not change the orientation angle γ_λ.. Since the total Hamiltonian does commute with the total (nuclear) orbital angular momentum operator $\widehat{J}$ and with one of its components, say $\widehat{J}_z$, the total nuclear wave function can be chosen as an eigenfunction of the previous operators with eigenvalues $J(J+1)\hbar^2$; $J = 0,\ 1,\ 2,\ 3,\ \ldots$ and $M\hbar$; $M = -J,\ -J+1,\ \ldots\ J-1,\ J$, respectively. Therefore, (cf. Ref. 13, chapter VI)

$$\Psi^\lambda(\mathbf{R}_\lambda, \mathbf{r}_\lambda) \equiv \psi^\lambda_{JM}(\mathbf{R}_\lambda, \mathbf{r}_\lambda) \tag{47}$$

The total angular momentum $\widehat{J}$ is given by the sum

$$\widehat{\mathbf{J}} = \widehat{\mathbf{l}} + \widehat{\mathbf{j}} \tag{48}$$

where $\widehat{l}$ is the orbital angular momentum produced by the rotation of the projectile around the CM the diatomic, and $\widehat{j}$ is the internal angular momentum produced by the rotation of the diatomic around its own CM. The eigenfunctions $\psi^{\lambda}_{JM}(\mathbf{R}_{\lambda}, \mathbf{r}_{\lambda})$ may be expressed in terms of the eigenfunctions of both $\widehat{l}$ and $\widehat{j}$ through the Clebsch-Gordan coefficient coupling scheme. This route is explicitly attempted in Ref. [13] and will not be presented here. The CC formalism is introduced when the eigenfunctions $\psi^{\lambda}_{JM}(\mathbf{R}_{\lambda}, \mathbf{r}_{\lambda})$ are expanded in terms of the spherical harmonics $Y_{j_{\lambda}M}(\theta_{\lambda}, \phi_{\lambda})$

$$\psi^{\lambda}_{JM}(R_{\lambda}, r_{\lambda}, \theta_{\lambda}, \phi_{\lambda}) = \sum_{j_{\lambda} \geq |M|} \left(\frac{1}{R_{\lambda} r_{\lambda}} \right) Y_{j_{\lambda}M}(\theta_{\lambda}, \phi_{\lambda}) F^{\lambda}_{j_{\lambda}M}(R_{\lambda}, r_{\lambda}) \tag{49}$$

where $F^{\lambda}_{j_{\lambda}M}(R_{\lambda}, r_{\lambda})$ are the radial component of the expansion. In some cases, the subsequent equations can be further simplified if a transformation from the previous space-fixed frame to a rotating body-fixed frame is effected. The body-fixed frame is oriented with its $\mathbf{z}$ axis along the $\mathbf{R}_{\lambda}$ vector and with its $\mathbf{y}$ axis normal to it (helicity representation). The new eigenfunctions $\psi^{\lambda}_{J\Omega_{\lambda}}(R_{\lambda}, r_{\lambda}, \gamma_{\lambda}, \chi_{\lambda})$ in the rotating frame are related to the old one by

$$\psi^{\lambda}_{JM}(\mathbf{R}_{\lambda}, \mathbf{r}_{\lambda}) = \sum_{\Omega_k} \sqrt{\frac{2J+1}{4\pi}} D^{J}_{M\Omega_{\lambda}}(\phi_{\lambda}, \theta_{\lambda}, 0) \psi^{\lambda}_{J\Omega_{\lambda}}(R_{\lambda}, r_{\lambda}, \gamma_{\lambda}, \chi_{\lambda}) \tag{50}$$

where the $D^{J}_{M\Omega_{\lambda}}$ are the Wigner rotation matrix elements, M and Ω_{λ} the azimuthal quantum numbers into the space-fixed and body-fixed $\mathbf{z}$ axes, respectively, and ϕ_{λ} θ_{λ} and χ_{λ} are three Euler angles. The inverse relationships can be obtained from the previous ones by appealing to the properties of the Wigner rotation matrices. The body-fixed function can also be factored out into angular and radial parts as

$$\psi^{\lambda}_{J\Omega_{\lambda}}(R_{\lambda}, r_{\lambda}, \gamma_{\lambda}, \chi_{\lambda}) = \sum_{j_{\lambda} \geq |\Omega_{\lambda}|} \left(\frac{1}{R_{\lambda} r_{\lambda}} \right) Y_{j_{\lambda}\Omega'_{\lambda}}(\gamma_{\lambda}, \chi_{\lambda}) F^{\lambda}_{j_{\lambda}\Omega_{\lambda}}(R_{\lambda}, r_{\lambda}) \tag{51}$$

If the space-fixed wave functions are set into the space-fixed Hamiltonian, an inextricable CC set of equations for the space-fixed radial part is obtained

$$\left[\frac{\partial^2}{\partial R_\lambda^2} + \frac{\partial^2}{\partial \tau_\lambda^2} + \frac{2\mu E}{\hbar^2} - \frac{l_\lambda(l_\lambda+1)}{R_\lambda^2} - \frac{j_\lambda(j_\lambda+1)}{\tau_\lambda^2}\right] F^\lambda_{J j_\lambda l_\lambda}(R_\lambda, \tau_\lambda) = \frac{2\mu}{\hbar^2} \sum_{l'_\lambda j'_\lambda} \langle j_\lambda l_\lambda | V^j | j'_\lambda l'_\lambda \rangle F^\lambda_{J j'_\lambda l'_\lambda}(R_\lambda, \tau_\lambda) \tag{52}$$

where the quantum numbers l_λ and j_λ are related, within the above coordinate transformation, to the orbital and the internal angular momenta. The matrix coupling terms $\langle j_\lambda l_\lambda | V^j | j'_\lambda l'_\lambda \rangle$ involve integrals over the adiabatic potential $V(R_\lambda, \tau_\lambda, \gamma_\lambda)$ and are explicitly shown in Ref. 28. Note that the above equations are for a fixed value of J and M. By applying the scattering boundary conditions to the above radial components, the S-matrix $S^J_{v^i_\alpha j^i_\alpha \to v^f_\lambda j^f_\lambda}$ in the helicity representation can be obtained. There, the labels denote a scattering process from the initial state with a diatomic molecule in the arrangement α with vibrational and rotational quantum numbers v^i_α and j^i_α to the final state with a diatomic in the arrangement λ with vibrational and rotational quantum numbers v^f_λ and j^f_λ. There are no labels for the final scattered projectile because it is in a unbounded state with no quantum numbers.

The derivation of a set of coupled equations for a three-atom system exhibiting either electron excitation or charge transfer involves the combination of the techniques shown in the treatment of the elastic collision of the atom-atom scattering with the present adiabatic treatment of the three-atom system. The final equations are very complicated, as the reader may suspect, and will not be presented here. However, some simplified equations for charge transfer processes will be shown in the next section.

Approximate time-independent methods: The infinite order sudden approximation

The full solution of the time-independent scattering problem demands the integration of the previous set of CC equations if this approach is adopted. Although the size

of the wave expansion is limited to the energetically accessible channels, rather long expansions are needed in most of the applications. The CC approach is exact if the full wave expansion for a given problem is employed. In most of the cases, this is "exact" only within the Born-Oppenheimer approximation since only one PES is being employed. If this is still too demanding, successively shorter truncations of the basis set can be tried until some convergence is achieved. In general, the heavier the particles, the higher the energy, the more degrees of freedom, and the stronger the couplings between them, the larger the basis set must be. It has been determined [28] that the use of N basis functions would require a computing time scale of N^3. This scaling factor usually makes the CC procedure difficult to apply to realistic systems. Therefore, different approximate treatments of the CC formalism have been proposed (see Ref. 13, 33 and 28, citations therein, and additional references below). Many of these approximations consist of imposing restrictions to some degrees of freedom or, equivalently speaking, freezing them. In this way, partial or total uncoupling of the CC equations is introduced. One approximation is the l label j_z conserving centrifugal sudden (CS) approximation where the orbital angular momentum operator $\widehat{l}^2$ is replaced by an effective fixed eigenvalue $\bar{l}(\bar{l}+1)\hbar^2$ whereas the diatomic angular momentum $\widehat{j}^2$ is treated exactly. It turns out that the component of j_z becomes conserved in this approximation. A complementary approximation to the CS scheme is the l_z conserving energy sudden (ES) approximation where now the diatomic angular momentum is replaced by an effective fixed eigenvalue $\bar{j}(\bar{j}+1)\hbar^2$. A more drastic but more workable approximation is the infinite order sudden approximation (IOSA) where both the CS and the ES schemes are simultaneously applied. This approximation was originally formulated for non reactive scattering processes but was later generalized to reactive processes (RIOSA). The resulting equations are totally uncoupled as far as the angular variables are concerned (*i.e.* the sudden uncoupling is

extended to all orders up to infinite). These equations are of pseudo-collinear type which, in the non reactive case, are solved for both R and r at different fixed ("frozen") values of the orientation angle γ. In the reactive or charge transfer case, two or three angles, one for the initial arrangement and the others for the reactive rearrangements, are held fixed. The (R)IOSA equations can be easily sketched from the previous CC equations. By setting the aforementioned effective eigenvalues into the CC equations, the set becomes

$$\begin{aligned}\left[\frac{\partial^2}{\partial R_\lambda^2}+\frac{\partial^2}{\partial r_\lambda^2}+\frac{2\mu E}{\hbar^2}-\frac{\bar{l}(\bar{l}+1)}{R_\lambda^2}-\frac{\bar{j}(\bar{j}+1)}{r_\lambda^2}\right]F^{\lambda(\bar{l}\bar{j})}_{Jj'_\lambda l'_\lambda}(R_\lambda,r_\lambda)\\ =\frac{2\mu}{\hbar^2}\sum_{l'_\lambda j'_\lambda}\langle j_\lambda l_\lambda|V^J|j'_\lambda l'_\lambda\rangle F^{\lambda(\bar{l}\bar{j})}_{Jj'_\lambda l'_\lambda}(R_\lambda,r_\lambda)\end{aligned} \tag{53}$$

By performing a special transformation to the body-fixed frame

$$\begin{aligned}F^{\lambda}_{J\bar{l}_\lambda\bar{\Omega}_\lambda}(R_\lambda,r_\lambda,\gamma_\lambda)=\sum_{l'_\lambda j'_\lambda}\sqrt{\frac{2l_\lambda+1}{2J+1}}\,\langle l0j\bar{\Omega}_\lambda|J\bar{\Omega}_\lambda\rangle\\ \times Y_{j\bar{\Omega}_\lambda}(\gamma_\lambda,0)F^{\lambda(\bar{l}\bar{j})}_{Jj'_\lambda l'_\lambda}(R_\lambda,r_\lambda)\end{aligned} \tag{54}$$

the (R)IOSA equations are obtained

$$\begin{aligned}\left[\frac{\partial^2}{\partial R_\lambda^2}+\frac{\partial^2}{\partial r_\lambda^2}+\frac{2\mu E}{\hbar^2}-\frac{\bar{l}(\bar{l}+1)}{R_\lambda^2}-\frac{\bar{j}(\bar{j}+1)}{r_\lambda^2}\right]F^{\lambda}_{J\bar{l}_\lambda\bar{\Omega}_\lambda}(R_\lambda,r_\lambda,\gamma_\lambda)\\ =\frac{2\mu}{\hbar^2}[V(R_\lambda,r_\lambda,\gamma_\lambda)-E]F^{\lambda}_{J\bar{l}_\lambda\bar{\Omega}_\lambda}(R_\lambda,r_\lambda,\gamma_\lambda)\end{aligned} \tag{55}$$

where $F^{\lambda}_{J\bar{l}_\lambda\bar{\Omega}_\lambda}(R_\lambda.r_\lambda,\gamma_\lambda)$ are the (R)IOSA nuclear functions. The effective value of $\bar{l}$ can be assigned to either the initial value l_0 of the orbital angular momentum, or to its final value l' or some average between them l_{av} (the first option is the most common). The same scheme can be applied to the effective value $\bar{j}$. The use of these effective values not only uncouples the CC equations but also simplifies further manipulations of the wave function involving space-fixed to body-fixed frame transformation and the coupling of the two mentioned angular momenta. The classical analogues of the three cited approximations are discussed in Ref. 34 and 28.

The extension of the IOSA scheme to charge transfer processes has been more recently formulated by Baer and coworkers [35, 36]. This formulation involves two diabatic PESs generated from two adiabatic DIM PES's. The IOSA equations to be solved are now [35, 36]

$$\left[-\frac{\hbar^2}{2\mu}\left(\frac{\partial^2}{\partial R^2}+\frac{\partial^2}{\partial r^2}\right)+W_{11}-\frac{\hbar^2}{2\mu}\frac{\bar{l}(\bar{l}+1)}{R^2}-E\right] \times\Psi_1(R,r,\gamma)+W_{12}\Psi_2(R,r,\gamma)=0 \tag{56}$$

and

$$\left[-\frac{\hbar^2}{2\mu}\left(\frac{\partial^2}{\partial R^2}+\frac{\partial^2}{\partial r^2}\right)+W_{22}-\frac{\hbar^2}{2\mu}\frac{\bar{l}(\bar{l}+1)}{R^2}-E\right] \times\Psi_2(R,r,\gamma)+W_{12}\Psi_1(R,r,\gamma)=0 \tag{57}$$

where $\Psi_1(R,r,\gamma)$ and $\Psi_2(R,r,\gamma)$ are the IOSA nuclear functions for the transfer and the non-transfer channels (PESs), and W_{11}, W_{12} and W_{22} are the elements of the DIM diabatic energy matrix. Note that the term in $\bar{j}$ has been omitted. In the case of charge transfer processes, the IOSA equations are not totally uncoupled since the interaction between the two diabatic (or adiabatic) states must obviously be present. The (R)IOSA method has been extensively applied to study different scattering systems. Bowman and Schinke [37] have used it to study the rotationally resolved scatterings of systems like $He + Na_2$, $He + Na_2$. Jellinek and Kouri [28] have applied the RIOSA approach to the reactive scattering of $H + H_2 \rightarrow H_2 + H$, $H + D_2 \rightarrow D_2 + H$, $F + H_2 \rightarrow HF + H$ and $F + D_2 \rightarrow DF + F$ *inter alia*. Baer and collaborators [35, 36] have employed their IOSA extension to electron transfer processes to study the reactions $Ar^+ + H_2 \rightarrow Ar + H_2^+$ and $H^+ + H_2 \rightarrow H + H_2^+$. The latter study will be compared with the END theory in a later chapter.

The numerical methods to integrate the CC equations and their many approximations are discussed by Secrest [38].

Time-Dependent Scattering Theory

Although the original formulation of Quantum Mechanics in the late 1920s was time-dependent (*e.g.* the original Schrödinger equation was the time-dependent one). The systematic study of realistic scattering problems in a time-dependent fashion has really begun only in the 1970s. Since then, the interest in time-dependent treatments have steadily increased. The neglect of the time-dependent approach had different causes. One of them was the initial interest to validate the quantum mechanics theory by calculating atomic and molecular stationary properties to be compared with accurate spectroscopic measurements. Another reason, typical in quantum chemistry, was the interest in some stationary properties (such as ionization potentials, electron affinities, heats of formation, electronic densities, etc.) to understand the basic chemical features of an isolated molecule. However, the most important cause for this delay was the strenuous difficulties found in integrating the time-dependent Schrödinger equation. The problems posed by this equation are far more demanding than those posed by its time-independent relative. Furthermore, many problems encountered in time-independent calculations are still present in the temporal scheme. The possibility of undertaking time-dependent studies on realistic systems became possible only with the advent of modern computers in the 1970s. Unlike their time-independent counterparts, the quantum time-dependent methods are not so developed and established. Therefore, a definite presentation on the subject is more difficult to trace. Two concise and complete reviews on the whole area have been written by Kröger [39] and Deumens *et al.* [1]. Additional information about some specific developments can be seen in the book edited by Broeckhove and Lathouwers [40] and in the review papers of the Faraday Transactions of the Royal Chemical Society **93**.

Two main philosophies exist to solve time-dependent molecular processes. In the first one, the time dependency is reserved only to the nuclear degrees of freedom. In the second one, the time dependency is given to all the degrees of freedom, nuclear and electronic. The first approach is a time-dependent nuclear dynamics on one or more predetermined PES. In this way, the electronic degrees of freedom have been previously treated time-independently in the PES calculation. In the second approach, the PES approach is abandoned and the simultaneous time evolution of electrons and nuclei is performed. However, this simultaneous dynamics is so demanding that all the nonPES methods so far use classical, SC, or quasi-classical descriptions for the nuclear degrees of freedom. The explicit way to perform this nonquantum nuclear description will be carefully analyzed in the next section on the SC theory and in later chapters of this thesis.

The most important time-dependent methods will be presented below. They are mainly classified according to whether they employ PESs or not.

Exact time-dependent dynamics on PESs: Wake-packet propagation

In the so-called "exact" methods, the numerical integration of the nuclear time-dependent Schrödinger equation is directly performed. The methods are not actually exact since conceptual and numerical approximations are in them. However, these approximations can be easily kept below some tolerance levels at will. The wave function in these simulations is not usually prepared in a plane wave but as a wave packet. This function can either be discretized on a grid of points in both position and time or be expanded in a convenient basis set. For instance, a discretized one-dimensional wave function is expressed as [39]

$$\psi_j^n = \psi(x = j\epsilon, t = n\delta) \tag{58}$$

where ε and δ are the position and the time steps, and j and n are two integers. The position grid is of course infinite and on its boundaries imaginary absorbing potentials are placed on the boundaries to avoid the non physical reflection of the wave packet on them. The methods using only one PES are obviously more established and are presented first.

Some exact methods can be classified according to the integration algorithm to be used. In the forward Euler algorithm [39], the discretizations in position and time up to second order imply

$$H\psi_j^n = -\left(\frac{1}{\epsilon^2}\right)\left(\psi_{j+1}^n - 2\psi_j^n + \psi_{j-1}^n\right) - V_j\psi_j^n \tag{59}$$

and

$$\psi_j^{n+1} = \exp\left(-\frac{i\delta H}{\hbar}\right)\psi_j^n = \left(1 - \frac{i\delta H}{\hbar}\right)\psi_j^n + O\left(\delta^2\right) \tag{60}$$

By setting these expressions in the time-dependent Schrödinger equation, it is obtained that

$$\psi_j^{n+1} = \psi_j^n + \left(\frac{i\delta}{\epsilon^2}\right)\left(\psi_{j+1}^n - 2\psi_j^n + \psi_{j-1}^n - \varepsilon^2 V_j\psi_j^n\right) \tag{61}$$

This is an explicit (no matrix inversion) scheme with a second-order local error. The function at time step $n+1$ is calculated from the function at time step n at three different positions. The algorithm is unfortunately unstable and does not preserve unitarity. An alternative option is the Euler backward algorithm [39] where one writes

$$\psi_j^n = \exp\left(\frac{i\delta H}{\hbar}\right)\psi_j^{n+1} \tag{62}$$

This leads to a stable integration but still without unitarity conservation. A stable algorithm conserving also unitarity is the Crank-Nicholson algorithm [39] where the Caley transform of the propagator is introduced

$$\exp\left(-\frac{i\delta H}{\hbar}\right) = \left(1 - \frac{i\delta H}{2\hbar}\right)\left(1 + \frac{i\delta H}{2\hbar}\right)^{-1} + O\left(\delta^2\right) \tag{63}$$

leading to the scheme

$$\psi_{j+1}^{n+1} + \left(i\lambda - \epsilon^2 V_j - 2\right)\psi_j^{n+1} + \psi_{j-1}^{n+1} = -\psi_{j+1}^{n} + \left(i\lambda + \epsilon^2 V_j + 2\right)\psi_j^{n} - \psi_{j-1}^{n} \,, \quad (64)$$

which is implicit, *i.e.* matrix inversion is required. However, the most useful algorithm is one originally devised by Harmuth for one-dimensional problems and further extended to higher dimensions [39, 41] and renamed as second-order differencing method (SOD). It consists in a first order expansion in Δt of the time evolution in a symmetric way under $t \rightarrow -t$

$$\psi^{n+1} = -\left(\frac{i}{\hbar}\right) 2\Delta t H \psi^n + \psi^{n-1} \,. \quad (65)$$

The algorithm is stable and conserves unitarity. Because it is explicit, the algorithm is also faster than the Crank-Nichlson one. For these reasons the SOD method has been used in a large variety of problems, including eigenspectra calculations [42], nonadiabatic coupled systems [43], photodetachment spectra [44] and for systems with time-dependent Hamiltonians [45].

In other exact methods, the emphasis is given on some approximation of the time evolution operator. The most celebrated of these approaches is the split operator (SO) method originally proposed by Feit and Fleck [46]. Given two operators A and B, one always has that

$$\exp\left[\Delta t(A+B)\right] = \exp\left(\frac{\Delta t}{2}A\right)\exp\left(\Delta B\right)\exp\left(\frac{\Delta t}{2}A\right) + O\Big[(\Delta t)^3\Big] \quad (66)$$

Then, by substituting A with the free Hamiltonian $H_0 = -\left(\frac{1}{2m}\nabla^2\right)$ and B what the potential V, it is obtained that

$$\psi(t+\Delta t) = \exp\left[-\left(\frac{i}{2\hbar}\right)\Delta t H_0\right]\exp\left[-\left(\frac{i}{\hbar}\right)\Delta V\right]\exp\left[-\left(\frac{i}{2\hbar}\right)\Delta t H_0\right]\psi(t) \,. \quad (67)$$

The actual implementation of this approximate operator requires a series of discrete Fourier transforms from position to momentum space and vice versa to make the above

operators plainly multiplicative (momentum space in the case of H_0 and position space in the case of V). Fast Fourier transform codes are therefore used. The authors have applied its method to compute spectra and wave functions in classically chaotic systems [46, 47]. Other approach is the Tchebychev expansion (TE) method proposed by Tal-Ezer and Kosloff [48]. There, an expansion in complex Tchebychev polynomials [49] in the interval $[-i, i]$ of the time-evolution operator is introduced.

$$= \exp\left(-i\Delta t H_0\right) = \sum_{n=0}^{N} a_n T_n(\omega) \tag{68}$$

where $\omega = a(-i\Delta t H) + b$ with a b being a scale factor and a shift, respectively. The algorithm has been applied by its authors to scattering problems from a surface in two dimension [48], and by Zhang *et al.* to the colinear exchange reaction $H + H_2$ [50]. A method similar in spirit to the Tchebychev expansion is the short-time iterative Lanczos (SIL) method developed by Park and Light [51]. This is based on replacing the full time evolution by an approximate one in a low-dimensional subspace (Krylov space) generated by the Lanczos method (a very brief outline of the method can be seen in Ref. [39]). The method has been applied to the evolution of wake packets in the Henon-Heiles potential [51].

Extensions of these methods to dynamics on multiple surfaces are known. For instance the wave-packet propagation on two coupled surfaces by Manthe [52–54] and Köppel [55].

Approximate time-dependent dynamics on PESs: Time-dependent self consistent field (TDSCF) methods

In these methods, the exact time evolution of the system is replaced with a model evolution which is easier to perform. One of these approaches is the Time-Dependent Self Consistent Field (TDSCF) method proposed by Bisseling *et al.* [56]. The nuclei

are represented by Hartree products of wave packets on a grid. Each nucleus is then moving in the average field of the other. Later developments of this method [57] allows different exit channels and include some correlation into the nuclear motion by using a multi-reference scheme of Hartree products. These methods have been applied to some model systems as the vibrational predissociation dynamics of the colinear $I_2(v)He$ cluster [56], the photodissociation of the $XeHI$ cluster [58], and the hydrogen transfer in the $ClHCl^-$ system, all giving promising results.

A multi-configuration time-dependent Hartree method on coupled surfaces have also been implemented by Manthe and collaborators [59].

Car-Parrinello Method

The Car-Parrinello (CP) method for dynamics has received a great deal of attention during the present decade. Because of its connection to some dynamical algorithms employed in liquid simulations, and of its *a la mode* use of DFT [24], the CP method has acquired a widespread popularity. More for its connections to the END theory than for its intrinsic value, the CP method is discussed in some detail below.

The original CP method [60] was an approximate, fast, and accurate algorithm to solve some minimization problems which imply the solution of eigenvalue problems. The method might in principle be applied to different eigenvalue determinations (DFT, HF, CI) but it has been used almost exclusively in a DFT context. In the Kohn Sham (KS) version of the DFT [24], the electronic density $n(\mathbf{r})$ of a close-shell system of N electrons in the BO approximation is

$$n(\mathbf{r}) = \sum_{i}^{N} |\psi_i(\mathbf{r})|^2 \tag{69}$$

where the one-particle molecular orthonormal orbitals $\psi_i(\mathbf{r})$ are to be determined. The total energy E of the system is given by the KS functional

$$E[\{\psi_i\}.\{R_I\}.\{\alpha_v\}] = \sum_i \int_\Omega d^3r \psi_i^*(\mathbf{r}) \left[-\left(\frac{\hbar^2}{2m}\right) \nabla^2 \right] \psi_i(\mathbf{r}) + U[n(\mathbf{r}), \{R_I\}, \{\alpha_v\}.] \tag{70}$$

where $\{R_I\}$ are the position of the nuclei ("ions") and $\{\alpha_v\}$ are all the possible external constraints imposed on the system, such as the volume Ω. The functional U contains the internuclear Coulomb repulsion and the effective electronic potential energy. The latter includes the external nuclear, Hartree, and exchange-and-correlation (E_{XC}) contributions. This functional is an upper bound to the exact ground electronic energy which is supposed to be obtained by minimization. In the KS formulation, the minimization is achieved by variation of the orbitals under the orthonormality constraint. This leads to the self-consistent KS equation

$$\left\{ -\frac{\hbar^2}{2m}\nabla^2 + \frac{\delta U}{\delta n(\mathbf{r})} \right\} \psi_i(\mathbf{r}) = \epsilon_i \psi_i(\mathbf{r}) \tag{71}$$

This problem can be solved in the conventional way by matrix diagonalization. This approach of the traditional DFT problem is difficult to apply to large systems. However, Carr and Parrinello realized that the search of that minimum value can be more easily done by introducing a parameter t so that now $\psi_i = \psi_i(t)$, $R_I = R_I(t)$ and $\alpha_v = \alpha_v(t)$. This parameter acts as "fictitious time" and through it the minimization search becomes a pseudo dynamics in the configuration space of the generalized "coordinates" ψ_i, R_I and α_v. To obtain the correct dynamical equation, Carr and Parrinello employed Lagrangian mechanics and constructed a Lagrangian [61] for the aforementioned generalized coordinates

$$L = \sum_i \frac{1}{2}\mu \int_\Omega d^3\mathbf{r} \left| \dot{\psi}_i \right|^2 + \sum_I \frac{1}{2} M_I \dot{R}_I^2 + \sum_v \frac{1}{2}\mu_v \dot{\alpha}_v^2 - E[\{\psi_i\}, \{R_I\}, \{\alpha_v\}] \tag{72}$$

subject to the "holonomic constraints" [61] of orthonormality

$$\int_{\Omega} d^3\mathbf{r}\, \dot{\psi_i}^*(\mathbf{r},\mathbf{t})\dot{\psi_j}(\mathbf{r},\mathbf{t}) = \delta_{ij} \tag{73}$$

There, M_I are the real masses of the nuclei, and μ and μ_v are "fictitious" masses of arbitrary values. Obviously, these masses are introduced to obtain a complete dynamical picture of the problem. From this Lagrangian, it is possible to obtain the Euler-Lagrange equation of motion by following the usual techniques of calculus of variations [61]

$$\mu\ddot{\psi_i}(\mathbf{r},t) = -\frac{\delta E}{\delta\psi_i^*(\mathbf{r},t)} + \sum_k \Lambda_{ik}\psi_k(\mathbf{r},t) \tag{74}$$

$$M_I\ddot{R}_I = -\nabla_{R_I} E \tag{75}$$

$$\mu_v\ddot{\alpha}_v = -\frac{\partial E}{\partial\alpha_v} \tag{76}$$

where the Λ_{ij} are the Lagrangian multipliers used to satisfy the above constraints. In the terminology of molecular dynamics (MD) [62], this is a set of Lagrangian equations of the first kind where the forces imposed by the constraints appear explicitly. In this formulation, the nuclear dynamics is rather real but the electronic and the additional parameters dynamics are obviously fictitious devices. It is also possible to define a classical kinetic energy K as

$$K = \sum_i \frac{1}{2}\mu \int_{\Omega} d^3\mathbf{r}\left|\dot{\psi_i}\right|^2 + \sum_I \frac{1}{2}M_I\dot{R}_I^2 + \sum_v \frac{1}{2}\mu_v\dot{\alpha}_v^2\,, \tag{77}$$

so that the temperature of the system can be defined as

$$K \sim \frac{3}{2}RT \tag{78}$$

It is easy to see that when the system achieves its dynamical equilibrium with $\ddot{\psi_i} = 0$, $\ddot{R}_I = 0$ and $\ddot{\alpha}_v = 0$ then the first dynamical equation is identical within a unitary transformation to the previous KS eigenvalue equation. The eigenvalues of the Lagrangian

multipliers matrix (Λ_{ij}) are the KS orbital energies ϵ_i. To achieve this equilibrium condition and then to solve the KS minimization problem, Car and Parrinello proposed a "dynamical simulated annealing" by borrowing some MD techniques. The system is given at initial time a certain amount of total kinetic energy. Then the system is allowed to evolve in time to explore the generalized configuration space. The constrained dynamics is simulated using MD algorithms usual in the field of liquid simulations [63]. After some time of evolution has elapsed, the temperature of the system is lowered by reducing the kinetic energy velocities ("dynamical simulated annealing"). By successively repeating this procedure of evolution and cooling, the system is supposed to get trapped in an absolute minimum of the energy functional. In this way, the optimization of the degrees of freedom (electronic, nuclear, and of the external constraints) is achieved simultaneously ("in parallel").

The original application of the CP method [60] was to the optimization of a Si structure. Only the valence electron were explicitly treated with the effect of the core electron described by pseudo-potentials. The KS orbitals were expanded in plane waves and the local density approximation (LDA) was employed to approximate the exchange and correlation functional. The constrained dynamics was simulated by the SHAKE algorithm [62, 64] which uses the Verlet integration algorithm in its original version. Arbitrary values of $\mu = 1\ a.u.$ and $\mu_\Omega = 10^{-5}\ a.u.$ were selected. After only 200 steps of 0.1 a.u. of time each, the values of the ϵ_i converged within some tolerance. The results were in good agreement with those obtained by conventional methods. Since this initial success, the CP method has been extensively used in solid state physics for optimization purposes. A review by Payne *et al.* [65] explained in detail the use of the CP method in that field.

In spite of the original goal of the CP method, it has been very tempting for many,

including its authors, to employ it in real dynamical studies. In that case, the annealing procedure is of course omitted ("constant temperature"). In fact, the original CP paper presented a dynamical simulation of an optical phonon mode of the same Si crystal. The calculation predicted a good value for the frequency mode. However, the physical interpretation of the fictitious kinetic energy becomes even more problematic in the case of dynamical simulations. The use of the CP method for dynamical purposes has been reviewed by Remler and Madden [66] although all their examples are again for solid state physics. Different MD algorithm have been numerically tested for stability in that review. The leapfrog version of the Verlet algorithm has been found to be the most stable for the cases studied. The authors ascribes the success of the CP method to the fact that the usually small electronic kinetic energy smoothly follows the motion of the nuclei. Therefore, the electronic state immediately adjusts to the ground state of the changing nuclear configuration. The electronic state stays very close to the BO surface all the time ("adiabaticity"). The use of the Hellmann-Feymann theorem to calculate the gradients in this method is therefore justified.

Time-dependent Hartree-Fock

There is a large class of methods that are variants of TDHF for the dynamics of electrons and that employ a SC or classical description for the atomic nuclei. Examples are the work of Kulander and collaborators [67–69], Micha, Feng and Runge [70–72], of Field [21], and of Mikkelsen and Ratner [73]. All these methods consider an explicit dynamical description of the electronic state. Sometimes the full *ab initio* Hamiltonian is considered (Runge and Micha), sometimes a model Hamiltonian is set up to drive the dynamics (Field, AM1 semiempirical Hamiltonian; Mikkelsen and Ratner). The coupling between the electrons and the nuclei in these models is through the (average) potential

energy surface. The nuclei feel the surface and the electrons feel the nuclei only through their instantaneous positions in the Fock operator. As a result, electron momenta are not treated correctly, a deficiency which shows up mainly in higher, non-chemical, energy regimes. To remedy this problem, electron translation factors (ETFs) are sometimes introduced [74–77].

Apparently, the work of Kulander and coworkers [67–69] is the first TDHF method ever prescribed for a molecular processes. This method describes the electronic orbitals numerically on a grid fixed in space and propagate them together with the classical nuclear positions as a coupled system of difference equations. Their study is restricted to collinear reactions in triatomic systems like $H^+ + H_2$, for which the equation for the (doubly occupied) orbital Φ becomes

$$\begin{aligned} i\frac{\partial}{\partial t}\Phi(\vec{r},t) &= h\Phi(\vec{r},t), \\ h &= -\frac{1}{2m}\nabla^2 + V_e(\vec{r},t) + V_{ne}(\vec{r},t), \\ V_e(\vec{r},t) &= \frac{1}{2}\int \frac{\rho(\vec{r}',t)}{|\vec{r}-\vec{r}'|}\mathrm{d}r', \\ V_{ne}(\vec{r},t) &= \sum_{j=1}^{3} -\frac{1}{|\vec{r}-Z_j(t)\vec{e}_z|}. \end{aligned} \tag{79}$$

The equations used by Runge and Micha [72, 71] introduce an elegant solution to the problem of largely differing time scales in the coupled system of equations. They start from the TDHF equation for the density matrix Γ

$$i\dot{\Gamma} = F\Gamma - \Gamma F, \tag{80}$$

where F is the Fock matrix. The nuclei are treated classically and alternatively follow prescribed trajectories, straight lines or Coulomb trajectories, or they follow trajectories computed from

$$m\ddot{\vec{R}}_k = \nabla_{\vec{R}_k} E(R,\Gamma), \tag{81}$$

where the average potential $E(R,\Gamma)$ is the expectation value of the molecular Hamiltonian, including the nuclear repulsion terms and the electronic energy of the state described by the density matrix Γ. To avoid having to integrate the fast electronic motion in eq. 80, Micha and Runge linearize the equation during time steps Δt, long compared to the electronic time scale, but short for the nuclei, with the assumption that the effect of the nuclei is a small perturbation on the evolution of the density matrix. They write $\Gamma(t) = \Gamma^0(t) + \Gamma^1(t)$, where the reference density Γ^0 is propagated assuming that the Fock matrix remains the same as at time t_0

$$i\dot{\Gamma}^0 = F(t_0)\Gamma^0 - \Gamma^0 F(t_0) \tag{82}$$

with $F(t_0) = F\big(R(t_0), \Gamma^0(t_0)\big)$. The correction Γ^1 then gives the effect of the motion of the nuclei, linear in the change of the Fock matrix, on the density

$$i\dot{\Gamma}^1 = F(t_0)\Gamma^1 - \Gamma^1 F(t_0) + \Delta F\,\Gamma^0 - \Gamma^0 \Delta F \tag{83}$$

where $\Delta F = F\big(R(t), \Gamma^0(t)\big) - F(t_0)$. These equations are integrated from t_0 to $t_0 + \Delta t$ by diagonalizing $F(t_0)$ and writing Γ^0 and Γ^1 as a superposition of the eigenmodes. An efficient algorithm is used to increase or decrease Δt during the evolution as needed. Runge and Micha write their equations in the traveling atomic orbital basis which is important for the quality of their results [72, 71]. A more recent treatment [78] using Liouville operators generalizes these equations to all orders in ΔF.

Time-dependent density functional

Recently Theilhaber [79] has implemented the rigorous time evolution used in the TDHF in the field of Density Functional Theory for extended systems as an alternative to the CP method. In this method, the electronic system is described by using KS orbitals

and to obtain the dynamical equations

$$
\begin{aligned}
i\frac{\partial}{\partial t}\psi_j(\vec{r},t) &= -\frac{1}{2m_e}\nabla^2\psi_j(\vec{r},t) + v_{\rm eff}(\vec{r},t,[n])\psi_j(\vec{r},t), \\
M\frac{\mathrm{d}^2}{\mathrm{d}t}\vec{R}_k(t) &= \vec{F}_k(t),
\end{aligned}
\tag{84}
$$

where $\vec{F}_k(t)$ is the total force on the k-ion and where, with double occupancy, the density is given again by

$$
n(\vec{r},t) = 2\sum_{j=1}^{N_e/2}|\psi(\vec{r},t)|^2. \tag{85}
$$

More details can be found in Theilhaber's paper [79]. The author points out that the TDDF approach has a physical kinetic energy as opposed to the fictitious kinetic energy of the CP method [60]. Furthermore, because of the rigorous relation to the Schrödinger equation for the full system, the TDDF equations conserve total momentum and total energy.

Time-dependent close coupling methods.

The time-dependent close-coupling (TDCC) method has nothing to do with a previously reviewed time-independent method. Reviews of the semiclassical and quantum version of the TDCC approach have been prepared by Delos [75], Kimura and Lane [80] and Fritsch and Lin [76]. It is a method to describe charge transfer processes in slow [75] and, recently, also fast [77] atomic collisions. One considers a target system originally at rest at the origin and a projectile atom approaching the target with given impact parameters and velocity. The method concentrates on describing one active electron, the others being frozen in core orbitals or treated by pseudo potentials. Some systems with two active electrons have been studied [76]. The semiclassical form of the method is briefly discussed below. Delos [75] gives a detailed discussion of the fully quantum mechanical form of the CC method.

The method has three ingredients: (i) a choice of nuclear trajectory, usually a prescribed trajectory, often a straight line or Coulomb trajectory, (ii) a choice of basis set for the electronic wave function, and (iii) the solution of coupled differential equations in time for the coefficients of the electronic wave function. The choice of basis set in the CC method has a rich history reviewed in detail by Fritsch and Lin [76]. The present consensus is to use molecular orbitals ψ_i depending on all nuclear coordinates *R* with electron translation factors (ETFs) of the form [80]

$$F_i(R,\vec{r}) = \exp\left[i\left(m\vec{v}\cdot\vec{r}f_i(R,\vec{r}) - mv^2t/2\right)/\hbar\right] \tag{86}$$

with a switching function *f*, which has the asymptotic values ±1 for the limit where the two atoms are far apart. The space independent kinetic energy term can be left off and incorporated in the wave function expansion coefficients.

The total molecular wave function is then written as

$$\Psi(R,\vec{r}) = \sum_i \chi_i(R)\psi_i(R,\vec{r})F_i(R,\vec{r}). \tag{87}$$

In the semiclassical approximation this becomes

$$\Psi(R,\vec{r}) = \sum_i a_i(t)\psi_i[R(t),\vec{r}]F_i[R(t),\vec{r}]\exp(f) \tag{88}$$

where

$$f = -i\int^t E_i\left[R(t')\right]\mathrm{d}t' - \frac{1}{2}\int^t v^2\mathrm{d}t'. \tag{89}$$

Substituting (88) in the time-dependent Schrödinger equation, projecting on the electronic basis, and expanding to first order in $\vec{v}$ give the coupled equations

$$i\mathbf{S}\frac{\mathrm{d}\mathbf{a}}{\mathrm{d}t} = \left[\mathbf{h} + \vec{v}\cdot\left(\vec{\mathbf{P}} + \vec{\mathbf{A}}\right)\right]\mathbf{a} \tag{90}$$

with

$$
\begin{aligned}
S_{ji} &= \langle \psi_j F_j | \psi_i F_i \rangle \\
\vec{P}_{ji} &= \langle \psi_j | -i \sum_k \nabla_{\vec{R}_k} | \psi_i \rangle \\
\vec{A}_{ji} &= \langle \psi_j F_j | [h_{\rm el}, \vec{r} f_i(R, \vec{r})] | \psi_i F_i \rangle \\
h_{ji} &= \langle \psi_j | h_{\rm el} | \psi_i \rangle .
\end{aligned}
\tag{91}
$$

The total Hamiltonian is defined as $H(R, \vec{r}) = T + h_{\rm el}$ with T the appropriate nuclear kinetic energy operator. **P** are the nonadiabatic coupling terms.

Note that the ETFs are used to derive the terms **A**, but are neglected in the evaluation of **P** and **h**. This is because the term **A** is essential to obtain the correct asymptotic behavior of the equations, whereas the low velocity makes the ETF almost equal to unity in the volume over which the matrix elements **P** and **h** are evaluated. It is then a good approximation to omit the ETF in that integration. See Riera [77] and Fritsch and Lin [76] for a detailed discussion.

The Perturbed Stationary State (PSS) method [26] was the first formulation (without ETFs) of the close-coupled equations for electronic dynamics in atomic collisions. Modern applications of the PSS method do include proper treatment of the velocity [77]. The original PSS equations only have the non adiabatic coupling term **P** of eq. (91) and rely on the completeness of the basis to accurately represent the other terms. The correct inclusion of ETFs [75] essentially brings out all terms linear in the nuclear velocities and is therefore less sensitive to the basis used.

Semiclassical Scattering Theory

The Semiclassical Theory in General

The SC theory or, if the reader prefers, approximation is as old as the quantum theory itself. Its primordial formulation, in the rig of the Jeffrey, Wentzel, Kramers and Brillouin (JWKB) approximation, dates back to 1925. Since this early origin, the SC theory has

been continuously evolving in form and expanding in scope, adopting more complex and accurate versions. Today, this theory has grown to a vast body of knowledge, covering the same kinds of systems and application as its quantum counterpart.

From the very beginning, the SC theory was supposed to undertake these two related tasks:

1. To show how quantum mechanics in principle goes to classical mechanics in cases where the energy and/or the masses of the system are high with respect to some value.
2. To generate an approximate procedure, easier to implement than the exact quantum one, to describe a system in the aforesaid regimen.

The kind of solutions given by the SC theory to these questions are not so "ideal" as they may have been expected. In first place, and as it was previously mentioned, quantum mechanics does not totally go to classical mechanics in the above limit. Vestiges of the exact quantum theory still remain there even though they may not be experimentally observable in some situations. In second place, the SC theory does provide high energy/high mass procedures which in many respects are less cumbersome than the original quantum ones. However, when these SC procedures are pushed beyond some level of detail they can become as difficult as or even more difficult than the original quantum solution. In that way, the original benefit of the SC approach is definitively lost and it may be advisable to go back to a quantum formulation of the problem at hand. Examples of the relationship between quantum and classical mechanics through the SC limit, and the difficulties of the SC techniques will be shown not only in this sections but throughout this thesis work.

The mentioned limit of high energies and/or masses is the seed of the SC formalism from the exact quantum mechanical expressions. To simplify and unify further manipu-

lations, this physical limit is always replaced by the totally formal but equivalent limit of

$$\hbar \to 0 \tag{92}$$

This physical limit, $\hbar$ is obviously a constant, is the hallmark of the SC theory although its use is not restricted to its realms only. As will be shortly seen in detail, it happens that in some quantum expressions there appear functions $F(E)$ of the energy E in fractions such as $\frac{F(E)}{\hbar}$. These functions take a very high value with respect to $\hbar$ when $E \to \infty$. Therefore, it is formally equivalent to keep the value of E fixed and applied the purely formal limit of $\hbar \to 0$ in the SC manipulations. The same is true with respect to a high mass limit since it implies a high value of E. Therefore, the SC theory can be very broadly defined as the asymptotic limit of the exact quantum mechanics in the limit of $\hbar \to 0$ when some appropriate mathematical techniques are used to take care of it. These techniques involve the expansion or the above functions $F(E)$ in powers of $\hbar$ and the evaluation of some integrals by the stationary phase approximation [81]. The present definition will become more precise with the definite examples reviewed below.

It is important to discern form the very beginning to what degrees of freedom the SC Theory can be meaningfully applied. Because of its high mass regime, the SC theory is scarcely useful for describing the electronic motion. Perhaps, it might be applied to highly excited electronic states near the continuum. But any attempt to describe the electronic motion of the ground state and of most of excited states in a molecule is bound to be inaccurate. The only exception to this behavior is the simple case of the hydrogen atom, where the SC theory predicts the same energy eigenvalues as the quantum theory does. In this respect, the reader may remember the failure of the Bohr's atomic model, a forerunner of the modern SC theory, when applied to many-electron systems. Therefore, the use of the SC theory in molecular and scattering problems is restricted to the nuclear degrees of

freedom. The SC theory is not independent of the exact quantum theory since a quantum description of the electronic motion is always necessary. In the traditional SC models, that electronic description comes in the form of a few predetermined PES. Thus, the most established SC methods show the same type of dependence to the PES calculation as many quantum methods do. However, the SC theory applied to the nuclear motion has shown a great deal of success because its results are very close to the quantum ones.

A review of the overwhelmingly vast SC theory follows. This presentation is specially focused on scattering problems and on those aspects of the SC which have some relevance to the END theory. A relatively recent review of the whole area is the book by Child [82]. However, this review will not be primarily employed during the next exposition.

The Jeffreys-Wentzel-Kramers-Brioullin (JWKB) Approximation.

This was one of the earliest manifestations of the SC theory. It can be applied to one-dimensional problems or to N dimensional problems separable in N one dimensional problems. It is a time-independent version of the SC theory which can be applied to both bound and unbound states. Given the unidimensional time-independent Schrödinger equation

$$\left[-\frac{\hbar^2}{2m}\frac{d^2}{dx^2}+V(x)\right]\psi(x)=E\psi(x) \tag{93}$$

it can be conveniently recast in the following way

$$\left[\hbar^2\frac{d^2}{dx^2}+p^2(x)\right]\psi(x)=0 \tag{94}$$

where the momentum function $p(x)$ is

$$p(x)=\{2m[E-V(x)]\}^{\frac{1}{2}} \tag{95}$$

If the potential is zero, an exact and independent solution of this equation is a plane wave

$$\psi(x)=\exp\left(\pm\frac{iS}{\hbar}\right):\ V(x)=0 \tag{96}$$

with momentum eigenvalue $S = p = (2mE)^{\frac{1}{2}}$. However, if the potential is non zero in at least some regions then it is possible to rewrite an exact and independent solution $\psi(x)$ as

$$\psi(x) = A(x) \exp\left[\pm \frac{iS(x)}{\hbar}\right] \tag{97}$$

where the complex functions $A(x)$ and $S(x)$ are to be determined. The former relates to the boundary conditions of the problem and the latter measures the departure of this system from the free motion. So far, this is only a reformulation of the original quantum problem. In the JWKB approximation, a expansion in powers of $\hbar$ is postulated to $S(x)$

$$S(x) = S_0(x) + S_1(x)\hbar + S_2\hbar^2 + \ ... \tag{98}$$

where the coefficients $S_i(x)$ are to be determined. If the SC limit of $\hbar \to 0$ is applied then the high order terms can be discarded. By setting the wave function with this expansion into the recast equation, it is easy to prove that first two terms are [13, 82]

$$S_0(x) = \int_{x_0}^{x} dx' \ p\Big(x'\Big) \tag{99}$$

and

$$S_1(x) = \frac{i}{2} \ln\left[p(x)\right] \tag{100}$$

where x_0 is an arbitrary point. The first term is a restricted action according to the terminology given by Goldstein [61]. It can be proven that the shortest expansion giving a meaningful wave function which satisfies flux conservation is that retaining the two first terms [13, 82]. This is exactly the case of the JWKB approximation. The function $S(x)$ also satisfies the classical Hamilton-Jacobi equation of motion [61]

$$\frac{1}{2m}\left[\frac{dS(x)}{dx}\right]^2 + V(x) = 0\text{: } \hbar \to 0 \tag{101}$$

making in this way the connection with classical mechanics[2]. The JWKB approximation is valid whenever the condition [13, 61, 82]

$$\left|\frac{d\lambda(x)}{dx}\right|^{\frac{1}{2}} \gg 1 \tag{102}$$

where the generalized wave length function is $\lambda(x) = \frac{\hbar}{p(x)}$. Obviously this approximation breaks down at and near the turning points of analogous classical problem. The incorporation of higher terms in the SC expansion has been investigated in detail by Fröman and Fröman [83]. However, this improvement of JWKB theory is extremely cumbersome and of few practical consequences in the scattering theory.

In the case of a simple potential with only two turning points a and b ($a \leq b$), the x axis can be divided into a classically allowed (CA) region or interval $[a, b]$, where $E \geq V(x)$: $x \in [a, b]$, and into two classically forbidden (CF) regions or intervals $(-\infty, a)$ and (b, ∞) where $E < V(x)$: $x \in (-\infty, a) \cap (b, \infty)$. In those regions, the general JWKB wave functions in term of two JWKB independent solutions of the above equation are

$$\begin{aligned}\psi_{CA}(x) = \left[\frac{1}{p(x)}\right]^{\frac{1}{2}} \{ & A' \exp\left[\frac{i}{\hbar}\int_{x_0}^{x} dx'\, p\,(x')\right] \\ & + B' \exp\left[-\frac{i}{\hbar}\int_{x_0}^{x} dx'\, p\,(x')\right]\}\end{aligned} \tag{103}$$

and

$$\begin{aligned}\psi_{CF}(x) = \left[\frac{1}{|p(x)|}\right]^{\frac{1}{2}} \{ & X \exp\left[\frac{1}{\hbar}\int_{x_0}^{x} dx'\, |p\,(x')|\right] \\ & + Y \exp\left[-\frac{1}{\hbar}\int_{x_0}^{x} dx'\, |p\,(x')|\right]\}\end{aligned} \tag{104}$$

2. The JWKB function $S(x)$ turns out to be the Hamilton-Jacobi characteristic function which is denoted as $W(q, P)$ in Ref. 61.

Note that the term $S_1(x)$ has been taken out of the exponent giving rise to the pre-exponential denominators having $p(x)$, which blow up at and near the turning points. The linear combination coefficients A', B', X and Y are to be determined. As is usual in quantum mechanical problems, these coefficients can be determined by appealing to the continuity of the wave function through the points connecting the three regions. However, these connecting points are here the turning points where the approximate wave functions are not longer valid. This special complication is the SC connection problem [13, 82], a far from trivial problem. The simplest (approximate) solution to this problem is to find the exact quantum expression for the wave function near the turning points by making a linear expansion of the potential from them, $V(x) \approx V(a) + \left[\frac{dV(x)}{dx}\right]_{x=a}(x-a)$ and $V(x) \approx V(b) + \left[\frac{dV(x)}{dx}\right]_{x=b}(x-b)$. The connection is made through these functions near the critical points. The most basic level of this approach, the previous CA solutions far from the turning points become

$$\psi_{CA}(x) \overset{x \gg a}{\approx} A\left[\frac{1}{p(x)}\right]^{\frac{1}{2}} \sin\left\{\frac{i}{\hbar}\left[\int_a^x dx'\, p\left(x'\right) + \frac{\pi}{4}\right]\right\} \tag{105}$$

$$\psi_{CA}(x) \overset{x \ll b}{\approx} B\left[\frac{1}{p(x)}\right]^{\frac{1}{2}} \sin\left[\frac{1}{\hbar}\int_x^b dx'\, p\left(x'\right) + \frac{\pi}{4}\right] \tag{106}$$

Note that the connection procedure has added a $\frac{\pi}{4}$ term to the CA function phase. The necessary condition that the CA function $\psi_{CA}(x)$ must be single-valued in its own interval imposes a severe constraint on the phases which implies that

$$\oint dx\, p(x) = \left(n + \frac{1}{2}\right)h;\ n = 0,\ 1,\ 2... \tag{107}$$

when the integral is evaluated over one complete period of oscillation between the two turning points. This expression indirectly imposes an energy quantization condition through the relationship between $p(x)$ and the total energy E. To obtain the expression of the quantized energy it is necessary to evaluate the previous integral for the specific

potential $V(x)$ at hand. Examples of quantized energy for different potentials can be found in Ref. 82. The agreement between the JWKB energies and the exact quantum values are remarkably good, including for the lowest levels. Surprisingly enough, the JWKB quantized energies for the harmonic and the Morse potentials are exact. The explicit solution of the quantum "patches" near the turning points and then the further determination of the coefficients A and B, and the coefficients in the CF wave function are rather cumbersome [82]. The same procedure can be applied to inverted potentials or barriers. In that situation, the interest is to obtain the transition coefficients of the tunneling process through the barrier. Typical examples are the JWKB transmission coefficient for the inverted harmonic, and the Eckart potentials [82]. The JWKB procedure can also be applied to scattering problems. The simplest case is the scattering from a totally repulsive potential which determines one turning point. In that case, the interest is not to quantize the total energy, which is a continuum for an unbound state, but to find a SC expression to the scattering phase shifts $\delta(l)$ introduced in a previous section. A more complicated case is the scattering from a potential with both a short-range repulsive and a long-range attractive parts. In that situation, the effective potential including the centrifugal term exhibits a finite well which determines three turning points for the low energy processes. The JWKB approximation has been successfully applied in that situation to find the eigenfunctions of the quasi-bound states in the well and expressions for corresponding resonance peaks and life times in scattering measurements [13].

The application of the JWKB procedure to cases of potentials with multiples minima and barriers is very cumbersome because of the increasing complication of the connection problem. A review of the methods to solve this problem can be seen in Ref. 13, appendix C; Ref. 82, chapter 3, and in the extensive bibliography cited in both. The application of these techniques to realistic systems seems to be impractical. A detailed relationship

between the JKWB approximation and the Hamilton-Jacobi theory in classical mechanics can be found in Ref. 61, chapter 10.

The Bohr-Sommerfeld Quantization Rule

Maslov [84] derived a general procedure to obtain the JWKB quantization rules, avoiding the explicit treatment of the connection problem. Using some topological properties of the phase space, this author determined that the action of the above SC wave function must necessarily satisfy the condition

$$\oint dx\, p(x) = (n + \delta_v)h \tag{108}$$

regardless of the nature of the potential being considered. In that expression, δ_v is the so-called Maslov index. From pure topological considerations, Maslov found that this index has a value of $\frac{1}{2}$ if the motion is of a libration type [61] (vibrational and orbital motion), or a value of 0 if the motion is of rotation type [61] (plane rotational motion). The index can be set in the more revealing form of

$$\delta_v = \frac{m}{4} \tag{109}$$

where m is the number of turning points in the potential generating the motion: two in a libration and zero in a rotation.[3]

This reshaped quantization rule can be directly applied to the one-dimensional systems examined in the JWKB approximation. However, the full power of Maslov's approach comes when it is applied to the bound motion of multidimensional separable systems. This application is strongly associated with the classical mechanics formalism of action-angle variables [61]. Given a classical Hamiltonian

$$H(p,q) = \frac{1}{2m}p^2 + V(q) = E \tag{110}$$

3. These statements are somewhat simplified. See Ref. 84 for a more rigorous presentation.

with N pairs of conjugated momenta p and positions q, the classical mechanics solution of the system dynamics implies the integration of $2N$ Hamilton equations [61]

$$\dot{p} = -\frac{\partial H(p,q)}{\partial q} \tag{111}$$

and

$$\dot{q} = \frac{\partial H(p,q)}{\partial p} \tag{112}$$

The solution of these equations is a challenge problem for some systems. In the action-angle formalism, there exists in principle a canonical transformation [61] to a new set of conjugated momenta and positions I ("actions") and α ('angles") so that the new Hamiltonian $\widetilde{H}$ has no explicit dependence on the generalized positions α

$$\widetilde{H}(I) = H(p,q) = E \tag{113}$$

Therefore, the transformed Hamilton equations are simply

$$\dot{I} = -\frac{\partial H(I)}{\partial \alpha} = 0 \tag{114}$$

and

$$\dot{\alpha} = \frac{\partial H(I)}{\partial I} = \omega(I) = Constant \tag{115}$$

Now, the I are constants of the motion and the α have simple linear solutions of the type $\alpha(t) = \omega(I)(t - t_0) + \alpha(t_0)$. Although the new solutions are disarmingly trivial, the procedure to obtain the adequate conjugate variables through the generating functions method [61] can be very convoluted. In the case of bound systems with periodic degrees of freedom, the constants $\omega(I)$ turn out to be the frequencies associated with the periodic motions, *i. e.* either librations or rotations. Also, each of the generalized momenta turns out to be an action in the restricted sense[4],

$$I = \frac{1}{2\pi} \oint dx\, p(x)\ , \tag{116}$$

4. Unlike other actions shown in a previous section this has a factor of $\frac{1}{2\pi}$. Different authors use slightly different definitions of this action.

where the integration is over one period of motion. Therefore, the conjugated positions α can be interpreted as angles describing the periodic motions. In that transformed Hamiltonian, the previous quantization rule can be imposed to each action I as $I = (n + \delta_v)\hbar$. This is the Bohr-Sommerfeld (BS) quantization rule in terms of the Maslov index theory. This rule has its remote origin in the so-called old quantum mechanics developed in the late 1920's. Since the energy E depends on the actions I, as shown above, this condition indirectly impose a quantization on it as well. In the case of a unidimensional harmonic oscillator, it is well-known that the action-angle Hamiltonian is simply [61]

$$H(I) = \omega I \tag{117}$$

which by applying the BS rules gives the exact quantum energy

$$E = \left(n + \frac{1}{2}\right)\hbar\omega;\ n = 0,\ 1,\ 2\ ... \tag{118}$$

Examples of the BS rule applied to the unidimensional Morse oscillator, the bidimensional harmonic oscillator, the (tridimensional) angular momentum problem and the hydrogen atom can be found in the literature [61, 82]. Remarkably, the BS quantization rule applied to the hydrogen atom renders the exact quantum results for the total energy, the total momentum and the azimuthal rotation. The action-angle treatment can in principle be applied to a diatomic molecule [85]. However, the resulting expressions are very cumbersome and some approximations must be introduced to make them of practical use[86]. The triatomic molecule is no longer a separable system. The BS rule can be used there if the problem is assumed to be approximately separable.

The Einstein-Broullin-Keller (EBK) Quantization Rule

The BS quantization rule can be generalized to the case of non separable dynamics in the case of regular, non chaotic motion. For a bound motion with N degrees of

freedom, it is necessary to find in phase space N topologically distinct closed contours C satisfying the condition

$$\frac{1}{2\pi}\oint_C \mathbf{dx}\cdot\mathbf{p} = (n_k + \delta_k)\hbar \tag{119}$$

where the conjugated momenta and positions are now seen as an$N$ dimensional vector. This is the Einstein-Brioullin-Keller (EBK) quantization rule. The determination of such contours can be done by direct inspection of the system evolution in terms of invariant tori, Poincaré surface sections, and Lissajous figures. The first application of this direct approach was done by Noid and Marcus for the Hennon-Heiles model potential [87]. An indirect and more workable procedure for the EBK rule was proposed by Percival and Pomphrey and was further implemented by Eaker and Schatz [88], *inter alia*. The method exploits the properties of a quasi-periodical motion using discrete Fourier transforms. The algorithm has been used by Schatz [10] to quantize the initial states of triatomic molecule involved in scattering processes. Detailed examples of that quantization in triatomic systems can be seen also in Ref. 82. There is no known quantization rule for the irregular, chaotic motion [84, 82].

Miller-Marcus Semiclassical S-matrix

The previously presented SC efforts (JWKB, BS, or EBK) have been primarily focused on the quantization of bound motions. In scattering problems, these techniques find an application in the quantization of the initial reactant state before the collision and in the determination of the final product states. In this application, the interest is in the quantization of the energy and other variables and not in the determination of the SC wave function. This function is never explicitly constructed. However, it is necessary to supply this SC initial and final state description with a SC propagation scheme to effect the transition from initial to final time. This SC propagation scheme has been independently

developed by Miller [85] and Marcus [89] since the 1970s. The former author has used an explicit time-dependent approach to the problem in terms of the Feyman path integral formulation of quantum mechanics [90]. The latter author has instead formulated a more direct extension of the JWKB and BS approaches to the scattering problem. The efforts by these two scientists and collaborators is usually termed the Miller-Marcus S-matrix theory. A review of the Marcus' version of this theory will not be presented here but it can be found in Ref. 13 and 82. Miller's version will be presented in some detail because of its occasional contacts with the END Theory.

In the Miller's version of the SC S-matrix[85, 86, 91], the SC limit of the quantum propagator in "position-position" representation $< q_2| \exp\left[\frac{-iH(t_2-t_1)}{\hbar}\right]|q_1\rangle$ is used as an starting point of the whole theory[90]

$$\lim_{\hbar\to 0} < q_2| \exp\left[\frac{-iH(t_2-t_1)}{\hbar}\right]|q_1\rangle \sim \exp\left[\frac{i\phi(q_2,q_1)}{\hbar}\right] \tag{120}$$

where the initial and final Cartesian coordinates $q_2 = q_2(t_2)$ and $q_1 = q_1(t_1)$ are taken at the final and initial times t_2 and t_1. The function $\phi(q_2, q_1)$ is the classical action along the classical path between the said initial and final points

$$\phi(q_2,q_1) = \int_{t_1}^{t_2} dt\ L[q(t),\dot{q}(t)] \tag{121}$$

Here $L[q(t), \dot{q}(t)]$ is the classical Lagrangian of the system. The previous SC limit of the propagator in "position-position" representation is then generalized to the "momentum-momentum", "position-momentum" and "momentum-position" representations by using the Dirac unitary transformation between sets of conjugate positions and momenta. The transformation relationships may be expressed in terms of action-angle variables. A definite relationship between the four representations and the different types of generating functions for canonical transformations [61] is be obtained. The dynamical picture is

introduced by realizing that an evolution in time can be seen as an active canonical transformation [61]. Thus, a general SC propagator in any of the mentioned representations can be formulated.

An illuminating example of this theory can be given by analyzing an atom-diatom scattering process. The classical Hamiltonian describing that system dynamics is

$$H(\mathbf{P},\mathbf{R}) = \frac{1}{2M_2}\mathbf{P_1}^2 + \frac{1}{2M_2}\mathbf{P_2}^2 + \frac{1}{2M_3}\mathbf{P_3}^2 + V(\mathbf{R_1},\mathbf{R_2},\mathbf{R_3}) \tag{122}$$

where $\mathbf{P}$ and $\mathbf{R}$ are the Cartesian conjugate momenta and positions. The problem has in principle nine degrees of freedom and implies the solution of a system of eighteen first-order differential Hamilton equations of the type

$$\dot{P}_i = -\left(\frac{\partial H}{\partial R_i}\right);\ i = 1,\ 2,\ \ldots,\ 9 \tag{123}$$

$$\dot{R}_i = \left(\frac{\partial H}{\partial P_i}\right);\ i = 1,\ 2,\ \ldots,\ 9 \tag{124}$$

However, these degrees of freedom can be reduced by physical considerations. First of all, in the molecular problem being discussed, the PES is always a function of the relative internal coordinates alone

$$V(\mathbf{R_1},\mathbf{R_2},\mathbf{R_3}) = V(\mathbf{R_1}-\mathbf{R_2},\mathbf{R_1}-\mathbf{R_3},\mathbf{R_2}-\mathbf{R_3}) \tag{125}$$

i.e. this function only involves six degrees of freedom. A complete reduction to a Hamiltonian with six degrees of freedom can actually be achieved if the Jacobi coordinates $\mathbf{R}$ and $\mathbf{r}$ are introduced again as in the previous example of the IOSA. This change of coordinates constitutes a point contact canonical transformation [61]. The Hamiltonian then becomes

$$H(\mathbf{P_R},\mathbf{R},\mathbf{p_r},\mathbf{r}) = \frac{1}{2\mu_R}\mathbf{P_R}^2 + \frac{1}{2\mu_r}\mathbf{p_r}^2 + V(R,r,\chi) \tag{126}$$

where $\mathbf{P_R}$ and $\mathbf{p_r}$ are the momenta conjugated to $\mathbf{R}$ and $\mathbf{r}$, respectively. As already defined in the IOSA example, χ is the orientation angle, and μ_R and μ_r the reduced masses. The omitted three degrees of freedom are those of the CM motion, which implies a trivial dynamics. A further reduction to a Hamiltonian with four degrees of freedom can be achieved if some canonical transformation to action-angle variables is introduced. One possibility is to employ the actions $I_l = |\mathbf{l}|$ and $I_j = |\mathbf{j}|$ which correspond to the projectile orbital angular momentum $\mathbf{l}$ and the molecule internal angular momentum $\mathbf{j}$, respectively. Their conjugated angles are $0 \leq \phi_l \leq 2\pi$ and $0 \leq \phi_j \leq 2\pi$. The total Hamiltonian can now be written [85]

$$H(P_R, p_r, I_l, I_j, R, r, \phi_j, \phi_m) = \frac{1}{2\mu_R}\left(P_R^2 + \frac{I_l^2}{R^2}\right) + \frac{1}{2\mu_r}\left(p_r^2 + \frac{I_j^2}{r^2}\right) + V(R, r, \chi) \tag{127}$$

Another possibility is to use the same previous action-angle variables plus the vibrational action n for the diatomic vibrational motion with conjugate angle $0 \leq \phi_n \leq 2\pi$. The Hamiltonian then becomes [85]

$$\begin{aligned} H(P_R, n, I_l, I_j, R, \phi_n, \phi_j, \phi_m) = {} & \frac{1}{2\mu_R}P_R^2 + \varepsilon(n, I_j) \\ & + \frac{1}{2\mu_R}[J^2 + j^2 - 2I_m^2 + \\ & + 2\left(J^2 - I_m^2\right)^{\frac{1}{2}}\left(j^2 - I_m^2\right)^{\frac{1}{2}}\cos\phi_m] + V(R, r, \chi) \end{aligned} \tag{128}$$

where $\varepsilon(n, I_j)$ is the vibration-rotation eigenvalue function of the diatomic[85, 86], and $\mathbf{J} = \mathbf{l} + \mathbf{j}$ is the total (constant) angular momentum. The angle χ can now be rewritten as [85]

$$\cos\chi = \left(1 - \frac{I_m^2}{I_{j^2}}\right)^{\frac{1}{2}}\cos\phi_j \tag{129}$$

The latter Hamiltonian is the most useful to calculate DCS. This Hamiltonian is closely related to the previously presented IOSA and allows a direct SC interpretation of that method. Furthermore, this Hamiltonian also allows an easy comparison of the SC S-matrix theory with the END scattering theory in the next chapters. In the Hamiltonian in

eq. 128, the initial internal conditions of the target are determined by the values assigned to ϕ_n^0,ϕ_j^0, ϕ_m^0, n^0,I_j^0 and I_m^0. The last three variables fully determine the orientation of the molecule because if a coordinate system is attached to it with the ***y*** axis along its bond and the ***z*** axis along the **j** vector then the molecule Euler angles $[\alpha,\ \beta,\ \gamma]$ [25] turn out to be $\alpha = \phi_m - \frac{\pi}{2}$, $\beta = \cos^{-1}\left(\frac{I_m}{I_j}\right)$, and $\gamma = \phi_j$. If the Miller's SC propagator is applied to this system then the SC S-matrix turns out to be [85]

$$S_{n^i,I_j^i,I_m^i \to n^f,I_j^f,I_m^f}(J) = \left[\frac{1}{(2\pi i\hbar)^3 D}\right]^{\frac{1}{2}} \exp\left[i\frac{\gamma^{cl}_{n^f,I_j^f,I_m^f,n^i,I_j^i,I_m^i}(J)}{\hbar}\right] \tag{130}$$

where D is the so-called "Van Vleck determinant" [92][5]

$$D = \left|\begin{pmatrix} \left(\frac{\partial I_n^f}{\partial \phi_n^i}\right)_{I_n^f,I_j^f,I_m^f} & \left(\frac{\partial I_n^f}{\partial \phi_j^i}\right)_{I_n^f,I_j^f,I_m^f} & \left(\frac{\partial I_n^f}{\partial \phi_m^i}\right)_{I_n^f,I_j^f,I_m^f} \\ \left(\frac{\partial I_j^f}{\partial \phi_n^i}\right)_{I_n^f,I_j^f,I_m^f} & \left(\frac{\partial I_j^f}{\partial \phi_j^i}\right)_{I_n^f,I_j^f,I_m^f} & \left(\frac{\partial I_j^f}{\partial \phi_m^i}\right)_{I_n^f,I_j^f,I_m^f} \\ \left(\frac{\partial I_m^f}{\partial \phi_n^i}\right)_{I_n^f,I_j^f,I_m^f} & \left(\frac{\partial I_m^f}{\partial \phi_j^i}\right)_{I_n^f,I_j^f,I_m^f} & \left(\frac{\partial I_m^f}{\partial \phi_m^i}\right)_{I_n^f,I_j^f,I_m^f} \end{pmatrix}\right| \tag{131}$$

and the classical action in terms of the action-angle variables is

$$\gamma^{cl}(J) = -\int_{t_1}^{t_2} dt\Big[R\dot{P} + \phi_n \dot{I}_n + \phi_j \dot{I}_j + q_m \dot{I}_m\Big]. \tag{132}$$

It will be seen in chapter 5 that the "Van Vleck determinant" is a purely classical entity. However, the exponential factor is a remanent of the original quantum theory although it contains the classical action. All the dynamical information of the scattering system can be further calculated from this SC version of the S-matrix. Notice that the SC wave function is never explicitly constructed at any time of the evolution. The implementation of this approach involves the integration of the above set of Hamilton equations starting at the proper initial conditions. The target molecule is initially set with its actions quantized according to the BS rule to reproduce the initial quantum state. The conjugate angles are

5. *In sensu stricto*, this is not the Van Vleck determinant because it contains derivatives of variables at final time w. r. t. variables at initial time. The name may have been proposed because of the superficial similarity between the two determinants.

given any value within their full ranges of $0 \leq \phi_n \leq 2\pi$, $0 \leq \phi_l \leq 2\pi$, and $0 \leq \phi_m \leq 2\pi$ The tree quantized actions determine a set of three integer quantum numbers at the initial time

$$I_n^i = n_n^i \hbar;\ n_n^i = 0,\ 1,\ 2,\ \ldots\ , \tag{133}$$

$$I_j^i = n_j \hbar;\ n_j^i = 0,\ 1,\ 2,\ \ldots\ , \tag{134}$$

and

$$I_m^i = n_m^i \hbar;\ n_m^i = -n_j^i,\ -n_j^i + 1,\ \ldots\ , n_j^i - 1,\ n_j^i\ . \tag{135}$$

The initial relative motion of the projectile is set by assigning to both R^0, and P^0 values corresponding to the experimental condition being simulated. By continuously varying the angles, different trajectories are generated. At final time, the target actions are examined to know whether they still have an integer value or not

$$I_n^f,\ I_j^f,\ I_m^f = Integer\ ? \tag{136}$$

Trajectories leading to final integer-valued actions are retained as the classical trajectories genuinely contributing to the true quantum evolution. Otherwise, the trajectories are totally discarded. This test for final integer-valued actions is called the root-searching (RS) problem, a very cumbersome procedure to undertake. An incredible waste of resources is thus employed to solely find the semiclassically correct trajectories. Another complication of the theory is the possibility of a singular value in the Van Vleck determinant. The extension of this scheme to rearrangement processes is relatively easy [85].

The previous SC S-matrix theory has been successfully applied to the collinear scattering of an atom by a non-rotating harmonic oscillator, the bidimensional scattering of an atom by a rigid rotor, the SC calculation of Clebsch-Gordan coefficients, different aspects of the $H + H_2$ reaction (all of them reviewed in Ref. 86 and 91), and the

tridimensional vibrational scattering of $He + H_2$ [93] *inter alia*. Interesting from a theoretical standpoint is the possibility to describe classically forbidden events (as tunneling) by letting the time develop an imaginary component [86]. The system may also acquire complex momenta and pierce some barriers. There have been many further improvements on the SC S-matrix theory. Relevant to this thesis work is the Initial Variable Representation (IVR) of the S-matrix to be referred in chapter 5.

Heller Semiclassical Wave Packet Dynamics

The previous SC dynamics has been skillfully reformulated by Heller in a series of very interesting theoretical papers [94–97]. This author has derived a representation of the SC theory in terms of frozen Gaussian wave packets. The original aim of his efforts has been to tailor a SC theory devoid of the previously discussed RS problem. Heller's derivations have explicitly exploited different properties of the canonical coherent state through its relationship to the Gaussian wave packets. This method has been mostly applied to theoretical models. Since Heller's theory bears some analogies with the END theory, it will be presented with some detail when discussing the latter in the next chapter. It can be stated without exaggeration that the present version of the END theory is the practical and efficient realization of some features of Heller's theory. An alternative presentation of the SC wave packet dynamics in Heller's sense can be seen in the review paper by Littlejohn [98].

Non-Adiabatic Semiclassical Methods: Transition Surface Hopping Model (TSHM)

The examples of the SC theory hitherto presented has been totally devoted to dynamical processes on one predetermined PES. However, there have been many attempts to extend the SC theory to treat non adiabatic processes on many PESs , especially electron transfer reactions. The first systematic developments for an electron transfer SC theory

was developed by Pechukas [99, 100] and Miller [86]. In their approach, the Feyman path integral formulation of the propagator is generalized to introduce electronic degrees of freedom in the classical Lagrangian through some PESs. An exact propagator for the evolution of the nuclei coupled to the electronic PESs can be derived in that way. By applying the SC limit to the nuclear degrees of freedom, a SC non adiabatic version of the propagator and of the S-matrix is obtained. The resulting SC propagation is started on one of the PES but allowing the time to be complex. In some trajectories, the nuclei evolve into a crossing point with other PES. This crossing point can lie on a complex-valued trajectory so that it is in a region of the PES obtained by analytical continuation. At this crossing point, the nuclei can smoothly pass from one surface to the other. If this the case, the evolution continues on the latter surface until an asymptotic state is reached, presumingly with real time, positions and momenta. This scheme describes the electron transfer processes is conceived as a classically forbidden event, as in the case of tunneling, because of the use of complex time and trajectories. This elaborate theory can exactly reproduce the results of some archetypal SC charge-transfer models [86] as those by Landau [101], and Zener [102], and by Demkov [103]. However, the application of this SC theory to more realistic systems has not been attempted yet because of its bizarre features, such as the use of complex variables. If this SC evolution is constrained on real trajectories only and some of its remnant quantum effects are discarded then this SC theory becomes almost equivalent to other SC models derived from less rigorous premises [86].

One of the most commonly used models is the Transition Surface Hopping Model (TSHM) originally derived by Tully and Preston [104]. This approach usually involve only two PES's. A classical dynamics is started on one of the PESs and the evolution is carefully followed thenceforth. If the trajectory pass through a region defining a crossing

or an avoided crossing with other PES then the system is allowed to pass or hop onto the other PES according to the Landau-Zerner transition probability. When the transition is effected the evolution will continue on the second PES until an asymptotic state is reached. Special care is devoted to guarantee the conservation of energy and linear momentum during the hopping. This implies an excessive intervention by the programmer at the transition moment. Examples of the performance of the TSHM model will be examined and compared with the END theory in a later chapter. The present efforts by Tully [105] are to develop a hopping method which includes multiple PES and allows transition at any time of the evolution.

CHAPTER 3
THE END THEORY FOR TIME-DEPENDENT DYNAMICS

General Outline of the END Theory

The END theory is a quite general time-dependent formalism to describe the dynamics of molecular systems. As stated in the introduction, chapter 1, this theory admits a hierarchy of realizations of increasing complexity. Although each particular realization calls for specific details, the END theory can be concisely formulated in a totally general way. The starting point of the END formalism is the quantum Time-Dependent Variational Principle (TDVP) [106] which bears a strikingly analogy to the "Hamilton's principle" in classical mechanics [61]. The TDVP formalism is a powerful technique well-known in the nuclear physics [107, 106] the coherent state [11] communities. However, this principle has remained virtually unknown in the field of quantum chemistry. The TDVP starts with the definition of the quantum mechanical action as [106]

$$A = \int_{t_1}^{t_2} L(\Psi^*, \Psi) dt, \tag{1}$$

where the quantum mechanical Lagrangian $L(\Psi^*, \Psi)$ is

$$L(\Psi^*, \Psi) = \langle \Psi | \frac{i\hbar}{2} \left(\frac{\partial}{\partial t} - \frac{\widetilde{\partial}}{\partial t} \right) - H_{total} | \Psi \rangle / \langle \Psi | \Psi \rangle \tag{2}$$

being H_{total} the quantum mechanical Hamiltonian of the whole system. The "left acting derivative" $\frac{\widetilde{\partial}}{\partial t}$ occurring in the integrand is defined as

$$f \frac{\widetilde{\partial}}{\partial t} = \frac{\partial}{\partial t} f \tag{3}$$

where f is an arbitrary function. In this way, the "Lagrangian operator" $\Theta = \frac{i\hbar}{2} \left(\frac{\partial}{\partial t} - \frac{\widetilde{\partial}}{\partial t} \right) - H_{total}$ becomes Hermitian[6]. The many-body wave functionΨ has a set of

6. The term "Lagrangian operator" must not be taken as that. There is no official name for the Θ operator.

variational complex parameters $\boldsymbol{\zeta} = \{\zeta_1, \zeta_2, ..., \zeta_M\}$ which depend on time: $\zeta_\alpha \equiv \zeta_\alpha(t)$. The notation $\Psi \equiv \Psi(\boldsymbol{\zeta}) \equiv |\boldsymbol{\zeta}\rangle$ is introduced where $|\boldsymbol{\zeta}\rangle$ is a (column) array of the complex parameters. Since the parameters depend only on time, it is easy to see that the Lagrangian parametrically depends on ζ, ζ^* and their respective "velocities" $\dot{\boldsymbol{\zeta}} = d\boldsymbol{\zeta}/dt$ and $\dot{\boldsymbol{\zeta}}^* = d\boldsymbol{\zeta}^*/dt$ .. Therefore,

$$L(\Psi^*, \Psi) \equiv L\left(\zeta^*, \dot{\zeta}^*, \zeta, \dot{\zeta}\right). \tag{4}$$

This dependency of the quantum Lagrangian strongly resembles that of its classical counterpart on generalized positions and velocities [61].

The TDVP states that the time evolution of the system can be determined by requiring the action to be stationary w. r. t. a variation of its parameters

$$\delta A = \delta \int_{t_1}^{t_2} L dt = 0, \tag{5}$$

subject to the boundary conditions

$$\delta|\Psi\rangle = \delta\langle\Psi| = 0 \tag{6}$$

at $t = t_1$ and t_2 (cf. its classical analogue in Ref [61]). The application of this principle along with the above boundary conditions implies that

$$\begin{aligned} \delta A &= \delta \int_{t_1}^{t_2} dt\ \langle\boldsymbol{\zeta}|\Theta|\boldsymbol{\zeta}\rangle/\langle\boldsymbol{\zeta}|\boldsymbol{\zeta}\rangle = 0 \\ &= \int dt \left[i\hbar \frac{\langle\delta\boldsymbol{\zeta}|\dot{\boldsymbol{\zeta}}\rangle}{\langle\boldsymbol{\zeta}|\boldsymbol{\zeta}\rangle} - \frac{\langle\delta\boldsymbol{\zeta}|H|\boldsymbol{\zeta}\rangle}{\langle\boldsymbol{\zeta}|\boldsymbol{\zeta}\rangle} - \frac{\langle\boldsymbol{\zeta}|\Theta|\boldsymbol{\zeta}\rangle}{\langle\boldsymbol{\zeta}|\boldsymbol{\zeta}\rangle^2}\langle\delta\boldsymbol{\zeta}|\boldsymbol{\zeta}\rangle + \ c.\ c. \right], \end{aligned} \tag{7}$$

where integration by parts has been used. If Ψ is varied in the full Hilbert space, the previous expression is equivalent to

$$\left[i\hbar \frac{\partial}{\partial t} - H_{total} \right] |\boldsymbol{\zeta}\rangle = \frac{\langle\boldsymbol{\zeta}|\Theta|\boldsymbol{\zeta}\rangle}{\langle\boldsymbol{\zeta}|\boldsymbol{\zeta}\rangle} |\boldsymbol{\zeta}\rangle \tag{8}$$

This is nothing but the time-dependent Schrödinger equation provided that the right hand side is zero. One can achieve this by explicitly considering the phase factor γ, *i. e.* by setting $|\zeta\rangle \rightarrow e^{-i\gamma}|\zeta\rangle$. Then,

$$\begin{aligned}
&\langle\zeta|e^{-i\gamma}\Theta e^{i\gamma}|\zeta\rangle = 0, \\
&\langle\zeta|e^{-i\gamma}\frac{1}{2}(i(i\dot{\gamma}) - i(-i\dot{\gamma}))e^{i\gamma}|\zeta\rangle + \langle\zeta|\Theta|\zeta\rangle = 0, \\
&\langle\zeta|\zeta\rangle\dot{\gamma} + \langle\zeta|\Theta|\zeta\rangle = 0, \\
&\dot{\gamma} = \frac{\langle\zeta|\Theta|\zeta\rangle}{\langle\zeta|\zeta\rangle}.
\end{aligned} \tag{9}$$

The last expression shows that the phase factor γ is the quantum action A itself since

$$\begin{aligned}
\gamma &= \int_{t_1}^{t_2} dt \;\; \dot{\gamma} \\
&= \int_{t_1}^{t_2} dt \; \frac{\langle\zeta|\Theta|\zeta\rangle}{\langle\zeta|\zeta\rangle} = A \; .
\end{aligned} \tag{10}$$

Note that this phase is a real function. By writing the quantum state $|\zeta\rangle$ as a wave function $\Psi(\vec{r}, \vec{R}, t) = \langle\vec{r}, \vec{R}|\zeta\rangle$, and including the phase factor to get$\Phi(\vec{r}. \vec{R}. t) = e^{i\gamma}\Psi(\vec{r}, \vec{R}, t)$, the Schrödinger equation is then recovered,

$$\left(i\hbar\frac{\partial}{\partial t} - H_{total}\right)\Phi(\vec{r}, \vec{R}, t) = 0. \tag{11}$$

If the variations of the action are restricted to a predetermined region of the Hilbert space, as it would be for a Ψ chosen to be of a specific form, then the Lagrangian will generate an approximate time evolution. This is the philosophy adopted in the different realizations of the END theory. However, a general set of dynamical equations can be obtained without introducing any further approximation. To that effect, the notations for the overlap $S(\boldsymbol{\zeta}^*, \boldsymbol{\zeta}) = \langle\boldsymbol{\zeta}|\boldsymbol{\zeta}\rangle$ and the energy $E(\boldsymbol{\zeta}^*. \boldsymbol{\zeta}) = \langle\boldsymbol{\zeta}|H\boldsymbol{\zeta}\rangle/\langle\boldsymbol{\zeta}|\boldsymbol{\zeta}\rangle$ are introduced

in eq. 7. This leads to

$$\delta A = \int_{t_1}^{t_2} \{\sum_{\beta} [-i \sum_{\alpha} (\frac{\partial^2 \ln S}{\partial \zeta_\alpha^* \partial \zeta_\beta} \dot{\zeta}_\alpha^* - \frac{\partial E}{\partial \zeta_\beta}) \delta \zeta_\beta + i \sum_{\alpha} (\frac{\partial^2 \ln S}{\partial \zeta_\alpha \partial \zeta_\beta^*} \dot{\zeta}_\alpha - \frac{\partial E}{\partial \zeta_\beta^*}) \delta \zeta_\beta^*]\} dt = 0 \,. \tag{12}$$

Since $\delta\zeta_\beta$ and $\delta\zeta_\beta^*$ are independent variations, one can write

$$i \sum_{\beta} C_{\alpha\beta} \dot{\zeta}_\beta = \frac{\partial E}{\partial \zeta_\alpha^*}, \qquad -i \sum_{\beta} C_{\alpha\beta}^* \dot{\zeta}_\beta^* = \frac{\partial E}{\partial \zeta_\alpha}, \tag{13}$$

where the complex Hermitian matrix $\mathbf{C} = \{C_{\alpha\beta}\}$ are defined as $C_{\alpha\beta} = \partial^2 \ln S / \partial \zeta_\alpha^* \partial \zeta_\beta$. The eq. 13 are the general END dynamical equations. These equations can be written in matrix form as

$$i \begin{pmatrix} C & 0 \\ 0 & -C^* \end{pmatrix} \begin{pmatrix} \dot{\zeta} \\ \dot{\zeta}^* \end{pmatrix} = \begin{pmatrix} \frac{\partial E}{\partial \zeta^*} \\ \frac{\partial E}{\partial \zeta} \end{pmatrix}. \tag{14}$$

For two, differentiable functions $f(\boldsymbol{\zeta}, \boldsymbol{\zeta}^*)$ and $g(\boldsymbol{\zeta}, \boldsymbol{\zeta}^*)$ the generalized Poisson bracket

$$\{f, g\} = -i \sum_{\alpha,\beta} [\frac{\partial f}{\partial \zeta_\alpha} (\mathbf{C^{-1}})_{\alpha\beta} \frac{\partial g}{\partial \zeta_\beta^*} - \frac{\partial g}{\partial \zeta_\alpha} (\mathbf{C^{-1}})_{\alpha\beta} \frac{\partial f}{\partial \zeta_\beta^*}] \tag{15}$$

is defined. The similarity of this generalized Poisson bracket and its well-known classical counterpart [61] is clearly manifest. It follows that $\dot{\boldsymbol{\zeta}} = \{\boldsymbol{\zeta}, E\}$ and $\dot{\boldsymbol{\zeta}}^* = \{\boldsymbol{\zeta}^*, E\}$ *i. e.* the time evolution of the wave function parameters is governed by Hamilton-like equations. The generalized phase space and the associated Poisson bracket, eq. (15, permit the relations

$$\{\zeta_\alpha, \zeta_\beta\} = \{\zeta_\alpha^*, \zeta_\beta^*\} = 0; \quad \{\zeta_\alpha, \zeta_\beta^*\} == -i(\mathbf{C^{-1}})_{\alpha\beta}, \tag{16}$$

which show that ζ*, and ζ behave as "classical" coordinates and momenta. If the matrix C was the unit matrix the corresponding phase space would be canonical or "flat". However,

in general, this generalized phase space is curved. Further details of the general structure and properties of the END dynamical equation can be found in Ref. [1] and [108].

In the previous derivations, the application of the TDVP has been carried out by a direct variation of the action. This approach is quite adequate in theoretical consideration of the TDVP [106, 1] but becomes very cumbersome when applied to realistic systems. A more expediting but equivalent algebraic procedure can be obtained if the central theorem of the calculus of variations is applied to the action stationary condition, eq. 5 (see for instance Ref. [61], chapter II). Through that theorem, the stationary condition turn out to be equivalent to set of Euler-Lagrange equations of the Lagrangian

$$\begin{aligned} \frac{d}{dt}\left[\frac{\partial L\left(\zeta^*,\dot{\zeta}^*,\zeta,\dot{\zeta}\right)}{\partial\zeta}\right] &= \frac{\partial L\left(\zeta^*,\dot{\zeta}^*,\zeta,\dot{\zeta}\right)}{\partial\dot{\zeta}} \,, \\ \frac{d}{dt}\left[\frac{\partial L\left(\zeta^*,\dot{\zeta}^*,\zeta,\dot{\zeta}\right)}{\partial\dot{\zeta}^*}\right] &= \frac{\partial L\left(\zeta^*,\dot{\zeta}^*,\zeta,\dot{\zeta}\right)}{\partial\dot{\zeta}^*} \,. \end{aligned} \tag{17}$$

These are the TDVP equations to be used henceforth. Aside form algebraic advantages, this set of equations facilitates even more the connection of the quantum theory with classical mechanics.

The QCSD END Wave Function

The simplest realization of the END theory rendering a realistic description is the QCSD END model. This is the only END realization which has been so far coded into the Endyne program package [2]. In this model, the END unnormalized wave function (in the Lab frame) $\Psi_{END}(\mathbf{X},\mathbf{x},t)$ is written as

$$\begin{aligned} \Psi_{END}(\mathbf{X},\mathbf{x},t) = F_{nucl}[\mathbf{X};\mathbf{R}(t),\mathbf{P}(t)]f_{el}[\mathbf{x};\mathbf{z}(t),\mathbf{R}(t)]\times \\ \exp\left[\frac{i}{\hbar}\gamma_{total}(t)\right] \end{aligned} \tag{18}$$

where $\mathbf{X}$ and $\mathbf{x}$ are the nuclear and electronic coordinates, $\mathbf{R}(t)$, $\mathbf{P}(t)$ and $\mathbf{z}(t)$ are the variational parameters, and $\gamma_{total}(t)$ is the total phase. Note that the time-dependency

of the wave function comes only through the parameters and the phase. Aside from the exponential factor $\exp\left[\frac{i}{\hbar}\gamma_{total}(t)\right]$, the QCSD END wave function has two essential parts, namely, the nuclear wave function $F_{nucl}[\mathbf{X};\mathbf{R}(t),\mathbf{P}(t)]$ and the electronic wave function $f_{el}[\mathbf{x};\mathbf{z}(t),\mathbf{R}(t)]$. The former is a simple product of unnormalized, "frozen ", Gaussian wave packets $\Phi_k(\mathbf{X_k};\mathbf{R_k},\mathbf{P_k})$

$$
\begin{aligned}
&F_{nucl}[\mathbf{X};\mathbf{R}(t),\mathbf{P}(t)] = \prod_{k=1}^{N_{nucl}} \Phi[\mathbf{X}_k;\mathbf{R}_k(t),\mathbf{P}_k(t)] \ , \\
&\Phi[\mathbf{X}_k;\mathbf{R}_k(t),\mathbf{P}_k(t)] = \exp\left\{-a_k[\mathbf{X}_k-\mathbf{R}_k(t)]^2 + \frac{i}{\hbar}\mathbf{P}_k(t)\cdot[\mathbf{X}_k-\mathbf{R}_k(t)]\right\} ,
\end{aligned}
\tag{19}
$$

where the variational parameters $\mathbf{R}(t)$ and $\mathbf{P}(t)$, and the constant a_k are taken real. The physical meaning of these variational parameters can be easily revealed if the averages of the Gaussian wave packets in the position $\widehat{\mathbf{X}}_k = \mathbf{X}_k$ and momentum $\widehat{\mathbf{P}}_k = -i\hbar\nabla_k$ operators are obtained by evaluating [109]

$$
\begin{aligned}
\frac{\langle\Phi_{ok}|\widehat{\mathbf{X}}_k|\Phi_{ok}\rangle}{\langle\Phi_{ok}|\Phi_{ok}\rangle} &= \mathbf{R}_k(t) \ , \\
\frac{\langle\Phi_{ok}|\widehat{\mathbf{P}}_k|\Phi_{ok}\rangle}{\langle\Phi_{ok}|\Phi_{ok}\rangle} &= \mathbf{P}_k(t) \ ,
\end{aligned}
\tag{20}
$$

i. e. $\mathbf{R}(t)$ and $\mathbf{P}(t)$ turn out to be the average positions and momenta of the wave packets. The constant a_k can be easily related to the width (normal deviation)b_k of the Gaussian probability (density) functions $\Phi_k^*(\mathbf{X_k};\mathbf{R_k},\mathbf{P_k})\Phi_k(\mathbf{X_k};\mathbf{R_k},\mathbf{P_k})$ through $a_k = \frac{1}{2\sqrt{b_k}}$ since by definition

$$
\begin{aligned}
\Phi^*[\mathbf{X}_k;\mathbf{R}_k(t),\mathbf{P}_k(t)]\Phi[\mathbf{X}_k;\mathbf{R}_k(t),\mathbf{P}_k(t)] &= \exp\left\{-2a_k[\mathbf{X}_k-\mathbf{R}_k(t)]^2\right\} \\
&= \exp\left\{-\frac{[\mathbf{X}_k-\mathbf{R}_k(t)]^2}{2b_k^2}\right\} .
\end{aligned}
\tag{21}
$$

Taking into account the physical meaning of the previous parameters and constants, each nuclear wave packet can be seen as a parametric plane wave function$\exp\left\{\frac{i}{\hbar}\mathbf{P}_k(t)\cdot[\mathbf{X}_k-\mathbf{R}_k(t)]\right\}$ localized around the position $\mathbf{R}_k(\mathbf{t})$ by a simple Gaussian factor $\exp\left\{-a_k[\mathbf{X}_k-\mathbf{R}_k(t)]^2\right\}$. Furthermore, since the constants a_k are

time-independent and the evolution is through the TDVP, each nuclear Gaussian will remain as such during the evolution without even changing their shape ("frozen" wave packets). The only change allowed for these nuclear wave packets is in their positions and momenta. This type of model evolution is in high contrast with the exact propagation of unconstrained Gaussian wave packets. There, the wave packets are allowed to spread out, lose shape, and even split into pieces. Obviously, the use of frozen wave packets has clear computational advantages over the exact wave packet propagation. Furthermore, the selection of Gaussian wave packets, and not of other type, has formal advantages in relating the nuclear dynamics to classical mechanics and the CS theory. The use of wave packets to describe translational degrees of freedom is commonplace in formal scattering theory [3] as it was discussed in chapter 1. Furthermore, the usual experimental conditions makes the scattering process so fast that the spreading of the translational wave packets is totally negligible [3]. Therefore, the use of "frozen " Gaussian wave packets in a model TDVP propagation is totally valid for the nuclear translational degrees of freedom if the tunneling effect is disregarded. However, the above QCSD Gaussian wave packets do describe both the translational and the internal (vibrational and rotational) degrees of freedom. The way in which this model description of the internal motion relates to the exact internal wave function will be discussed in detail in chapters 6 and 7.

The electronic function $f_{el}[\mathbf{x}; \mathbf{z}(t), \mathbf{R}(t)]$ is a single-determinant wave function throughout the time evolution. One reason for this choice is that this type of wave function has the precedent of a known and established model propagation: the TDHF of the nuclear many-body theory [110, 111, 107]. However, it must be bore in mind that the END theory far exceeds those nuclear physics schemes by simultaneously treating both the nuclear and electronic degrees of freedom. Another reason for this choice is that

this single determinant is also related to either a restricted HF (RHF) or an unrestricted HF (UHF) description of the reagents and products ground states. In other words, the (stationary) ground states of both reagents and products are described at the level of the HF theory and a model propagation compatible with them is being employed. The construction of a wave function which remains as a single determinant during the time evolution is not a trivial pursuit. The solution to this problem was obtained by Thouless in the 1960's [110, 111] but in the context of the stability conditions of the HF theory. His mathematical proof, the so-called Thouless theorem, was immediately applied to time-dependent problems in nuclear physics [111, 107]. The QCSD END single determinant wave function $f_{el}[\mathbf{x}; \mathbf{z}(t), \mathbf{R}(t)]$ will be presented mostly following the original derivation by Thouless [110, 111]. Further details on this subject can be found in Ref. [107]. In the context of a determinantal state, it is meaningful to divide the set of K spin orbitals into *N occupied* and *K-N unoccupied* spin orbitals. When a linear array q refers to the set of all, of only occupied, or of only unoccupied spin orbitals, it is denoted by q, $q^{\bullet}$, and q°, respectively. Atomic spin orbitals may also be partitioned in two sets which may be called occupied and unoccupied. This should be understood as a mere mathematical construct. For the purpose of dynamics, the reference determinant is simply made up of nonorthogonal atomic spin orbitals which are said to be "occupied". The rest are "unoccupied". The reference determinant does not necessarily have any physical meaning. It only provides a suitable mathematical reference. With this in mind, the atomic spin orbitals can be partitioned as follows

$$\phi = (\phi^{\bullet} \quad \phi^{\circ}) \tag{22}$$

Similarly, for matrices four sub blocks are identified: the occupied $N \times N$ and unoccupied $(K\text{-}N) \times (K\text{-}N)$ diagonal blocks, and the upper and lower off diagonal blocks. The

transformation to the molecular basis becomes, in block form

$$(\psi^{\bullet} \quad \psi^{\circ}) = (\phi^{\bullet} \quad \phi^{\circ}) \begin{pmatrix} W^{\bullet} & W^{>} \\ W^{\vee} & W^{\circ} \end{pmatrix}. \tag{23}$$

A full circle is used to denote the occupied part and an empty circle to denote the unoccupied part. The right-angle > denotes the upper off-diagonal block, reminding us of the horizontal rectangular shape with the number of occupied orbitals (the number of rows of that block) usually being smaller than the number of unoccupied orbitals (the number of columns). Similarly the down-angle denotes the lower off-diagonal block which has a vertical rectangular shape, where the opposite is true. With this notation many messy index manipulations are avoided. As a mnemonic device, *p,q,r* are reserved for indices running over the *particle* or unoccupied range *N+1,...,K*, and *h,g,f* for the *hole* or occupied range *1,...,N*. It is important to emphasize that the atomic spin-obitals are functions placed on the centers of the nuclear wave packets $\mathbf{R}(t)$. Therefore, both the atomic ϕ and the molecular ψ spin-orbitals depend parametrically on $\mathbf{R}(t)$. This is finally manifested in the electronic wave function $f_{el}[\mathbf{x}; \mathbf{z}(t), \mathbf{R}(t)]$[7]

Introducing a general unitary transformation U of the orthonormal molecular spin orbital basis one can write

$$(c^{\bullet\dagger} \quad c^{\circ\dagger}) = (b^{\bullet\dagger} \quad b^{\circ\dagger}) \begin{pmatrix} U^{\bullet} & U^{>} \\ U^{\vee} & U^{\circ} \end{pmatrix} \tag{24}$$

---

7. A more flexible END electronic wave function which also depends on the parameter $\mathbf{P}(t)$ has been formulated by Mogensen et *al.* [112].

for the basis field operators, and obtain for a determinantal state [110, 113]

$$
\begin{aligned}
|\Psi\rangle = |c^{\bullet\dagger}\rangle &= \prod_{h=1}^{N} c_h^{\bullet\dagger}|vac\rangle \\
&= \prod_{h=1}^{N}\left(\sum_{k=1}^{N} b_k^{\bullet\dagger}U_{kh}^{\bullet} + \sum_{p=N+1}^{K} b_p^{\circ\dagger}U_{ph}^{\vee}\right)|vac\rangle \\
&= \prod_{h=1}^{N}\left(\sum_{l=1}^{N}\left(b_l^{\bullet\dagger} + \sum_{p=N+1}^{K}\sum_{k=1}^{N} b_p^{\circ\dagger}U_{pk}^{\vee}U_{kl}^{\bullet -1}\right)U_{lh}^{\bullet}\right)|vac\rangle \\
&= \alpha\prod_{h=1}^{N}\left(b_h^{\bullet\dagger} + \sum_{p=N+1}^{K}\sum_{k=1}^{N} b_p^{\circ\dagger}U_{pk}^{\vee}U_{kh}^{\bullet -1}\right)|vac\rangle \\
&= \alpha\prod_{h=1}^{N}\left(1 + \sum_{p=N+1}^{K}\sum_{k=1}^{N} b_p^{\circ\dagger}U_{pk}^{\vee}U_{kh}^{\bullet -1}b_h^{\bullet}\right)\prod_{l=1}^{N} b_l^{\bullet\dagger}|vac\rangle,
\end{aligned}
\tag{25}
$$

where the invariance, up to a constant α, of a determinantal wave function under a linear transformation of its occupied spin orbitals is used. Defining the Thouless parameters $z_{pq}\ \sum_{k=1}^{N} U_{pk}^{\vee}U_{kh}^{\bullet -1} = z_{ph}$, and the reference state $|\Psi_0\rangle$

$$
|\Psi_0\rangle = |b^{\bullet\dagger}\rangle = \prod_{h=1}^{N} b_h^{\bullet\dagger}|vac\rangle \tag{26}
$$

one can write the unnormalized Thouless determinant $|\mathbf{z}, \mathbf{R}\rangle = f_{el}[\mathbf{x}; \mathbf{z}(t), \mathbf{R}(t)]$ as

$$
\begin{aligned}
|\mathbf{z}, \mathbf{R}\rangle &= \prod_{h=1}^{N}\left(1 + \sum_{p=N+1}^{K} b_p^{\circ\dagger}z_{ph}b_h^{\bullet}\right)|\Psi_0\rangle \\
&= \prod_{h=1}^{N}\prod_{p=N+1}^{K}\left(1 + b_p^{\circ\dagger}z_{ph}b_h^{\bullet}\right)|\Psi_0\rangle \\
&= \prod_{h=1}^{N}\prod_{p=N+1}^{K}\exp\left(z_{ph}b_p^{\circ\dagger}b_h^{\bullet}\right)|\Psi_0\rangle \\
&= \exp\left(\sum_{h=1}^{N}\sum_{p=N+1}^{K} z_{ph}b_p^{\circ\dagger}b_h^{\bullet}\right)|\Psi_0\rangle.
\end{aligned}
\tag{27}
$$

In eq. (27) the nilpotency of the operators $b_p^{\circ\dagger}b_h^{\bullet}$ is exploited. Note that the parameters z_{pq} are complex numbers. The determinantal wave function of this state is $\det\{\chi_h(\vec{r}_n)\}$

in terms of the occupied *dynamical orbitals*

$$\chi_h = \psi_h + \sum_{p=N+1}^{K} \psi_p z_{ph}. \tag{28}$$

These orbitals are not orthogonal. The function $|\mathbf{z}.\mathbf{R}\rangle = f_{el}[\mathbf{x}{:}\,\mathbf{z}(t), \mathbf{R}(t)]$, shown in eq. 27 is the sought general single-determinant wave function (Thouless determinant) for the QCSD END theory. If the arbitrary reference state $|\Psi_0\rangle$ is selected as the HF ground state of the system$|\Psi_0\rangle = |\Psi_0\rangle_{HF}$ then the Thouless determinant contains this state plus all its excitations (single, double, triple, *etc.*). Further mathematical properties of this construct, specially about its symplectic [61] structure, can be found in Ref. [1] and the many references cited therein. The relationship of the wave functions $F_{nucl}[\mathbf{X}; \mathbf{R}(t), \mathbf{P}(t)]$ and $f_{el}[\mathbf{x}{:}\,\mathbf{z}(t), \mathbf{R}(t)]$ with the CS theory will be discussed in chapter 4[8].

Finally, the QCSD END total phase $\gamma_{total}(t)$ is the quantum action corresponding to the QCSD END wave function $\Psi_{END}(\mathbf{X}.\mathbf{x}.t)$. The relationship of this action with the SC action will be discussed in chapter 7.

The QCSD Dynamical Equations

The QCSD END dynamical equations can be obtained by constructing its quantum Lagrangian and deriving its corresponding Euler-Lagrange equations. The "exact" QCSD END Lagrangian can be obtained if finite values of the wave packet constants a_k are used. In that case, the derivation involves different types of Gaussian integrals with the additional complication of the plane wave component $\exp\{\frac{i}{\hbar}\mathbf{P}_k(t)\cdot[\mathbf{X}_k - \mathbf{R}_k(t)]\}$. A detailed account for this procedure along with the final expressions will not be presented

8. It is worth noticing that the standard presentations of the Thouless theorem [110, 111, 107] make no reference to the CS theory. In fact, a thorough understanding of this theorem can be achieved without resorting to the concept of CS. This is the point of view adopted in this chapter. Nonetheless, the further relationship of the Thouless single determinant with the CS theory will bring about additional mathematical properties.

here for brevity but it can be found in Ref. [114]. However, the "exact" QCSD END dynamical equations are not the END equations currently implemented in the program ENDyne since the SC limit

$$\begin{aligned} &\hbar \rightarrow 0 \,, \\ &a_k \rightarrow \infty \; (\equiv \; b_k \rightarrow 0) \,, \\ &a_k \hbar \rightarrow \; finite \;\; constant \,, \end{aligned} \tag{29}$$

is applied to the nuclear part of this wave function [1]. This "triple limit" will be reduced to the first one (*i.e.* to the traditional SC limit, eq. 92, chapter 2) when the connection between the END with both the CS and the SC theories is established in chapter 6. The second limit in eq. 29 makes the nuclear Gaussian wave packets be highly localized around the positions $\mathbf{R}(t)$. Loosely speaking, the Gaussian function becomes a Dirac delta function in that limit (see appendix A). The third limit in eq. 92 prevents the indeterminacy of some terms when the other two limits are applied. The actual value of the finite constants is irrelevant since they cancel out in all the expressions. The justification for using the SC approximation in the QCSD END theory has different facets. The resulting dynamical equations from this approximation obviously omit all the nuclear Gaussian integrals and, therefore, have clear computational advantages. It is then assumed that the gain in computational efficiency will compensate the loss of accuracy in the nuclear description. In fact, this SC approximation is not so drastic as it might appear in the present context. The use of very wide Gaussian wave packets (*e. g.* wave packets with a width being more than 5 % of a characteristic bond distance) would be meaningful if some subtle quantum effects, such as tunneling, were to be described. But if a proper account for those effects is desired the model TDVP propagation must be replaced by the exact wave packet propagation. The use of very wide, "frozen" wave packets in a model TDVP evolution is of dubious physical meaning. Therefore, narrow but still finite,

"frozen" Gaussian wave packets (*e. g.* wave packets with a width being less than 5% of a bond distance) are compatible with a TDVP propagation. It will be assumed henceforth that the zero-width SC limit of the QCSD END theory is numerically very close to its "exact", narrow-width version. Although nuclear delta functions are actually used in the dynamical equations below, Gaussian wave packets with nonzero width will be employed in further theoretical treatments of the END theory. Only by retaining a finite width a relationship between the END and SC theory can be elaborated (see chapter 6).

In order to calculate the QCSD END Lagrangian, the total Hamiltonian of the system is partitioned as

$$H_{total} = T_N + H_{el} \tag{30}$$

where T_N is the nuclear kinetic operator

$$T_N = -\sum_{l}^{3N_{nucl}} \frac{\hbar^2}{2M_l} \left(\frac{\partial^2}{\partial X_l^2} \right) \tag{31}$$

with nuclear mass M_k, and H_{el} is the electronic Hamiltonian including nuclear repulsion. Note that the above sum runs through the $3N_{nucl}$ components X_l of the nuclear coordinate $\mathbf{X}$. The resulting QCSD END Lagrangian in the SC limit is obtained by setting the QCSD END wave function, eq. 18, into the definition of the quantum Lagrangian, eq. 2 and by then applying the above SC limit, eq. 29 (see Ref. [115] for a step-by step derivation). The result is

$$\begin{aligned} L &= L\Big(\mathbf{R}, \mathbf{P}, \mathbf{z}, \mathbf{z}^*, \dot{\mathbf{R}}, \dot{\mathbf{P}}, \dot{\mathbf{z}}, \mathbf{z}^*\Big) \\ &= \sum_{l}^{3N_{nucl}} P_l \dot{R}_l + \frac{i\hbar}{2} \sum_{l}^{3N_{nucl}} \left(\frac{\partial \ln S}{\partial R_l} - \frac{\partial \ln S}{\partial R_l'} \right) \dot{R}_l \\ &\quad + \frac{i\hbar}{2} \sum_{p}^{N_p} \left(\frac{\partial \ln S}{\partial z_p} \dot{z}_p - \frac{\partial \ln S}{\partial z_p^*} \dot{z}_p^* \right) - E \ , \end{aligned} \tag{32}$$

where S is the overlap between the electronic functions at different parametric positions

$$S = \langle \mathbf{z}, \mathbf{R}' | \mathbf{z}, \mathbf{R} \rangle \ , \tag{33}$$

and E is the total energy of the system

$$E = \sum_{l}^{N_{nucl}} \frac{P_l^2}{2M_l} + \frac{\langle \mathbf{z}, \mathbf{R} | H_{el} | \mathbf{z}, \mathbf{R} \rangle}{\langle \mathbf{z}, \mathbf{R} | \mathbf{z}, \mathbf{R} \rangle} . \tag{34}$$

Note that sums in the $3N_{nucl}$ components R_l of $\mathbf{R}$ and in the $3N_{nucl}$ components P_l of $\mathbf{P}$ are being used, respectively. The occurrence of different parametric positions in the overlap S is a mathematical device used in the intermediate steps of the END derivations. This double dependency will disappear when the limit $\mathbf{R}' \rightarrow \mathbf{R}$ is taken in the final expressions below. Note also that because of the use of nuclear Gaussian wave packets the total overlap is only in terms of the electronic function. The term, $\sum_{l}^{3N_{nucl}} P_l \dot{R}_l$ in the above Lagrangian comes directly from the nuclear operator T_N and plays for the nuclei a similar role as that in the Legendre transformation connecting the Lagrangian and the Hamiltonian in classical mechanics [61].

By deriving the Euler-Lagrange equations from the above Lagrangian, according to eq. 17, the QCSD END dynamical equations in the SC limit are obtained [1, 115]. They are in matrix form (cf. eq. 14)

$$\begin{bmatrix} i\mathbf{C} & \mathbf{0} & i\mathbf{C}_{\mathbf{R}} & \mathbf{0} \\ \mathbf{0} & -i\mathbf{C}^* & -i\mathbf{C}^*_{\mathbf{R}} & \mathbf{0} \\ i\mathbf{C}_{\mathbf{R}}{}^{\dagger} & -i\mathbf{C}_{\mathbf{R}}{}^{T} & \mathbf{C}_{\mathbf{RR}} & -\mathbf{I} \\ \mathbf{0} & \mathbf{0} & \mathbf{I} & \mathbf{0} \end{bmatrix} \begin{bmatrix} \dot{\mathbf{z}} \\ \dot{\mathbf{z}}^* \\ \dot{\mathbf{R}} \\ \dot{\mathbf{P}} \end{bmatrix} = \begin{bmatrix} \partial E/\partial \mathbf{z}^* \\ \partial E/\partial \mathbf{z} \\ \partial E/\partial \mathbf{R} \\ \partial E/\partial \mathbf{P} \end{bmatrix} , \tag{35}$$

where the definitions of the dynamical metric matrices are

$$(C_{XY})_{ij;kl} = -2\mathrm{Im} \frac{\partial^2 \ln S}{\partial X_{ik} \partial Y_{jl}} \Big|_{R'=R} , \tag{36}$$

$$(C_{X_{ik}})_{ph} = \frac{\partial^2 \ln S}{\partial z^*_{ph} \partial X_{ik}} \Big|_{R'=R} , \tag{37}$$

and

$$C_{ph;qg} = \frac{\partial^2 \ln S}{\partial z^*_{ph} \partial z_{qg}} \Big|_{R=R'} . \tag{38}$$

Note that the two first matrices contain couplings between the nuclear and the electronic degrees of freedom. The eq. 35 is a set of highly nonlinear, first-order differential equations. These are the END dynamical equations coded into the Endyne program package

[2]. Further details about their mathematical properties and numerical implementation can be found in Ref. [1], [2], and [108].

General Character of the QCSD END Dynamical Equations

Before advancing in this thesis dissertation, it will be illuminating to discuss some general properties of the proposed QCSD END theory. The first aspect to be examined is the nature of the QCSD END wave function. The comparison of this wave function, eq. 18, with both the adiabatic and the diabatic expansions, eq. 15 and 22, chapter 2immediately reveals its diabatic character. Furthermore, by effecting the product of the nuclear function $F_{nucl}[\mathbf{X}\colon \mathbf{R}(t), \mathbf{P}(t)]$, eq. 19, with its electronic counterpart $f_{el}[\mathbf{x}\colon \mathbf{z}(t), \mathbf{R}(t)] = |\mathbf{z}, \mathbf{R}\rangle$, eq. 27, it can be seen that the QCSD END wave function provides a diabatic expansion in which different electronic states correspond to the same diabatic nuclear wave function $F_{nucl}[\mathbf{X}\colon \mathbf{R}(t), \mathbf{P}(t)]$. This constraint imposed on the exact diabatic expansion does not carries a serious loss of accuracy unless a very detailed description of the dynamics is sought. This particular aspect will be further addressed in the next section and in chapter 7. Note that the above END metric matrices, eq. 36, 37 and 38, play a role similar to that of the diabatic coupling. A detailed mathematical relationship between the END metric matrices and the diabatic couplings will be postponed for future research. The diabatic nature of the END theory must not be emphasized too much when the SC limit is applied. In that case, the only contributing value of $\mathbf{X}$ to the nuclear delta functions is when $\mathbf{X} = \mathbf{R}(t)$. This identity introduces a kind of coupling between the electronic and the nuclear parts which resembles that of the adiabatic expansion.

A second aspect to be examined is the nature of the TDVP propagation used in the QCSD END theory. By adopting that dynamical scheme, the exact and linear propagation

given by the time evolution operator is replaced by the nonlinear approximation of the TDVP [1]. This implies that the END equations are not micro reversible [1]. This feature does not introduce any serious limitation when the END theory is applied to systems such as those studied in chapter 7. However, some special care must be exerted when defining the END analogue of the S-matrix (see chapter 6). However, TDVP do provides conservation laws associated with the energy, the linear momentum, and the angular momentum (see Ref. [1] and references cited therein). Detailed proofs for the QCSD END conservation laws of the total (*i.e.* nuclear plus electronic) energy, linear momentum and angular momentum can be found in Ref. [1]. These proofs are similar to their classical counterparts in exploiting the time, translational, and rotational invariance of the Lagrangian (cf. Ref. [61]). Some of these conservation laws will be used in chapter 6.

The general evolution scheme of the QCSD END theory in the SC limit is summarized as follows. The initial state of the system is constructed by first placing the nuclear wave packets (delta functions) in the positions $\mathbf{X} = \mathbf{R}(t_1)$ with parametric momenta $\mathbf{P}(t_1)$. Then, the electronic single determinant wave function is constructed from the atomic basis set placed on the centers of the wave packets. This electronic wave function is either a RHF or UHF ground state. By selecting a convenient reference state, the initial Thouless parameters $\mathbf{z}(t_1)$ and $\mathbf{z}^*(t_1)$ are determined. Then, from this set of initial conditions $\mathbf{X}(t_1)$, $\mathbf{P}(t_1)$, $\mathbf{z}(t_1)$ and $\mathbf{z}^*(t_1)$, the propagation of the total wave function is effected by solving the END dynamical equations, 35. Any intermediate state of the system at time t will be totally determined by the values of the parameters $\mathbf{X}(t)$, $\mathbf{P}(t)$, $\mathbf{z}(t)$ and $\mathbf{z}^*(t)$. At final time, a projection of the total wave function onto stationary states with the same final position and momentum $\mathbf{X}(t_2)$, $\mathbf{P}(t_2)$ will render the transition amplitudes of the reaction under study. This procedure will be further discussed in

chapter 3. Note that the description of the initial and the final stationary states is within the BO approximation, as is the usually done in electronic structure and spectroscopy. However, the propagation scheme does not make use of the BO approximation. As soon as the propagation starts, the initial HF single determinant will evolve into a general Thouless determinant which combines many electronic PES. A multi-surface, non BO propagation is therefore obtained.

The QCSD END theory have implicit some less general methods as particular cases. For instance, a molecular dynamics (MD) version of the END theory [2] can be obtained if the variation given by the Thouless determinant is discarded and the electronic function is constrained to the ground state HF PES throughout the propagation. This MD END theory has clear computational advantages but it heavily relies on the BO approximation. If the nuclei are fixed and some approximations are introduced [1] then the QSCD END dynamical equations will coincide with the TDHF of the quantum many-body theory [110, 111, 107]. Finally, if the nuclei are again fixed and the time dependency is discarded then the variation in the Thouless parameters can be still done time-independently. In that case, the TDVP will transform into its time-independent counterpart and the END dynamical equations will be the HF stationary condition expressed in terms of the Thouless parameters.

Other END Models: The Double Wave Packet END Theory

The previously presented QCSD END model is not the only realization of the END theory. Different END models with higher degrees of sophistication have been proposed. An electronic multi-configurational END theory [116] was theoretically devised by Deumens *et al.* to improve the electronic description of the QCSD END theory. This development has yet to be implemented. Another effort is the generalization of the END

theory done by Mogensen *et al.* [112] to treat electron scattering processes by molecular targets. This model has been recently implemented and is being tested for accuracy.

In addition of these developments, a double wave packet (DWP) END theory has been formulated during this thesis research. This new model aims at overcoming the previously mentioned constraints imposed on the diabatic expansion of the QCSD END theory. The fact that all the electronic states in the Thouless determinant shares the same nuclear wave function implies that all the exit channels have the same nuclear dynamics (*i. e.* all channels have the same final values of $\mathbf{R}(t)$ and $\mathbf{P}(t)$). This constraint may be a limitation when a highly detailed description of the dynamics is desired (see chapter 7). In order to obtain a higher variational flexibility between the transfer and the nontransfer channels, the DWP END wave function Ψ_{END}^{DWP}, which is double configurational in both the nuclear and the electronic degrees of freedom, is proposed

$$\begin{aligned}\Psi_{END}^{DWP} =& \Psi_{END}^{DWP}(\mathbf{R_1}, \mathbf{P_1}, \mathbf{R_2}, \mathbf{P_2}, A, B, C) \\ =& F_1(\mathbf{R_1}, \mathbf{P_1})[f_1(\mathbf{z_1}, \mathbf{R_1}) + B f_2(\mathbf{z_2}, \mathbf{R_2})] \\ &+ A F_2(\mathbf{R_2}, \mathbf{P_2})[C f_1(\mathbf{z_1}, \mathbf{R_1}) + f_2(\mathbf{z_2}, \mathbf{R_2})]\end{aligned} \tag{39}$$

where $\mathbf{R}_i(t)$ and $\mathbf{P}_i(t)$ are the nuclear variational parameter of the nuclear functions F_i , $i = 1, 2$. These two functions are defined as products of generalized, "frozen" Gaussian wave packets as before. The electronic functions f_i , $i = 1, 2$ are single determinant wave functions which depends parametrically on Thouless parameters $\mathbf{z}_i(t)$ and $\mathbf{R}_i(t)$. The complex coefficients $A(t)$, $B(t)$ and $C(t)$ are related to the probability amplitudes of the different components in the wave function. The three are treated as variational parameters as well. Note that the nuclear and electronic coordinates $\mathbf{X}_i$ and $\mathbf{x}_i$, the total phase, and the time dependency are not explicitly shown in eq. 39 for brevity. If the conditions $A(t) = A = 0$ and $B(t) = B = 0$ are imposed throughout the time evolution then the previous QCSD END wave function is recovered. If only

$A(t) = A = 0$ is imposed then a simplified version of the electronic multi-configuration END wave functions mentioned in the previous section is obtained. By applying the same mathematical procedures as those used in the QCSD END theory, the Lagrangian and the dynamical equations of the DWP END theory can be obtained. The algebra involved and the final expressions are far more complicate than their QCSD END counterparts. These expressions are not reproduced here for brevity but they can be found in Ref. [115]. However, the main idea of the DWP END theory can be easily understood without knowing these final equations. At initial time t_1, when the reactants are far apart, the DWP END wave function is forced to be that of the QCSD END theory by fixing $A(t) = A(t_1) = 0$, $t_1 \leq t < t_c < t_2$ and $B(t) = B(t_1) = 0$, $t_1 \leq t < t_c < t_2$ up to some critical time t_c. At that time, when the reactants are close enough to interact, these two constraints are released and a full DWP END dynamics is allowed to start. At final time t_2, when the products are far apart, the coefficients $B(t)$ and $C(t)$ are supposed to go to zero so that the final wave function will be

$$\Psi_{END}^{DWP} = F_1(\mathbf{R_1}, \mathbf{P_1}) f_1(\mathbf{z_1}, \mathbf{R_1}) + A F_2(\mathbf{R_2}, \mathbf{P_2}) f_2(\mathbf{z_2}, \mathbf{R_2}) \quad (t = t_2 \rightarrow \infty) \,. \tag{40}$$

This asymptotic form corresponds to two independent QCSD END wave functions, one for the nontransfer channels and the other for the transfer ones.

The DWP END theory can be seen as the exact TDVP formulation of the TSH model reviewed in chapter 2. Applications for the DWP END theory will be discussed in chapter 7.

CHAPTER 4
THE COHERENT STATE THEORY IN THE END CONTEXT

The General Theory of Coherent and States

Definition of Coherent States

In a Hilbert space $\mathcal{H}$, a set of states $|\mu\rangle \in \mathcal{H}$, which are functions of the complex parameter(s) μ, forms a set of CS if they satisfy the following two conditions [11]:

1. The states $|\mu\rangle$ are continuous functions of the parameter(s) μ

$$\lim_{\mu \to \mu_0} |\mu\rangle = |\mu_0\rangle \tag{1}$$

2. (Stronger) There exists a positive measure $d\mu_+$ for which the resolution to unity holds

$$1 = \int d\mu \, |\mu\rangle\langle\mu| \, . \tag{2}$$

These states form a complete set in the Hilbert space which in most of the cases is nonorthogonal. A complete set of nonorthogonal functions is called overcomplete [11].

The previous definition of a CS is the most general and the most widely accepted. However, in some occasions the above second condition is adopted in a weaker form

1. (Weaker) The closed linear span of the CS $|\mu\rangle$ is the Hilbert space $\mathcal{H}$. This alternative condition means that any state vector in the Hilbert space may be represented as a (possible infinite) linear sums of CS [11]. A way to satisfy this condition is to have a

resolution of unity as in eq. 2 but with a signed measure $d_{\pm}\mu$ (*i.e.* a measure which can acquire both positive and negative values.)

Several sets of CS related to different quantum mechanical problems have been derived. The first constructed CS, and the most widely known, is the canonical CS $|\alpha\rangle$ [117, 11], also known as the Glauber state because of its applications to optical problems [118]. These states are associated to the harmonic oscillator Hamiltonian H_{vib} [119]

$$H_{vib} = \hbar\omega\left(a^{\dagger}a + \frac{1}{2}\right) \tag{3}$$

where ω is the angular frequency of the oscillator, and the creator and annihilation boson operators $a^{\dagger}$ and a are defined

$$\begin{aligned} a^{\dagger} &= \frac{1}{\sqrt{2}}(x - ip) \ , \\ a \ &= \frac{1}{\sqrt{2}}(x + ip) \ . \end{aligned} \tag{4}$$

The reduced position and momentum operators x and p are in turn defined

$$\begin{aligned} x &= \sqrt{\frac{m\omega}{\hbar}}X \ , \\ p &= \sqrt{\frac{\hbar}{m\omega}}P \ , \end{aligned} \tag{5}$$

where X and P are the position and momentum operator, and m the oscillator mass. The canonical CS $|\alpha\rangle$ in the complex parameter α are the eigenfunctions of the annihilation operators a with eigenvalues α

$$a|\alpha\rangle = \alpha|\alpha\rangle \ . \tag{6}$$

This CS can be explicitly written as [119, 11]

$$\begin{aligned} |\alpha\rangle &= exp\left\{-\frac{1}{2}|\alpha|^2\right\}\sum_{n=0}^{\infty}\frac{\alpha^n}{\sqrt{n!}}|n\rangle \\ &= exp\left\{-\frac{1}{2}|\alpha|^2\right\}\exp\left\{\alpha a^{\dagger}\right\}|0\rangle \ , \end{aligned} \tag{7}$$

where the $|n\rangle$ are the eigenstates of the Hamiltonian H_{vib}

$$H_{vib}|n\rangle = \left(n + \frac{1}{2}\right)\hbar\omega|n\rangle \; ; \; n = 0,\ 1,\ 2,\ \ldots \tag{8}$$

eq. 7 can be seen as a resolution of the canonical CS into the eigenstates of the Hamiltonian H_{vib}. Furthermore, the probability $P_n(\alpha)$ to find the eigenstate $|n\rangle$ in the CS $|\alpha\rangle$ is neatly given by a Poisson distribution in $|\alpha|^2$

$$\begin{aligned} P_n(\alpha) &= |\langle n|\alpha\rangle|^2 \\ &= exp\Big\{-|\alpha|^2\Big\}\frac{|\alpha|^{2n}}{n!} \; . \end{aligned} \tag{9}$$

The overlap between two canonical CS is

$$\langle\alpha|\alpha'\rangle = \exp\left(-\frac{|\alpha|^2}{2} - \frac{\left|\alpha'\right|^2}{2} + \alpha^*\alpha'\right) . \tag{10}$$

which implies that

$$\left|\langle\alpha|\alpha'\rangle\right|^2 = \exp\left[-\left|\alpha - \alpha'\right|^2\right] . \tag{11}$$

The canonical CS are nonorthogonal. The measure for this CS is

$$d\mu_+(\alpha) = \frac{1}{\pi} d\left[\mathrm{Re}(\alpha)\right] d\left[\mathrm{Im}(\alpha)\right] \tag{12}$$

so it holds that

$$1 = \frac{1}{\pi}\int_{-\infty}^{\infty}\int_{-\infty}^{\infty} d\left[\mathrm{Re}(\alpha)\right] d\left[\mathrm{Im}(\alpha)\right] |\alpha\rangle\langle\alpha| \; . \tag{13}$$

A second example of a CS is the spin CS [120, 121] which is associated to the general spin operators S_i $(i = x,\ y,\ z)$. By defining, as usual, the operators $S_\pm$ as

$$S_\pm = S_x \pm iS_y \; , \tag{14}$$

the set of spin CS $|\beta\rangle$ is defined

$$\begin{aligned} |\beta\rangle &= \sum_{M=-S}^{S} \sqrt{\frac{(2S)!}{(S-M)!(S+M)!}} \left[\frac{\beta^{S+M}}{\left(1+|\beta|^2\right)^S}\right] |SM\rangle \\ &= \frac{1}{\left(1+|\beta|^2\right)^S} \exp\left(\beta S_+\right)|S - S\rangle \end{aligned} \tag{15}$$

where β is the CS complex parameter, and the $|SM\rangle$; $S = 0,\ \frac{1}{2},\ 1,\ \ldots\ ;\ M = 0,\ \pm 1,\ \ldots\ S$ are the spin eigenstates. The overlap between two spin CS is

$$\langle\beta|\beta'\rangle = \frac{\left(1+\beta^*\beta'\right)^{2S}}{\left(1+|\beta|^2\right)^S\left(1+|\beta'|^2\right)^S}\ , \tag{16}$$

which implies

$$\left|\langle\beta|\beta'\rangle\right|^2 = \left(1-\frac{\left|\beta-\beta'\right|^2}{\left(1+|\beta|^2\right)^S\left(1+|\beta'|^2\right)^S}\right)^{2S}\ . \tag{17}$$

The spin CS are nonorthogonal as well. The measure of the spin CS is

$$d\mu_+(\beta) = \frac{d\left[\mathrm{Re}(\beta)\right]d\left[\mathrm{Im}(\beta)\right]}{\left(1+|\beta|^2\right)^2}\left(\frac{2s+2}{\pi}\right)\ . \tag{18}$$

A final example is the (bilinear) fermion CS [11], also known as the Thouless CS because of its direct relationship with the Thouless determinant function [110, 111], eq. 27, chapter 3[9]. For N identical fermions in a basis of dimension $K \geq N$, the normalized Thouless coherent state $|z\rangle$ is

$$|z\rangle = \det\left(I+z^\dagger z\right)^{-\frac{1}{2}}\exp\left[\sum_{h=1}^{N}\sum_{p=N+1}^{K} z_{ph}b_p^\dagger b_h\right]|\Psi_0\rangle \tag{19}$$

where the z_{ph}; $1 \leq h \leq N$; $N+1 \leq p \leq K$ is a set of complex parameters, the $b_i^\dagger$ and b_i the fermion creation and annihilation operators, and $|\Psi_0\rangle$ a single determinantal reference function. The overlap between two Thouless CS is $\langle z|z'\rangle = \det\left(I+z^\dagger z\right)^{-\frac{1}{2}}\det\left(I+z'^\dagger z'\right)^{-\frac{1}{2}}\det\left(I+z^\dagger z'\right)^{-\frac{1}{2}}$, which exemplifies another nonorthogonal CS. The measure of this CS is

$$d\mu_+(z) = d^2z\frac{\eta}{\det\left(I+z^\dagger z\right)^K} \tag{20}$$

where

$$d^2z = \prod_{ph}\frac{d\left[\mathrm{Re}\left(z_{ph}\right)\right]d\left[\mathrm{Im}\left(z_{ph}\right)\right]}{\pi}\ , \tag{21}$$

9. There exist other types of fermion CS; see Ref. [11] for further details.

and

$$\eta = \frac{1!2! \ldots K!}{1!2! \ldots (K-J)!1!2! \ldots J!} \tag{22}$$

Note that all the CS exemplified above satisfy the stronger version of the second condition for a CS.

The construction of a set of CS was, and partially still is, a matter of mathematical intuition since there was no general prescription to generate it. However, Perelomov [122] defined the so-called group-related CS which provides a general prescription for their construction. In brief, given an arbitrary Lie Group$G$ and one of its irreducible representations T on the Hilbert space $\mathcal{H}$, then all the elements $h \in G$ satisfying

$$T(h)|\psi_0\rangle = \exp\left[if(h)\right]|\psi_0\rangle \tag{23}$$

where $|\psi_0\rangle \in \mathcal{H}$ form the stability subgroup $H \subset G$. Then, the states

$$|\psi_{g(x)}\rangle = T[g(x)]|\psi_0\rangle \tag{24}$$

where $g(x)$ is one of the representatives of all elements of the group G, for which the vectors $|\psi\rangle = T(g)|\psi_0\rangle$ differ only from each other by a phase factor, do satisfy the above conditions of a CS, The three CS shown above belong to this category of CS. For instance, in the harmonic oscillator case, the group defining the set of CS is the Weyl group with generators $a^\dagger$ and a satisfying

$$\left[a^\dagger, a\right] = 1 \tag{25}$$

Although Perelomov prescription plays a very important role in the CS theory, there are many known CS which do not belong to this type (see Ref. 11 for different types of non group-related CS).

Quasi-Classical Coherent States

One of the most remarkable features of some sets of CS is their quasi-classical behavior. The definition of a quasi-classical state was already advanced in chapter 2 and will be further refined below. A state $|\psi_{qc}\rangle$, which is not necessarily a CS, is classified as quasi-classical if its operator averages in position x, momentum p, and some associated Hamiltonian H

$$\begin{aligned} x_{cq}(t) &= \langle\psi_{qc}|x|\psi_{qc}\rangle \ , \\ p_{cq}(t) &= \langle\psi_{qc}|p|\psi_{qc}\rangle \ , \\ H_{cq} &= \langle\psi_{qc}|H|\psi_{qc}\rangle \ , \end{aligned} \tag{26}$$

do generate a genuine set of classical Hamilton equations [61]

$$\begin{aligned} H_{qc} \ &= H_{qc}(x,p) \ , \\ \dot{x}_{qc}(t) &= \left(\frac{\partial H_{qc}}{\partial \dot{x}_{qc}}\right) \ , \\ \dot{p}_{qc}(t) &= \left(-\frac{\partial H_{qc}}{\partial \dot{p}_{qc}}\right) \ . \end{aligned} \tag{27}$$

In other words, the average position and momentum of the quasi-classical state evolve in time as the position and momentum some classical analogue do. Note that the definition of a quasi-classical state does not demand the SC limit of $\hbar \to 0$. It is important to emphasize that there is no *a priori* guaranty that a quasi-classical state may even exit for a given Hamiltonian. In general, the construction of a possible quasi-classical state is a very demanding task. To verify whether or not a proposed state $|\psi\rangle$ is quasi-classical, it is possible to make use of the Ehrenfest's theorem [119]

$$\begin{aligned} i\hbar\frac{d}{dt}\langle\psi|x|\psi\rangle &= \langle\psi|[x,H]\psi|\psi\rangle \ , \\ i\hbar\frac{d}{dt}\langle\psi|p|\psi\rangle &= \langle\psi|[p,H]\psi|\psi\rangle \ . \end{aligned} \tag{28}$$

Then, the state $|\psi\rangle$ is quasi-classical if the above Ehrenfest's set of equations reduces to the quasi-classical set, eq. 27. Note that the Ehrenfest's theorem itself does not provide a set of quasi-classical equations for an arbitrary state.

It can be proven through eq. 28 that the canonical CS $|\alpha\rangle$, eq. 7, is a quasi-classical state in the harmonic oscillator Hamiltonian H_{vib}. In ultimate instance, its quasi-classical equations turn out to be

$$\begin{aligned} \langle\alpha|x|\alpha\rangle &= x_\alpha(t) = \sqrt{\frac{2\hbar}{m\omega}}\,\mathrm{Re}[\alpha\exp(-i\omega t)]\,, \\ \langle\alpha|p|\alpha\rangle &= p_\alpha(t) = \sqrt{2m\hbar\omega}\,\mathrm{Im}[\alpha\exp(-i\omega t)] \end{aligned} \tag{29}$$

Moreover, the total energy E_α of the canonical CS is

$$\begin{aligned} E_\alpha &= H_{cq} \\ &= \langle\alpha|H_{vib}|\alpha\rangle \\ &= \hbar\omega|\alpha|^2 + \frac{\hbar\omega}{2} \\ &= E^\alpha_{class} + \frac{\hbar\omega}{2}\,, \end{aligned} \tag{30}$$

where E^α_{class} is the classical energy of the harmonic oscillator with the same values of x_α and p_α

$$E^\alpha_{class} = \frac{1}{2m}p^2_\alpha + m\omega^2 x^2_\alpha\,. \tag{31}$$

In addition, this CS also satisfies the interesting dynamical property that

$$\begin{aligned} |\alpha(t)\rangle &= \exp\left(-\frac{iH_{vib}}{\hbar}\right)|\alpha\rangle\,, \\ \alpha(t) &= \alpha\exp(-i\omega t)\,, \\ |\alpha(t)|^2 &= |\alpha|^2\,, \end{aligned} \tag{32}$$

i.e. the canonical CS remains as such during a time evolution in the harmonic oscillator Hamiltonian. Note also that the resolution of the canonical CS into the eigenstates $|n\rangle$, eq. 9 is time-independent. The canonical CS also satisfies the minimum uncertainty condition

$$\Delta x_\alpha(t)\Delta p_\alpha(t) = \hbar \tag{33}$$

where the deviations $\Delta x_\alpha(t)$ and $\Delta p_\alpha(t)$ are, respectively

$$\begin{aligned} \Delta x_\alpha(t) &= \Delta x_\alpha = \sqrt{\frac{\hbar}{2m\omega}}\,, \\ \Delta p_\alpha(t) &= \Delta p_\alpha = \sqrt{\frac{m\hbar\omega}{2}}\,, \end{aligned} \tag{34}$$

The minimum uncertainty condition seems to be related to the quasi-classical nature of some CS. Finally, it can be proven that the coordinate representative $\psi_\alpha(x,t)$ of this CS is

$$\begin{aligned}\psi_\alpha(x,t) &= \langle x|\alpha(t)\rangle \\ &= \exp\left[i\theta_\alpha(t)\right]\left(\frac{m\omega}{\pi\hbar}\right)^{\frac{1}{2}} \exp\left(-i\omega t\right)\times \\ &\quad \exp\left\{-\frac{\left[x-x_\alpha(t)\right]^2}{2\Delta x_\alpha}\right\}\exp\left[\frac{ip_\alpha(t)x}{\hbar}\right]\end{aligned} \tag{35}$$

where $\theta_\alpha(t)$ is a global phase.

The spin CS, eq. 15, can not be classified as quasi-classical because there is no Hamiltonian associated with it (however, see the section on rotational states in this chapter). On the other hand, minimum uncertainty conditions are known for this CS (see Ref. [11]). The Thouless CS is not a quasi-classical state. However, it is possible to obtain classical-like equations for the Thouless parameter via the TDVP as was shown by the QCSD END dynamical equations, eq. 35. In general, not all the types of CS exhibit a quasi-classical behavior. The construction of a quasi-classical state, coherent or not, for a given Hamiltonian is not a trivial pursuit. This problem is still an open area of research.

The Coherent State Theory and the QCSD END Theory

At this point, it is possible to make a comparison between the CS and the QCSD END theories. By inspecting the QCSD END wave function, eq. 18, it is immediate that the END electronic wave function $f_{el}[\mathbf{x}:\mathbf{z}(t),\mathbf{R}(t)]$, eq. 27, is exactly the unnormalized Thouless CS$|\mathbf{z}\rangle$, eq. 19. The very role of this CS is to provide a nonredundant and continuous parametrization of the single-determinant electronic wave function. The fact that this CS is not a quasi-classical state is irrelevant because it would be unrealistic to have a classical description for the average electronic position $\langle\mathbf{z}|x_{el}|\mathbf{z}\rangle$ and momentum $\langle\mathbf{z}|p_{el}|\mathbf{z}\rangle$. However, this CS does provide a set of classical-like equations for the Thouless

parameters $\mathbf{z}(t)$ and $\mathbf{z}^*(t)$ when subjected to a TDVP propagation as shown by the QCSD END dynamical equations, eq. 35.

The status of the END nuclear wave function $F_{nucl}[\mathbf{X}; \mathbf{R}(t), \mathbf{P}(t)]$ with respect to the CS theory is less direct. An inspection of the QCSD END dynamical equations, eq. 35, first reveals that its nuclear wave function is a model quasi-classical state. In other words, this nuclear function is not a genuine quasi-classical state but one generated by the model TDVP. Furthermore, by comparing the END nuclear function, eq. 19, with the coordinate representative of the canonical CS, eq. 35, it is easy to see that the coordinate components, $\mathbf{X}_k = \left(X_x^k, X_y^k, X_z^k\right)$, $k = 1, 2, \ldots N_{nucl}$, of the END Gaussian wave packets constitute a set of $3N_{nucl}$ independent canonical CS provided that the widthsb_k are equated to the position uncertainty Δx_α, eq. 34. Therefore, the QCSD END nuclear wave function is the canonical CS associated with a Hamiltonian which is the sum of $3N_{nucl}$ independent harmonic oscillator Hamiltonians H_{vib}. If the system Hamiltonian H_{total} happens to be that peculiar sum then both the TDVP and the exact propagations will generate the same quasi-classical dynamics when applied to the QCSD END wave function[10]. But if the system Hamiltonian is not of this type, as is the case of all the realistic system, then the TDVP must be applied if a quasi-classical behavior is sought.

The exact relationship between the CS and END theories shown in the previous paragraph can be restated in an approximate way of higher practical consequences. It will be proven in chapter 6 that under very general conditions the END nuclear wave function can be approximately factorized as

$$F_{nucl}[\mathbf{X}; \mathbf{R}(t), \mathbf{P}(t)] \approx F_{trans} F_{vib} F_{rot} \tag{36}$$

10. To this effect, it id necessary to constraint the electronic wave function to produce $3N_{nucl}$ independent harmonic potentials for the nuclei.

where F_{trans}, F_{vib} and F_{rot} are some functions associated with the translational, vibrational, and rotational degrees of freedom. If the vibrational and rotational functions can be further related to adequate quasi-classical states, respectively, then it will be possible to map the classical parameters $\mathbf{X}(t)$ and $\mathbf{P}(t)$ into the exact vibrational and rotational eigenstates of the system. For instance, it will be proven in chapter 6 that the vibrational function F_{vib} is closely related to the (quasi-classical) canonical CS if the system vibrational modes are nearly harmonic. In that case, each quasi-classical vibrational mode can be resolved into the harmonic oscillator eigenstates$|n\rangle$ through eq. 29 and 9. It is then possible to associate the (quasi-classical) canonical CS with the vibrational function F_{vib}. However, an analogous (quasi-classical) CS corresponding to the rotational function F_{rot} is still unknown. Unlike the canonical and the Thouless CS, the theory of rotational CS is by far less developed and known. In fact, it has been necessary to formulate a new rotational CS to complete the factorization scheme proposed in eq. 36. The derivation of this rotational CS is a mathematical problem in its own and it will be presented in the next section. After the rotational CS problem is solved in the next lines, the discussion about the factorization proposed in eq. 36 will be resumed in chapter 6.

It is worth noting that no attempt will be made to associate the translational function F_{trans}, with a CS. The reason for this deceptive inconsistency is that there is no CS theory for the unbound (continuous) translational states. However, it will be seen in chapter 6 that this translational function can be associated with the conventional SC theory.

A Proposed Rotational Coherent State for The END Theory

Previous Rotational Coherent States

Thera are relatively few references in the literature about the rotational CS theory. The most important contribution in that field was done by D. Janssen in 1977[123, 11].

This author derived a non group-related, quasi-classical, rotational CS for the general asymmetric rotor. Janssen CS $|xyz\rangle_{Janssen}$ can be expressed as

$$|xyz\rangle_{Janssen} = \sum_{\mathcal{I}\mathcal{M}\mathcal{K}} J_{\mathcal{I}\mathcal{M}\mathcal{K}}(x,y,z)|\mathcal{I}\mathcal{M}\mathcal{K}\rangle \tag{37}$$

where $|\mathcal{I}\mathcal{M}\mathcal{K}\rangle : \mathcal{I} = 0,\ \frac{1}{2},\ 1,\ \ldots\ ;\ \mathcal{M},\ \mathcal{K} = 0,\ \frac{1}{2},\ \ldots \pm\mathcal{I}$ are the integer (fermion) and half-integer (boson) rotational states associated with the symmetric rotor Hamiltonian, x, y, and z the CS parameters, and $J_{\mathcal{I}\mathcal{M}\mathcal{K}}(x,y,z)$ a set of coefficients. This CS satisfies quasi-classical dynamical equations when evolved by the asymmetric rotor Hamiltonian in the abstract Hilbert space containing the states $|\mathcal{I}\mathcal{M}\mathcal{K}\rangle$. It is obvious that this mathematical construct has not physical application since any real system has either integer (boson) or half-integer (fermion) quantum numbers associated to its angular degrees of freedom. Almost at the same time that Janssen, D. Bhaumik *et al.* formulated a relatively similar CS in terms of both integer and half-integer rotational states but for the simpler case of a symmetric rotor. This CS behaves quasi-classically only in the limit of $\hbar \to 0$. L. Fonda *et. al.* [124] wrote a more recent review about this subject. These authors analyzed a great variety of proposed rotational CS but again only for the symmetric rotor. Although their paper shed light into some aspects of the rotational CS theory, the examples therein presented seem to be scarcely useful for the END theory. The same reference did not analyzed the CS quasi-classical behavior in high detail and failed to mention the two rotational CS cited above.

In the rest of this chapter, a new rotational CS is derived in the spirit of Janssen CS formulation. This CS is expressed only in terms of integer rotational states so that it is quite appropriate to describe molecular rotors within the QCSD END theory. The derived CS does not exhibit an exact quasi-classical behavior; but this departure from the classical equations can be easily remedied. Also, a general proof is also presented

that if the half-integer rotational states are excluded from this type of constructs then an exact quasi-classical rotational CS can not be obtained. This proof does not necessarily denies the existence of a quasi-classical rotational CS with only integer rotational states of another type. However, the formulation of such an hypothetical CS remains still unknown.

Rotational Hamiltonian and Related Operators

The pure rotational Hamiltonian for a molecular system can be written as [25]

$$H_{rot} = \frac{L_x^2}{2I_x} + \frac{L_y^2}{2I_y} + \frac{L_z^2}{2I_z} \tag{38}$$

where $I_i \quad (i = x,\ y,\ z)$ are the principal axis momenta of inertia, and L_i the body-fixed components of the angular momentum. The problem is restricted to orbital angular momentum of integer quantum numbers. Given the space-fixed components of the angular momentum J_i ($J^2 = L^2$), the following relationships hold

$$[J_i, J_j] = i\varepsilon_{ijl}J_l: \quad [L_i, L_j] = -i\varepsilon_{ijl}L_l \tag{39}$$

and

$$[J_i, L_k] = \quad \left[L^2, L_z\right] = \left[J^2, J_z\right] = 0 \tag{40}$$

where ε_{ikl} are the components of the Levi-Civita tensor. Note the anomalous commutation relationships [25] in the L_i components. As a result of these commutation relationships, there exists a complete set of rotational eigenstates $|IMK\rangle$ so that

$$\begin{aligned} L^2|IMK\rangle &= I(I+1)|IMK\rangle: \quad I = 0,\ 1,\ 2,\ ... \\ L_z|IMK\rangle &= K|IMK\rangle: \qquad K = 0,\ \pm 1,\ ...,\ \pm I \\ J_z|IMK\rangle &= M|IMK\rangle: \qquad M = 0,\ \pm 1,\ ...,\ \pm I \end{aligned} \tag{41}$$

These rotational eigenstates in position ("angular") representation are

$$\langle\phi, \theta, \chi|IMK\rangle = \left[\frac{2I+1}{8\pi^2}\right]^{\frac{1}{2}} D^{I*}_{MK}(\phi, \theta, \chi) \tag{42}$$

where $D^{I}_{MK}(\phi, \theta, \chi)$ is a rotation matrix (Wigner D function) [25].

From the previous commutators, it is immediate that the rotational Hamiltonian satisfies the flowing relationships

$$\begin{aligned} [H_{rot}, J_i] &= 0 \\ \left[H_{rot}, J^2\right] &= 0 \end{aligned} \tag{43}$$

It follows from them that the Hamiltonian eigenfunctions Ψ^{α}_{IM} must satisfy

$$\begin{aligned} H_{rot}\Psi^{\alpha}_{IM} &= E^{\alpha}_{rot}\Psi^{\alpha}_{IM} \\ J^2\Psi^{\alpha}_{IM} &= I(I+1)\Psi^{\alpha}_{IM} \qquad I = 0,\ 1,\ 2,\ \ldots \\ J_z\Psi^{\alpha}_{IM} &= M\Psi^{\alpha}_{IM} \qquad\quad M = 0,\ \pm 1,\ \ldots,\ \pm I \end{aligned} \tag{44}$$

where the superscript α is, after I and M. a third quantum number to label a particular rotational eigenstate. On the other hand, and with respect to the L_i operators, it is not difficult to prove by appealing to their commutator relationships that

$$[H_{rot}, L_i] = i \sum_{j} \frac{\varepsilon_{ijk}}{2I_k}(L_j L_k + L_k L_j) \tag{45}$$

The Ψ^{α}_{IM} eigenfunctions can be accordingly expressed as

$$\Psi^{\alpha}_{IM} = \sum_{K} c^{IM\alpha}_{K} |IMK\rangle \tag{46}$$

where the coefficients $c^{IM\alpha}_{K}$ are to be determined.

In the special case of a spherical rotor, $I = I_x = I_y = I_z$ (*e.g.* CH_4 and SF_6), and the eigenvalue problem simplifies considerably

$$\begin{aligned} H_{rot} &= \frac{L^2}{2I} = \frac{J^2}{2I} \\ \Psi^{\alpha}_{IM} &= \Psi_{IM} = |IMK\rangle \\ E^{IM\alpha}_{rot} &= E^{I}_{rot} = \frac{I(I+1)}{2I} \end{aligned} \tag{47}$$

In the case of a prolate symmetric rotor, $I_x \leq I_y = I_z$ (*e.g.* CH_3Cl and PCl_5), and the eigenvalue problem becomes

$$\begin{aligned} H_{rot} &= \frac{L^2}{2I_z} + \left(\frac{1}{2I_x} - \frac{1}{2I_z}\right) L_z^2 \\ \Psi_{IM}^{\alpha} &= \Psi_{IM} = |IMK\rangle \\ E_{rot}^{IM\alpha} &= E_{rot}^{IM} = \frac{I(I+1)}{2I_z} + \left(\frac{1}{2I_x} - \frac{1}{2I_z}\right) K^2 \end{aligned} \tag{48}$$

The equivalent expressions for the case of a oblate symmetric rotor, $I_x = I_y \leq I_z$ (*e.g.* $CHCl_3$ and C_6H_6) can be obtained by interchanging the I_x with the I_z in the last equations. The linear rotor (*e.g.* all the diatomics, CO_2 and C_2H_2) is the $I_x = 0$ limit of the prolate symmetric one. In that case,

$$\begin{aligned} H_{rot} &= \frac{J^2}{2I} \\ \Psi_{IM}^{\alpha} &= \Psi_{IM} = |IM0\rangle \\ E_{rot}^{IM\alpha} &= E_{rot}^{I} = \frac{I(I+1)}{2I} \\ \langle \theta, \phi | IM0 \rangle &= Y_{IM}(\theta, \phi) \end{aligned} \tag{49}$$

where the $Y_{IM}(\theta, \phi)$ are the spherical harmonics [25]. Finally, in the case of an asymmetric rotor, $I_x \leq I_y \leq I_z$ (e.g. CH_2H_2), the eigenfunctions Ψ_{IM}^{α} keep their linear combination form, and the $c_K^{IM\alpha}$ coefficients must be specifically calculated.

Group Relationships

Although the present CS is no group-related, the group relationship around the rotational states is briefly discussed for sake of completeness. The (orbital) rotational states $|IMK\rangle$ span the irreducible representation of the semidirect product of the $SO(3) \times SO(3)$ group with an abelian group. The generators of the first $SO(3)$ group are the L_i which satisfy

$$[L_i, L_k] = -i\varepsilon_{ikl} L_l \tag{50}$$

For the second $SO(3)$ group, we have the generators J_i, which satisfy

$$[J_i, J_k] = i\varepsilon_{ikl} J_l \tag{51}$$

The generators of the abelian group belong to a family of operators $T^{\lambda}_{\mu\nu}$ $\left(\lambda = 0,\ \frac{1}{2},\ 1,\ \frac{3}{2},\ ...;\ \mu,\ \nu = 0,\ \pm\frac{1}{2},\ ....,\ \pm\lambda\right)$ which satisfy

$$\left[T^{\lambda}_{\mu\nu}, T^{\lambda}_{\mu'\nu'}\right] = 0 \tag{52}$$

These operators are a three -subscript generalization of the regular spherical tensor operators . In Ref. 123, $\lambda = \frac{1}{2}$ was used, rendering four generators for the abelian group. However, these operators connect integral (boson) and half-integral (fermion) states. In our case, we should use $\lambda = 1$ to avoid such a "mixing" (see Appendix A). This selection renders nine generators for the abelian group. The relationships among the two $SO(3)$ groups generators are

$$[J_i, L_k] = 0 \tag{53}$$

To obtain the remaining cross relationships among the generators, the commutator properties of the regular two-subscript spherical tensor operators are generalized to act [25] with both L_i and J_i. The new relationships turn out to be (for a general λ)

$$\begin{aligned} \left[L_z, T^{\lambda}_{\mu\nu}\right] &= \nu T^{\lambda}_{\mu\nu} \\ \left[J_z, T^{\lambda}_{\mu\nu}\right] &= \mu T^{\lambda}_{\mu\nu} \end{aligned} \tag{54}$$

and

$$\begin{aligned} \left[L_{\pm}, T^{\lambda}_{\mu\nu}\right] &= \left[\lambda(\lambda+1) - \nu(\nu \pm 1)\right]^{\frac{1}{2}} T^{\lambda}_{\mu\nu\pm\lambda} \\ \left[J_{\pm}, T^{\lambda}_{\mu\nu}\right] &= \left[\lambda(\lambda+1) - \mu(\mu \pm 1)\right]^{\frac{1}{2}} T^{\lambda}_{\mu\pm\lambda} \end{aligned} \tag{55}$$

where

$$\begin{aligned} L_{\pm} &= L_x \pm iL_y \\ J_{\pm} &= J_x \pm iJ_y \end{aligned} \tag{56}$$

Note that these relationships have been equally defined in both the body and the space frames.

The action of the $T^{\lambda}_{\mu\nu}$ operators on the rotational states $|IMK\rangle$ deserves more attention since they are little known (or unknown) out of this context. By appealing to the above commutator relationships, it is possible to prove that these operators change the three indexes of $|IMK\rangle$ and multiply this function by a factor. These properties are explicitly derived in appendix B. Such formulae also complete the proof that the $|IMK\rangle$ spans the irreducible representations of the above groups products. Here, it suffices to bear in mind that

$$T^{\lambda}_{-\lambda-\lambda}|I\ -I\ -I\rangle = |I+\lambda\ -I-\lambda\ -I-\lambda\rangle \tag{57}$$

Coherent State Construction

Because the rotational quantum mechanical problem involves three quantum number, we need three independent complex parameter $x,\ y,\ and\ z$ to define a new set of CS $|xyz\rangle$. Perelemov's prescription [122] would make that set be

$$|xyz\rangle_{Perelemov} \sim e^{xJ_+}e^{zL_+}e^{yT^1_{-1-1}}|000\rangle \tag{58}$$

However, this CS does not exhibit the sought quasi-classical properties of a rotor. Therefore, by modifying Janssen's construction [123], the proposed CS state CS $|xyz\rangle$ is

$$\begin{aligned}|xyz\rangle = &\exp\left[-\frac{1}{2}yy^*(1+xx^*)^2(1+zz^*)^2\right]\times \\ &e^{xJ_+}e^{zL_+}exp\left[y\sqrt{\widehat{I}}\ T^1_{-1-1}\right]|000\rangle\end{aligned} \tag{59}$$

where the operator $\widehat{I}$ is defined by (cf. Ref. [123])

$$\widehat{I}|IMK\rangle = I|IMK\rangle \tag{60}$$

This operator is a pure mathematical device to simplify some expressions not having any physical meaning. Notice the subtle differences in the normalization factor and in the

right exponential operator with respect to those in Ref. [123]. It can be seen that

$$\begin{aligned}\exp\left(y\sqrt{\hat{I}}\,T_{-1-1}^{\frac{1}{}}\right)|000\rangle &= \sum_{I=0,\,1,\,...}^{\infty}\frac{\left(y\sqrt{\hat{I}}\,T_{-1-1}^{\frac{1}{}}\right)^{I}}{I!}|000\rangle \\ &= \sum_{I=0,\,1,\,...}^{\infty}\frac{y^{I}}{\sqrt{I!}}|I-I-I\rangle\end{aligned} \tag{61}$$

and

$$\begin{aligned}e^{zL_{+}}|I-I-I\rangle &= \sum_{n=0}^{\infty}\frac{z^{n}}{n!}L_{+}^{n}|I-I-I\rangle \\ &= \sum_{n=0}^{2I}\frac{z^{n}}{n!}\{2I(2I-1)\,...[2I-(n-1)]\}^{\frac{1}{2}}(n!)^{\frac{1}{2}}|I-I-I+n\rangle \\ &= \sum_{K=-I}^{I}\frac{z^{(I+K)}}{[(I+K)!]^{\frac{1}{2}}}\{2I(2I-1)\,...[2I-(I+K-1)]\}^{\frac{1}{2}} \\ &\qquad |I-I\;\;K\rangle \\ &= \sum_{K=-I}^{I}\frac{z^{(I+K)}}{[(I+K)!]^{\frac{1}{2}}}\left[\frac{(2I)!}{(I-K)!}\right]^{\frac{1}{2}}|I-I\;\;K\rangle\end{aligned} \tag{62}$$

where $n = I + K$ has been used from the second to the third line. By changing M for K, and L_+ for J_+, the analogous expansion of $e^{xJ_+}|I-I-I\rangle$ is obtained. Notices that these two expressions are still valid for a half-integer I. Therefore, the set of CS becomes

$$\begin{aligned}|xyz\rangle = &\exp\left[-\frac{1}{2}yy^{*}(1+xx^{*})^{2}(1+zz^{*})^{2}\right]\times \\ &\sum_{IMK}\left\{\frac{[(2I)!]^{2}}{(I+M)!\,(I-M)!\,(I+K)!\,(I-K)!}\right\}^{\frac{1}{2}}\times \\ &\frac{x^{(I+M)}y^{I}z^{(I+K)}}{(I!)^{\frac{1}{2}}}|IMK\rangle\end{aligned} \tag{63}$$

Each CS in this set is normalized to one since

$$\begin{aligned}
\langle xyz|xyz\rangle &= \exp\left[-yy^*(1+xx^*)^2(1+zz^*)^2\right]\times \\
&\quad \sum_{IMK}\frac{[(2I)!]^2}{(I+M)!\,(I-M)!\,(I+K)!\,(I-K)!}\times \\
&\quad \frac{(xx^*)^{(I+M)}\;(yy^*)^I\;(zz^*)^{(I+K)}}{I!} \\
&= \exp\left[-yy^*(1+xx^*)^2(1+zz^*)^2\right]\times \\
&\quad \sum_{I=0}^{\infty}\frac{(yy^*)^I}{I!}\sum_{M=-I}^{I}\frac{(2I)!\,(xx^*)^{(I+M)}}{(I+M)!\,(I-M)!} \\
&\quad \sum_{K=-I}^{I}\frac{(2I)!\,(zz^*)^{(I+K)}}{(I+K)!\,(I-K)!} \\
&= \exp\left[-yy^*(1+xx^*)^2(1+zz^*)^2\right]\times \\
&\quad \sum_{I=0}^{\infty}\frac{\left[(yy^*)(1+xx^*)^2(1+zz^*)^2\right]^I}{I!} \\
&= 1
\end{aligned} \tag{64}$$

where the power expansion of $(1+zz^*)^{2I}$

$$(1+zz^*)^{2I} = \sum_{K=-I}^{I}\frac{(2I)!}{(I+K)!\,(I-K)!}(zz^*)^{I+K} \tag{65}$$

and the analogous one of $(1+xx^*)^{2I}$ have been used from the second to the third line. Notice the appearance of a Poisson distribution in the variable $yy^*(1+xx^*)^2(1+zz^*)^2$ in the third line. By the same token, it is quite similar to prove that the overlap $\langle x'y'z'|xyz\rangle$ between two different Coherent States is

$$\begin{aligned}
\langle x'y'z'|xyz\rangle = &\exp\left[-\frac{1}{2}yy^*(1+xx^*)^2(1+zz^*)^2\right]\times \\
&\exp\left[-\frac{1}{2}y'y'^*\left(1+x'x'^*\right)^2\left(1+z'z'^*\right)^2\right]\times \\
&\exp\left[yy'^*\left(1+xx'^*\right)^2\left(1+zz'^*\right)^2\right]
\end{aligned} \tag{66}$$

i.e. the set of states is nonorthogonal.

Because of their construction, the $|xyz\rangle$ states do satisfy the first CS condition. To certify whether these states also satisfy the second condition, it is necessary to construct a

proper measure $d\mu$, a procedure with no predetermined prescription. Taken into account the signed measure of Ref. 123 and after considerable thinking, it is obtained (see appendix C)

$$d\mu_{\pm}(x,y,z) = \frac{1}{\pi^3}\{4\left[(1+xx^*)(1+zz^*)\right]^4 (yy^*)^2 \\ -8\left[(1+xx^*)(1+zz^*)\right]^2 yy^*+1\}\, dxdydz \tag{67}$$

where

$$dx = dRe(x)dIm(x),\ dy = dRe(y)dIm(y),\ dz = dRe(z)dIm(z) \tag{68}$$

so that

$$\int d\mu_{\pm}(x,y,z)|xyz\rangle\langle xyz| = \sum_{IMK} |IMK\rangle\langle IMK| \\ = 1 \tag{69}$$

Then, it is almost immediate that

$$|IMK\rangle = \int d\mu_{\pm}(x,y,z)\ \exp\left[-\frac{1}{2}yy^*(1+xx^*)^2(1+zz^*)^2\right]\times \\ x^{*I+M}y^{*I}z^{*I+K}\times \\ \left\{\frac{[(2I)!]^2}{I!\,(I+M)!\,(I-M)!\,(I+K)!\,(I-K)!}\right\}^{\frac{1}{2}}|xyz\rangle. \tag{70}$$

Note that both the CS from Ref. 123 and the present one satisfy the weaker version of the second condition for a CS.

Operator Averages in The Coherent State

The next step is to evaluate some important operator averages in the CS. This can be done by direct evaluation of the integrals shown below. Such a procedure involves using some properties of the binomial power expansion and of the Poisson distribution, as in the case of the normalization. Some examples of these calculations are shown in appendix D. The net results are

$$\langle xyz|I|xyz\rangle = yy^*(1+xx^*)^2(1+zz^*)^2 \tag{71}$$

$$\begin{aligned}
\langle xyz|L_x|xyz\rangle &= \frac{z+z^*}{1+zz^*}\langle xyz|I|xyz\rangle \\
\langle xyz|L_y|xyz\rangle &= \frac{i(z-z^*)}{1+zz^*}\langle xyz|I|xyz\rangle \\
\langle xyz|L_z|xyz\rangle &= \frac{(zz^*-1)}{1+zz^*}\langle xyz|I|xyz\rangle
\end{aligned} \tag{72}$$

$$\begin{aligned}
\langle xyz|L_x^2|xyz\rangle &= \langle xyz|L_x|xyz\rangle^2 \\
&\quad + \frac{\left[1+4zz^*+z^2+z^{*2}+(zz^*)^2\right]}{2\left(1+zz^*\right)^2}\langle xyz|I|xyz\rangle \\
\langle xyz|L_y^2|xyz\rangle &= \langle xyz|L_y|xyz\rangle^2 \\
&\quad + \frac{\left[1+4zz^*-z^2-z^{*2}+(zz^*)^2\right]}{2\left(1+zz^*\right)^2}\langle xyz|I|xyz\rangle \\
\langle xyz|L_z^2|xyz\rangle &= \langle xyz|L_z|xyz\rangle^2 + \left(\frac{2z^*}{1+zz^*}\right)^2\langle xyz|I|xyz\rangle
\end{aligned} \tag{73}$$

and

$$\begin{aligned}
\langle xyz|L_iL_j+L_jL_i|zyz\rangle &= 2\langle xyz|L_i|xyz\rangle\langle xyz|L_j|xyz\rangle \\
&\quad + \frac{\langle xyz|L_i|xyz\rangle\langle xyz|L_j|xyz\rangle}{\langle xyz|I|xyz\rangle}
\end{aligned} \tag{74}$$

By changing L_i for J_i, and z for x, the averages of the components of J are immediately obtained. The integral $\langle xyz|I|xyz\rangle$ turns out to be slightly different from that of Ref. 123. However, the form of the first-order averages as a function of that primordial integral remains the same.

Parameterization in Physical Terms

In order to physically interpret the CS, a new parameterization must be introduced. This is

$$\begin{aligned}
x &= -e^{-i\alpha}tg\left(\frac{\beta+\pi}{2}\right) \\
z &= -e^{-i\gamma}tg\left(\frac{\theta+\pi}{2}\right) \\
y &= r\cos^2\left(\frac{\beta}{2}\right)\cos^2\left(\frac{\theta}{2}\right)e^{i(\alpha+\gamma+\varphi)}
\end{aligned} \tag{75}$$

where $0 \le r \le \infty$, $0 \le \alpha,\ \gamma,\ \varphi \le 2\pi$ and $0 \le \beta,\ \theta \le \pi$. The interpretation of these new variables will be clear shortly. Note that the new parameterization differs form that

in Ref. [123]. From the above definition, it follows that

$$
\begin{aligned}
& xx^* = \tan^2\left(\frac{\beta+\pi}{2}\right); \quad zz^* = \tan^2\left(\frac{\theta+\pi}{2}\right) \\
& (1+xx^*)^2 = \left[1+\tan^2\left(\frac{\beta+\pi}{2}\right)\right]^2 = \frac{1}{\cos^4\left(\frac{\beta+\pi}{4}\right)} \\
& (1+zz^*)^2 = \left[1+\tan^2\left(\frac{\theta+\pi}{2}\right)\right]^2 = \frac{1}{\cos^4\left(\frac{\theta+\pi}{4}\right)} \\
& yy^* = r\cos^4\left(\frac{\beta+\pi}{4}\right)\cos^4\left(\frac{\theta+\pi}{4}\right) \\
& yy^*(1+xx^*)^2(1+zz^*)^2 = r
\end{aligned}
\tag{76}
$$

The CS then becomes

$$
\begin{aligned}
|xyz\rangle &= |\alpha\beta\gamma\theta\varphi r\rangle \\
&= \exp\left(-\frac{r}{2}\right)\sum_{IMK}(-1)^{M+K}\left\{\frac{[(2I)!]^2}{(I+K)!(I-K)!(I+M)!(I-M)!}\right\}^{\frac{1}{2}}\times \\
&\qquad \left[e^{-iM\alpha}\sin^{I+M}\left(\frac{\beta}{2}\right)\cos^{I-M}\left(\frac{\beta}{2}\right)e^{iI\gamma}\right]\times \\
&\qquad \left[e^{-iK\alpha}\sin^{I+K}\left(\frac{\theta}{2}\right)\cos^{I-K}\left(\frac{\theta}{2}\right)\right]\frac{r^{\frac{I}{2}}}{\sqrt{I!}}|IMK\rangle
\end{aligned}
\tag{77}
$$

$$
= \exp\left(-\frac{r}{2}\right)\sum_{IMK} D^I_{M-I}(\alpha,\beta,\gamma)D^I_{K-I}(\varphi,\theta,0)\frac{r^{\frac{I}{2}}}{\sqrt{I!}}|IMK\rangle
$$

where the analytical definition of the rotation matrices (Wigner D functions)$D^I_{MK}(\alpha,\beta,\gamma)$ [25] has been used in the last line.

The operator averages in the CS are now ($|\alpha\beta\gamma\theta\phi r\rangle = |coh\rangle$)

$$
\langle coh|I|coh\rangle = r \tag{78}
$$

$$
\begin{aligned}
&\langle coh|L_x|coh\rangle = r\cos(\varphi)\sin(\theta); \qquad \langle coh|J_x|coh\rangle = r\cos(\alpha)\sin(\beta) \\
&\langle coh|L_y|coh\rangle = r\sin(\varphi)\sin(\theta); \qquad \langle coh|J_y|coh\rangle = r\sin(\alpha)\sin(\beta) \\
&\langle coh|L_z|coh\rangle = r\cos(\theta); \qquad\qquad \langle coh|J_z|coh\rangle = r\cos(\beta)
\end{aligned}
\tag{79}
$$

and

$$
\langle coh|L^2|coh\rangle = \langle coh|J^2|coh\rangle = r(r+2) \tag{80}
$$

From these expressions, it follows that the parameter r is the angular momentum modulus, the pairs of angles $\varphi,\ and\ \theta$, and $\alpha\ and\ \beta$ are the azimuthal and the polar angle of $\langle\vec{L}\rangle\ and\ \langle\vec{J}\rangle$ vectors in the body-fixed and laboratory frame, respectively. The angle γ determines the relative orientation of the body-fixed frame with respect to the space-fixed one. Finally, the probability P_{IMK} to find the rotational state $|IMK\rangle$ in the CS is

$$P_{IMK}(\beta,\theta) = \left\{\frac{[(2I)!]^2}{(I+K)!(I-K)!(I+M)!(I-M)!}\right\}\times \left[\sin^{2(I+M)}\left(\frac{\beta}{2}\right)\cos^{2(I-M)}\left(\frac{\beta}{2}\right)\right]\times \left[\sin^{2(I+K)}\left(\frac{\theta}{2}\right)\cos^{2(I-K)}\left(\frac{\theta}{2}\right)\right]\exp(-r)\frac{r^I}{I!} \tag{81}$$

$$= \left\{\frac{[(2I)!]^2}{(I+K)!(I-K)!(I+M)!(I-M)!}\right\}p^{(I+M)}(1-p)^{(I-M)}\times q^{(I+K)}(1-q)^{(I-M)}\exp(-r)\frac{r^I}{I!}$$

where p is $0 \le p = \sin^2(\theta) \le 1$, and q is $0 \le q = \sin^2(\beta) \le 1$. Notice that the resolution P_{IMK} combines a binomial distribution in p, a binomial distribution in q, and a Poisson distribution in r. It is easy to see that

$$\sum_{I=0,\,1,\,\ldots}^{\infty}\ \sum_{M=-I}^{I}\ \sum_{K=-I}^{I} P_{IMK}(\beta,\theta) = 1 \tag{82}$$

Time Evolution of The Coherent State

The time-evolution of the proposed set of CS is now analyzed. The Ehrenfest's theorem applied to the operators L_i is now

$$\frac{d}{dt}\langle coh|L_i|coh\rangle = i\langle coh|[H_{rot}, L_i]|coh\rangle = -\langle coh|\sum_j \varepsilon_{ijk}\frac{1}{2I_k}(L_jL_k + L_kL_j)|coh\rangle \tag{83}$$
$$(i = x,\ y,\ z)$$

By introducing a quasi-classical definition for the angular velocity $\boldsymbol{\omega}$ as

$$\omega_i = \frac{\langle coh|L_i|coh\rangle}{I_i} \tag{84}$$

and using the previous averages, it is finally obtained that

$$\begin{aligned}
\dot{\omega}_x &= \frac{\omega_y \omega_z}{I_x}(I_y - I_z)\left(1 + \frac{1}{2r}\right) , \\
\dot{\omega}_y &= \frac{\omega_x \omega_z}{I_y}(I_x - I_z)\left(1 + \frac{1}{2r}\right) , \\
\dot{\omega}_z &= \frac{\omega_x \omega_y}{I_z}(I_x - I_y)\left(1 + \frac{1}{2r}\right) , \\
& r > 0 .
\end{aligned} \tag{85}$$

This is almost a set of Euler's equations of motion for a rigid body with one point fixed [61]. The last equations show the **almost** quasi-classical behavior of the proposed set of CS. The rotational CS will be exactly quasi-classical in the limit of $r \to \infty$ (high angular momentum) which is equivalent to the SC limit of $\hbar \to 0$. Since the value of r is time-independent, it is possible to define an effective quasi-classical angular velocity $\boldsymbol{\omega}^{eff}$

$$\omega_i^{eff} = \frac{\langle coh|L_i|coh\rangle}{I_i}\left(1 + \frac{1}{2r}\right); \ (r > 0), \tag{86}$$

so that eq. 85 can be rewritten as

$$\begin{aligned}
\dot{\omega}_x^{eff} &= \frac{\omega_y^{eff} \omega_z^{eff}}{I_x}(I_y - I_z) , \\
\dot{\omega}_y^{eff} &= \frac{\omega_x^{eff} \omega_z^{eff}}{I_y}(I_x - I_z) , \\
\dot{\omega}_z^{eff} &= \frac{\omega_x^{eff} \omega_y^{eff}}{I_z}(I_x - I_y) .
\end{aligned} \tag{87}$$

Note that

$$\lim_{r \to \infty} \boldsymbol{\omega}^{eff} = \boldsymbol{\omega} . \tag{88}$$

The behavior of these equations when $r = 0$ can be seen in appendix D The proof that an exact quasi-classical CS in terms of only integer rotational states can not be constructed in the spirit of Janssen CS is shown in Ref. 125.

CHAPTER 5
THE CROSS SECTIONS IN THE DIFFERENT THEORIES

Quantum Cross Sections

General Definition

The quantum mechanical formulation of cross sections stems directly from their general definitions given in chapter 2 . The S-matrix plays a central role in the quantum formulation. Once this matrix has been determined from the system dynamics, the further calculation of the cross sections is relatively less demanding. The formulation of the cross sections is usually done in the time-independent scheme [13] despite the fact that the dynamics and the S-matrix may have been calculated time-independently. A more involving time-dependent formulation of cross sections can be found in Ref. [3]. Below, the time-independent version of this subject is presented. Some of these expressions will be of use in the further discussion of the subject.

For a general scattering processes, the asymptotic boundary conditions of the nuclear function $G_j^{\lambda}(\mathbf{X})$ in the CM frame can be written, eq.30, 2,

$$\lim_{\mathbf{X}_\lambda \to \infty} G_j^{\lambda}(\mathbf{X}_\lambda) = \delta_{ij}\delta_{\lambda,1} e^{ik_j z_1} + f_{ij}^{\lambda}(\theta_\lambda, \gamma_\lambda)\frac{e^{ik_j^{\lambda} r_\lambda}}{r_\lambda}. \tag{1}$$

The index λ denotes the different arrangements of the products; the value $\lambda = 1$ has been adopted for the non reactive arrangement. The index i for the entrance channel, and the indices j for the exit channels are a shorthand notation of the quantum numbers corresponding to the initial and final state at the proper arrangements. Note that both the plane wave $e^{ik_i^1 z_1}$ and the spherical $\frac{e^{ik_j^1 r_\lambda}}{r_\lambda}$ components are not normalized. The different

ingredients to derive the quantum DCS according to its general definition, eq. 2, chapter 2, can be obtained by evaluating the modulus of the current density $\mathbf{j}_j^\lambda$

$$\mathbf{j}_\mathbf{j}^\lambda = \frac{i\hbar}{2m_\lambda}\left(\Psi_j^{\lambda *}\nabla\Psi_j^\lambda - \Psi_j^\lambda\nabla\Psi_j^{\lambda *}\right) \tag{2}$$

where m_λ and Ψ_j^λ are the reduced mass and the wave function components in the channel j of the arrangement λ. The symmetry of the incoming component in the entrance channel, the plane wave $e^{ik_i^1 z_1}$, calls for a gradient operator in Cartesian form

$$\nabla_\lambda = \mathbf{i}\frac{\partial}{\partial \mathbf{x}_\lambda} + \mathbf{j}\frac{\partial}{\partial \mathbf{y}_\lambda} + \mathbf{k}\frac{\partial}{\partial \mathbf{z}_\lambda}. \tag{3}$$

Then, it is straightforward to prove that the current density of the incoming components at the entrance channel $\mathbf{j}_i^{\lambda\,(in)}$ is

$$\begin{aligned}\mathbf{j}_i^{\lambda\,(in)} &= -\frac{i\hbar}{2m_i}\left[e^{ik_i^1 z_1}\nabla_1 e^{-ik_i^1 z_1} + e^{-ik_i^1 z_1}\nabla_1 e^{ik_i^1 z_1}\right] \\ &= \frac{\hbar}{m_i}\mathbf{k}_\mathbf{i}^\mathbf{1} \\ &= \mathbf{v}_\mathbf{i}^\mathbf{1}\end{aligned} \tag{4}$$

where $\mathbf{v}_\mathbf{i}^\lambda$ is the reactants relative velocity. The initial beam intensity I_0 is within an unknown normalization factor proportional to that velocity

$$I_0 \propto v_i \tag{5}$$

The current density associated with the spherical outgoing components (including that of the entrance channel) can be calculated with the gradient operator in orthogonal spherical coordinates [49]

$$\nabla_\lambda = \mathbf{n}\frac{\partial}{\partial r_\lambda} + \mathbf{l}\frac{\partial}{r_\lambda \partial\theta_\lambda} + \mathbf{m}\frac{\partial}{r_\lambda \sin\theta_\lambda \partial\phi_\lambda}. \tag{6}$$

However, only the first term of the above gradient must be retained in the asymptotic region because there $r_\lambda \to \infty$. Therefore, the current density of the outgoing channels is

$$\begin{aligned}\mathbf{j}_j^\lambda &= -\frac{i\hbar}{2m_\lambda}|f_{ij}(\theta_\lambda,\gamma_\lambda)|^2\left[\frac{e^{-ik_j^\lambda r_\lambda}}{r_\lambda}\nabla\left(\frac{e^{ik_j^\lambda r_\lambda}}{r_\lambda}\right)+\frac{e^{ik_j^\lambda r_\lambda}}{r_\lambda}\nabla\left(\frac{e^{-ik_j r}}{r_\lambda}\right)\right]\\ &= \frac{\hbar}{m_\lambda r_\lambda^2}|f_{ij}(\theta_\lambda\colon\gamma_\lambda)|^2\mathbf{k}_j^\lambda\\ &= \frac{1}{r_\lambda^2}\left|f_{ij}^\lambda(\theta;\gamma)\right|^2\mathbf{v}_j^\lambda\end{aligned} \tag{7}$$

where $\mathbf{v}_\mathbf{j}^\lambda$ is the velocity vector associated to the channel j. The number of particles $d\dot{N}_i^\lambda(\theta_\lambda,\gamma_\lambda)$ scattered per unit time through an areas $dS_\lambda = r_\lambda^2\sin\theta_\lambda\ d\theta_\lambda d\gamma_\lambda$ is within an undetermined normalization factor proportional to the last current density

$$\begin{aligned}d\dot{N}_j^\lambda(\theta_\lambda,\gamma_\lambda) &\propto \left|\mathbf{j}_j{}^{out}\right|r_\lambda^2\sin\theta_\lambda\ d\theta_\lambda d\gamma_\lambda\\ &\propto \left|f_{ij}^\lambda(\theta_\lambda\colon\gamma_\lambda)\right|^2 v_j^\lambda\sin\theta_\lambda\ d\theta_\lambda d\gamma_\lambda\end{aligned} \tag{8}$$

Therefore, the DCS through the solid angle $d\Omega_\lambda(\theta_\lambda,\gamma_\lambda) = \sin\theta_\lambda\ d\theta_\lambda d\gamma_\lambda$ for the scattering processes from the initial state i to the final state j is

$$\begin{aligned}\frac{d\sigma_{i\to f}^\lambda}{d\Omega_\lambda}(\theta_\lambda,\varphi_\lambda) &= \frac{d\dot{N}_{i\to f}^\lambda(\theta_\lambda,\varphi_\lambda)}{I_0 d\Omega(\theta_\lambda,\varphi_\lambda)}\\ &= \frac{m_1 k_j^\lambda}{m_\lambda k_i^1}\left|f_{ij}^\lambda(\theta_\lambda\colon\gamma_\lambda)\right|^2.\end{aligned} \tag{9}$$

The scattering amplitude $f_{ij}^\lambda(\theta_\lambda\colon\gamma_\lambda)$ is then strongly associated to the DCS. Notice the ratio of reduced masses and wave vectors in the DCS expression accounting for the change of arrangement and relative translational kinetic energy, respectively. In the case of a non reactive, elastic scattering it holds that $m_\lambda = m_1$ and $k_i^1 = k_j^\lambda$, and therefore this ratio cancels out. It is important to briefly discuss some features of the previous DC expression since it will be compared with its time-dependent END counterpart in the next chapter. First of all. this DCS is the so-called CM DCS because the coordinates involved in it are the CM variables: θ_λ and φ_λ. This CM DCS is not the observed Lab DCS and some transformation must be applied to allow a comparison with the experimental data.

The CM-Lab transformations for DCS will be discussed in a later section of this chapter. The two CM angles are the polar and the azimuthal angles of the relative position vector between the target and the projectile CM's at final time. Therefore, their particular definitions depend on the kind of arrangement being considered. Another point of note is the role of the wave vector per channel k_i^λ. For a given arrangement λ and a given channel j, the wave vector k_j^λ is the same regardless of the direction $(\theta_\lambda, \gamma_\lambda)$ being considered. According to its definition, eq. 31 chapter 2, the wave vector is proportional to the difference between the total energy of the system and the internal energy of the projectile and the target at infinite separation. Therefore, this difference is the available translational kinetic energy of the two participants which in a time-independent approach is fixed. It will be seen later that in a time-dependent approach the wave vector do depend of the direction being considered.

Atom-Atom Scattering

The DCS formula can be made more explicit if the proper expression of the scattering amplitude is set. In the simple case of an atom-atom scattering process with a rapidly decreasing potential, it is obtained from eq. 39 chapter 2 that

$$\frac{d\sigma_{i\to j}}{d\Omega}(\theta) = \frac{1}{4k_i^2}\left|\sum_{l=0}^{\infty}(2l+1)S_{ij}^l P_l(\cos\theta)\right|^2 ;\ \theta \neq 0 \tag{10}$$

where the arrangement index and the azimuthal angle have been omitted because they are superfluous in this case. The expression for the ICS $\sigma_{i\to f}$ can be obtained easily by

$$\begin{aligned}\sigma_{i\to j} &= \int_0^{2\pi}\int_0^{\pi} d\gamma d\theta\, \frac{d\sigma_{i\to j}}{d\Omega}(\theta) \\ &= \frac{\pi}{k_i^2}\sum_{l=0}^{\infty}(2l+1)\left|S_{ij}^l\right|^2\end{aligned} \tag{11}$$

where the orthogonality properties of the Legendre polynomials has been exploited [27]. The elastic σ_{el} and the inelastic σ_{in} and the total σ_{tot} ICS are defined as

$$\sigma_{el} = \sigma_{ii} \ , \tag{12}$$

$$\sigma_{in} = \sum_{j \neq i} \sigma_{ij} \ , \tag{13}$$

and

$$\sigma_{tot} = \sigma_{el} + \sigma_{in} \ . \tag{14}$$

It is easy to prove from the previous definitions a more direct relationship between the total ICS and the scattering amplitude

$$\sigma_{tot} = \frac{4\pi}{k_i^2} \mathrm{Im}[f_{ii}(\theta = 0)] \tag{15}$$

This last expression is termed the optical theorem [13]. In view of the symmetry of the S-matrix is easy to see that the following relationships hold

$$k_i^2 \frac{d\sigma_{i \to j}}{d\Omega}(\theta) = k_j^2 \frac{d\sigma_{j \to i}}{d\Omega}(\theta) \tag{16}$$

and

$$k_i^2 \sigma_{i \to j} = k_j^2 \sigma_{j \to i} \tag{17}$$

which are termed the equations of detailed balance [13]. In the very case of elastic scattering (*e. g.* scattering of noble gas atoms at very low energy), only one channel is opened and the S-matrix $S_{el}^l = S_{ii}^l$ adopts a very simple form

$$S_{el}^l = \exp\left(2i\eta_l\right) , \tag{18}$$

where the phase shift η_l is the difference of the phase factors δ_l and $\widetilde{\delta}_l$ of the asymptotic nuclear wave functions with and without the real potential applied, respectively [26, 13]

$$\eta_l = \delta_l - \widetilde{\delta}_l \ . \tag{19}$$

When the inelastic channels are open, the elastic S-matrix can still be written as

$$S_{ii}^{l} = \exp\left[2i(\lambda_l + i\mu_l)\right] \tag{20}$$

with $\lambda_l > 0$ and $\mu_l > 0$. The last term accounts for the depletion from the initial channel. Further properties and relationships of this type of cross section can be found in Ref. [13]

The quantum DCS's for rapidly decreasing potentials are always bound functions at all the values of the scattering angle θ although sharp peaks can be seen in some circumstances. The DCS's also exhibit a typical oscillatory pattern when plotted w. r. t. the scattering angle θ. The sharp peaks and the oscillatory pattern are strongly associated to the SC limit of the DCS's and will be studied in detail in later sections. The quantum ICS for this kind of potentials always converge to a finite number, including in the case of elastic ICS's. In the case of the Coulomb potential, a not rapidly decreasing potential. some modifications must be introduced in the asymptotic conditions and in the spherical wave component (see Ref. [26] for more details). For a repulsive Coulomb potential (Rutherford scattering), the DCS has a closed form expression

$$\frac{d\sigma}{d\Omega}(\theta) = \left(\frac{ZZ'e^2}{4E}\right)^2 \csc^4\left(\frac{\theta}{2}\right) \tag{21}$$

where Z and Z' are the charge numbers of the scattering particles$e$ the electron charge and E is the total CM energy. However, the ICS does not converge for a Coulomb potential as can easily be confirmed by attempting the integration of the above expression. Aside form known historical reason, the neat DCS and divergent ICS in the Rutherford scattering constitute the only case in which the quantum and the classical theory predicts the same expressions.

Atom-Diatom Scattering

The quantum formulation of the cross sections for more complicated systems can be done by extending the previous analysis of the atom-atom scattering. However some

extra complications will arise due to the increasing number of degrees of freedom. An important case in subsequent developments is that of atom-diatom scattering. To simplify the presentation, only the example of a nonreactive scattering with a nonvibrating diatom will be discussed. The extension to the reactive and/or vibrating cases is relatively straightforward. The scattering amplitude for such a scattering process is [126]

$$f_{jm_j,j'm'_j}(\theta,\phi) = \sum_{J\,l\,l'\,m'_l} \left[\frac{(2l+1)\pi}{k_j k_{j'}}\right] i^{l-l'}(jlm_j0|jlJm_j)\times \\ T^J_{jM\,j'M'J}\left(j'l'Jm_j|j'l'm_{j'}m_{l'}\right)\times \\ Y_{lm'_l}(\theta,\phi)\ , \tag{22}$$

where $(jlm_j0|jlJm_j)$ and $(j'l'Jm_j|j'l'm_{j'}m_{l'})$ are Clebsch-Gordan coefficients [25] and $Y_{lm'_l}(\theta,\phi)$ are the spherical harmonics [25]. J is the orbital quantum number of the conserved total angular momentum, and j and m_j are the orbital and the azimuthal quantum numbers of the diatomic angular momentum in the entrance channel with their primed analogues in the exit channels. The T-matrix $T^J_{jm_j\,j'm'_l}$ relates to the corresponding S-matrix $S^J_{jm_j\,j'm'_l}$ so that

$$T^J_{jm_j\,j'm'_l} = i\left[S^J_{jm_j\,j'm'_l} - \delta_{ll'}\delta_{jj'}\right]\ , \tag{23}$$

Note that both matrices are a function of the quantum number J. The whole scattering processes is now labeled by the quantum numbers l, m_l, l' and $m_{l'}$. The proliferation of angular momentum indices, coefficients, and functions is a direct consequence of the coupling between the orbital angular momentum of the projectile moving around the target and the internal angular momentum of the target rotating around its CM. The use of this scattering amplitude to obtain the corresponding DCS 's and ICS' is cumbersome and is seldom attempted in this representation. A drastic simplification is achieved if the full problem is represented in the a rotating body-fixed CM frame attached to the target (the helicity representation already introduced in chapter 2) instead of the representation

in the space-fixed CM frame. In the helicity representation, the scattering amplitude is more concisely

$$f_{jM,j'M'}(\theta,\phi) = \frac{(-1)^{j-j'+M-M'}}{(k_j k_{j'})^{\frac{1}{2}}} \sum_{J=0}^{\infty} (2J+1)\times \\ S^J_{jM\ j'M'} \left[D^J_{MM'}(\phi,\theta,0)\right]^* ;\ \theta \neq 0\ , \tag{24}$$

where now M and M' are the azimuthal quantum numbers with respect to the rotating **z**—axis and $D^J_{MM'}(\phi,\theta,\chi)$ are the elements of the Wigner D matrices [25]. This expression bears a strong resemblances to that for the atom-atom scattering. Furthermore, it reduces to the latter when $j = j' = 0$ because then $J = l$, $M = M' = 0$ and $D^{l*}_{00}(\phi,\theta,\chi) = P_l(\cos\theta)$ [25]. The T- and S-matrices, and the corresponding scattering amplitudes in different representation do not have the same value since they correspond to different processes. Explicit relationships between properties in different representations can be obtained, but are intricate as the reader might suspect. By repeating the same steps as those made for the atom-atom scattering, the partial DCS in both angular quantum numbers in the helicity representation is

$$\frac{d\sigma_{jM\to j'M'}}{d\Omega}(\theta) = \frac{1}{4k_j^2}\left|\sum_{l=0}^{\infty}(2J+1)S^J_{jM\ j'M'}d^J_{M,M'}(\theta)\right|^2 , \\ (\theta \neq 0) \tag{25}$$

with $d^J_{MM'}(\theta) = D^J_{MM'}(0,\theta,0)$. Note that the resulting DCS is not a function of the azimuthal scattering angle ϕ as anticipated in chapter 2. The partial ICS in both angular quantum numbers is

$$\sigma_{jM\to j'M'} = \frac{\pi}{k_j^2}\sum_{J=0}^{\infty}(2J+1)S^J_{jM\ jM'} \tag{26}$$

However, these two detailed cross sections in both angular quantum numbers are not experimentally measured even with the state-of-the-art technology. Less detailed partial DCS and ICS in only the orbital quantum numbers are defined as

$$\frac{d\sigma_{j\to j'}}{d\Omega}(\theta) = \frac{1}{(2j+1)}\sum_{MM'}\frac{d\sigma_{jM\to jM'}}{d\Omega}(\theta)\ , \tag{27}$$

and

$$\sigma_{j\to j'} = \frac{1}{(2j+1)} \sum_{MM'} \sigma_{jM\to jM'} \ , \tag{28}$$

where the denominator $(2j+1)$ accounts for the rotational degeneracy of the entrance channel. These expressions are the same in both the space-fixed and the helicity representation because the effect of the azimuthal quantum numbers have been cancelled by the previous sum. Finally the total DCS and the ICS are defined as

$$\frac{d\sigma_{tot}}{d\Omega}(\theta) = \sum_{jj'} \frac{d\sigma_{j\to j'}}{d\Omega}(\theta) \ , \tag{29}$$

$$\sigma_{tot} = \sum_{jj'} \sigma_{j\to j'} \ , \tag{30}$$

respectively, and obviously are the least detailed cross sections for this type of scattering. It is easy to prove again that all these expressions transform into their atom-atom counterparts when $j = j' = 0$. Further properties of these expressions, such as the detailed balance equation and the optical theorem, can be easily deduced. They can be fond in Ref. 13. The cross sections for the case of a reactive and/or vibrating rotor follow directly from the previous expression and will be given in a later section.

The cross sections for approximate time-independent methods follows directly from the previously discussed exact expressions. The RIOSA cross sections for both the reactive and the non reactive processes can be found in Ref. 28, and the IOSA cross sections for charge transfer processes in Ref. 35 and 36.

Classical and Semiclassical Cross Sections

Coordinate Transformations: Center of Mass and Laboratory Frames

The transformation form Lab coordinates to their CM counterparts is commonplace in all quantum and SC calculations [13]. Both the dynamics and the calculation of the measured properties are totally done in the latter frame. The reason for that selection is

that in the CM frame the uninterested and trivial evolution of the CM of the whole system is eliminated from the very beginning. Although employed in quantum calculations, the transformation itself is classical in spirit. In time-dependent quantum calculations with fast wave packets [3], the average positions and momenta allow a kind of quasi-classical treatment which brings about classical transformations. This situation also includes our QCSD-END theory. But, including in a time-independent quantum calculation, the actual quantum coordinates are treated classically for the transformations [13]. In the case of SC calculations, the classical trajectories of this the theory easily allow such kinds of transformations [85, 86, 91].

It is not intrinsically necessary to change to CM coordinates in the END theory. However, we usually perform such a transformation for the final state because of the two following reasons:

1. All the SC techniques necessary to obtain the END cross sections have been derived in the CM frame. Instead of transforming such complicated expression back to the END Lab frame, it is easier to transform the final END state to the CM frame, employ the SC expressions, and transform the resulting properties back to the Lab system.
2. Most of the old and many of the new quantum and SC calculations have been reported in the CM frame, and for sake of comparison with the END theory it is necessary to transform the END results.

For a given calculation (classical, SC or quantum) the transformation form one frame to the other, or vice versa, is simple. The use of the CM frame in those calculations has given rise to the so-called CM properties (*e.g.*, CM cross sections) which can not be directly compared with experimental results. Since many of these studies are not reported in full detail, a final transformation to the Lab frame can not be accomplished.

On the other hand, it is in principle impossible to transform experimental (Lab) results to the CM frame since the experiments can not give all the intrinsic dynamical information necessary to apply the transformation formulas. If an experiment is to be compared with preexisting CM calculations then some iterative procedures, which combine both experimental and theoretical data, must be applied [127, 128].

The transformation of positions and velocities (or momenta) from a CM to a Lab frame, or vice versa, is a simple matter known from textbooks on classical mechanics [61]. However, the transformation of some derived properties (scattering angles, cross sections, etc.) from a few known parameters (mass change during the collision, energy loss, etc.) is a more involved issue. The most complete presentation of the subject is due to R. K. B. Helbing [129] whose main findings are presented below. Additional aspects are discussed in Ref. 130 and 131.

A Lab-to-CM transformation begins with the position transformations. Then, by derivation and algebraic manipulations, the velocity and momenta transformations are obtained. The emphasis is made on the last two transformations ("velocity space") since the actual positions of the particles during an experiment is rather uncertain. For a general colliding system, the CM transformations for the velocities are simply

$$\begin{aligned} \mathbf{v}_i &= \mathbf{v}_0 + \mathbf{u}_i \\ \mathbf{v}_i{}' &= \mathbf{v}_0 + \mathbf{u}_i{}' \end{aligned} \tag{31}$$

where $\mathbf{v}$ and $\mathbf{u}$ are the particle velocities in the CM and Lab frames, respectively; and $\mathbf{v}_0$ the velocity of the CM of the nuclei in the system. The index $i = t \ \ or \ \ p$ denotes either the target or the projectile. The primed and unprimed variables are for initial and final time, respectively. With this notation, the polar CM and Lab scattering angles $0 \leq \theta_{Lab} \leq \pi$ and $0 \leq \theta_{CM} \leq \pi$ are respectively defined such that

$$\tan \theta_{Lab} = \frac{|\mathbf{u}_p \times \mathbf{u}_p{}'|}{(\mathbf{u}_p \cdot \mathbf{u}_p{}')} \ . \tag{32}$$

$$\tan\theta_{CM} = \frac{|\mathbf{v}_p \times \mathbf{v}_p{}'|}{(\mathbf{v}_p \cdot \mathbf{v}_p{}')} \ , \tag{33}$$

or, equivalently,

$$\cos\theta_{Lab} = \frac{(\mathbf{u}_p \cdot \mathbf{u}_p{}')}{|\mathbf{u}_p||\mathbf{u}_p|} \ , \tag{34}$$

$$\cos\theta_{CM} = \frac{(\mathbf{v}_p \cdot \mathbf{v}_p{}')}{|\mathbf{v}_p||\mathbf{v}_p{}'|} \ . \tag{35}$$

In physical terms, they are the angles between the initial and final directions of the projectile in each frame. If the initial travelling direction of the projectile is along the Lab **z**-axis then the scattering angle θ_{Lab} will coincide with the final spherical coordinate θ of the projectile. In the case of two normal beams, it is sometimes convenient to set positive or negatives signs to θ_{Lab} if the final projectile velocity has a positive or negative projection onto the initial secondary beam direction [127]. The definition of the azimuthal scattering angles γ_{Lab} and γ_{CM} is more cumbersome if totally general expressions are desired. Helbing's definition in the LAB case is [129]

$$\tan|\gamma_{Lab}| = \frac{|\mathbf{T}_o \times \mathbf{T}|}{(\mathbf{T}_o \cdot \mathbf{T})} \tag{36}$$

where the unit vectors $\mathbf{T}_o$ and $\mathbf{T}$ are in the direction of $\mathbf{v}_o \times \mathbf{v}$ and $\mathbf{v} \times \mathbf{v}'$, respectively. The range an sign of this angle is determined by the conditions

$$\begin{aligned} 0 \le \gamma \le +\pi &\leftrightarrow det\left(\mathbf{v}, \mathbf{v}_o, \mathbf{v}'\right) \ge 0 \ , \\ -\pi \le \gamma \le 0 \quad &\leftrightarrow det\left(\mathbf{v}, \mathbf{v}_o, \mathbf{v}'\right) \le 0 \ . \end{aligned} \tag{37}$$

The definition of γ_{CM} can be obtained by simply changing the Lab velocities for their CM counterparts in the above expressions. In the case of a dynamics on a predetermined PES (*i.e.* a dynamics excluding the electronic dynamics), it can be proven that the angle γ_{Lab} is the difference between the final azimuth of the projectile and the initial azimuth of the target in the Lab frame [129]. If the initial target have zero azimuth then the angle

γ_{Lab} is the net increase in the azimuth of the projectile at final time. The two scattering angles have been defined in terms of intrinsic dynamical variables being independent of both the position and orientation of the coordinate axes. This justifies the somewhat cumbersome definition of γ angles. It is possible to define the same scattering angles for the final target, although they are of less practical value.

In an END calculation, the scattering angles in both frames can be calculated by the direct application of the above formulas to the final state. The transformation of the CM angles to the Lab ones can be displayed as a numerical mapping. However, to obtain explicit formulas for such angle transformations, it would be necessary to use the above definition of the scattering angles and of the CM-Lab transformation, and to appeal to the conservation laws ruling the dynamics (specially, the momentum and energy conservation laws). In Ref. 129, those explicit formulas are shown for the case of a PES classical dynamics. They are not difficult to derive but they involved tedious vectorial and trigonometric manipulations. Some of these expressions reduce to those for more simple cases found in the textbooks [61] after adapting the notation. The application of the formulas to an END calculation may only be approximate since they do not take into account the electron dynamics. When the END dynamics neither imply considerable electron transfer nor high electron excitations, the previous equations are almost exact. It might be possible to derive the analogous END formulas by incorporating the electron dynamics into the conservation laws. That derivation would be somewhat cumbersome and it is not attempted here. Although approximate in an END context, the above equations give some insight about the CM-Lab scattering angle transformation, specially about its relationship to the energy ΔE, and mass Δm change .

Classical Total Cross Sections

Initial conditions and calculation strategy

The most familiar derivations of classical cross sections are done for total cross sections, *i. e.* without any concern of the final internal state of the projectile and target. It is important to remember here that it is impossible to describe charge transfer or electron excitation processes in a pure classical way. Therefore, the next examples will be concentrated on classically derived cross sections which only involve explicitly nuclear degrees of freedom.

The calculation of a classical cross sections stems from the calculation of the system trajectory. In classically describing a scattering process, a Lagrangian or a Hamiltonian scheme can be adopted. In either case, the solution of the system dynamics requires the knowledge of its initial conditions, *i.e.* the initial positions and velocities (momenta). (It is theoretically possible to solve the problem by knowing all the initial and final positions, or all the initial and final velocities (momenta), or any combination of both initial and final positions and velocities (momenta). This scheme is sometime used in SC derivations [85, 86, 91] but it is rare in pure classical contexts). For a system consisting of N_{nucl} nuclei, its is necessary to specify $3N_{nucl}$ initial positions and $3N_{nucl}$, initial velocities in the Lagrangian formulation, or $3N_{nucl}$ initial positions and $3N_{nucl}$ initial conjugate momenta in the Hamiltonian one. In either case, this set of $6N_{nucl}$ total initial conditions can be split into the following groups of variables

1. The initial positions and velocities (or conjugate momenta) of the CM's of the projectile and the target (12)
2. The initial orientation and angular velocities (or conjugate angular momenta) of the projectile and target (12). The initial orientation will be collectively denoted by o

from now on.

3. The remaining internal positions and velocities (or conjugate momenta) of the projectile and target ($6N_{nucl} - 12$. These initial conditions will be collectively denoted by ι from now on.

A given trajectory is a function of all these initial conditions. the explicit definition of those initial internal conditions will be discussed in chapter 7. For a system under study, specific values of the initial conditions must be set to simulate a given experimental situation. The full investigation involves series of calculations in which some initial conditions are necessarily the same. The scheme of such calculations is as follows:

1. The initial target and projectile velocities (or momenta), and their internal initial conditions ι are set according to the experimental setup. The initial velocities (momenta) should be in accordance with the collision energy, meanwhile the internal coordinates should correspond to the reactants initial states.
2. It is customary in scattering theory to place the target in the center of the coordinate system and to choose the initial direction of the projectile as the positive z-direction. The initial separation of the two partners should be set to a large value in molecular terms (the actual experimental value is never precisely known). For sake of ease during serial calculations, a fix z- separations of the reactants is adopted in the present study.
3. Then, some relevant initial orientations of both the target and the projectile are selected. Batches of different calculations are done, each of them with the same initial orientations for the projectile and the target.
4. For a given orientation o, different calculations are performed by varying the lateral separation of the reactants. This is the impact parameter b, always chosen in the

y direction in the present study. This initial condition is taken to be positive $(0 \leq b \leq \infty,)$

It will be see in the next section that the cross sections can be defined for each orientation o, so that the final cross sections is averaged over such orientations.

The calculation strategy shown above is not unique, and equivalent other ones can be conceived. However, this has proven to be the most convenient for the END simulations.

Total cross section derivation

The derivation of a classical total cross section follows from an interpretation of its definition in terms of classical mechanics. Curiously, the purely classical scattering theory is less known than its SC and quantum counterparts. Obviously, a careful reexamination of the subject is essential in the context of the END theory. Except for the simple cases shown in some textbooks and books [13, 61, 4], the advanced classical scattering theory is dispersed among different works (Ref. [132–134] are the most relevant to the present discussion). The derivation outlined below is a substantial reformulation of the consulted sources.

In figures 7.1, 7.20, and 7.35, chapter 7, different collisions are depicted showing different projectiles and targets with the collective orientations o and internal initial conditions ι. The projectile center of mass position is specified by the coordinates (r_0, b, φ_0), *i.e.* the **z** separation, the impact parameter, and the azimuth on the **x-y** plane with respect to the **z** axis. The coordinate r_0 is very large on the molecular scale and its actual value is not accurately known in a given experimental setup. The impact parameter can also be increased to a macroscopic value but that situation will be equivalent to no collision. Therefore, the practical values of the impact parameter are on the microscopic scale. It is assumed that there are far more target molecules than

projectiles so that a given projectile can always be coupled with a target. Of course, many target molecules are without a projectile counterpart. At a given initial time t_1, many of these pairs are in the shown initial conditions, although they might differ in the separation r_0. At the final time t_2, all these projectiles will have a certain probability to reach the detector placed at (r, θ, γ). More precisely, each individual projectile will have a probability density $\Pi(r, \theta, \gamma; o, \iota) = \Pi(r, \theta, \gamma; r_0 b, \gamma_0, t_2, t_1, o, \iota)$ to be found in the volume $dV = r^2 \sin\theta dr d\theta d\gamma$ at time t_2 after having the initial conditions (r_0, b, φ_0) at time t_1 so that

$$\int_0^{2\pi} d\gamma \int_0^{\pi} d\theta \int_0^{\infty} d\ r r^2 \sin\theta\ \Pi(r, \theta, \gamma; o, \iota) = 1\ . \tag{38}$$

Since the values of both r_0 and r are uncertain, they are put outside of the formalism under certain assumptions. First, the value of r_0 will be fixed to the same large value for all the pairs. Secondly, the value of r is supposed to be almost the same for all the pairs, differing only microscopically. Because of the last assumption, a less detailed probability $P(\theta, \gamma; o, \iota) = P(\theta, \gamma; b, \gamma_0, r_0, r, t_2, t_1, o, \iota)$

$$P(\theta, \gamma; o, \iota) = \int_0^{\infty} d\ r r^2 \sin\theta \Pi(r, \theta, \gamma; o, i) \tag{39}$$

can be introduced since all the particles will be almost at the same radius r at time t_2. Notice that $\sin\theta$ has been incorporated into the new probability so that

$$\int_0^{2\pi} d\gamma \int_0^{\pi} d\theta\ P(\theta, \gamma; o, \iota) = 1\ . \tag{40}$$

Each collision pair can be seen as an independent "scattering experiment," all of them making up a big "statistical ensemble." Therefore, if in a short time Δt N_0 projectiles are sent to be scattered and $dN(b, \gamma_0; \iota, o)$ of them have the initial conditions $(b, \gamma_0; \iota, o)$ then the probability $dp(b, \gamma_0; \iota, o) = dp(b, \gamma_0; \iota, o; r_0, t_1)$ to find an individual pair with

such initial conditions is

$$\begin{aligned} d\,p(b,\gamma_0;\iota,o) &= \frac{dN(b,\gamma_0;\iota,o)}{N_0} \\ &= \left(\frac{b\;dbd\gamma_0}{A_0}\right)_{\iota,o} . \end{aligned} \tag{41}$$

In the last line, it has been assumed that both the projectiles and the targets are randomly distributed on the collision transverse area A_0. Then, the total number of projectiles scattered with the noted initial conditions $dN(b,\gamma_0;\iota,o)$ during the time Δt is

$$dN(b,\gamma_0;\iota,o) = \left(\frac{N_0}{A_0}\;b\;dbd\gamma_0\right)_{\iota,o} , \tag{42}$$

and the number of projectiles per unit time (rate) $d\dot{N}(b,\gamma_0;\iota,o)$ scattered is

$$\begin{aligned} d\dot{N}(b,\gamma_0;\iota,o) &= \left(\frac{\dot{N}_0}{A_0}\;b\right)_{\iota,o} dbd\gamma_0 \\ &= (I_0 b)_{\iota,o}\;dbd\gamma_0 , \end{aligned} \tag{43}$$

where I_0 is the beam intensity. Finally, the number per unit time $d\dot{N}(\theta,\gamma;\iota,o)$ of these particles reaching the detector placed in the direction (θ,γ) is then

$$\begin{aligned} d\dot{N}(\theta,\gamma;\iota,o) &= d\dot{N}(\theta,\gamma;\iota,o;r,t_2) \\ &= I_0 P(\theta,\gamma;\iota,o)\;dbd\gamma_0 d\theta d\gamma . \end{aligned} \tag{44}$$

An implicit assumption used to obtain the last equation is that there exists a stationary flux between the incoming particles to be scattered and the outgoing scattered particles (cf. Ref. 61). The differential contribution of these scattering processes with initial conditions $(b,\gamma_0;\iota,o)$ to the total DCS is

$$\left[\frac{\partial^3\sigma}{\partial\Omega\partial b\partial\gamma_0}\right](\theta,\gamma;\iota,o)\;dbd\gamma_0 = \frac{bP(\theta,\gamma;\iota,o)}{\sin\theta}\;dbd\gamma_0 . \tag{45}$$

In order to obtain the total DCS for the orientation o, it is necessary to integrate the last expression over all the initial conditions (b,γ_0)

$$\begin{aligned} \frac{d\sigma}{d\Omega}(\theta,\gamma) &= \int_0^{2\pi} d\gamma_0 \int_0^{\infty} db\,\left[\frac{\partial^3\sigma}{\partial\Omega\partial b\partial\gamma_0}\right](\theta,\gamma;\iota,o) \\ &= \frac{1}{\sin\theta}\int_0^{2\pi} d\gamma_0 \int_0^{\infty} db\;P(\theta,\gamma;\iota,o) . \end{aligned} \tag{46}$$

The last equation has been derived mainly from statistical considerations. However, to go further it is necessary to make explicit the probability density $P(\theta, \gamma; \iota, o)$. That is accomplished by calling the classical mechanics into play. By finding the classical trajectory with initial conditions (b, γ_0), its possible to obtain an explicit expressions for the final polar Θ and azimuthal Φ angles of the projectile.

$$\Theta = \Theta(b, \gamma_0; \iota, o; r_0, r; t_2, t_1) = \Theta(b, \gamma_0; \iota, o) \ , \tag{47}$$

and

$$\Phi = \Phi(b, \gamma_0; \iota, o; r_0, r; t_2, t_1) = \Phi(b, \gamma_0; \iota, o) \ , \tag{48}$$

These are the classical polar and azimuthal deflection functions, respectively. Their ranges are $-\infty \leq \Theta \leq \infty$ and $-\infty \leq \Phi \leq \infty$ when the $\pm$ sign accounts for the direction of rotation. The lack of the traditional boundaries $[0, \pi]$ and $[0, 2\pi]$, as for θ and γ, indicates that the projectile can rotate many times around the deflection axes as dictated by its classical trajectory. Because of the imposition of the classical mechanics, the probability density becomes

$$P(\theta, \gamma; \iota, o) = \delta[\theta - \Theta(b, \gamma_0; \iota, o)]\delta[\gamma - \Phi(b, \gamma_0; \iota, o)] \tag{49}$$

being nonzero only when the following congruence conditions are satisfied

$$\theta = \pm[\Theta(b, \gamma_0; \iota, o) - 2\pi n]; \ 0 \leq \theta \leq \pi \ , \tag{50}$$

and

$$\gamma = \pm[\Phi(b, \gamma_0; \iota, o) - 2\pi m]; \ 0 \leq \gamma \leq 2\pi \ . \tag{51}$$

There, the integers n and m account for the number of turns rotated by the projectile around the respective deflection axes. It is worth noting that different initial conditions (branches) $(b_i, \gamma_{0,i}) \quad i = 1, \ 2, \ 3, \ \ldots \ ; \ (\iota, o)$ can satisfy the above relations. This

physically means that the projectile can be travelling in the direction (θ, γ) at time t_2 starting form different initial conditions. The deflection functions can be thought of as a general transformation

$$[\Theta(b, \gamma_0; \iota, o), \Phi(b, \gamma_0; \iota, o)] = (b, \gamma_0) \tag{52}$$

with the Jacobian matrix J

$$\begin{aligned} J &= \begin{pmatrix} \left[\frac{\partial \Theta(b,\gamma_0)}{\partial b}\right] & \left[\frac{\partial \Theta(b,\gamma_0)}{\partial \gamma_0}\right] \\ \left[\frac{\partial \Phi(b,\gamma_0)}{\partial b}\right] & \left[\frac{\partial \Phi(b,\gamma_0)}{\partial \gamma_0}\right] \end{pmatrix} \\ &= \begin{pmatrix} \left(\frac{\partial \theta}{\partial b}\right) & \left(\frac{\partial \theta}{\partial \gamma_0}\right) \\ \left(\frac{\partial \gamma}{\partial b}\right) & \left(\frac{\partial \gamma}{\partial \gamma_0}\right) \end{pmatrix} \end{aligned} \tag{53}$$

where the initial conditions (ι, o) have been omitted for brevity. In the second line, it has been introduced the widespread short notation for each derivative despite the fact that both θ and γ are fixed values not functions. A justification of this notation abuse, aside from brevity, is that each derivative will actually be evaluated when the above congruence conditions are satisfied. Therefore, the DCS becomes (cf. Ref. 134 and 132)

$$\frac{d\sigma(\theta, \gamma; \iota, o)}{d\Omega} = \frac{1}{\sin\theta} \int_0^{2\pi} d\gamma_0 \int_0^{\infty} db\, b\delta[\theta - \Theta(b, \gamma_0; \iota, o)]\delta[\gamma - \Phi(b, \gamma_0; \iota, o)] \,. \tag{54}$$

To further evaluate this integral, it is necessary to invert both δ functions to the (b, γ_0) domain by (see appendix A),

$$\delta[\theta - \Theta(b, \gamma_0)]\delta[\gamma - \Phi(b, \gamma_0)] = \sum_i |\det(J_i)|^{-1} \delta(b - b_i)\delta(\gamma_0 - \gamma_{0,i}) \,. \tag{55}$$

where $\det(J_i)$ is the transformation Jacobian evaluated at the branch i

$$\det(J_i) = \begin{pmatrix} \left(\frac{\partial \theta}{\partial b}\right)_{b_i, \gamma_{0,i}} & \left(\frac{\partial \theta}{\partial \gamma_0}\right)_{b_i, \gamma_{0,i}} \\ \left(\frac{\partial \gamma}{\partial b}\right)_{b_i, \gamma_{0,i}} & \left(\frac{\partial \gamma}{\partial \gamma_0}\right)_{b_i, \gamma_{0,i}} \end{pmatrix} . \tag{56}$$

where again the initial conditions (ι, o) have been omitted. Then, the DCS becomes (cf. Ref. 134 and 132) In the case of a central interaction potential, the projectile will not

$$\begin{aligned}\frac{d\sigma(\theta,\gamma;o,\iota)}{d\Omega} &= \sum_i \frac{1}{\sin\theta}\int_0^{2\pi} d\gamma_0 \int_0^{\infty} db\, b|\det(J_i)|^{-1}\delta(b-b_i)\delta(\gamma_0-\gamma_{0,i}) \\ &= \frac{1}{\sin\theta}\sum_i b_i \det(J_i)^{-1}\ .\end{aligned} \tag{57}$$

change its initial azimuth γ_0 and will always remain in the plane containing its initial velocity (momentum) vector and the target center of mass. Therefore,

$$\theta = \pm[\Theta(b;\iota,o) - 2\pi n];\ 0 \le \theta \le \pi\ , \tag{58}$$

$$\gamma = \gamma_0;\ 0 \le \gamma \le 2\pi\ , \tag{59}$$

and

$$J = \begin{pmatrix} \left(\frac{\partial\theta}{\partial b}\right) & 0 \\ 0 & 1 \end{pmatrix}\ , \tag{60}$$

with

$$det(J_i) = \left(\frac{\partial\theta}{\partial b}\right)_{b_i}\ . \tag{61}$$

The previous DCS then simplifies to

$$\frac{d\sigma(\theta,\gamma;\iota,o)}{d\Omega} = \frac{1}{\sin\theta}\sum_i \frac{b_i}{\left|\left(\frac{\partial\theta}{\partial b}\right)_{b_i}\right|}\ . \tag{62}$$

The expression just derived for the classical differential cross section has a great theoretical value. However, it has scarcely been used for calculations because the numerical evaluation of its Jacobian is rather cumbersome. A proposed histogram procedure can partially avoid this difficulty, but even in that case the task remains difficult (see Ref. 132 and references therein). It will be shown in the next section that this problem can be easily overcome since the practical expression in use is similar to that of a central potential even though the interaction may not be of that sort

Effect of the orientation average on the total differential cross section

It must be remembered that the total differential cross section refers only to the initial orientation o. The measured differential cross section is an average over all the possible orientations initial orientation o. This can be denoted by

$$\frac{d\sigma}{d\Omega}(\theta, \gamma; \iota, o) = \frac{1}{\Delta o} \int do \, \frac{d\sigma}{d\Omega}(\theta, \gamma; \iota, o) \, , \tag{63}$$

where the normalization factor is $\Delta o = \int do$. The details of this averaging procedure will be discussed in chapter 7 and appendix E. For the present discussion, the above expression suffices. If the general formula of the DCS is substituted into the average integral, it follows that

$$\frac{d\sigma}{d\Omega}(\theta, \gamma; \iota) = \frac{1}{\Delta o} \int do \, \frac{1}{\sin\theta} \int_0^\infty b db \int_0^{2\pi} d\gamma_0 \, \delta[\theta - \Theta(b, \gamma_0; \iota, o)] \times \delta[\gamma - \Phi(b, \gamma_0; \iota, o)] \, . \tag{64}$$

As mentioned before, the DCS's are independent of the scattering angle γ. Taking into account the congruence between the angles γ and Φ, it holds that $d\gamma = \pm d\Phi$. Therefore,

the differential cross section can be rewritten (cf. 132) as

$$\begin{aligned}
\frac{d\sigma}{d\Omega}(\theta;\iota) &= \frac{d\sigma}{d\Omega}(\theta,\gamma;\iota) \\
&= \frac{\int_0^{2\pi} d\gamma\ \frac{d\sigma}{d\Omega}(\theta,\gamma;\iota)}{\int_0^{2\pi} d\gamma} \\
&= \frac{\int_0^{2\pi} d\Phi\ \frac{d\sigma}{d\Omega}(\theta,\gamma;\iota)}{\int_0^{2\pi} d\Phi} \\
&= \frac{1}{2\pi\Delta o}\int do\ \frac{1}{\sin\theta}\int_0^{\infty} bdb\int_0^{2\pi} d\gamma_0\int_0^{2\pi} d\Phi\ \delta[\theta-\Theta(b,\gamma_0;\iota,o)]\times \\
&\qquad \delta[\gamma-\Phi(b,\gamma_0;\iota,o)] \\
&= \frac{1}{2\pi\Delta o}\int do\ \frac{1}{\sin\theta}\int_0^{\infty} bdb\int_0^{2\pi} d\gamma_0\ \delta[\theta-\Theta(b,\gamma_0;\iota,o)]\ .
\end{aligned} \tag{65}$$

Appealing again to the properties of the δ functions (see appendix A)

$$\delta[\theta-\Theta(b,\gamma_0)] = \sum_i \left|\left(\frac{\partial\theta}{\partial b}\right)\right|^{-1}_{\gamma_0,b=b_i}\delta(b-b_i);\ \gamma_0 = constant \tag{66}$$

the differential cross section becomes

$$\frac{d\sigma}{d\Omega}(\theta,\iota) = \frac{1}{2\pi\Delta o}\int do\int_0^{2\pi} d\gamma_0\left\{\sum_i \frac{1}{\sin\theta}b_i\left|\left(\frac{\partial\theta}{\partial b}\right)\right|^{-1}_{\gamma_0,b=b_i}\right\}. \tag{67}$$

This expression can further be simplified by a closer examination of the orientation variables o. One of them can always be chosen as an azimuthal angle, say χ, with respect to the frame **z**-axis. It is easy to see that if the angles γ_0 and χ are changed by the same amount then the dynamics will not change. In other words, the dynamics rather depends on $\chi-\gamma_0$ than on

$$\gamma_0 \tag{68}$$

alone. Thus, if the integral in γ_0 is performed first then the result will be independent of χ, and the remaining integration in χ will become trivial. This procedure can be inverted

by taking the γ_0 integration to be trivial and keeping the integration in χ in full. By adopting the latter point of view, the differential cross section becomes

$$\begin{aligned}\frac{d\sigma}{d\Omega}(\theta,\iota) &= \frac{1}{\Delta o}\int do\left\{\sum_i \frac{1}{\sin\theta} b_i \left|\left(\frac{\partial\theta}{\partial b}\right)\right|_{b=b_i}^{-1}\right\} \\ &= \frac{1}{\Delta o}\int do\ \frac{d\sigma}{d\Omega}(\theta;o,\iota)\ ,\end{aligned} \tag{69}$$

where

$$\frac{d\sigma}{d\Omega}(\theta;o,\iota) = \frac{1}{\sin\theta}\sum_i b_i \left|\left(\frac{\partial\theta}{\partial b}\right)\right|_{b=b_i}^{-1}. \tag{70}$$

Note that as result of the previous discussion, the dependence on γ has been eliminated. This is the equation used in the evaluation of a classical DCS. This expression has the clear advantage of having a an ordinary derivative instead of the original Jacobian.

Classical integral cross sections

The classical ICS can be easily derived by integrating the previous classical DCS. For internal conditions ι and orientation o, the classical integral cross section $\sigma(\iota,o)$ is

$$\begin{aligned}\sigma(\iota,o) &= \int_\Omega d\Omega \frac{d\sigma}{d\Omega}(\theta;\iota,o) \\ &= \int_0^{2\pi} d\gamma \int_0^{\pi} d\theta \sin\theta\ \frac{d\sigma}{d\Omega}(\theta;\iota,o) \\ &= 2\pi\sum_i \int_0^{\pi} d\theta b_i \left|\left(\frac{\partial\theta}{\partial b}\right)\right|_{b=b_i}^{-1} \\ &= 2\pi\int_0^{b_{max}} b\ db\ .\end{aligned} \tag{71}$$

Note that from the third to the fourth line the integration in θ has been changed to one in b. Therefore, b_{max} is the highest impact parameter for which the above congruence condition can be satisfied. In most cases, b_{max} is infinite but in practical calculations it is a finite value, large on the molecular scale.

Laboratory and center-of-mass differential cross sections

In the previous derivations, not specific selection of the reference frame has been made (that is the reason the angles θ and γ bear no label so far). However, the derivation can equally be repeated in both the Lab and the CM frame yielding, respectively

$$\frac{d\sigma}{d\Omega}(\theta_{Lab}; o_{Lab}) = \frac{1}{\sin\theta_{lab}} \sum_i b_i \left| \left(\frac{\partial \theta_{Lab}}{\partial b} \right) \right|^{-1}_{b=b_i} \tag{72}$$

$$\frac{d\sigma}{d\omega}(\theta_{CM}; o_{CM}) = \frac{1}{\sin\theta_{CM}} \sum_i b_i \left| \left(\frac{\partial \theta_{CM}}{\partial b} \right) \right|^{-1}_{b=b_i} \tag{73}$$

Note that both b and (the missing) γ_0 are the same in both frames since they are relative coordinate between the projectile and the target.

General features of classical differential cross secrions

The first understanding of cross sections, either classical, SC, or quantum, came from the study of some model systems with one predetermined PES. A brief exposition of this type of approach in the case of classical mechanics is presented above. Further details can be learned form the abundant examples of Ref. [82]. Most of those traditional examples involved systems with a central projectile-target interaction. Collisions involving atoms and atomic ions do lie in that category. The use of one PES along with classically mechanics will implies that neither electronic excitation nor charge transfer can be taken into account. It is assumed in those methods that the central potential between the projectile and the target $V(r)$ is known as a function of their relative separation r. Therefore, the application of standard classical mechanics techniques will give the

following results for the deflection function in the CM frame [61, 13]

$$\begin{aligned}\Theta_{CM}(E,L) &= \pi - 2b\int_{r_m}^{\infty}\frac{dr}{r^2\Big[1-\big(\frac{b}{r}\big)^2-\frac{V(r)}{E}\Big]^{1/2}} \\ &= \pi - 2bE\int_{r_m}^{\infty}\frac{dr}{r^2\Big[E-\frac{L^2}{2\mu r^2}-V(r)\Big]^{1/2}}\end{aligned} \tag{74}$$

where E is the collision energy, r_m the relative separation at the classical turning point, and μ the projectile-target reduced mass. The derivative $\left(\frac{\partial\theta}{\partial b}\right)$ can be readily obtained form these expressions.

Different model potentials have been tested to calculate classical DCS. The archetypal examples of the hard sphere and the repulsive Coulomb (Rutherford scattering) potentials can be found in Ref. [82]. For the case of atomic collisions, purely repulsive, purely attractive, and both attractive and repulsive potentials have been tested. In the last case, the potentials are attractive in the long separation range and repulsive in the short one, exhibiting a characteristic "well" at intermediate separations. A well-known example of attractive and repulsive potentials are the Lennard-Jones n-6 potentials

$$V(r) = 4\epsilon\left\{\frac{6}{n-6}\Big(\frac{r_0}{r}\Big)^n - \frac{n}{n-6}\Big(\frac{r_0}{r}\Big)^6\right\} \tag{75}$$

where the parameters ε and r_0 are the depth and the position of the "well bottom". The first exponent is usually $n = 12$ although other values are possible. These potentials belong to the category of two-parameter potentials. Studies of the deflection function from such potentials have been done usually in terms of the effective potential

$$V_L(r) = V(r) + \frac{L^2}{2\mu r^2} \tag{76}$$

i. e. the actual potential plus a centrifugal term. In the case of attractive-repulsive interactions, the centrifugal term can overcome the attractive well for high values of L

(high value of impact parameter b) making the effective potential purely repulsive. The main features of the defection functions from these potentials are [13, 4]

1. Purely attractive potentials: the deflection function is monotonically decreasing from π to 0 as the impact parameter goes from 0 to ∞. Only one branch contributes per each value of the scattering angle.
2. Purely attractive potentials: the deflection function is initially decreasing form a 0 value at 0 impact parameter. However, at an intermediate impact parameter the CM energy matches the maximum of $V_L(r)$ the projectile begins to follow an stable orbit around the target. This phenomenon is called orbiting or spiraling [61, 13]. During orbiting, the deflection function decreases indefinitely to $-\infty$ rendering a singularity. Beyond this critical impact parameter, the deflection function increases, going to 0 at infinite impact parameter. Because of the orbiting singularity, an infinite number of branches can contribute to a given scattering angle.
3. Attractive-repulsive potentials: at relatively high energies, the deflection function starts behaving similarly to a purely repulsive one. In other words, the repulsive part of the potential prevails at low impact parameters. However, the deflection function reaches a zero value (glory angle) at a finite impact parameter (glory impact parameter). At that point, the repulsive and attractive parts to the potential counterbalance each other, and the projectile is not scattered. Beyond this point, the attractive part dominates making the deflection function negative and decreasing. This attractive effect weakens at even higher impact parameters so that the deflection function reaches a minimum at the so-called rainbow angle. Beyond this point, the deflection function increases, going to 0 value at infinite impact parameter. Because of this pattern, three branches, one repulsive and two attractive, can contribute to a scattering angle below the absolute value of the rainbow angle. Beyond that point,

only the repulsive branch can still contribute. Therefore, the classical differential cross section has a sudden decrease in intensity. By analogy with some optical phenomena, the region of three contributing branches is called the lit region, whereas that of only one branch is called the dark region. If the energy is relatively high, a similar behavior is observed but the rainbow angle degenerate to an orbiting singularity in the deflection function. The number of branches are then infinite.

The features previously discussed refer of course to classical calculations with central PES. However, they also manifest in more complicated situations (*e.g.*non-central potentials, multi-surface dynamics) as will be seen in the systems studied in chapter 7.

Accuracy of the classical total differential cross section: classical singularities

Many classical cross sections calculations have been done with either model or *ab initio* potentials. The comparison of these total classical cross sections with their quantum and experimental counterparts is a very established subject in the literature [82]. It is generally recognized that far from some singularities, to be explained below, classical differential cross sections do make a qualitatively acceptable prediction, the classical values always being smaller than the corresponding quantum and experimental ones. However, the overall performance of the classical DCS is not satisfactory. The main reason is the occurrence of some singularities at certain scattering angle values. These singularities or "effects" are not present in quantum calculations or experimental results. By inspecting the general definition of the total DCS. eq. 70, it is possible to discern the following classical effects:

1. Rainbow effect: It occurs when the conditions

$$\left(\frac{\partial\theta}{\partial b}\right)_{b=b_{rainbow}} = 0 \,, \tag{77}$$

in eq. 70 is satisfied by and impact parameter $b_{rainbow}$. This effect manifests as a sharp peak in a plot of a classical DCS w.r.t. the scattering angle θ. The peak appears at the values of θ when

$$\theta = \pm[\Theta(b_{rainbow}) - 2\pi n];\ 0 \leq \theta \leq \pi\ . \tag{78}$$

is satisfied. Taking into account the qualitative description of the previous section, a rainbow singularity happens at the impact parameters when the attractive or the repulsive part of the projectile-target interaction reaches an extreme value (the attractive rainbow effect is the most common). There, two branches contributing to the DCS coalesce into one. In physical terms this means that an increasing number of scattered particles will end up at the same scattering angle. This infinite peak is not observed experimentally but a finite peak somewhat shifted from the classical rainbow angle is usually observed.

2. Glory effect: It occurs when either the condition

$$\begin{gathered} 0 = \theta = \pm\left[\Theta\left(b^j_{fglory}\right) - 2\pi n\right],\ j = 1,\ 2,\ \ldots \\ \sin\left[\theta = 0\right] = 0\ , \end{gathered} \tag{79}$$

or

$$\begin{gathered} \pi = \theta = \pm\left[\Theta\left(b^j_{bglory}\right) - 2\pi n\right],\ j = 1,\ 2,\ \ldots \\ \sin\left[\theta = \pi\right] = 0\ , \end{gathered} \tag{80}$$

is satisfied in eq. 70 with finite values of the finite impact parameters $b_{bglory}\ ,\ j = 1,\ 2,\ \ldots$ or $b_{fglory}\ ,\ j = 1,\ 2,\ \ldots$. The first conditions belong to the forward glory effect and the second to the backward glory effect. Both effects manifest as an infinite value of the DCS at $\theta = 0$. The forward glory effect happens at impact parameters when the projectile-target interaction changes from attractive to repulsive. The projectile at those impact parameters feels a null effective force and is not deflected. The backward glory effect happens at relatively low impact parameters

when the projectile is exposed to the repulsive part of the interaction. The collision energy must be also very low to allow a back scattering. The backward glory effect is far less common then its forward counterpart. The physical reason for both glory effects is that as soon as the scattering angle goes to either 0 or π, the solid angle $d\Omega = \sin\theta d\theta d\gamma$ goes to zero; therefore, a finite flux of outgoing particles are being sent to an infinitely small solid angle. The infinite value of the glory effect is not observed experimentally because the measured DCS is always finite, including at zero scattering angle.

3. Small angle effect: It occurs when the condition

$$\begin{gathered} \lim_{b\to\infty} \theta = \pm[\Theta(b) - 2\pi n] \, , \\ \sin\left[\theta = 0\right] = 0 \, , \end{gathered} \tag{81}$$

it is satisfied in eq. 70. This effects manifests as an infinite value of the DCS at $\theta = 0$ but with higher intensity than the glory effect. This effect is caused by the unscatterd projectiles at high impact parameters. Again this effect is not observed in quantum calculations or experimental measurement.

This classical effects "happens" in situations when classical mechanics is most likely to fail from a quantum mechanical point of view. For instance, the classical rainbow effects is not really observed because the definite classical trajectories coalescing at the rainbow impact parameter are not appropriate to describe a quantum phenomenon. If this trajectories are replaced by interfering partial waves then the classical, infinite peak will become into a shifted, finite peak. The relationship between these classical effects and the real, quantum mechanics DCS is shown by the SC theory. This theory also provides some mathematical techniques to correct this unphysical effects in a classical calculation. This topic will be discussed by the end of this chapter.

The rainbow effect can not be seen in the classical ICS since the integration procedure over the impact parameter b washes this singularity off. However, the classical ICS diverges for elastic processes. This lack of convergence can be linked to the glory and small angle effect previously discussed. The convergency in the elastic classical ICS can be restored if some SC techniques are applied.

Classical Partial Cross Sections

So far, only total classical cross sections has been described. Partial differential cross sections are concerned with the final state of the target and the projectile. The term final state refers to the internal degrees of freedom of the two collision partners, which have been collectively denoted by ι at initial time. The description of the internal state at a given time is attained by knowing the values of either all the internal generalized position and velocities, in the Lagrangian formulation, or all the internal generalized position and their conjugated momenta in the Hamiltonian one. Many different but equivalent selections of internal variables can be made freely, and, in fact, classical mechanics does not favor any of them from a purely theoretical point of view. The selection of a given set of internal positions and velocities (or momenta) might be made on the basis of the ease of their transformations, the accuracy of their description for a given problem, or their convenience for a numerical implementation.

The simple example of an atom-diatom scattering processes is again used to simplify the presentation. The vibrational degree of freedom is considered frozen and will not be explicitly shown. By generalizing the arguments used in the derivation of the total differential cross section, it is easy to prove that the classical partial cross section for

this scattering system (cf. 134)

$$\left[\frac{\partial^3\sigma}{\partial\Omega\partial I_j\partial I_m}\right]\left(\theta,\gamma,I_j^f,I_m^f\right)=\frac{1}{4\pi^2\sin\theta}\int_0^\infty db\,b\int_0^{2\pi}d\gamma_0\int_0^{2\pi}d\phi_j^i\int_0^{2\pi}d\phi_m^i \times\delta(\theta-\Theta)\delta(\gamma-\Phi)\delta\left(I_j-I_j^f\right)\delta\left(I_m-I_m^f\right), \tag{82}$$

In this case, the orientation variables are $do=d\phi_j d\phi_m$ with normalization $\Delta o=4\pi^2$. The deflection functions Θ and Φ are now

$$\Theta=\Theta\left(b,\gamma_0,\phi_j^i,\phi_m^i;R^0,P^0,t_2,t_1\right)=\Theta\left(b,\gamma_0,\phi_j^i,\phi_m^i\right), \tag{83}$$

and

$$\Phi=\Phi\left(b,\gamma_0,\phi_j^i,\phi_m^i;R^0,P^0,t_2,t_1\right)=\Phi\left(b,\gamma_0,\phi_j^i,\phi_m^i\right). \tag{84}$$

and the final actions

$$I_j^f=I_j^f\left(b,\gamma_0,\phi_j^i,\phi_m^i;R^0,P^0,t_2,t_1\right)=I_j^f(b,\gamma_0,\phi_j,\phi_m), \tag{85}$$

and

$$I_m^f=I_m^f\left(b,\gamma_0,\phi_j^i,\phi_m^i;R^0,P^0,t_2,t_1\right)=I_m^f(b,\gamma_0,\phi_j,\phi_m). \tag{86}$$

A characteristic feature of the present classical mechanics treatment is that the labeling of the cross sections is by the continuous variables I_j and I_m through their partial derivatives. By similar arguments, as those used in the total cross section case, the functionality in γ_0 can be removed[11]). A more practical expression is therefore

$$\left[\frac{\partial^3\sigma}{\partial\Omega\partial I_j\partial I_m}\right]\left(\theta,I_j^f,I_m^f\right)=\frac{1}{4\pi^2\sin\theta}\int_0^\infty db\,b\int_0^{2\pi}d\phi_j^i\int_0^{2\pi}d\phi_m^i \times\delta(\theta-\Theta)\delta\left(I_j-I_j^f\right)\delta\left(I_m-I_m^f\right), \tag{87}$$

where now

$$\Theta=\Theta(b,\phi_j,\phi_m), \tag{88}$$

11. In the opinion of Ref. 34, this may not be true for other quantization axes.

$$\Phi = \Phi\left(b, \phi_j^i, \phi_m^i\right) , \tag{89}$$

$$I_j^f = I_j^f(b, , \phi_j, \phi_m) , \tag{90}$$

and

$$I_m^f = I_m^f(b, , \phi_j, \phi_m) . \tag{91}$$

The last two integrals can be evaluated first at a constant value of the impact parameter b. Therefore, by invoking once more time the delta function properties (see appendix A, it is possible to write

$$\delta\left(I_j - I_j^f\right)\delta\left(I_m - I_m^f\right) = \delta\left(\phi_j - \phi_j^i\right)\delta\left(\phi_m - \phi_m^i\right)\left|det\left(J\left(\phi_j^i, \phi_m^i; b\right)\right)\right|^{-1} , \tag{92}$$

where the determinant $det\left[J\left(\phi_j^i, \phi_m^i; b\right)\right]$ is

$$det\left[J\left(\phi_j^f \phi_m^f; b\right)\right] = \left| \begin{pmatrix} \left(\frac{\partial I_j^f}{\partial \phi_j^i}\right)_{I_j^f, I_m^f; b} & \left(\frac{\partial I_j^f}{\partial \phi_m^i}\right)_{I_j^f, I_m^f; b} \\ \left(\frac{\partial I_m^f}{\partial \phi_{j,k}^i}\right)_{I_j^f, I_m^f; b} & \left(\frac{\partial I_m^f}{\partial \phi_{m,k}^i}\right)_{I_j^f, I_m^f; b} \end{pmatrix} \right| . \tag{93}$$

This is again the "Van Vleck's determinant" [92] already shown in eq. 131, chapter 2. Now this determinant has appear in a purely classical context. Note that the impact parameter b is taken as a constant in the last expression. The differential cross section is now

$$\left[\frac{\partial^3 \sigma}{\partial \Omega \partial I_j \partial I_m}\right]\left(\theta, I_j^f, I_m^f\right) = \frac{1}{4\pi^2 \sin\theta} \int_0^\infty db\, b\delta(\theta - \Theta)\left|det\left(J\left(\phi_j^i, \phi_m^i; b\right)\right)\right|^{-1} . \tag{94}$$

By performing the remaining integration, the final result is obtained as[12]

$$\left[\frac{\partial^3 \sigma}{\partial \Omega \partial I_j \partial I_m}\right]\left(\theta, I_j^f, I_m^f\right) = \frac{1}{\sin\theta} \sum_k \frac{b_i P_{class}\left(I_j^f, I_m^f; b_k\right)}{\left|\frac{\partial \theta}{\partial b}\right|_{b_k}} , \tag{95}$$

12. Note that in Ref. 134 this final expression is not derived.

where the classical probability $P_{class}\left(I_j^f, I_m^f; b_i\right)$ is

$$P_{class}\left(I_j^f, I_m^f; b_i\right) = \frac{1}{4\pi^2}\left|\begin{pmatrix}\left(\frac{\partial I_j^f}{\partial \phi_j^i}\right)_{I_j^f, I_m^f; b} & \left(\frac{\partial I_j^f}{\partial \phi_m^i}\right)_{I_j^f, I_m^f; b} \\ \left(\frac{\partial I_m^f}{\partial \phi_j^i}\right)_{I_j^f, I_m^f; b} & \left(\frac{\partial I_m^f}{\partial \phi_m^i}\right)_{I_j^f, I_m^f; b}\end{pmatrix}\right|^{-1} \tag{96}$$

and the index k denotes the different branches rendering a diatomic molecule with final actions I_j^f and I_j^f and a projectile asymptotically travelling in the θ direction.

In order to obtain classical differential cross sections from the last expression a series of classical trajectories must be run with fixed initial values of R^0, P^0, I_j^i and I_m^i, and varying values of $0 \leq b \leq \infty$, $0 \leq \phi_j \leq 2\pi$ and $0 \leq \phi_m \leq 2\pi$. As in the total cross section case, the evaluation of the "Van Vleck determinant" is a cumbersome task but there is no simple way to circumvent its evaluation here. Furthermore, a continuum of values of I_j^f and I_j^f can be classically obtained. Therefore, to obtain realistic results for the differential cross section, it is imperative to abandon the pure classical description and impose the SC quantizations rules to both actions

$$I_j = n_j \hbar \tag{97}$$

and

$$I_m = n_m \hbar \tag{98}$$

where $n_j = 0,\ 1,\ 2,\ \ldots$ and $n_m = -n_j,\ -n_j + 1,\ \ldots,\ n_j - 1,\ n_j$ are the orbital and the azimuthal quantum numbers, respectively. This is almost the SC prescription explained in detail in chapter 2.

Expressions for less resolved differential cross sections can be obtained by successive integration of the original expression above. An integration in only I_m renders the differential cross section $\frac{\partial^2 \sigma}{\partial \Omega \partial I_j}$ (see Ref. 134 and references therein for both theoretical and experimental results about it). An integration in both I_m and I_l renders the

unresolved, total differential cross section $\frac{d\sigma}{d\Omega}$ as in the previous section. A generalization of these expressions to the case of a non rigid rotor target is relatively simple to obtained and it is omitted. The final result resembles the purely classical part of the SC S-matrix presented in chapter 2.

In some approaches, there is no interest to express the classical cross sections in terms of the action-angle formalism. There, the direct inspection of some less elaborated positions and conjugate momenta are of primary importance (see Ref. 135–138). The disadvantage of these approaches is that the relationship to quantum mechanics is indirect and that the selections of variables by the different authors make the comparison of their results somewhat difficult. In one study of atom-molecule collisions [136], the DCS is expressed in terms of the usual impact parameter b and the initial projectile azimuth γ_0 plus some particular internal variables for the molecular target. They are the initial molecular angular momentum modulus $j = |\mathbf{j}|$, their spherical polar and the azimuthal angles α β in a space fixed frame; and the angle δ between the bond vector and the projection of the angular momentum $\mathbf{j}$ onto the plane of rotation. The differential cross section is derived by appealing to the Liouville theorem in classical mechanics [61].[13] The DCS turns out to be

$$\begin{aligned}\frac{\partial^5\sigma}{\partial\theta\partial\phi\partial\alpha'\partial\beta'\partial j'} &= \frac{\rho^f}{8\pi^2\rho^i} \\ &= \sum \frac{b\sin\beta}{8\pi^2\sin\theta\sin\beta'}\left|\frac{\partial(b,\gamma_0,\alpha,\beta,\delta)}{\partial(\theta,\phi,\alpha',\beta',j')}\right|\end{aligned} \tag{99}$$

The integration over all the variables except θ and j' leads to [139]

$$\frac{\partial^2\sigma\left(\theta,j'\right)}{\partial j'\partial\Omega} = \int_0^{2\pi} d\alpha \int_0^{\pi} \sin\beta d\beta \left[\frac{\partial^2\sigma\left(\theta,j';\alpha,\beta\right)}{\partial j'\partial\Omega}\right] \tag{100}$$

13. This is also the case of Ref. 137. The use of this approach has the advantages to simplify the derivation of a classical cross section but it has the disadvantage to not show the many theoretical and experimental assumptions around it. This is the reason it has not been employed in the previous section on total differential cross sections.

where the differential cross section $\frac{\partial^2\sigma\left(\theta,j';\alpha,\beta\right)}{\partial j'\partial\Omega}$ for the initial molecular orientation $[\alpha,\ \beta]$ is

$$\frac{\partial^2\sigma\left(\theta,j';\alpha,\beta\right)}{\partial j'\partial\Omega}=\sum_k\frac{b_k}{4\pi\sin\theta}\left|\frac{\partial\left(b_k,\gamma_{0,k}\right)}{\partial(j',\theta)}\right| \tag{101}$$

with $d\Omega=2\pi\sin\theta d\theta$. This expression is equivalent to the previously mentioned $\frac{\partial^2\sigma}{\partial\Omega\partial I_f}$ differential cross section in the action-angle scheme. This formula is preferred when the action-angle transformation are not desirable and when direct relationship between the variables in the Jacobian are relevant. Similar expressions can be found in Ref. 137.

Singularities in the classical partial cross sections: rotational rainbows

The knowledge of singularities in the partial differential cross section is less extensive than that in the total cross sections. Conclusive but not exhaustive examples of these phenomena are known from theory and experiments [139, 134, 37]. In the context of action-angle differential cross section, the occurrence of singularities can be found whenever the partial derivatives $\left(\frac{\partial\theta}{\partial b}\right)$, $\left(\frac{\partial I_i^f}{\partial\sigma_i'}\right)$, or $\left(\frac{\partial I_m^f}{\partial\sigma_m'}\right)$ are zero. The first case seems to be analogous in effect and origin to the previous angular rainbow discussed for total differential cross sections. However, studies of this singularity are not complete (see for example Ref. 85). This subject will be addressed in more detail in the END cross section The singularities arising from the other two derivative are not called rainbows and have been studied in detail in the context of the SC theory and will be discussed in a later section. A complete analysis of the singularities in the non action-angle differential cross section has been done in Ref. 139. Obviously, there will be a singularity in the cross section whenever the Jacobian

$$\frac{\partial(b,\gamma_0)}{\partial(j',\theta)}=\left(\frac{\partial b}{\partial j'}\right)_\theta\left(\frac{\partial\gamma_0}{\partial\theta}\right)_{j'}-\left(\frac{\partial b}{\partial\theta}\right)_{j'}\left(\frac{\partial\gamma_0}{\partial j'}\right)_\theta \tag{102}$$

is infinite. In principle, this might happen whenever at least one of the four partial derivatives is infinite, a situation leading to four types of singularities or "rainbows". However, its is easy to prove by two-variable calculus that when one derivative is singular the other three are also. In other terms, if the an extrema exists for, say, $j' = j'(b, \gamma_0)$ subject to the constraint of a constant θ then it holds that $\left(\frac{\partial j'}{\partial b}\right)_\theta = \left(\frac{\partial j'}{\partial \gamma_0}\right)_\theta = 0$ for some particular values $(b_r, \gamma_{0,r})$; but this immediately implies that the function $\theta = \theta(b, \gamma_0)$ subject to the constraint of a constant j' has also an extremum $\left(\frac{\partial \theta}{\partial b}\right)_{j'} = \left(\frac{\partial \theta'}{\partial \gamma_0}\right)_{j'} = 0$ at the same point, making the fourth derivatives zero. If plots are made of this classical differential cross sections $\frac{\partial^2 \sigma\left(\theta, j'; \alpha, \beta\right)}{\partial j' \partial \Omega}$ both as a function of j' at constant θ and vice versa then strong singularities will be shown in both plots at the points $j'_r = j'(b_r, \gamma_{0,r})$ and $\theta_r = \theta(b_r, \gamma_{0,r})$, respectively. These singularities will survive in the observable differential cross section $\frac{\partial^2 \sigma\left(\theta, j'; \alpha, \beta\right)}{\partial j' \partial \Omega}$ provided that the averaging over the orientation does not wash out this effect. This singularity has been called "rotational rainbow" [140] for its manifestation in a $\left[\frac{\partial^2 \sigma\left(\theta, j'; \alpha, \beta\right)}{\partial j' \partial \Omega}\right]_\theta$ vs. j' plot. Theoretical and experimental examples of this phenomenon can be found in Ref. 139 and references therein. Those examples show a more complicated relationship to the details of the potential energy surface and are not necessarily related to a transition from a repulsive to an attractive part of the potential. Of course, the experimental results do not show a singularity but a strong, bound peak which can be ascribed to a classical singularity. A more general view of this subject comprising the singularities from both types of differential cross sections is not known in the literature, and it will not be attempted here.

Semiclassical Cross Sections

The relationship between the quantum DCS, presented in the first sections of this chapter, and their classical counterparts, presented in the preceding sections, is effected by the SC theory. This undertaking is not only explanatory since the SC theory also

provides useful mathematical techniques to correct the unphysical singularities in the classical DCS. In essence, the SC approach to the DCS [13, 82] consists in replacing the discrete sums in the quantum expressions by integrals and then in evaluating them in the limit of $\hbar \to 0$. This last operation involves the use of the stationary phase approximation [81] and other more sophisticated techniques related to it. The derivation of the SC DCS from the exact quantum ones is more a mathematical problem than a physical one. Except for the simplest scattering cases, the mathematics involved is rather intricate. Furthermore, the SC treatment of some complicated scattering situations seem to be unknown.

Most of the knowledge about the SC DCS is about elastic scattering of atoms and will be presented first. Despite its original range of application, these SC methods can be extended to treat inelastic scattering with the END theory as will be seen in chapter 6. The first prescribed SC treatment for the rainbow effect was formulated by Ford and Wheeler [141] and was later extended by M. V. Berry [142]. This prescription can be applied when the rainbow singularity is either unique or far away form other rainbow peaks. The rainbow angle must be far away from a possible glory angle as well. This whole situation is extremely common and it will be exemplified by the scattering systems in chapter 7. The case of two or more rainbow peaks close to each other constitutes a much more complicated mathematical problem. These situations have been exhaustively studied by Connor in a series of papers [143–147] in which the catastrophe theory [148] played and important role. System exhibiting this type of rainbow effect are fortunately rare although an example is shown in chapter 7. However, the implementation of Connor's SC techniques is rather cumbersome as will be briefly discussed in chapter 6. The SC treatment of the glory effect and the small angle effect are mathematically different from that in the rainbow effect. A thorough treatment of both effects has been given by M.

V. Berry [142]. These techniques are being implemented in the framework of the END theory as well [115]. However, they will not be explained in detail here since they are not used in the systems studied in chapter 7. Further details can be found in Ref. [115].

The knowledge about SC DCS for inelastic scattering process is very narrow. A method proposed by Miller [85], which apparently has never been tried, will be discussed in chapter 6. Another known example is the application of the SC techniques to the IOSA approximation done by Schinke and Bowman [37] in the context of the rotational rainbows. This effort seems to be of little relevance for the END theory.

Finally, there exist SC methods to correct the singularities in the derivatives of the Van Vleck's determinant of the SC S-matrix, eq. 131 and 93 [82]. These techniques are called "non-generic" [82] as opposed to the "generic" treatments of rainbows presented above. These methods are of no use within the END theory.

CHAPTER 6
THE END CROSS SECTIONS

The END S-Matrix

General Overview

The derivation of cross sections for the QCSD END theory can be now undertaken. The point of view adopted here is that the QCSD END wave functions and its TDVP propagation are quantum in nature. It is very important to bear in mind that the full QCSD END theory is a model, approximated but quantum theory. Therefore, a quantum derivation of the END properties can be done by adapting the quantum formalism explained in the beginning of chapter 6. After this quantum stage is completed, the SC limit of $\hbar \rightarrow 0$ will be finally applied to be in accordance with the END dynamical equations, eq. 35. In applying that limit, an special care will be exerted to retain as much quantum dynamical information as the model allows. At this stage, the previously presented CS and SC theories will be heavily invoked.

As seen in the previous chapter, the key element in the formulation of quantum cross sections is the S-matrix. The definition of the exact, quantum mechanical of the S-matrix $S^{qm}_{a\rightarrow b}$ is in terms of the evolution operator, eq. 9 is [4, 3]

$$S^{qm}_{a\rightarrow b} = \lim_{t\rightarrow\infty} \langle \psi_b | \exp\left[i \frac{H_{total}(t_2 - t_1)}{\hbar} \right] \psi_a \rangle \qquad (1)$$
$$(t = t_2 - t_1)$$

where H_{total} is the Hamiltonian of the whole system, and the ψ_a, ψ_a are the initial and final wave function describing the process. In turn, these function can be expressed as

[3] $\psi_a = w_a\phi_a$ and $\psi_b = w_b\phi_b$, where w_a and w_b are two wave packets describing the translational degrees of freedom, and ϕ_a and ϕ_b are two stationary eigenstates describing the reagents and the products, respectively. The labels a and b are collections of quantum numbers denoting the internal quantum states of reagents and products, respectively. The meaning of the S-matrix is very clear: it is the probability amplitude to find the system in the state b at time t_2 after being in the state a at time t_1. By writing the evolved wave function $\psi_a(t)$ at final time as

$$\psi_a(t) = \exp\left[i\frac{H_{total}(t_2 - t_1)}{\hbar}\right]\psi_a \ , \tag{2}$$

the S-matrix can be rewritten in a form which omits the evolution operator

$$S^{qm}_{a\to b} = \lim_{t\to\infty}\langle\psi_b|\psi_a(t)\rangle \ . \tag{3}$$

The QCSD END wave function is not evolved by the exact evolution operator but by a nonlinear, approximate TDVP scheme. Therefore, the definition of a END S-matrix in the form of eq. 1 is impossible unless an effective, nonlinear operator $f^{END}_{eff}(t_2 - t_1)$ is used to replaced the exact evolution operator $U(t_2 - t_1)$, $f^{END}_{eff}(t_2 - t_1)$. However, that approach seems to be not very useful. However, a END S-matrix, or an END analogue of the S-matrix, can be easily formulated in the lines of eq. 3

$$S^{END}_{a\to b} = \lim_{t\to\infty}\langle\psi^{END}_b|\psi^{END}_a(t)\rangle \ . \tag{4}$$

Here, $\psi^{END}_a(t)$ will be the QCSD END wave function, eq. 18, which has been evolved with the END dynamical equations, eq. 35; and ψ^{END}_b will be a wave function describing the state of the product in a way compatible with the END theory. Conceptually, the END S-matrix is the probability amplitude to find the system the END-equivalent state b at time t_2 after being in the END-equivalent state a at time t_1 after evolving with the END dynamical equations. The term "END-equivalent" does not mean something artificially

created but the END closest approximation to the exact quantum states. The END S-matrix will be an approximation to the exact, quantum S-matrix. This approximation might exhibit some departures from its exact counterpart The most conspicuous of this departure is the failure of the END propagation scheme to satisfy the detailed balanced principle, eq. 17, as explained in chapter 3. However, this limitation poses no serious problem when the END theory is applied to the systems studied in chapter 7. Having defined the END S-matrix, the definition of the END cross sections will stem from it.

The END Cross Sections I: Atom-Atom Scattering

The Atom-Atom END Wave Function

The first step in this derivation is to rewrite the END wave function in the CM frame. This is only necessary for purposes of interpretation at initial and final times. The actual END propagation is always done in the Lab frame. The QCSD END wave function is. eq. 18, is again

$$\Psi_{END}(\mathbf{X},\mathbf{x},t) = F_{nucl}[\mathbf{X}:\mathbf{R}(t),\mathbf{P}(t)]f_{el}[\mathbf{x}:\mathbf{z}(t),\mathbf{R}(t)]\times \exp\left[\frac{i}{\hbar}\gamma_{total}(t)\right] \tag{5}$$

where all its components have been previously discussed in chapter 3. For the case of two colliding atoms (or for a diatomic molecule) the nuclear part consists of two Gaussian wave packets (cf. 19)

$$F_{nucl}(\mathbf{X}:\mathbf{R},\mathbf{P}) = \prod_{k=1}^{2}\exp\left\{-a_k[\mathbf{X_k}-\mathbf{R_k}(t)]^2+\frac{i}{\hbar}\mathbf{P_k}(t)\cdot[\mathbf{X_k}-\mathbf{R_k}(t)]\right\}. \tag{6}$$

The electronic part $f_{el}[\mathbf{z}(t),\mathbf{R}(t)]$ is the Thouless single determinant wave function. The total phase $\gamma_{total}(t)$ is the action $A(t)$ of the END generalized Lagrangian $L(\mathbf{R},\mathbf{P},\mathbf{z})$:

$$\gamma_{total}(t) = A(t) = \int_{t_1}^{t_2} dt' L[\mathbf{R}(t'),\mathbf{P}(t'),\mathbf{z}(t')] \tag{7}$$

where $t = t_2 - t_1$.

So far, Gaussian wave packets of finite coefficients a_k and the real finite value of $\hbar$ are being used. The nuclear coefficients can be explicitly defined as those of a canonical CS (cf. eq. 34 and 35)

$$a_k = \frac{m_k \omega_k}{2\hbar} \quad k = 1, 2 \tag{8}$$

where m_k and ω_k are the mass of and the angular frequency, respectively associated with the nucleus k. Those frequencies can in principle have any value. However, since the END theory assumes frozen wave packets, both m_k and ω_k will not vary during the time evolution. This selection of Gaussian parameters also makes the "triple" SC limit used in chapter 3

$$\begin{aligned} &\hbar \to 0 \ , \\ &a_k \to \infty \ , \\ &a_k \hbar \to \ finite \ constant \ , \end{aligned} \tag{9}$$

reduce to the first one alone as previously anticipated.

The transformation to the CM coordinates is effected by adapting to the present situation the Jacobi coordinates mentioned in chapter 2. This is

$$\begin{aligned} \mathbf{X_0} &= \frac{1}{M}(m_1 \mathbf{X_1} + m_2 \mathbf{X_2}) \ , \\ \mathbf{x} &= \mathbf{X_2} - \mathbf{X_1} \ , \end{aligned} \tag{10}$$

with a similar transformation for the parameters of the average nuclear positions

$$\begin{aligned} \mathbf{R_0}(t) &= \frac{1}{M}(m_1 \mathbf{R_1}(t) + m_2 \mathbf{R_2}(t)) \ , \\ \mathbf{r}(t) &= \mathbf{R_2}(t) - \mathbf{R_1}(t) \ , \end{aligned} \tag{11}$$

where M is the total mass ($M = m_1 + m_2$). Obviously, $\mathbf{X_0}$ ($\mathbf{R_0}$) and $\mathbf{x}$ ($\mathbf{r}$) refer to the nuclear CM and the nuclear relative positions, respectively. This transformation is set into $F_{nucl}(\mathbf{X}; \mathbf{R}, \mathbf{P})$ in order to write this function as a product:

$$F_{nucl}(\mathbf{X}; \mathbf{R}, \mathbf{P}) = F_0(\mathbf{X_0}; \mathbf{R_0}, \mathbf{P_0}) F_{int}(\mathbf{x}; \mathbf{r}, \mathbf{p}) \ . \tag{12}$$

After some few algebraic steps, omitted for brevity, it is easy to find that this factorization can be achieved only if the condition: $\omega_1 = \omega_2 = \omega$ is imposed. In that case, it is obtained that

$$F_0(\mathbf{X_0}; \mathbf{R_0}, \mathbf{P_0}) = \exp\left\{-a_0[\mathbf{X_0} - \mathbf{R_0}(t)]^2 + \frac{i}{\hbar}\mathbf{P_0}(t) \cdot [\mathbf{X_0} - \mathbf{R_0}(t)]\right\}, \tag{13}$$

and

$$F_{int}(\mathbf{x}; \mathbf{r}, \mathbf{p}) = \exp\left\{-a_\mu[\mathbf{x} - \mathbf{r}(t)]^2 + \frac{i}{\hbar}\mathbf{p}(t) \cdot [\mathbf{x} - \mathbf{r}(t)]\right\}. \tag{14}$$

Here, the new momentum parameters $\mathbf{P_0}(t)$ ("total nuclear momentum") and $\mathbf{p}(t)$ ("relative nuclear momentum") are

$$\mathbf{P_0}(t) = \mathbf{P_1}(t) + \mathbf{P_2}(t) \tag{15}$$

and

$$\mathbf{p}(t) = \mu\left(\dot{\mathbf{R}}_2 - \dot{\mathbf{R}}_1\right) = \mu\dot{\mathbf{r}}\ . \tag{16}$$

respectively, where μ is the translational reduced mass ($\mu = \frac{m_1 m_2}{m_1 + m_2}$). The transformed nuclear coefficient turn out to be

$$a_0 = \frac{M\omega}{2\hbar} \tag{17}$$

and

$$a_\mu = \frac{\mu\omega}{2\hbar}\ . \tag{18}$$

The electronic part of the wave function undergoes the same transformation. However, that part is, aside from electronic parameters, a function of relative nuclear positions only. Therefore, its form will not be affected by this transformation. A similar partition of the total phase means that

$$\gamma(t) = \gamma_0(t) + \gamma_{int}(t)\ , \tag{19}$$

where $\gamma_0(t)$ contains only the nuclear CM variables and $\gamma_{int}(t)$ the remaining nuclear (relative) variables along with the electronic parameters. These terms will be explicitly given in the SC limit in the next section.

By the previous procedure, the total QCSD END wave function has been divided into two parts: one part totally in terms of the CM nuclear coordinates and parameters and another in terms of the remaining (relative) nuclear and electronic coordinates and parameters. The CM part is a canonical CS with a trivial time evolution that of the system CM. This part can be totally separated together with its phase $\gamma_0(t)$ from the rest leaving the internal END wave function

$$\Psi_{int}^{END}(t) = F_{int}[\mathbf{r}(t), \mathbf{p}(t)] f_{el}[\mathbf{z}(t), \mathbf{r}(t)] \exp\left(\frac{i}{\hbar}\gamma_{int}(t)\right) \tag{20}$$

alone. In most of the cases, it is convenient to transform the Cartesian nuclear coordinates and parameters in $F_{int}(\mathbf{x}; \mathbf{r}, \mathbf{p})$ into a spherical polar representation. Because of the symmetry of the problem, the dynamics will be constrained to a plane (this is also true in a full quantum treatment). For the case of a diatomic molecule, the nonrotating coordinate system is oriented with the z-axis normal to the dynamics plane ($\theta = \frac{\pi}{2}$) whereas the azimuthal angle φ is free to vary in its full range, $0 \leq \varphi \leq 2\pi$. In the case of a two-atom scattering, the coordinate system is oriented with the z-axis in the direction of the incoming projectile. The expression is the same but with φ replaced by the polar angle θ ($0 \leq \theta \leq \pi$). In either case, it is obtained that

$$\begin{aligned} F_{int}(x, \varphi, ; r, \widetilde{\varphi}) =& \exp\left\{-a_\mu\left[x^2 + r^2(t) - 2xr(t)cos(\varphi - \widetilde{\varphi}(t))\right]\right\} \times \\ & \exp\left\{\frac{i}{\hbar}\mu[\dot{r}(t)xcos(\varphi - \widetilde{\varphi}(t)) - \dot{r}r]\right\} \times \\ & \exp\left\{\frac{i}{\hbar}\mu\left[xr\dot{\widetilde{\varphi}}(t)sin(\varphi - \widetilde{\varphi}(t))\right]\right\} \end{aligned} \tag{21}$$

where $0 \leq x\ (r) \leq \infty$ is the (parametric) relative position of the two atoms, $0 \leq \dot{r}(t) \leq \infty$ and $-\infty \leq \dot{\widetilde{\varphi}}(t) \leq \infty$ are the (parametric) linear and angular velocities.

The first two lines in this equation would form a canonical CS for the atomic relative positions if some angular term could be separated out. The third line would be a pure angular function if some linear term could also be separated out. However, the coupling between the angular and the linear variables is a real effect and there is not an exact way to decuple them (a situation similar to that in molecular spectroscopy theory). Note that except for the assumption of a unique frequency ω, all this steps are exact. Furthermore, a unique frequency for a two-atom system is not a problem because it is related to the one vibrational mode of the system. In the description of a diatomic molecule, this frequency can be set to the real vibrational frequency of the system at the initial time. However, in the description of an atom-atom scattering, this frequency can not be assigned to a vibration.

Uncoupling of the Angular and Linear Coordinates

Further analysis of this problem is difficult unless some approximations are introduced into the above internal function. In the same spirit as that of the molecular spectroscopy theory, the following approximation will be considered (cf. eq. 36):

$$F_{int}(x,\varphi,;r,\widetilde{\varphi}) \approx F_{vib}(x{:}\, r)F_{rot}(\varphi;\widetilde{\varphi}) \;, \tag{22}$$

where

$$F_{vib}(x{:}\, r) = \frac{1}{x}\exp\left\{-a_\mu[x-r(t)]^2 + \frac{i}{\hbar}\mu\dot{r}(t)[x-r(t)]\right\} \tag{23}$$

and

$$\begin{aligned} F_{rot}(\varphi{:}\,\widetilde{\varphi}) =& \exp\{-2a_\mu r_0^2[1-cos(\varphi-\widetilde{\varphi}(t))]\}\times \\ & \exp\left\{\frac{i}{\hbar}\mu r_0^2\dot{\widetilde{\varphi}}(t)sin(\varphi-\widetilde{\varphi}(t))\right\} . \end{aligned} \tag{24}$$

The $\frac{1}{x}$ factor in F_{vib} cancels the x^2 in the spherical volume $x^2 sin\theta dx d\theta d\varphi$ during integration. In the case of a diatomic molecule, the terms r_0 and $\dot{r}_0$ are the separation and the linear velocity at equilibrium, respectively. In the scattering case, they are

an arbitrarily large separation and the final linear velocity, respectively. Notice that the vibrational part has a time variation only through the parameter $r(t)$, and the rotational part only through $\dot{\widetilde{\varphi}}(t)$. This approximate separation into vibrational and rotational degrees of freedom might be justified in the following way. First, the exact internal END function is rewritten as

$$\begin{aligned} F_{int}(x,\varphi,;r,\widetilde{\varphi}) =& \exp\left\{-a_\mu[x-r(t)]^2+\frac{i}{\hbar}\mu\dot{r}(t)[x-r(t)]\right\}\times \\ & \exp\{-2a_\mu xr(t)[1-cos(\varphi-\widetilde{\varphi}(t))]\}\times \\ & \exp\left\{\frac{i}{\hbar}\mu[x\dot{r}(t)cos(\varphi-\widetilde{\varphi}(t))-1]\right\}\times \\ & \exp\left\{\frac{i}{\hbar}\mu\left[xr\dot{\widetilde{\varphi}}(t)sin(\varphi-\widetilde{\varphi}(t))\right]\right\}. \end{aligned} \tag{25}$$

Then, the main part of the third factor can be exactly expanded as

$$\begin{aligned} \exp\left\{\frac{i}{\hbar}\mu[x\dot{r}(t)cos(\varphi-\widetilde{\varphi}(t))]\right\} &= \sum_{l=0}^{\infty} i^l(2l+1)j_l\left[\frac{\mu\dot{r}(t)x}{\hbar}\right]P_l[cos(\varphi-\widetilde{\varphi}(t))] \\ &= \sum_{l=0}^{\infty} i^l(2l+1)j_l[k_r(t)x]P_l[cos(\varphi-\widetilde{\varphi}(t))]\,, \end{aligned} \tag{26}$$

where the $j_l's$ are the spherical Bessel functions [27], the $P_l's$ are the Legendre functions [27],, and $k_r(t)=\frac{\mu\dot{r}(t)}{\hbar}$. If either $x\ or\ k_r(t)\to\infty$ then it holds the asymptotic form [27],

$$j_l[k_r(t)x]\to\frac{1}{k_r(t)x}\sin\left[k_r(t)x-\frac{l\pi}{2}\right]. \tag{27}$$

If $\hbar$ is taken as very small then the above limit can be applied. Also in that situation , the Gaussian terms make the total function be significant only if $\varphi\simeq\widetilde{\varphi}(t)\ and\ x\simeq r$; then $P_l[cos(\varphi-\widetilde{\varphi}(t))]\underset{\hbar\ small}{\approx}1$ [27], and from this

$$\exp\left\{\frac{i}{\hbar}\mu[x\dot{r}(t)cos(\varphi-\widetilde{\varphi}(t))]\right\}\underset{\hbar\ small}{\approx}\sum_{l=0}^{\infty}i^l(2l+1)\frac{1}{k_r(t)x}\sin\left[k_r(t)x-\frac{l\pi}{2}\right]. \tag{28}$$

Then, the approximate replacement

$$xr(t)\underset{\hbar\ small}{\approx}r(t)^2\approx r_0^2 \tag{29}$$

is introduced in the second and fourth factor of the exact internal function, eq. 25,

$$k_r(t)x \approx k_r^0 r_0 \tag{30}$$

in the sine argument of the expansion, and

$$k_r(t) \approx k_r^0 \tag{31}$$

in the sine denominator. By putting all together and discarding the constant terms, the separation in eq. 22 is obtained.

The study of the mechanical behavior of this approximate function in the full classical limit ($\hbar \to 0$) can also justify this separation. In that limit , we can even substitute the approximate rotational function in an integrand for its expansion up to quadratic terms

$$\begin{aligned} F_{rot}(\varphi;\widetilde{\varphi}) \underset{\hbar\ small}{\approx} & \exp\left\{-a_\mu r_0^2[\varphi-\widetilde{\varphi}(t)]^2\right\}\times \\ & \exp\left\{\frac{i}{\hbar}\mu r_0^2\dot{\widetilde{\varphi}}(t)(\varphi-\widetilde{\varphi}(t))\right\} \end{aligned} \tag{32}$$

and to enlarge the integrations limits of φ from $[0,\ 2\pi]$ to $[-\infty,\ \infty]$, For the same reason, the integration limits of x can be expanded from $[0,\ \infty]$ to $[-\infty,\ \infty]$ as usual in molecular spectroscopy theory[14]. For an angular operator $\widehat{A}$, its average value in the approximate internal function is

$$\langle A\rangle = \frac{\langle F_{int}\left|\widehat{A}\right|F_{int}\rangle}{\langle F_{int}|F_{int}\rangle} = \frac{\langle F_{rot}\left|\widehat{A}\right|F_{rot}\rangle}{\langle F_{rot}|F_{rot}\rangle}\ . \tag{33}$$

Then, in the SC limit, it is easy to prove that

$$\lim_{\hbar\to 0}\langle L_x\rangle = \lim_{\hbar\to 0}\langle L_y\rangle = 0\ , \tag{34}$$

$$\lim_{\hbar\to 0}\langle L_z\rangle = \mu r_0^2\dot{\widetilde{\varphi}}(t)\ , \tag{35}$$

14. It is not possible to use the stationary phase approximation to evaluate these integrals because the phase will cancel out in the integrands. However, the method suggested above turned out to be equivalent to the Laplace approximation for integrals [81].

and

$$\lim_{\hbar\to 0}\langle L^2\rangle = \left[\mu r_0^2\dot{\widetilde{\varphi}}(t)\right]^2 . \tag{36}$$

These expressions are the classical values.

To evaluate the energy and the Lagrangian of this function, the discussion can be simplified by treating the electrons through an effective potential $V(x-r_0)$ expanded in a Taylor series around its minimum r_0. Using a Hamiltonian in spherical coordinates

$$\widehat{H}_{int} = -\frac{\hbar^2}{2\mu}\left(\frac{\partial^2}{\partial x^2}+\frac{2}{x}\frac{\partial}{\partial x}\right)+\frac{1}{2\mu x^2}\widehat{L}^2+V(x-r_0) \tag{37}$$

it can be obtained, after some manipulations, the total energy

$$\begin{aligned}\lim_{\hbar\to 0} E_{int} &= \lim_{\hbar\to 0}\frac{< F_{int}|\widehat{H}_{int}|F_{int}\rangle}{< F_{int}|F_{int}\rangle}\\ &= \frac{1}{2\mu}(\mu\dot{r}(t))+\frac{1}{2\mu r^2(t)}\langle L^2\rangle + V[r(t)-r_0]\end{aligned} \tag{38}$$

and the Lagrangian

$$\lim_{\hbar\to 0} L_{int}\left[r(t),\widetilde{\varphi}(t),\dot{r(t)},\dot{\widetilde{\varphi}(t)}\right] = [\mu\dot{r}(t)]\dot{r}(t)+\left[\mu r_0^2\dot{\widetilde{\varphi}}(t)\right]\dot{\widetilde{\varphi}}(t)-E_{int} \tag{39}$$

where $< L^2 >$ has been given above. Notice that these results are in accordance with a classical mechanics description. The potential $V[r(t)-r_0]$ can be expanded up to second order, with its second derivative set $\omega=\sqrt{\frac{V''_{r_0}}{2\mu}}$, and $r(t)$ can be approximated by the constant r_0 in the momentum of inertia. Thus, the resulting equations describe the time evolution of a harmonic oscillator-rigid rotor model system. The relationship between the rotational function and the rotational CS will be investigated later.

The Atom-Atom END S-Matrix

Now, it is possible to evaluate the END S-matrix for a atom-atom scattering according to eq. 4. In this case, the final normalized wave function $\Psi_{int}^{END}(t)_a$

$$\Psi_{int}^{END}(t)_a = \frac{F_{int}[\mathbf{r_a}(t),\mathbf{p_a}(t)]f_{rl}[\mathbf{z_a}(t),\mathbf{r_a}(t)]\exp\left(\frac{i}{\hbar}\gamma_{int}(t)\right)}{N_a} \tag{40}$$

where N_a is a total (nuclear plus electronic) normalization constant, and a is the label of the initial state, *i. e.* a indicates that the present function has evolved from the initial state a. That label comprises the quantum number(s) of the initial electronic state and the values of the parameter $R(t_1)$ and $P(t_1)$. The state to project on is constructed as

$$\left(\Psi_{int}^{END}\right)_b = \frac{F_{int}[\mathbf{r_b}, \mathbf{p_b}] f_{el}[\mathbf{z_b}, \mathbf{r_b}]_b}{N_b} \tag{41}$$

i.e. a frozen Gaussian wave packet $F_{int}(\mathbf{r_b}, \mathbf{p_b})$ with arbitrary final scattering positions and momentar$_\mathbf{b}$ and $\mathbf{p_b}$ carrying a SCF electronic function $f_{el}[\mathbf{z_b}, \mathbf{r_b}]_b$ and with total normalization constant N_b. Then, the S-matrix elements are (the infinite time limit is implicitly assumed henceforth)

$$S_{a\to b}^{END} = A_{nucl}(\mathbf{r_b}, \mathbf{p_b}, \mathbf{r_a}, \mathbf{p_a}) A_{el}(\mathbf{r_b}, \mathbf{z_b}, \mathbf{r_a}, \mathbf{z_a}) exp\left(\frac{i}{\hbar}\gamma_{int}\right) . \tag{42}$$

where the nuclear amplitude is [114]

$$\begin{aligned} A_{nucl}(\mathbf{r_b}, \mathbf{p_b}, \mathbf{r_a}, \mathbf{p_a}) &= \langle \frac{F_{int}(\mathbf{r_b}, \mathbf{z_b})}{N_{nucl}^b} | \frac{F_{int}(\mathbf{r_a}, \mathbf{z_a})}{N_{nucl}^a} \rangle \\ &= \prod_{k=1}^{3} M_k \exp\left\{ -\frac{[P_k^b - P_k^a]^2}{4[2a_\mu \hbar]\hbar} \right\} , \end{aligned} \tag{43}$$

with

$$\begin{aligned} M_k =& \exp\left\{ -\frac{a}{2}\left[R_k^b - R_k^a\right]^2 \right\} \times \\ & \exp\left\{ \frac{i}{\hbar}\left[P_k^a\left(R_k^C - R_k^b\right) - P_k^b\left(R_k^C - R_k^a\right) \right] \right\} , \end{aligned} \tag{44}$$

and

$$R_k^C = \frac{[R_k^a + R_k^b]}{2} . \tag{45}$$

The nuclear amplitude is similar to the Gaussian semiclassical generalized amplitude by Heller [97]. The electronic amplitude is

$$A_{el}(\mathbf{r_b}, \mathbf{z_b}, \mathbf{r_a}, \mathbf{z_a}) = \langle \frac{f_{el}^b(\mathbf{r_b}, \mathbf{z_b})}{N_{el}^b} | \frac{f_{el}(\mathbf{r_a}, \mathbf{z_a})}{N_{el}^a} \rangle \tag{46}$$

being a quantum amplitude. Notice that in general, the electronic functions are at different nuclear positions. If the classical limit is applied, then the nuclear amplitude will be non zero only if the positions and momenta of the final state are the same as those from the evolution. Then, it is obtained that

$$\lim_{\hbar\to 0} S_{a\to b}^{END} = \delta(\mathbf{r_b}-\mathbf{r_a})\delta(\mathbf{p_b}-\mathbf{p_a})A_{el}(\mathbf{r_b},\mathbf{z_b},\mathbf{r_a},\mathbf{z_a})\exp\left(\frac{i}{\hbar}\gamma_{int}\right) \tag{47}$$

Now, it is the proper time to consider in detail the phase involved in the last expression. In the SC limit, the total phase $\gamma_{total}(t)$ becomes

$$\lim_{\hbar\to 0}\gamma_{total}(t) = \lim_{\hbar\to 0}\gamma_0(t) + \lim_{\hbar\to 0}\gamma_{int}(t) \tag{48}$$

There, the nuclear CM phase $\gamma_0(t)$ in that limit is

$$\begin{aligned}\lim_{\hbar\to 0}\gamma_0(t) &= \int_{t_1}^{t_2} dt'\,\mathbf{P_0}(t')\cdot\dot{\mathbf{R}}_\mathbf{0}(t') - E_0(t_2-t_1)\\ &= \frac{1}{2M}\mathbf{P}_0(t)^2\\ &\qquad (t=t_2-t_1\to\infty)\end{aligned} \tag{49}$$

Also, the internal phase $\gamma_{int}(t)$ becomes

$$\begin{aligned}\lim_{\hbar\to 0}\gamma_{int}(t) = \int_{t_1}^{t_2} dt'\,\left[\mathbf{p}(t')\cdot\dot{\mathbf{r}}(t') + \dot{\gamma_{el}}(t')\right] - E_{int}(t_2-t_1)\\ (t=t_2-t_1\to\infty)\end{aligned} \tag{50}$$

with the electronic part $\dot{\gamma}_{el}(t)$ in the atomic basis being

$$\begin{aligned}\dot{\gamma_{el}} = -ImTr\{\dot{z}\Lambda^{\bullet}(z,\mathbf{r})^{-1}\Big[\Delta^{>}(\mathbf{r}) + z^{\dagger}\Delta^{\circ}(\mathbf{r})\Big]\\ + [\dot{\mathbf{r}}\cdot\nabla_{\mathbf{r}}\Delta(\mathbf{r})]\Gamma(z,\mathbf{r})\}\end{aligned} \tag{51}$$

where the electronic matrices Δ, Γ, and Λ are defined in Ref. [1]. Note that the dependance of these matrices with respect to the internal parameters z and $\mathbf{r}$ has been explicitly shown. In a bundle of END trajectories only differing in the impact parameter, the internal energy and the time difference $t_2 - t_1$ are the same. Therefore, the last term

of the internal phase can be omitted in actual calculations since only differences between phases are experimentally observed. However, that term will be kept in theoretical derivations to maintain a direct relationship to the action functional. From the standpoint of classical mechanics, both $\gamma_0(t)$ and $\gamma_{int}(t)$ as actions belong to the $F_1\left(q_i^0, q_i^\infty\right)$—type of generating functions [61], which implies that

$$\lim_{\hbar \to 0} \gamma_0(t) = \gamma_0\left(\mathbf{Q}_i^\mathbf{0}, \mathbf{Q}_i^\infty; t\right) \qquad (t = t_2 - t_1 \to \infty) \tag{52}$$

and

$$\lim_{\hbar \to 0} \gamma_{int}(t) = \gamma_{int}\left(\mathbf{q}_i^\mathbf{0}, \mathbf{q}_i^\infty; t\right) \qquad (t = t_2 - t_1 \to \infty) \tag{53}$$

where the $\{\mathbf{Q}_i\}$ and $\{\mathbf{q}_i\}$ are the CM (nuclear) and internal (both nuclear and electronic) canonical positions at the trajectory extrema, respectively. This general functionality for both phases must be considered in theoretical derivations. However, in actual calculations of the S-matrix, all its components can be ultimately written as a function of only one canonical position, say, the impact parameter b. This is so because all the final canonical position can be written as functions of the initial canonical position and momenta, and many of these are the same for a bundle of trajectories (*e.g.* the initial transversal separation of the two particles, all the electronic parameters, the initial nuclear and electronic canonical momenta) Then, the S-matrix elements can be written in a more convenient form

$$\lim_{\hbar \to 0} S_{ab}^{end}(b) = A_{el}(b)_{ab} \exp\left[\frac{i}{\hbar}\gamma_{int}(b)\right]. \tag{54}$$

It is interesting to compare the END S-matrix in the classical limit with that in Miller's semiclassical theory [91]. For the case of a single PES (an elastic non-transfer atom-atom process), the SC S-matrix is, after adapting the original notation to the present one, (cf. chapter 2)

$$\lim_{\hbar \to 0} S_{a \to b}^{SC}(b) = \exp\left[\frac{i}{\hbar}\gamma_{semi}(b)\right] \tag{55}$$

where the semiclassical phase is

$$\gamma_{semi}(b) = -\int_{t_1}^{t_2} dt' \, \mathbf{r}(t') \cdot \dot{\mathbf{p}}(t') \tag{56}$$

Note that there are no electronic terms in the pre-exponential factor and in the phase of the SC version. The nuclear part of the SC phase is the negative of the END nuclear phase but with the roles of the positions and momenta in reversed order. This is because the SC S-matrix is obtained in the momentum representation. The nuclear part of the END phase indeed corresponds the SC phase in the position representation [85]. A formulation of the END theory in the momentum representation will render in the SC limit the same expression as that of the semiclassical theory plus additional electronic terms. Although a momentum representation treatment of the nuclear Gaussian wave packets is relatively simple, a similar treatment of the electronic wave functions may be cumbersome. However, a simple relationship between the two representations can be obtained along the following lines. Consider the sums $\sum_i \mathbf{p}_\mathbf{i}^\mathbf{c} \cdot \mathbf{q}_\mathbf{i}^\mathbf{c}$ where $\{\mathbf{p}^\mathbf{c}{}_i\}$ and $\{\mathbf{q}^\mathbf{c}{}_i\}$ are the nuclear canonical momenta and position at the initial $(c = 0)$ and final $(c = \infty)$ time. at initial time, it is

$$\begin{aligned} \sum_i \mathbf{p}_\mathbf{i}^\mathbf{0} \cdot \mathbf{q}_\mathbf{i}^\mathbf{0} &= p_r^0 r^0 + p_\theta^0 \theta^0 \\ &= pZ^0 + pb\theta^0 \, , \end{aligned} \tag{57}$$

where p is the total nuclear momentum and Z^0 the relative transversal separation of both nuclei (here thought to be in the z-coordinate in accordance to the convention in chapter 5). In a bundle of END trajectories, only b is the differing initial position. However as the limit $t = t_2 - t_1 \to \infty$ is approached, all the above variables remained finite except Z^0

$$\lim_{t\to\infty} X^0 = large\ number \, . \tag{58}$$

Then,

$$\lim_{t\to\infty} \sum_i \mathbf{p}_\mathbf{i}^\mathbf{0} \cdot \mathbf{q}_\mathbf{i}^\mathbf{0} \approx pX^0 = large\ number \, . \tag{59}$$

which is the same for all the trajectories. At final time, it can be written

$$\sum_i \mathbf{p_i^\infty} \cdot \mathbf{q_i^\infty} = p_r^\infty r^\infty + p_\theta^\infty \theta^\infty \tag{60}$$

Similarly, when the time limit is approached, all the above variables remained finite except r^∞

$$\lim_{t\to\infty} r^\infty = large\ number\ . \tag{61}$$

Then

$$\lim_{t\to\infty} \sum_i \mathbf{p_i^\infty} \cdot \mathbf{q_i^\infty} \approx p_r^\infty r^\infty = large\ number\ . \tag{62}$$

The value of r^∞ (the detector position) is the almost same for all the trajectories. If it is assumed on the basis of a large initial nuclear momentum that p_r^∞ is almost the same for all the trajectories, then the quantity $\lim_{t\to\infty} \sum_i \left(\mathbf{p_i^\infty} \cdot \mathbf{q_i^\infty} - \mathbf{p_i^0} \cdot \mathbf{q_i^0}\right)$ can be added to the phase in the S-matrix expression. Then the following equalities up to a phase factor can be written

$$\begin{aligned}
\lim_{\hbar\to 0} S_{a\to b}^{END} &= A_{el} \exp\left[\frac{i}{\hbar}\gamma_{int}\left(\mathbf{q_i^0}, \mathbf{q_i^\infty}\right)\right] \\
&= A_{el} \exp\left[\frac{i}{\hbar}\left(\gamma_{int}\left(\mathbf{q_i^0}, \mathbf{q_i^\infty}\right) + \sum_i \left(\mathbf{p_i^\infty} \cdot \mathbf{q_i^\infty} - \mathbf{p_i^0} \cdot \mathbf{q_i^0}\right)\right)\right] \\
&= A_{el} \exp\left[\frac{i}{\hbar}\gamma'_{int}\left(\mathbf{p_i^0}, \mathbf{p_i^0}\right)\right]
\end{aligned} \tag{63}$$

The transformed internal phase $\gamma'_{int}\left(\mathbf{p_i^0}, \mathbf{p_i^\infty}\right)$ without the electronic and the energy terms is identical in its nuclear part to the above semiclassical phase γ_{SC}. Note that this transformed phase is a $F_4\left(p_i^0, p_i^\infty\right)$ generating function in the nuclear variables. In some theoretical derivation it is better to transform the original END S-matrix expression in its F_4 version to take advantage of its derivative properties [61]

$$\begin{aligned}
\frac{\partial F_4}{\partial p_i^0} &= -q_i^0\ , \\
\frac{\partial F_4}{\partial p_i^\infty} &= q_i^\infty\ .
\end{aligned} \tag{64}$$

END Cross Sections for the Atom-Atom Scattering

Now, it is possible to derive the END expressions for the DCS and ICS. This can be done by the following route. First, the partial-wave definition of the differential cross section for the central-field inelastic process is recalled form chapter 5, eq. 10,

$$\left[\frac{d\sigma(\theta)}{d\Omega}\right]_{a\to b} = \left(\frac{k_b}{k_a}\right)|f_{a\to b}(\theta)|^2 \tag{65}$$

where $f_{ab}(\theta)$ is the scattering amplitude

$$f_{a\to b}(\theta) = \frac{1}{i[2\pi k_a k_b sin\theta]^{\frac{1}{2}}}\sum_{l=0}^{\infty}(2l+1)S_{ab}(l)P_l(cos\theta)\ , \tag{66}$$

where $P_l(cos\theta)$ is a Legendre function, and l is the angular quantum number associated with the relative motion. Then, the exact, quantum S-matrix is replaced by its approximate END analogue and the resulting expression is treated in the SC limit for sake of consistency

$$\begin{aligned}\left[\frac{d\sigma(\theta)}{d\Omega}\right]_{ab}^{end} &= \lim_{\hbar\to 0}\frac{1}{4k_a^2}|s|^2 \\ &= \lim_{\hbar\to 0}\frac{1}{4k_a^2}\left|\sum_{l=0}^{\infty}(2l+1)S_{ab}^{end}(l)P_l(cos\theta)\right|^2 .\end{aligned} \tag{67}$$

In the SC limit, the connection between the quantum number l and the final nuclear angular momentum $\mathbf{L}_{\mathbf{nuc}}^{\infty}$ is through the Langer condition [13]

$$\mathrm{L}_{\mathrm{nuc}}^{\infty} = |\mathbf{L}_{\mathbf{nuc}}^{\infty}| = \hbar(l+1/2)\ . \tag{68}$$

The relationship of l with the impact parameter b is through the conservation of the total (nuclear plus electronic) angular momentum [1]

$$\begin{aligned}\mathbf{L}_{\mathbf{total}}^{0} &= \mathbf{L}_{\mathbf{total}}^{\infty} \\ \hbar\mathbf{k_a}\cdot\mathbf{b}+\mathbf{L}_{\mathbf{el}}^{0}+\mathbf{s}_{\mathbf{el}}^{0} &= \hbar(l+1/2)\mathbf{n}_{\mathbf{nuc}}+\mathbf{L}_{\mathbf{el}}^{\infty}+\mathbf{s}_{\mathbf{el}}^{\infty}\end{aligned} \tag{69}$$

where $\mathbf{n}^{\infty}_{\mathbf{nuc}}$ is a unit vector in the direction of $\mathbf{L}^{\infty}_{\mathbf{nuc}}$, and $\mathbf{L_{el}}$ and $\mathbf{s_{el}}$ are the (expectation value of the) electronic orbital and spin angular momenta respectively. Since by symmetry all these vectors are normal to the scattering plane, we obtain

$$l = k_a b + \frac{\left[\left(L^0_{el} - L^{\infty}_{el}\right) + \left(s^0_{el} - s^{\infty}_{el}\right)\right]}{\hbar} - \frac{1}{2}\,. \tag{70}$$

If the conditions

$$\theta \neq 0 \; or \; \pi \tag{71}$$

and

$$l \sin\theta >> 1 \Rightarrow l >> \frac{1}{2} \tag{72}$$

are satisfied, then the Legendre polynomial can be replaced by its asymptotic expansion in that range [27]

$$P_l(cos\theta) \approx \left(\frac{2}{\pi l sin\theta}\right)^{\frac{1}{2}} cos\left[\left(l + \frac{1}{2}\right)\theta - \frac{\pi}{4}\right]. \tag{73}$$

Then, the sum in the scattering expression can be approximated as

$$\begin{aligned} s &= \lim_{\hbar \to 0}\left[\frac{2}{\pi \sin\theta}\right]^{1/2} \sum_{l=0}^{\infty} \frac{(2l+1)}{l^{1/2}} A_{el}(l) cos\left[\left(l + \frac{1}{2}\right)\theta - \pi/4\right] exp\left[\frac{i}{\hbar}\gamma_{int}(l)\right] \\ &= \left[\frac{2}{\pi \sin\theta}\right]^{1/2} \int_0^{\infty} dl\, l^{\frac{1}{2}} A_{el}(l_j)_{ab} \{\exp[i\chi_+(l)] + \exp[i\chi_-(l)]\}\,, \end{aligned} \tag{74}$$

where the original sum has been converted into an integral, and

$$\chi_{\pm}(l) = \frac{\gamma_{int}(l)}{\hbar} \pm \left(l\theta - \frac{\pi}{4}\right). \tag{75}$$

Invoking, one more time, the SC limit of $\hbar \to 0$, this last integral can be evaluated by stationary phase techniques [81]. The result is

$$s = \frac{1}{(\sin\theta)^{\frac{1}{2}}} \sum_j \left\{\frac{l_j}{\left|\chi''_{\pm}(l_j)\right|}\right\}^{\frac{1}{2}} \mathrm{A_{el}(l_j)_{ab}} \exp\left[i\chi_{\pm}(l_j) + \frac{i\pi}{4}\right], \tag{76}$$

if the roots l_j of the stationary condition

$$\frac{\partial\chi(lj)}{\partial l} = \frac{1}{\hbar}\frac{\partial\gamma_{int}}{\partial l}(l_j) \pm \theta = 0 \tag{77}$$

are well separated from each other. Taking advantage of the equality up to a phase of the S-matrix elements, this expression is equivalent to

$$\frac{\partial\chi(lj)}{\partial l} = \frac{1}{\hbar}\frac{\partial\gamma'_{int}}{\partial l}(l_j) \pm \theta = 0\ . \tag{78}$$

But, since l is related to the canonical moment l through

$$l = \frac{L_{nuc}}{\hbar};\ l >> \frac{1}{2} \tag{79}$$

then

$$\frac{1}{\hbar}\frac{\partial\gamma'_{int}}{\partial l}(l_j) \pm \theta \Rightarrow \frac{\partial\gamma'_{int}}{\partial L^{\infty}_{nuc}}(l_j) \pm \theta = 0\ . \tag{80}$$

which through the F_4 nature of γ'_{int} renders

$$\pm\varphi(t \rightarrow \infty) = \theta + 2\pi n;\ n = 0,\ \pm 1,\ \pm 2... \tag{81}$$

as expected (*i.e.* the absolute value of final angular position is congruent to the selected scattering direction). Note that $\varphi(t \rightarrow \infty)$ results form the full electronic plus nuclear dynamics throughout. The $\pm$ sign can be ascribed to repulsive or attractive scattering, respectively. The differential cross section thus becomes

$$\begin{aligned}\left[\frac{d\sigma(\theta)}{d\Omega}\right]^{EXD}_{a\rightarrow b} &= \frac{1}{k_a^2}\left|\sum_j\left(\frac{l_j}{\sin\theta|\chi''(l_j)|_{b_j}}\right)^{\frac{1}{2}} A_{el}(lj)_{ab}\exp\left[i\chi_{\pm}(lj)+\frac{i\pi}{4}\right]\right|^2 \\ &= \sum_j\left[\frac{d\sigma^{cl}(\theta)}{d\Omega}\right]_{j;ab} + \\ &\quad 2\sum_{j<k}\left\{\left[\frac{d\sigma^{cl}(\theta)}{d\Omega}\right]_{j;ab}\left[\frac{d\sigma^{cl}(\theta)}{d\Omega}\right]_{k;ab}\right\}^{\frac{1}{2}}\cos[\chi_{\pm}(b_j)-\chi_{\pm}(b_k)]\ .\end{aligned} \tag{82}$$

This expression can be simplified even more if in the above relationship between l and b it is recognized that at the present level of END the change in $\mathbf{s_{el}}$ is null and the change in $\mathbf{L_{el}}$ is usually small. Then

$$\left[\frac{d\sigma(\theta)}{d\Omega}\right]_{a\to b}^{END} = \sum_j \left[\frac{d\sigma^{cl}(\theta)}{d\Omega}\right]_{j;ab} + 2\sum_{j<k}\left\{\left[\frac{d\sigma^{cl}(\theta)}{d\Omega}\right]_{j;ab}\left[\frac{d\sigma^{cl}(\theta)}{d\Omega}\right]_{k;ab}\right\}^{\frac{1}{2}} \cos[\chi_{\pm}(b_j) - \chi_{\pm}(b_k)] \tag{83}$$

where

$$\left[\frac{d\sigma^{cl}(\theta)}{d\Omega}\right]_{j;ab} = \frac{b_j P_{cl}(b_j)_{ab}}{sin\theta\left|\frac{d\theta}{db}\right|_{b_j}} , \tag{84}$$

and $P_{cl}(b)_{ab} = |A_{cl}(b)_{ab}|^2$.

The situation when at the least two of the roots l_j are very close or coalesce into one corresponds to a rainbow singularity in classical mechanics as discussed in chapter 5. In such a case, the scattering amplitude integral can not be evaluated by the simple stationary phase but by more sophisticated SC techniques. This gives rise to the transitional and the uniform approximations for the rainbow singularities [142–147]. For instance, the END scattering amplitude, $f_{a\to b}^{END}(\theta)$, in the uniform SC approximation for an isolated rainbow angle [142, 143, 146] is

$$f_{a\to b}^{END}(\theta) = f_{1,2}^{END}(\theta) + f_3^{END}(\theta) , \tag{85}$$

where the one-repulsive-branch amplitude $f_3^{END}(\theta)$ is

$$f_{3;\,a\to b}^{END}(\theta) = \left[\frac{d\sigma^{cl}(\theta)}{d\Omega}\right]_{3;\,a\to b}^{\frac{1}{2}} \exp\left\{i\left[\chi_{3,+}(\theta) - \frac{1}{2}\pi\right]\right\} \tag{86}$$

and the two-attractive-branch amplitude $f_{1,2}^{END}(\theta)$ containing the rainbow angle is

$$f_{1,2;\,a\to b}^{END\,(UA)}(\theta) = \pi^{\frac{1}{2}} \exp\left[i\left(A_{1,2}(\theta) - \frac{1}{4}\pi\right)\right]\times \left\{S_{1,2}^{+}(\theta)\xi_{1,2}^{1/4} Ai(-\xi_{1,2}) - iS_{1,2}^{-}(\theta)\xi_{1,2}^{-1/4} Ai'(-\xi_{1,2})\right\} , \tag{87}$$

where

$$A_{1,2;\ a\to b}(\theta) = \frac{1}{2}[\chi_{1,-}(\theta) + \chi_{2,-}(\theta)] \ .$$
$$S^{\pm}_{1,2;\ a\to b}(\theta) = \left\{ \left[\frac{d\sigma^{cl}(\theta)}{d\Omega}\right]^{\frac{1}{2}}_{2;\ a\to b} \pm \left[\frac{d\sigma^{cl}(\theta)}{d\Omega}\right]^{\frac{1}{2}}_{1;\ a\to b} \right\} . \tag{88}$$
$$\xi_{1,2;\ a\to b}(\theta) = \left\{ \frac{3}{4}[\chi_{1,-}(\theta) - \chi_{2,-}(\theta)]^{2/3} \right\} ,$$

and $Ai(-\xi_{1,2})$ and $Ai'(-\xi_{1,2})$ are the Airy function and its first derivative [27]. The Airy function occurs in many instances of the SC theory as can be seen in Ref. [82]. The DCS resulting from the previous expressions does not exhibit the infinite rainbow peak of the classical theory at a scattering angle θ_r^{class}. Instead, a finite peak at almost the first maximum of the Airy function occurs at a scattering angle θ_r^{SC}. This "semiclassically corrected" rainbow is approximately given by the equation [13]

$$\left(\theta_r^{SC} - \theta_r^{class}\right) = -1.019 \times q_r^{1/3} \ . \tag{89}$$

where

$$q_r = \frac{1}{2k_a^2}\left[\frac{d^2\theta}{db^2}\right]_{b_r} , \tag{90}$$

and b_r is the impact parameter at the rainbow singularity. θ_r^{SC} turns out to be lower than its classical counterpart in the present example. The term "uniform" ascribed to the SC approximation given by eq. 85 through 88 denotes the fact the DCS arising from it goes uniformly (continuity in the first derivatives) to the simpler expression of eq. 83 when applied far away from the rainbow singularity. The transitional SC approximation can be obtained form the previous one if the limiting value of the amplitude $f^{EXD}_{1,2}(\theta)$ near rainbow singularity is forcefully applied at all the values of θ [142, 143, 146]

$$f^{END\ (TA)}_{1,2;\ a\to b}(\theta) = \left[\frac{2\pi b_r}{k_a \sin\theta}\right]^{\frac{1}{2}} \frac{\exp\left\{i\left[\chi_-(b_r) - \frac{\pi}{4}\right]\right\}}{|q_r|^{1/2}} Ai\left(\frac{\theta_r^{class} - \theta}{q_r^{1/3}}\right) . \tag{91}$$

This expression is only exact near the classical rainbow and does not go uniformly to the exact expression of the DCS far from this singularity, eq. 83. In eq. 91, θ_r^{SC} do exactly

happens at the first maximum of the Airy function and its exactly given by eq. 89. Also, θ_r^{class} corresponds to an inflection point in the Airy function. Of course, the transitional approximation less uniform counterpart but it si easier to implement.

Finally, if the above condition of the scattering angle

$$\theta \neq 0 \; or \; \pi \tag{92}$$

is not satisfied then the SC approximation to the glory and the small angle singularities can be applied [149].

The derivation of the integral cross sections starts from its partial-wave expression for a central-field inelastic process given in chapter 5

$$\sigma_{a\to b}(\theta) = \sum_{l=0}^{\infty} (2l+1)|S_{a\to b}(l)|^2 \; . \tag{93}$$

By transforming the sum into an integral and by replacing semiclassically l with b, it is obtained that

$$\begin{aligned} \sigma_{ab}^{end}(\theta) &= \lim_{\hbar\to 0} \frac{\pi}{k_a^2} \int_0^{\infty} dl \; (2l+1) \left| S_{ab}^{end}(l) \right|^2 \\ &= 2\pi \int_0^{\infty} db \; b P_{el}(b)_{ab} \end{aligned} \tag{94}$$

This expression has no singularities except for the elastic case in which $\lim_{b\to\infty} P_{el}(b)_{aa} = 1$. SC approximations can be again applied to overcome this problem [142].

The END Cross Sections II: Atom-Diatom Scattering

The Atom-Diatom END Wave Function

The next stage in this study is to derive the END cross sections for an atom-diatom process. This is the first scattering process in which the rotational and vibrational degrees

of freedom of a molecule will manifest themselves. The END nuclear part of a three center system is now

$$F_{nucl}(\mathbf{X}:\mathbf{R},\mathbf{P}) = \prod_{k=1}^{3} \exp\left\{-a_k[\mathbf{X_k} - \mathbf{R_k}(t)]^2 + \frac{i}{\hbar}\mathbf{P_k}(t)\cdot[\mathbf{X_k} - \mathbf{R_k}(t)]\right\} \tag{95}$$

with

$$a_k = \frac{m_k \omega k}{2\hbar} \quad k = 1,\ 2,\ 3 \tag{96}$$

To be more specific, a non-rearrangement process is considered. The projectile nucleus is label 3 as usual. The rearrangement process will follow a similar treatment. As in the previous section, the Jacobi coordinate transformation is introduced

$$\begin{aligned} \mathbf{X_0} &= \frac{1}{M}(m_1\mathbf{X_1} + m_2\mathbf{X_2} + m_3\mathbf{X_3})\ , \\ \mathbf{X_{ad}} &= \mathbf{X_3} - \frac{1}{m_d}(m_1\mathbf{X_1} + m_2\mathbf{X_2})\ , \\ \mathbf{x} &= \mathbf{X_2} - \mathbf{X_1}\ . \end{aligned} \tag{97}$$

where M is the total mass ($M = m_1 + m_2 + m_3$) and m_d is the mass of the diatomic fragment ($m_d = m_1 + m_2$). In this transformation, $\mathbf{X_0}$ is the nuclear CM position, $\mathbf{X_{ad}}$ is the atom-diatom relative position, and $\mathbf{x}$ is the relative position of the diatom atoms. A similar transformation for the parameters of the average nuclear position can be written. The inverse transformation is

$$\begin{aligned} \mathbf{R_1} &= \mathbf{R_0} - \frac{m_3}{M}\mathbf{R_{ad}} - \frac{m_2}{m_d}\mathbf{r}\ , \\ \mathbf{R_2} &= \mathbf{R_0} - \frac{m_3}{M}\mathbf{R_{ad}} + \frac{m_1}{m_d}\mathbf{r}\ , \\ \mathbf{R_3} &= \mathbf{R_0} + \frac{m_d}{M}\mathbf{R_{ad}}\ . \end{aligned} \tag{98}$$

By repeating the same algebra as that in the atom-atom scattering, we can achieve the separation of the CM degrees of freedom from the remainder if we impose the condition: $\omega = \omega_1 = \omega_2 = \omega_3$. Then, we obtain

$$\begin{aligned} F_{nucl}(\mathbf{X}:\mathbf{R},\mathbf{P}) =& F_0(\mathbf{X_0}:\mathbf{R_0},\mathbf{P_0})F_{ad}(\mathbf{X_{ad}}:\mathbf{R_{ad}},\mathbf{P_{ad}})\times \\ & F_d(\mathbf{x}:\mathbf{r},\mathbf{p})\ , \end{aligned} \tag{99}$$

where

$$F_0(\mathbf{X_0}\colon \mathbf{R_0}, \mathbf{P_0}) \quad = \exp\left\{-a_0[\mathbf{X_0} - \mathbf{R_0}(t)]^2 + \frac{i}{\hbar}\mathbf{P_0}(t)\cdot[\mathbf{X_0} - \mathbf{R_0}(t)]\right\},$$
$$F_{ad}(\mathbf{X_{ad}}\colon \mathbf{R_{ad}}, \mathbf{P_{ad}}) = \exp\left\{-a_d[\mathbf{X_{ad}} - \mathbf{R_d}(t)]^2 + \frac{i}{\hbar}\mathbf{P_{ad}}(t)\cdot[\mathbf{X_{ad}} - \mathbf{R_{ad}}(t)]\right\}, \tag{100}$$

and

$$F_d(\mathbf{x}\colon \mathbf{r}, \mathbf{p}) = \exp\left\{-a_\mu[\mathbf{x} - \mathbf{r}(t)]^2 + \frac{i}{\hbar}\mathbf{p}(t)\cdot[\mathbf{x} - \mathbf{r}(t)]\right\}. \tag{101}$$

Here, the momentum parameters $\mathbf{P_0}(t)$ ("total nuclear momentum"), $\mathbf{P_{ad}}(t)$ ("atom diatom relative momentum"), and $\mathbf{p}(t)$ ("atoms in the diatomic relative momentum") are

$$\begin{aligned}\mathbf{P_0}(t) \quad &= \mathbf{P_1}(t) + \mathbf{P_2}(t) + \mathbf{P_3}(t)\,,\\ \mathbf{P_{ad}}(t) &= \frac{m_d}{M}\mathbf{P_3}(t) - \frac{m_3}{M}[\mathbf{P_1}(t) + \mathbf{P_2}(t)]\,,\end{aligned} \tag{102}$$

and

$$\mathbf{p}(t) = \mu\left(\dot{\mathbf{R}}_2 - \dot{\mathbf{R}}_1\right) = \mu\dot{\mathbf{r}}\,, \tag{103}$$

where μ is the diatomic reduced mass ($\mu = \frac{m_1 m_2}{m_1+m_2}$). The transformed nuclear coefficients are

$$a_0 = \frac{M\omega}{2\hbar}\,, \tag{104}$$

$$a_{ad} = \frac{\mu_{ad}\omega}{2\hbar}\,, \tag{105}$$

and

$$a_\mu = \frac{\mu\omega}{2\hbar}\,, \tag{106}$$

where μ_{ad} is the atom-diatom reduced mass ($\mu_{ad} = \frac{m_d m_3}{md+m_3} = \frac{(m_1+m_2)m_3}{m_1+m_2+m_3}$). The Gaussian associated with the atom-diatom relative motion will be treated as its analogue in the atom-atom scattering. On the other hand, the Gaussian associated with the diatomic internal motion will be treated as the rotational-vibrational uncoupled function of the previous section

$$F_d(\mathbf{x}\colon \mathbf{r}, \mathbf{p}) \approx F^d_{vib}(x; r)F^d_{rot}(\varphi; \widetilde{\varphi}) \tag{107}$$

The electronic part of the wave function and the total phase undergo the same transformations as those in the previous section.

In the case of a rearrangement, the above transformation is used up to the time of the interchange. Thenceforth, a similar transformation is used in terms of the final projectile and molecular fragments. .

The Atom-Diatom END S-Matrix

In this case, the state to project on is constructed as

$$\Psi_{int_b}^{end} = \frac{F_{ad}[\mathbf{R_b}, \mathbf{P_b}] F_{v,l,m}(x,\theta,\varphi) f_{el}[\mathbf{z_b}, \mathbf{r_b}]}{N_b} \tag{108}$$

i.e. a frozen Gaussian wave packet $F_{ad}\left(\mathbf{R}_{\mathbf{ad}}^{\mathbf{b}}, \mathbf{P}_{\mathbf{ad}}^{\mathbf{b}}\right)$ with arbitrary atom-diatom relative positions $\mathbf{R}_{\mathbf{ad}}^{\mathbf{b}}$ momenta $\mathbf{P}_{\mathbf{ad}}^{\mathbf{b}}$ carrying a quantum rovibrational function for the diatom $F_{v,l}(x,\theta,\varphi)$ and a SCF electronic function $f_{el}[\mathbf{z_b}, \mathbf{r_b}]$ with total normalization constant N_b. The final label b (or the initial label a) comprises the final (initial) position and momenta $\mathbf{R}_{\mathbf{ad}}^{\mathbf{b(a)}}$ and $\mathbf{P}_{\mathbf{ad}}^{\mathbf{b(a)}}$, the vibrational quantum number $v^{(')}$, and the rotational quantum numbers $l^{(')}$ and $m^{(')}$. The diatom rovibrational function is [19]

$$F_{v,l,m}(x,\theta,\varphi) = \frac{1}{x} S_v(x) Y_{l,m}(\theta,\varphi) \tag{109}$$

where $S_v(x)$ is an harmonic oscillator eigenfunction of frequency ω, and $Y_{l,m}(\theta,\varphi)$ is a spherical harmonic. Then, the S-matrix elements are (omitting some arguments for brevity)

$$S_{a\to b}^{END} = A_{ad}\left(\mathbf{R}_{\mathbf{ad}}^{\mathbf{b}}, \mathbf{P}_{\mathbf{ad}}^{\mathbf{b}}, \mathbf{R}_{\mathbf{ad}}^{\mathbf{a}}, \mathbf{P}_{\mathbf{ad}}^{\mathbf{a}}\right) A_{vib}^{ab} A_{rot}^{ab} A_{el}^{ab} exp\left(\frac{i}{\hbar}\gamma_{int}\right), \tag{110}$$

where the atom-diatom amplitude $A_{ad}\left(\mathbf{R}_{\mathbf{ad}}^{\mathbf{b}}, \mathbf{P}_{\mathbf{ad}}^{\mathbf{b}}, \mathbf{R}_{\mathbf{ad}}^{\mathbf{a}}, \mathbf{P}_{\mathbf{ad}}^{\mathbf{a}}\right)$ and the electronic amplitude A_{el} are the analogues of $A_{nucl}(\mathbf{r_b}, \mathbf{p_b}, \mathbf{r_a}, \mathbf{p_a})$ and A_{el} from the previous section,

respectively. The vibrational amplitude A_{vib} is

$$\begin{aligned} A_{vib}^{v'v} &= \int dx \, \frac{1}{x} S_v(x) F_{vib}(x; r, \dot{r}) x^2 \\ &= \int dx \; S_v(x) \exp\left\{ -a_\mu [x - r(t)]^2 + \frac{i}{\hbar} \mu \dot{r}(t) [x - r(t)] \right\} \\ &= \frac{(\alpha_{v'})^v}{\sqrt{v!}} \exp\left(-\frac{|\alpha_{v'}|^2}{2} \right) . \end{aligned} \tag{111}$$

where the canonical coherent state parameter $\alpha_{v'}$ is

$$\alpha_{v'} = \frac{E_{vib}^{v'}}{\hbar\omega} , \tag{112}$$

with $E_{vib}^{v'}$ the classical vibrational energy at final. In the non-rearrangement case, the parametric frequency ω can be set to the diatomic frequency at the initial time. In the rearrangement case, the initial value of ω must be changed to that of the final diatomic molecule. The rotational amplitude A_{rot} is

$$\begin{aligned} A_{rot}^{l',m',l,m} &= \int d\varphi d\theta \sin\theta Y_{l,m}^*(\theta, \varphi) F_{rot}^d(\theta, \varphi) \\ &= \left(\lim_{\hbar \to 0} P_{lM0}(\beta) \right) . \end{aligned} \tag{113}$$

where $P_{lM0}(\beta)$ is the rotational CS resolution, eq. 81 for a diatom. In the SC limit of $\hbar \to 0$, the atom-diatom amplitude A_{ad} will go to a delta function and we can write similarly to the atom-atom case

$$\lim_{\hbar \to 0} S_{ab}^{end} = A_{vib}^{ab}(\mathbf{I}) A_{rot}^{ab}(\mathbf{I}) A_{el}^{ab}(\mathbf{I})_{ab} \exp\left[\frac{i}{\hbar} \gamma_{int}(\mathbf{I}) \right] \tag{114}$$

where $\mathbf{I}$ denotes all the classical initial conditions: the projectile impact parameter, and the diatom angular orientations. Also in that limit, the internal phase $\gamma_{int}$is

$$\lim_{\hbar \to 0} \gamma_{int}(t) = \int_{t_1}^{t_2} dt' \left[\mathbf{P_{ad}}(\mathbf{t'}) \cdot \dot{\mathbf{R}}_{\mathbf{ad}}(\mathbf{t'}) \mathbf{p}(t') \cdot \dot{\mathbf{r}}(t') + \dot{\gamma}_{el}(t') \right] - E_{int}(t_2 - t_1) , \tag{115}$$
$$(t = t_2 - t_1 \to \infty) .$$

The expression for the electronic phase γ_{el} will be given later. As before, the internal energy E_{int} term can be omitted.

It is very instructive to compare the END S-matrix in the classical limit with that of the semiclassical theory [85, 86, 91]. For the classical actions$n,\ l,\ and\ M$ associated with the vibrational, total angular and the helicity angular diatomic motions with conjugated angles $q_n,\ q_l,\ and\ q_M$, respectively, the semiclassical S-matrix is (adapting the notation to ours)

$$S^{SC}_{a\rightarrow b}(J) = \left[\frac{D}{(2\pi i\hbar)^3}\right]^{\frac{1}{2}} exp\left[\frac{i}{\hbar}\gamma^{SC}_{ab}(J)\right], \tag{116}$$

where J is the total angular momentum of the system, D is the Van Vleck's determinant

$$D^{-1} = \left|\frac{\partial n(t_2)}{\partial q_n(t_1)}\ \frac{\partial l(t_2)}{\partial q_l(t_1)}\ \frac{\partial M(t_2)}{\partial q_M(t_1)}\right|, \tag{117}$$

and $\gamma^{SC}_{a\rightarrow b}$ is the SC action

$$\gamma^{SC}_{a\rightarrow b}(J) = -\int_{t_1}^{t_2} dt\left[R_{ad}\dot{P}_{ad} + q_n\dot{n} + q_j\dot{j} + q_M\dot{M}\right] \tag{118}$$

By examining these two versions of the S-matrix, we notice the following differences

1. There are no electronic terms in either the pre-exponential factor or the phase in the semiclassical S-matrix
2. The semiclassical S-matrix and its subjacent dynamics are in terms of the above action-angle variables. In the a END dynamics there is no attempt to use such variables since a transformation to them becomes increasingly cumbersome for more complicated systems.
3. The semiclassical rovibrational amplitude is given by the classical Van Vleck's determinant whose numerical evaluation is complicated. On the other hand, the END rovibrational amplitude is obtained via a CS mapping of the classical motion onto the quantum states. The evaluation of the CS amplitudes is quite simple.
4. Finally, the dynamical schemes are very different. In the semiclassical dynamics, not all the trajectories going to a given direction contribute to the S-matrix but

only those ending with integer values of the actions. This is the cumbersome root-searching problem of the semiclassical scheme. In the END dynamics, there is no such a problem. Every trajectory ending in a given direction will definitely contribute to the S-matrix via a coherent state amplitude.

The END Cross Sections for the Atom-Diatom Scattering

In the most convenient helicity representation, the scattering amplitude is, eq. 24,

$$f_{n_a j_a M_a n_b j_b M_b}(\theta) = \frac{1}{i[2\pi k_a k_b sin\theta]^{\frac{1}{2}}} \sum_{l=0}^{\infty} (2J+1) d^J_{M_b M_a}(\theta) S_{ab}(J) \qquad (119)$$

where

$$n,\ l,\ and\ M \qquad (120)$$

are the vibrational, total angular, and helicity angular quantum numbers (which correspond SC to the previously defined actions), and the $d^J_{M_2 M_1}(\theta)'s$ are the central part of the rotation matrices $D^J_{M_2 M_1}(\phi, \theta, \chi)'s$ (Wigner D functions) [25]. The presence of the above matrices, the sum over J instead of l, and the more complex phase make the SC evaluation of this sum more difficult. Furthermore, it seems that a close resemblance of the final expression to the pure classical result, as in the atom-atom scattering case, can be derived for some special cases. The analysis is partially hindered by the absence of SC techniques to be applied to this inelastic scattering as discussed in the last section of chapter 5. The study of this more complex expression can be done in the following paragraphs.

Initial nonrotating target: approximate treatment

If the initial target is not rotating, having or not vibrational motion, then $M_1 = 0$. For the same reason, the total angular momentum is at the initial time totally due to the relative motion of the two fragments.$J = l$. If the initial velocities of the three atoms

are all in the same then, by conservation of the total angular momentum, the dynamics is constrained on that plane. This is the situation of the $[\alpha,\ \beta = 0^0]$ orientations in the $H^+ + H_2$ system studied in chapter 7. Also, it must be verified that $M_2 = 0$ even though there is rovibrational excitation. In such a case [25],

$$d^J_{0,0}(\theta) = P_J(\cos\theta)\ . \tag{121}$$

If the diatom contribution in the dynamics is small compared with that of the relative motion of the two fragments, we can neglect that contribution in the phase. This is the classical analogue of the sudden approximation [134] discussed in chapter 2. If we also neglect the electronic phase, as in the previous section, we obtain an expression formally identical to that of the atom-atom scattering which can be treated in the same way. The evaluation of the cross sections and the treatment of the rainbow, glory, and small angle singularities can be done identically. The special case of a homonuclear target, the orientation $[\alpha = 90^0,\ \beta = 0^0]$ shares the same characteristics so far explained and undergoes an identical treatment.

If the initial velocities of the three atoms are not in the same plane then the dynamics is of course not constrained onto that plane. In other words, the final projectile is scattered off that plane and its asymptotic motion is described by the two scattering angles $\theta\ and\ \varphi$. M_2 can acquire any value but if the body-fixed approximation [134] is applied then it holds that $M_2 \approx 0$. If the electronic and the diatom contributions are further neglected in the phase, it is obtained that

$$\begin{aligned}\lim_{\hbar\to 0}\gamma_{int} &= \int_{t_1}^{t_2} dt'\ \mu_{ad}\Big[\dot{R_{ad}}^2 + R^2_{ad}\dot{\theta}^2_{ad} + R^2_{ad}\sin^2\theta_{ad}\dot{\varphi}^2_{ad}\Big] \\ &= \int_{t_1}^{t_2} dt'\ \mu_{ad}\Big[\dot{R_{ad}}^2 + L^m_{ad}\dot{\theta}_{ad} + L^I_{ad}\dot{\varphi}_{ad}\Big]\ .\end{aligned} \tag{122}$$

If the third term is also neglected in the phase, the DCS can be derived as that of the dynamics in the plane. This has been the theoretical approach used in the systems studied in chapter 7.

The motivation of using all these approximations is to obtain analytical expressions similar to those of the atom-atom scattering. These expressions closely resemble the classical result and the treatment of its singularities is well-known. It is important to remember that these approximations become exact for high impact parameter collisions. The combination of the above sudden and body-fixed approximations is the classical analogue of the quantum infinite order approximation (IOSA) discussed in chapter 2. However, these approximations have been introduced only to evaluate semiclassically the differential cross sections: the END evolution does not invoke them and the full dynamics is still reflected in the S-matrix of the cross section.

Initial rotating target: approximate treatment

It is obvious from the previous discussion that this case is even more difficult to treat. No END study has been attempted on this initial condition yet. If we crudely approximate the rotational matrix $d^J_{M_2 M_1}(\theta)'s$ by the Legendre function, as before, approximate the total angular momentum by

$$J = l \tag{123}$$

and apply all the other approximations of the previous case, then we obtain the same equivalent expressions. Of course, these approximation are more drastic in this context.

Exact treatment

Now the question arises about how to SC evaluate the differential cross section without any approximation. In terms of the traditional semiclassical theory, that evaluation

is known [85]. It implies the use of the SC limit of the $d^J_{M_2 M_1}(\theta)$ matrices [150] and the evaluation of the resulting integral by stationary phase with respect to J. The final expression for the cases without singularities is known [85] and its implementation does not seems to be very difficult. However, it seems that this expression has never been used and its extension to the cases with singularities is unknown. Aside from these concerns, the use of that expression is problematic in our END context because it depends on the pure semiclassical phase which is not the same as that of the END theory. Furthermore, this expression could be more properly used if the nuclear dynamics were entirely done in terms of action-angle variables, and a root-searching algorithm were employed to select the proper trajectories. This scheme of work is not advocated here and has been systematically avoided from the very beginning. If that effort is discarded, the previously described approach can be adopted.

Other END Scattering Properties

The END Average Energy Loss

The derivation of the END average energy loss stems from the previous derivation of the differential cross section. An example is shown below for a non-transfer, atom-atom (or equivalently reduced case) scattering process; the transfer case can be treated in the same way. In a classical END description, the denominator of the energy loss, eq. 5, becomes

$$\begin{aligned}\sum_{b'} \frac{d\sigma^{NT}_{a\to b'}}{d\Omega} &= \sum_{b'} \sum_{i} \frac{b_i P_i^{NT} P_{a\to b'}}{\sin\theta \left(\frac{\partial\theta}{\partial b}\right)_i} \\ &= \sum_{b'} \frac{b_i P_i^{NT}}{\sin\theta \left(\frac{\partial\theta}{\partial b}\right)_i} \\ &= \left(\frac{d\sigma}{d\Omega}\right)^{NT}_{total} .\end{aligned} \tag{124}$$

At the same time, the numerator turns out to be

$$\begin{aligned}\sum_a \left(\frac{d\sigma_{a\to b}}{d\Omega}\right)\Delta E_{a\to b} &= \sum_a \sum_i \frac{b_i P_i^{NT} P_{a\to b}\Delta E_{a\to b}}{\sin\theta\left(\frac{\partial\theta}{\partial b}\right)_i} \\ &= \sum_i \frac{b_i P_i^{NT}\Delta E_i^{NT}}{\sin\theta\left(\frac{\partial\theta}{\partial b}\right)_i} \,.\end{aligned} \tag{125}$$

where

$$\Delta E_i^{NT} = \sum_b P_{a\to b}\Delta E_{a\to b} \,. \tag{126}$$

Notice that the $\Delta E'_{a\to b}s$ are the (time-independent) energy eigenvalues of the final target in the basis set being used. Therefore, ΔE_i^{NT} is immediately interpreted as the average energy transferred by the projectile to the target in the branch i. For processes with low electron transfer and excitation probability, this transferred energy is correct within the numerical accuracy. But for very mixed processes (*i.e.* those with comparable transfer and non-transfer probabilities) the correctness of this value and of its physical meaning is questionably. The final expression for the energy loss is

$$\begin{aligned}\langle\Delta E(\theta)\rangle &= \frac{\sum_i \frac{b_i P_i^{NT}\Delta E_i^{NT}}{\sin\theta\left(\frac{\partial\theta}{\partial b}\right)_i}}{\sum_i \frac{b_i P_i^{NT}}{\sin\theta\left(\frac{\partial\theta}{\partial b}\right)_i}} \\ &= \frac{\sum_i \frac{b_i P_i^{NT}\Delta E_i^{NT}}{\sin\theta\left(\frac{\partial\theta}{\partial b}\right)_i}}{\left(\frac{d\sigma}{d\Omega}\right)_{total}^{NT}} \,.\end{aligned} \tag{127}$$

Note that the numerator is identical to the classical differential cross section withΔE_i^{NT} as an additional factor. A subsequent average over all the orientations completes the energy loss calculations.

A semiclassical version of this expression can be easily obtained by applying the SC procedures of the DCS.

CHAPTER 7
CALCULATION RESULTS

General Considerations

In this chapter, the previously derived formalism to quasi-classically and semiclassically describe a scattering process within the END theory will be numerically tested. Three gas phase scattering systems:

$$H^+ + H_2 \tag{1}$$

$$H^+ + CH_4 \tag{2}$$

and

$$H^+ + H_2O \tag{3}$$

experimentally studied by P. Toennies and collaborators[36, 151, 152] have been selected. The choice of these beam experiments is made for several reasons. First of all, these measurements rendered time-of-flight (TOF) spectra and ICSs and DCSs for both the transfer and the non-transfer channels. This wealth of information about a chemical reaction is not usually attained in beam experiments. Secondly, the somewhat high, in chemical terms, collision energies of 30 eV in the first two experiments and of 46 eV in the last one are within the range of validity of the SC and quasi-classical theory developed in this thesis. Furthermore, the possibility of subtle quantum effects, such as tunneling, not tractable within the present formalism are unlikely to happen in that energy regime. Furthermore, the use of excited state PESs is mandatory if an accurate dynamical description is desired at those energies. These excited states are automatically generated

by the single determinant electronic wave function of the END formalism. This certainly guaranties a proper treatment of the dynamics.

In the case of the first system, the TOF spectra is relatively simple and allowed the experimental group to evaluate vibrationally resolved ICSs and DCSs. These highly detailed properties are successfully reproduced by the present END formalism as will be seen in the next section. The other two experiments did not rendered vibrationally resolved ICSs and DCSs because of the complexity of their respective TOF spectra. However, the successful END reproduction of their properties for such complex systems is far from trivial. These two last systems also exhibit a great deal of chemical features which are pictorially described in the next sections. Unfortunately, these experiments did not yield any rotationally resolved property. A test of the rotational part of the present formalism is left for future investigations. However, some properties not measured in these experiments are also theoretically investigated in the next sections. They are compared with independent experimental work cited below.

The Proton-Hydrogen Molecule System

Experiments and Previous Theory

From a theoretical point of view, the

$$H_1^+ + H_2H_3\ (v_i = 0)\ , \tag{4}$$

system of reactants exhibits four distinct processes, namely, the no-transfer (NT) inelastic channel with the products

$$H_1^+ + H_2H_3\ (v_f)\ , \tag{5}$$

the charge transfer (CT) channel, yielding

$$H_1 + H_2H_3^+\ (v_f)\ . \tag{6}$$

the rearrangement (R) or "reactive" channels with products

$$H_{2/3}^{+} + H_1 H_{3/2}\ (v_f)\ , \tag{7}$$

and

$$H_{2/3} + H_1 H_{3/2}^{+}\ (v_f)\ ; \tag{8}$$

and the collision-induced dissociation (D) channels, producing

$$H_1 + H_{2/3}^{+} + H_{3/2}\ . \tag{9}$$

or

$$H_1^{+} + H_2 + H_3\ . \tag{10}$$

Such detail is not possible to observe in the experiments used here for comparison. In fact, the established theoretical methods usually make simplifying assumptions that eliminate from consideration some of the channels. For instance, constraints on the range of some interparticle distances will prevent the dynamics to reach the dissociative channels.

The END calculations are compared with results from experimental studies on the NT product channel showing vibrational (rotational) excitation of the H_2 molecule [153–156] and on the charge transfer (CT) channel [157]. DCSs both for scattered protons and hydrogen atoms have been measured at collision energy of 30 eV in the laboratory frame (20 eV in the center of mass frame).

A number of theoretical models has been applied to this system. The trajectory surface hopping model (TSHM) [158, 104] (see chapter 2) was used for comparison with a TOF experiment [157]. Disagreements were attributed to unspecified inadequacies of the chosen potential energy surfaces. In particular, the experimental results show a more pronounced angular dependence of the DCSs for charge transfer than do the theoretical ones. A quite extensive and elaborate three-dimensional quantum mechanical study of

this system[36] employing the DIM surface suggested by Ellison[22], and invoking the infinite order sudden approximation (IOSA) [36] (see chapter 2), has been carried out with some better agreement with experiments than that of TSHM. Still there are discernible differences between some of the results of this study, which will be referred to as IOSA for short, and experiment. Particularly, the position of the rainbow angle, and vibrationally resolved differential cross sections deviate from the experimental results. As explained in chapter 2, the IOSA method employs Jacobi internal coordinates consisting of the distance R, between the projectile and the center of mass of the target molecule, the bond distance r of the diatomic, and an orientation angle γ, are used in this approach. The discretization of γ, the determination of the limits of R and r, and their influence on the results are said to represent a considerable effort. Yet, it appears that the value chosen for r_{max} of 2.2 Å excludes any of the processes involving proton exchange, or total breakup, both of which take place at this energy. Furthermore, R_{max} = 4.7 Å seems a bit too small a product separation when one of the fragments is charged. Thus, even the three-dimensional quantum mechanical treatment on two coupled surfaces involves a rather constrained dynamics.

In view of these difficulties, it is interesting to perform a END study of this system with a full dynamics of electrons and nuclei. Particularly, since the END allows for all possible product channels and does not employ PESs.

Initial Conditions and Final State Analysis

The present END calculations were performed with the ENDyne program package and its auxiliary programs EVOLVE, PROJECT and ECROSS [2] to evaluate cross sections other final properties. Parameters defining the initial conditions of the reactants are depicted in fig. 7.1. The nuclei originally of the H_2 molecule are labeled 1 and

2, respectively and the H^+ projectile is labeled 3. The electronic state is described in a pVDZ [4s1p]/(2s1p) basis [159] centered on each of the three nuclei. This basis has shown to be adequate in earlier END studies on hydrogenic systems[7]. The H_2 molecule is initially in its electronic ground state and at its equilibrium geometry as given by the single determinant approximation in the given basis. It is initially at rest with its center of mass at the origin of the laboratory frame. The classical description of the nuclei means that the nuclei are stationary in the vibrational ground state. The H^+ projectile is placed 15 a.u. from the target with a momentum corresponding to E_{lab} 30 eV in the z-direction. A number of END trajectories are then calculated for varying initial orientation [α, β] of the target (see fig. 7.1) and for different values of the projectile impact parameter b. The values of the polar angle α of the bond vector are chosen in steps of 15° from 0° to 180°, and it was found sufficient to consider only the values 0°, 45°, and 90° for the azimuthal angle β of the bond vector. The impact parameter b assumes values in steps of 0.1 a.u. from 0.0 to 2.0 a.u. and in steps of 0.2 a.u. from 2.0 to 6.0 a.u. . Advantage can be taken of the symmetry so that, say, results of an orientation [α, 90°] are equivalent to those of the orientation [180° – α, 90°]. Still, the full study involves about 1,120 fully dynamical trajectories. Each trajectory evolution ran for 900 a.u. of time in order to achieve full separation of the product fragments. The calculations were performed on an IBM RS/6000–580 computer. The version of the ENDyne code used in this study allowed a total evolution to be carried out in about two hours of CPU time. For example, in the case of the orientation [75°, 0°] with an evolution time of 900 a.u., the CPU time decreased steadily from 2.5 hours for b = 0.0 a.u. to 2.0 hours for b = 6.0 a.u. .

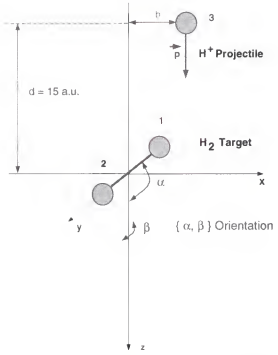

Figure 7.1: Initial conditions for the $H^+ + H_2$ system for the END calculations. α and B are the polar and the azimuthal angles, respectively, of the bond vector in the depicted Lab frame.

Each ENDyne run produces the final state of the system of product species, *i.e.* the final electronic wave function and the final nuclear positions and momenta. From the END evolution selected properties can be calculated with the previously cited auxiliary programs. For instance, the electronic charge distribution, say, as given by the Mulliken population is readily obtained by the program EVOLVE. An analysis of the electronic state is essential in terms of its components that describe the various possible distributions of electronic charge among the separate product species. The program ECROSS, introduced in this thesis work, calculate the END cross sections according to the theory developed in chapter 6. Inspection of the END nuclear trajectories, interparticle distances, and atomic charges (Mulliken populations) as function of time permits the determination of the type of process (CT, NT, etc).). The scattering angle θ_{Lab} can be calculated according to eq. 32. The vibrational final state can be obtained by using the canonical CS resolution into

the harmonic oscillator eigenstates, eq. 9, chapter 4, reproduced below

$$P_n(\alpha) = exp\Big\{-|\alpha|^2\Big\}\frac{|\alpha|^{2n}}{n!} \ . \tag{11}$$

This procedure is accomplished by matching the final END vibrational energy E_{vib}^{END} with the classical energy associated with the canonical CS E_{class}^{α}, 30,

$$\begin{aligned} E_{vib}^{END} &= E_{class}^{\alpha} \\ &= \hbar\omega|\alpha|^2. \end{aligned} \tag{12}$$

In this way, the squared modulus of the CS parameter α is obtained and subsequently used in eq. 11. The END vibrational energy E_{vib}^{END} derives directly from the electron nuclear dynamics, since the total nuclear energy is calculated throughout each trajectory and at final separation can be evaluated for the molecule in question. Subtracting the center of mass translational energy leaves the kinetic energy of the rovibrational motion. In the present case, the rotational energy estimated from the angular momentum and the moment of inertia at equilibrium is found to be negligible. The final electronic state of the product molecule comes from projecting, say, the total $H^+ + H_2$ electronic state onto that of H_2. Then, the electronic energy of this projected state, possibly an excited state, minus the ground state energy in the given basis yields the excitation energy, which, when added to the rovibrational kinetic energy gives the energy E available for quantum vibration and rotation of the molecule.

END Results

The principal assumption in the END theory applied to this system is that the TDVP yields an appropriate approximation to the time-dependent Schrödinger equation. The approximations then consist only of the choice of wave function (*e.g.* single determinant and classical nuclei) and that of a basis set. There are no further assumptions about the system of electrons and atomic nuclei. The electron-nuclear dynamics within these

approximations is exact within a given numerical precision. This approach is capable of describing details of the "microdynamics" on electronic time scales, far beyond what is observable with current experimental techniques. Nevertheless, such details give interesting and potentially useful informations about short-time processes. Furthermore, END does not exclude any of the possible processes. In table 7.1, the initial conditions $[\alpha, \beta]$ for the $H^+ + H_2$ system are grouped according to which processes are generated. In summary a number of observations can be made:

i. The dynamics starting from a target orientation $[\alpha, \beta]$ is similar in all respects to that of an orientation [180° - α, β]. This is expected in view of the rather isotropic interaction between the projectile and the target.

ii. Effects due to anisotropy of the interaction are mostly apparent for impact parameters below 2.0 a.u. . For instance, the rotational excitation, a clear manifestation of such effects, is important in this range.

iii. The occurrence of dissociation and rearrangement is more prominent for the $[\alpha, 0°]$ orientations than for others, and these two channels become less important as α goes to 0° or 180°.

iv. Initial $[\alpha, 0°]$ orientations lead to dissociation and rearrangement for impact parameters less than 1.0–1.5 a.u., while $[\alpha, 45°]$ and $[\alpha, 90°]$ produce the same processes for impact parameters below 0.5–0.8 a.u. .

In order to illustrate some detailed END results for the processes listed in table 7.1, figures 7.2 through 7.7 depict evolutions for 2000 a.u. of time. These figures refer to the initial target orientation [90°, 0°] and impact parameter$b$ = 0.3, 1.0, and 1.6 a.u., which lead to dissociation, rearrangement, and NT and CT scattering processes, respectively.

Table 7.1: Type of process produced by various initial conditions as given by target orientation and projectile impact parameter. D means dissociation, R rearrangement, and NT & CT non transfer inelastic and charge transfer scattering, respectively.

END product analysis		
[α, β] target orientation (deg)	Impact parameter range (a.u.)	Type of process
[90°, 0°]	0.0 - 0.5	D
	0.6 - 1.1	R
	1.2 -1.4	D
	1.5 -6.0	NT & CT
[90°, 45°]	0.0 - 0.5	D
	0.6 - 6.0	NT & CT
[90°, 90°]	0.0 - 0.6	D
	0.6 - 6.0	NT & CT
[60°, 0°]	0.0	R
	0.1 - 0.2	D
	0.3 - 1.0	R
	1.1 - 1.3	D
	1.4 - 6.0	NT & CT
[60°, 45°]	0.0	R
	0.1 -0.6	D
	0.7 - 6.0	NT & CT
[60°, 90°]	0.0	R
	0.1 - 0.3	D
	0.4 - 6.0	NT & CT
[30°, 0°]	0.0 - 0.1	NT & CT
	0.2 - 0.9	D
	1.0 - 6.0	NT & CT
[30°, 45°]	0.0 - 6.0	NT & CT
[30°, 90°]	0.0 - 6.0	NT & CT

The figures 7.2, 7.3, and 7.4 show the trajectories of the three nuclei (in the yz-plane), and the figures 7.5, 7.6 and 7.7 give the Mulliken populations versus time.

In the dissociation case, the incoming projectile transfers a great deal of momentum inducing the target to dissociate. In this case the outgoing projectile also carries a significant amount of charge from the target molecule. The rearrangement case trajectories and atomic charges depict a rovibrationally excited product molecule. The details in fig. 7.8 of the evolution of the three internuclear distances for the NT & CT case indicate that the first change in the target molecule bond distance is the so called bond "dilution", first found in a calculation by Giese *et al.*[160] and also in other treatments[161, 157] using classical nuclei .

In the CT scattering case the rovibrational excitation of the target molecule occurs simultaneously with the electron transfer. It is noteworthy in this context that Niedner *et al.* based on their theoretical analysis of the experimental results proposed a two-step mechanism for the CT scattering. An initial step consists of a vibrational excitation of the H_2 molecule to $v_f \geq 4$ followed by a second step of electron transfer from the excited molecule. The END dynamics does not support this picture.

Another dynamical quantity of interest is the scattering angle θ_{Lab} which enters into the expressions for the classical differential cross sections. This magnitude can be calculated directly form eq. 32, or from one of its many variants

$$\cos\theta_{Lab} = \frac{(p^2 - p_x^2 - p_y^2)^{1/2}}{p}, \tag{13}$$

where $\vec{p} = (p_x \quad p_y \quad p_z)$ with $p = |\vec{p}|$ is the final momentum of the fragment going to the detector (usually the fastest).

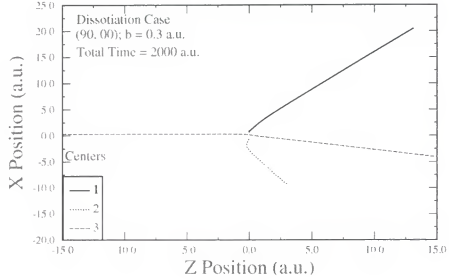

Figure 7.2: x vs. z position for the three centers (nuclei) in a END $H^+ + H_2$ trajectory belonging to the orientation [90°, 0°] for which the dynamics remains in the xz plane. The total evolution time is 2000 a.u. The process shown is for a dissociation (D) at impact parameter b = 0.3 a.u. The dissociation of the original target is clearly depicted

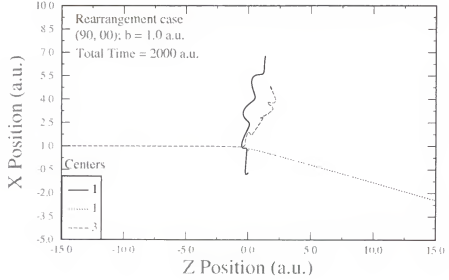

Figure 7.3: The same as in Fig. 7.2 but for a rearrangement process (R) at b = 1.0 a.u.

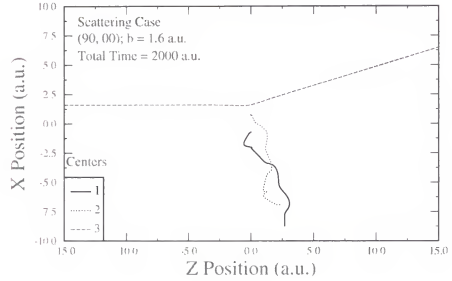

Figure 7.4: The same as in Fig. 7.2 but for a non transfer/charge transfer (NT/CT) at b = 1.6 a.u.

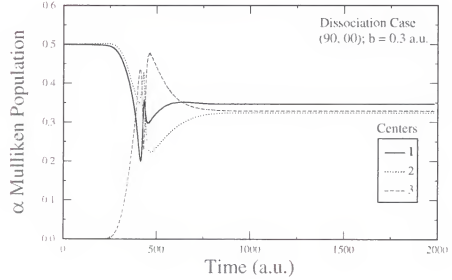

Figure 7.5: Mulliken population of α spin electrons vs. time for the three centers (nuclei) in a END $H^+ + H_2$ trajectory belonging to the orientation [90°, 0°]. The process shown is for a dissociation (D) at impact parameter b = 0.3 a.u.

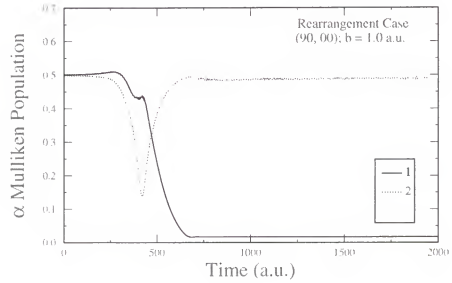

Figure 7.6: The same as in Fig. 7.5 but for a rearrangement process (R) at b = 1.0 a.u.

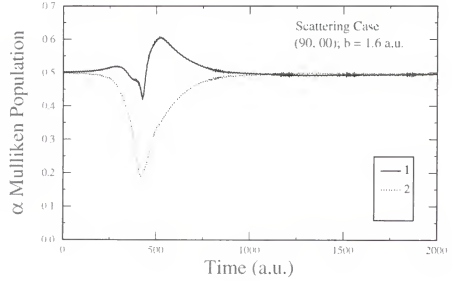

Figure 7.7: The same as in Fig. 7.5 but for a non transfer/charge transfer (NT/CT) at b = 1.6 a.u.

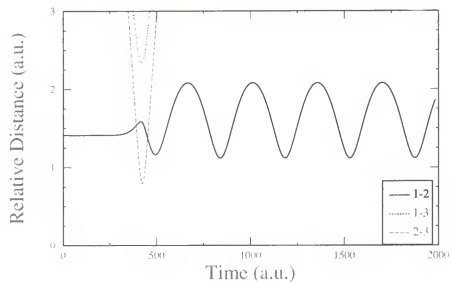

Figure 7.8: Relative nuclear distances vs. time for the orientation [90°, 0°] and impact parameter b = 1.6 a.u. The bond "dilution" of the H_2 as the projectile approaches, the initial vibrational excitation (correlated to the CT process, see Fig. 7.7), and the vibrational excitation after the collision can readily be discerned.

Figure 7.9 shows the scattering angle as a function of impact parameter for some representative initial reactant orientations. Impact parameter values in this figure apply only to NT & CT scattering (*i.e.* no breakup or rearrangement). The maximum in the range of b from 2.0 to 3.0 a.u. can be identified with the primary rainbow angle. Analogously to the case of ion-atom collisions [13, 4] this rainbow angle corresponds to the maximum of the attractive part of the interaction between projectile and target. The value of the classical rainbow angle is minimum for the [90°, 0°] initial target orientation, and shows a monotonic increase for α going to either to 0° or 180°, or for β approaching 90°. For the [90°, 90°] and for all the [α, 0°] trajectories a scattering angle of 0°, the glory angle[13, 4], arises for impact parameters smaller than those of the primary rainbow. As is the case for ion-atom collisions this glory singularity in the classical cross section occurs where the interaction changes from repulsive to attractive. For trajectories with other

initial target orientations a non zero minimum in the scattering angle replaces the glory angle giving rise to a so called secondary rainbow. This was first described in a DECENT calculation by Giese *et al.*[160] and also found in the TSHM calculations by Niedner *et al.*[157]. This secondary rainbow is associated with the projectile being scattered out of the original xz-plane. More precisely its x and y components of momentum pass through zero for close but different values of the impact parameter. Therefore, a zero scattering angle cannot occur (see eq. 13) when the projectile goes from the region of repulsive to the region of attractive interaction. However, the corresponding scattering angle is small, which causes a blurring of the rainbow and glory characteristics Analysis of the NT and CT probabilities as discussed below shows that the rearrangement and dissociation processes are far more efficient in transferring electronic charge than is the scattering. It is noteworthy that the CT probability as well as the transfer of energy into vibrations both reach a maximum at the impact parameter of the primary rainbow.

Vibrational resolution of various dynamical properties is achieved by subjecting the END trajectories to the analysis using the canonical CS. The result of that procedure for the case of weighted probabilities averaged over all target orientations is shown in fig. 7.10. The straight line represents $b\sum_i P_i = b$, since the sum over all probabilities must add to unity. The vibrational resolution of the NT channel permits the calculation of the classical vibrationally resolved NT integral cross sections, which show excellent agreement [162] with experiment.

The END vibrational energy transfer averaged over all molecular orientations is depicted in fig. 7.11 as a function of scattering angle together with the IOSA [36], the TSHM, and the experimental results [157]. There is a satisfactory agreement with experiment. The dip in the END results reflects the absence of some contributions to the energy transfer. Addition of more trajectories would tend to make this dip less

pronounced.

As discussed in chapter 5 and 6, the purely classical DCS for this system is (cf. eq. 83 and 84, chapter 6)

$$\frac{d\sigma(\theta_{Lab},[\alpha,\beta])}{d\Omega} = \sum_i \frac{b_i P_i(b_i,[\alpha,\beta])}{\sin\theta\left|\left[\partial\theta_{Lab}/\partial b\right]_{[\alpha,\beta],b=b_i}\right|} \,. \tag{14}$$

The classical DCS calculated in this manner provide a good initial estimate of the experimental results in spite of their typical singularities discussed in chapter 5. For instance, the average of the END results over the target orientations yields a classical rainbow angle θ_r^{class} at 8.8° as compared to the experimental value somewhere between 6° and 7°. The TSHM result is close to 10°.

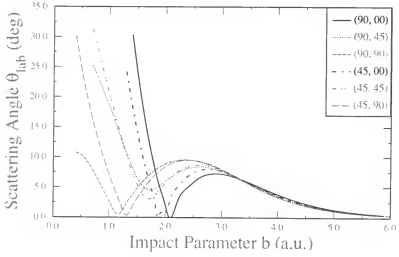

Figure 7.9: Laboratory scattering angle θ_{lab} vs. impact parameter b for some representative orientations [α, β]. The case depicted correspond only to the NT/CT scattering (no dissociation of rearrangement) for sake of simplicity. The primary rainbow angle can be seen for 2.0 $a.u. \leq b \leq$ 3.0 $a.u.$ in all cases. In the orientations with β = 0°, a (zero) glory angle can be observed at impact parameters lower than that of the primary rainbow. In the other orientations, a (nonzero) secondary rainbow angle can be seen.

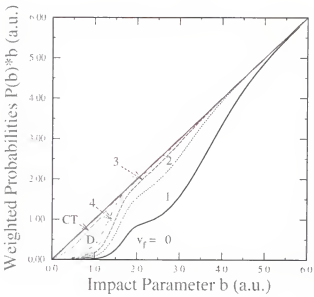

Figure 7.10: Orientation-averaged weighted probability vs. impact parameter. All the channels shown along with $b \sum_i P_i(b) = b$ as the upper straight line. CT is the total charge transfer via either dissociation or rearrangement or pure scattering, D is non transfer dissociation, and $v_f = 0,\ 1,\ 2,\ 3,\ 4$, final vibrational state of the H_2 molecule in the NT scattering case. The CT probability is a continuous function of the impact parameter but is low at high impact parameter. Observe the predominance of the dissociation and charge transfer processes at low impact parameters, and the higher vibrational excitation at the impact parameters of the rainbow.

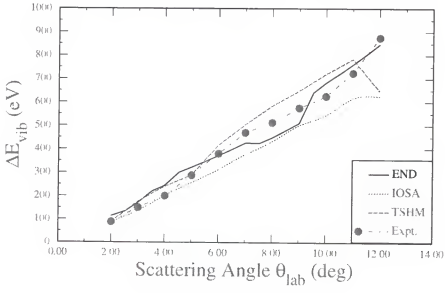

Figure 7.11: H_2 NT vibrational energy transfer ΔE_{vib} vs laboratory scattering angle θ_{lab}. Orientation-averaged results from END, IOSA [36], and THSM [157] calculations along with experimental data [157].

SC corrections yield cross sections that better agree with experiment as will be seen below. The transitional SC approximation for the END theory, eq. 85, 86 and 91, is employed for the primary rainbow. The treatment of the secondary rainbow is less straightforward. As discussed in the last section of chapter 5, there exists in the literature SC treatments of elastic isotropic scattering exhibiting a maximum and a minimum in the deflection function [143–145, 163]. The direct application of either the uniform or the transitional Airy approximation to both rainbow angles has been discussed in the cited works, but fails when they are too close to each other as in the present case. Approaches based on catastrophe theory [148], such as the uniform and transitional Pearcey approximation [163] are the correct SC treatment for both rainbow angles, but it is implementation is too cumbersome in this context. Therefore, no corrections have been made for the secondary rainbow. Other studies[160, 157] have adopted the same philosophy, and the averaging procedure of the END smooths effects of the secondary rainbow, anyway.

Figure 7.12 displays the total NT DCS for laboratory scattering angles of 2° through 12°. END is compared to IOSA [36], TSHM, and the experimental result [157]. The latter has been normalized to the END results by matching the experimental DCS at the experimental rainbow to the END total DCS at the END rainbow angle. The fig. 7.13 through 7.18 similarly show the vibrationally resolved NT DCSs for $v = 0, 1, 2, 3, 4, 5$. The agreement of the END results with experiment is superb with respect to position of the primary rainbow, overall shape, and vibrational resolution. Actually, the position of the END primary rainbow in all cases agree better with experiment than does the so called full quantum mechanical study using a DIM surface and the IOSA. The latter predicts values somewhat greater than do either TSHM or END.

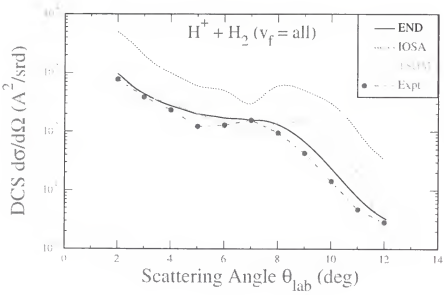

Figure 7.12: Total non transfer differential cross sections vs laboratory scattering angle. orientation averaged results from END, IOSA [36], and THSM [157] along with experimental data [157]. The latter have been normalized to the END results by matching the experimental total NT differential cross section at the experimental rainbow angle.

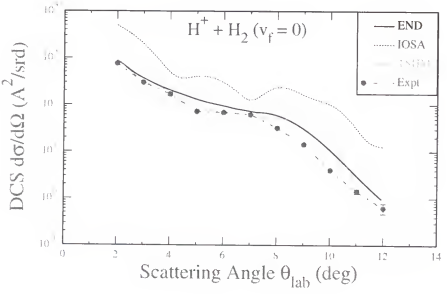

Figure 7.13: The same as in Fig. 7.12 but for the final vibrational state v_f = 0.

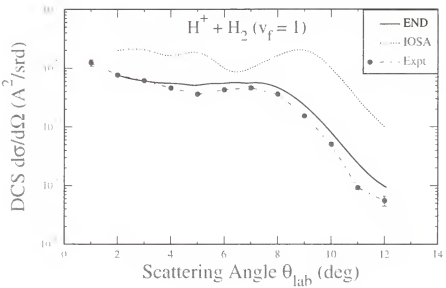

Figure 7.14: The same as in Fig. 7.12 but for the final vibrational state $v_f = 1$.

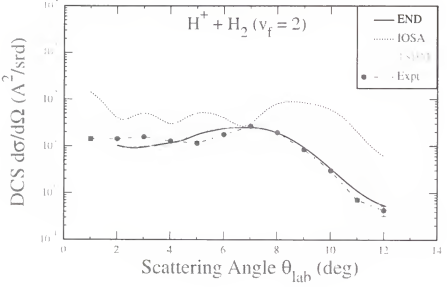

Figure 7.15: The same as in Fig. 7.12 but for the final vibrational state $v_f = 2$.

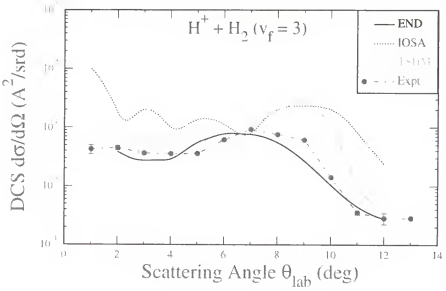

Figure 7.16: The same as in Fig. 7.12 but for the final vibrational state $v_f = 3$.

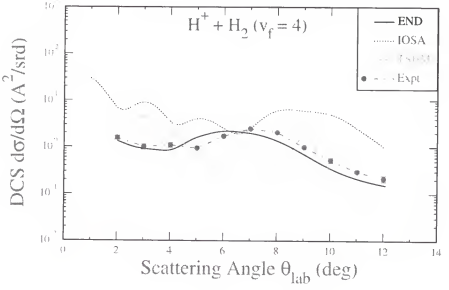

Figure 7.17: The same as in Fig. 7.12 but for the final vibrational state $v_f = 4$.

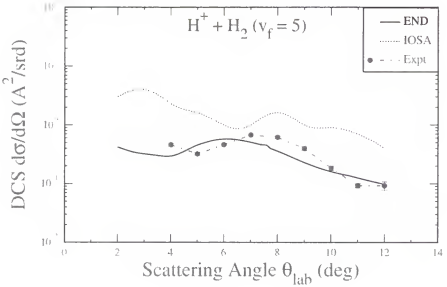

Figure 7.18: The same as in Fig. 7.12 but for the final vibrational state v_f = 5.

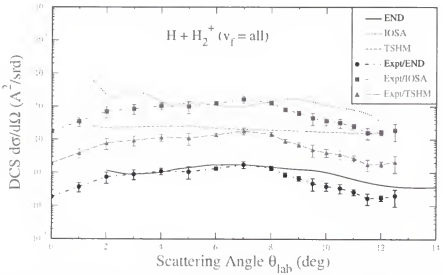

Figure 7.19: Charge Transfer total differential cross sections vs. laboratory scattering angle. Orientation-averaged results from END, IOSA [36], and THSM [157] calculations along with experimental data [157] normalized to the three calculations.

The END, IOSA, and TSHM total CT DCSs are given in Fig. 7.19 together with the experimental one, which has been reproduced three times for ease of comparison by normalizing it in turn to the three theoretical curves. The END results again show

satisfactory agreement with experiment. The END transfer cross section does better overall than the structureless TSHM results. It also seems to give a better account of the low angle portion than does IOSA, particularly in showing the proper decrease down to 2°.

The END description might be judged less satisfactory at greater scattering angles. The decrease of the theoretical curve is less rapid than the experimental one. The reason for this behavior is understood. For scattering angles greater than the primary rainbow, the repulsive interactions determines the differential cross section. As the scattering angle increases further and the impact parameter decreases, the dissociative region is reached. END shows no dissociation for $\theta \leq 12°$. Beyond the primary rainbow angle the CT probability function first decreases but then steeply increases into the region where dissociation dominates. This situation is particularly pronounced for the [α, 90°] orientations, which show less repulsion and permits the projectile to get close, interchange a considerable amount of charge, and then scatter. When energy losses higher than 3 eV are excluded the CT differential cross section assumes a reasonable fall-off for the higher scattering angles. This makes sense for the purpose of comparison, since it appears that such contributions cannot be seen by experiment[157]. None of the theories, including multi-trajectory method[164], reproduces the sharp fall-off of the experimental differential cross section at very low scattering angles. The END results down to 1° is no different. This increase in the calculated differential cross section for charge transfer seems to have its origin in the secondary rainbow, and particularly involve trajectories with [α, 90°] target orientations. Such a pronounced discrepancy between theory and experiment deserves further study. A vibrational resolution of the transfer DCS. similar to that in the non-transfer DCS, was attempted but it was not very satisfactory. A detailed discussion on this issue is provided in chapter 8.

An intriguing feature of the studies of this simple ion-molecule system is the quite

different absolute magnitudes of the total transfer cross section produced by the various theoretical approaches. Unfortunately, the TOF experiment referred to throughout this study [157] did not yield absolute results, which means that independent investigations must be consulted for comparison. Past experiments on the CT pprocesses of $H^+ + H_2$ measured only ICS, and most of those experiments were not carried out at energies close to E_{lab} = 30 eV. Some experiments at 30 eV actually failed to detect any transfer whatsoever[165]. Therefore, the value used here for comparison is one interpolated from data compiled by Phelps[166]. This data collection contains quite a few experimental results for $3.16\ \text{eV} \leq E_{lab} \leq 10,000\ \text{eV}$. Among these data, the experiment closest to our collision energy is the one by Gealy *et al.*[167]. The fitted values are also consistent with those in the classical works by Cramer [165] and Koopman[168]. Table 7.2 compares the interpolated experimental CT cross sections with the available theoretical ones. The END values are the classical ones obtained by (cf. eq. 94)

$$\sigma([\alpha,\beta]) = \int_{b_1}^{b_2} P(b,[\alpha,\beta])b\mathrm{d}b \tag{15}$$

followed by an average over orientations. The integration limits are chosen to correspond to the scattering angle interval of interest. It is not possible to ascertain whether the experimental values include dissociation and rearrangement contributions to the total CT process. Therefore, Table 7.2 contains the three different columns:

i. $0 \leq \theta_{lab} \leq 12°$ the span of scattering angle in the experiment of Niedner *et al.*[157]. END does not predict dissociation or rearrangement in this range.

ii. The full range of scattering angle but excluding the contributions from dissociation and rearrangement, *i.e.* scattering CT integral cross section.

iii. The full range of scattering angle with all contributing processes included (dissociation, rearrangement, and scattering), *i.e.* the full CT integral cross section.

Table 7.2: The integral charge transfer cross section in $Å^2$ calculated in three different ways, IOSA [36], TSHM [157] and END, compared to an interpolated experimental. value [166].

Method	$0° \leq \theta_{lab} \leq 12°$	All θ_{lab} excluding D and R	All θ_{lab} all processes
IOSA	0.73	-	1.10
TSHM	-	-	0.3
END	1.44×10^{-2}	0.121	0.275
Experiment	-	-	0.371

The Proton-Methane System

Initial Conditions and Final State Analysis

The QCSD END theory is now applied to the proton-methane system. As was the case in the proton-hydrogen system, the first concern is the choice of the initial orientations of the methane molecule. Because of its high symmetry, only a small number of orientations suffice. An average over initial target orientations requires an integration over the Euler angles. A reasonable grid for this integration is the one shown in Table 7.21. The six basic orientations displayed in Figure 7.20 generate 132 grid points. The target molecule is held fixed at the origin of the laboratory Cartesian frame and the proton is given a momentum commensurate with the desired collision energy. In these calculations the proton is initially at a distance of 15 a.u. from the target and the methane molecule is in its electronic ground state and equilibrium geometry, computed in the given basis at the SCF level. A full range of impact parameters is considered for each basic orientation. The nuclei being classical particles have no zero-point vibrations.

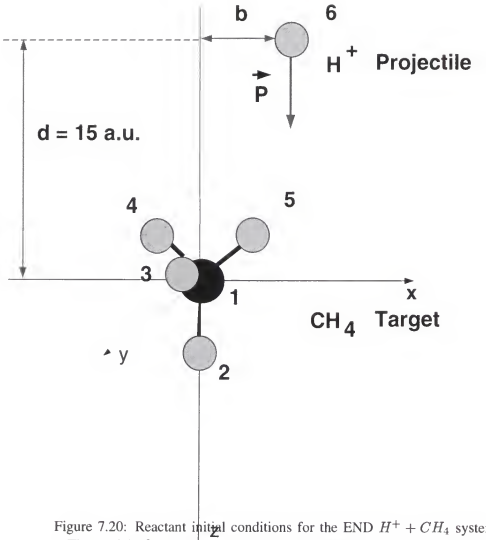

Figure 7.20: Reactant initial conditions for the END $H^+ + CH_4$ system. The nuclei of the methane molecule are labeled C_1, H_2, H_3, H_4, H_5.

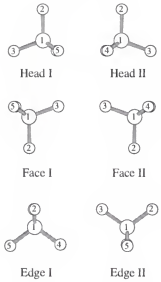

Figure 7.21: The six target orientations considered are shown with the labels Head I, and II, Face I and II, and Edge I and II.

Table 7.3: Integration grid for the orientations of the target methane molecule. The six basic orientations are shown in Figure 1

γ	0	$\pi/3$	-	$2\pi/3$	π	$4\pi/3$	-	$5\pi/3$	2π
	H1	H2	-	H1	H2	H1	-	H2	H1

β\ α	0	$\pi/3$	$\pi/2$	$2\pi/3$	π	$4\pi/3$	$3\pi/2$	$5\pi/3$	2π
0	H1	H1	-	H1	H1	H1	-	H1	H1
π-θ	F2	F1	-	F2	F1	F2	-	F1	F2
θ	E1	-	E2	-	E1	-	E2	-	E1
π	F1	F1	-	F1	F1	F1	-	F1	F1
0	H2	H2	-	H2	H2	H2	-	H2	H2
$\theta/2$	E2	-	E1	-	E2	-	E1	-	E2
θ	H1	H2	-	H1	H2	H1	-	H2	H1
π	F2	F2	-	F2	F2	F2	-	F2	F2

The six basic orientations include the proton approach parallel to the C_3 axis and heading into a hydrogen with two distinct target orientations (Head I and Head II), the opposite orientation with the proton approach into the triangular face of three hydrogens

again with two distinct target orientations (Face I and Face II), and the approach parallel to an S_4 axis also with two distinct methane orientations (Edge I and Edge II). The impact parameter, b, assumes values in steps 0.1 from 0.0 to 6.0 Bohr and 0.5 between 6.0 and 8.0 Bohr. This yields 390 fully dynamical trajectories, each with an evolution time of 1,200 a.u. to achieve a clear separation of the product species. For all these trajectories the proton enters the collision region after about 400 a.u. of time.

The electronic basis set is chosen as the minimal STO-3G. The behavior of END results with change of basis sets is the subject of an ongoing study. However, experience [169, 7, 170] with the ENDyne calculations on several smaller systems has shown that this level of description is capable of yielding results that will not be greatly changed when the basis is augmented. Typically one observes somewhat different behavior of individual trajectories with basis set changes, but the resulting effects on cross sections, average energy transfers, etc. are not dramatic. One possible piece in the puzzle to understand the behavior of this level of END theory is the effective potential surface on which the dynamics may be considered to take place. For each trajectory one can at each time step of integration subtract the nuclear kinetic energy from the constant total energy of the system and in such a manner obtain an effective potential surface (including the effects of electron-nuclear couplings). Such effective surfaces studied so far are very smooth and structureless indicating that a modest basis might be sufficient for a reasonable description of the electron dynamics.

Since the END treats the electrons and the nuclei on an equal footing this system represents a sixteen particle collision. For such an encounter at 30 eV many possible processes can result. The initial system can be represented as

$$p^+ + CH_4(\nu_i = 0) \tag{16}$$

where we have denoted the projectile proton as p^+ and where $\nu_i = 0$ denotes the lack of rovibrational excitation in the target molecule. The product channels observed in this application of the END theory are as follows:

The proton departs having excited the methane molecule. This is referred to as non transfer (NT) inelastic scattering,

$$p^+ + CH_4(\nu_f). \tag{17}$$

Simple electron charge transfer (CT) leaves the products

$$p + CH_4^+(\nu_f). \tag{18}$$

In both the above cases there exist also the exchange processes (E)

$$H^+ + CH_3p\ (\nu_f). \tag{19}$$

or

$$H + CH_3p^+(\nu_f). \tag{20}$$

Another process is the so called collision-induced dissociation (D2) involving three product fragments, two of which are hydrogenic particles,

$$p + H^+ + CH_3(\nu_f) \quad \text{or} \quad p^+ + H + CH_3(\nu_f) \quad \text{or} \quad p + H + CH_3^+(\nu_f). \tag{21}$$

A very small number of trajectories also yield products with three hydrogenic particles (D3) leaving with various amount of electron charge. Finally, a molecular hydrogen formation (F) channel (or hydrogen abstraction channel) is observed yielding the products

$$CH_3(\nu_{f1}) + pH^+(\nu_{f2}) \ \text{ or } CH_3^+(\nu_{f1}) + pH(\nu_{f2})\ . \tag{22}$$

This channel may also exhibit a dissociation (FD2) of the productCH_3 fragment into a CH_2 and a hydrogenic particle.

Obviously this classification of product channels can be further refined with a discussion of which vibrational or rovibrational states are reached. Such calculations are deferred to a later publication. No total fragmentation of methane comes from the END calculations. These general results of the END calculations are in agreement with the experiments, where CH_4^+,CH_3^+, and CH_2^+ fragments have been detected, but no CH^+ or C^+. The END calculations with distinguishable nuclei can, of course, yield details that are beyond what the experiment can do. The TOF [151] generally only detects the fastest product particle irrespective of its past history.

It should be noted that the END dynamics of the CT and NT channels have trajectories where the hydrogenic particles leave partially charged and actually the majority of trajectories are of the NT variety with effectively a proton leaving. This means that the classical nuclei, which can, of course, only present one evolving product geometry is weighted towards the CH_4 rather than CH_4^+. This situation can only be remedied by the double-wave packet END theory sketched in chapter 3. However, even with classical nuclei the experience shows that the calculated transfer probabilities are reasonable and so is the dynamics of the dominant process.

END Results.

For this system different initial conditions yield different product channels and in table 7.4 the initial conditions are classified as functions of the process generated. It is interesting to note that the type of process depends strongly on the orientation of the methane. Some, such as the Face II orientations, yield only non reactive NT and CT channels, while others are extremely reactive and involve bond breaking and bond making. The value of the impact parameter is also decisive in steering the system to a particular channel. For instance, the Face I orientation yields thirteen different processes as the impact parameter varies from 0.0 to 8.0 Bohr. Processes where the incoming

proton does not encounter a *C-H* bond are the less violent as one would expect. Indeed, impact parameters greater that 2.9 Bohr always lead to CT and NT channels. Although a different system, this is consistent with the calculations by Raff [171] on hydrogen atom collisions with methane which showed that the probability for chemical reaction falls off to zero for impact parameters $b > 3.0$ Bohr. For smaller impact parameters the dissociation, the hydrogen exchange, and the formation of molecular hydrogen are the dominant channels, while the D3 and FD2 processes are rare events occurring almost exclusively for very small impact parameters in the Head orientations.

The atoms in the methane target are labeled C_1, H_2, H_3, H_4, and H_5, while the initial proton is labelled H_6 (see figure 7.21). It is often instructive to study some typical trajectories in order to get an understanding of the relevant dynamics. The NT and CT channels result in trajectories similar to what has been observed in the previous section for the proton collisions with molecular hydrogen. The electron charge, as given by the Mulliken population on the incoming proton, increases as the proton approaches methane and then decreases to an asymptotic value corresponding to the final charge transfer probability. In the region of the rainbow angle the CT probability is considerable (about 30%). The dissociation process D2 is illustrated in figures 7.22 through 7.24. The initial conditions are orientation Head II and $b = 1.00$ Bohr. The H_3 hydrogen is the fastest outgoing particle, the incoming proton being slowed by the interaction, and the remaining CH_3 fragment leaves vibrationally excited as illustrated by the evolution of the $C\text{-}H_2$ bond distance. In this trajectory the fastest outgoing particle, which happens to be H_3, carries off a significant amount of charge (0.51e) and the slower H_6 hydrogen, which interacts a long time with the carbon center leaves with almost a full electron (0.95e). The Mulliken populations of the remaining CH_3 fragment oscillate illustrating the sharing of the electrons between these atoms forming a bound species.

Table 7.4: Types of process produced by different initial conditions (orientation of target and impact parameter of projectile)

Target orientation	Impact parameter range	Process
Head I	0.0-0.0	F
	0.1-0.1	E
	0.2-0.4	D3
	0.5-8.0	NT and CT
Head II	0.0-0.0	F
	0.1-0.1; 2.1-2.4	E
	0.2-0.2	FD2
	0.3-0.4	D3
	0.5-2.0; 2.5-2.9	D2
	3.0-8.0	NT and CT
Face I	0.0-0.2;2.7-8.0	NT and CT
	0.3-0.4; 0.6-0.6; 0.9-1.4;	D2
	1.9-1.9; 2.6-2.6	
	0.5-0.5; 0.7-0.8; 1.5-1.8;	F
	2.5-2.5	
	2.0-2.3	E
	2.4-2.4	D3
Face II	0.0-8.0	NT and CT
Edge I	0.0-1.0; 2.7-8.0	NT and CT
	1.1-2.6	D2
Edge II	0.0-0.1; 2.4-8.0	NT and CT
	0.2-0.3; 1.5-1.6; 2.1-2.1;	D2
	2.3-2.3	
	0.4-1.4; 2.2-2.2	F
	1.7-2.0	E

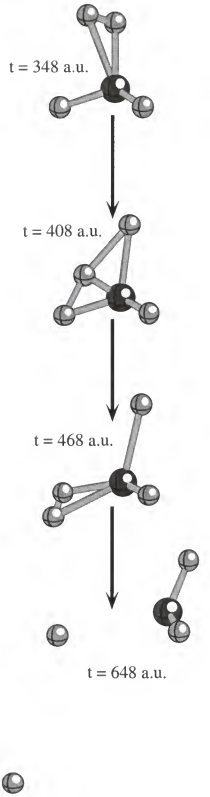

Figure 7.22: Depiction of the END trajectory in the xz-plane for target orientation Head II and impact parameter 1.0 Bohr. The nuclear evolution is shown at four different time points. The lines between atoms only registers proximity during the evolution and has the meaning of a bond only at the very end of the trajectory. This is part of channel D2.

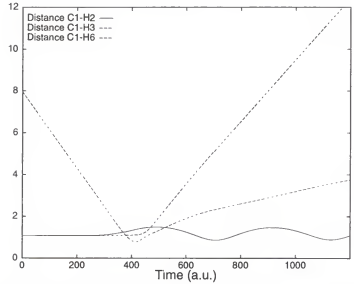

Figure 7.23: The time evolution of the relevant *C-H* distances is shown.

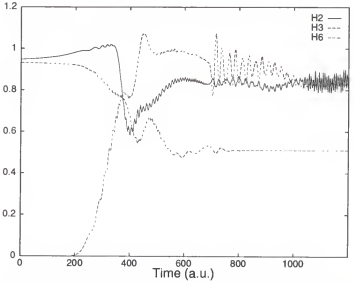

Figure 7.24: The electron charge evolution is shown in terms of the Mulliken populations on the hydrogens H_2 that stays on the carbon fragment, and H_3 (fast) that comes from the original CH_4 and the original proton projectile that leaves as H_6 (slow).

A typical F process is shown in figures 7.25 through 7.27 for initial conditions corresponding to the orientation Edge II and impact parameter 1.30 Bohr. This process is not detected experimentally.

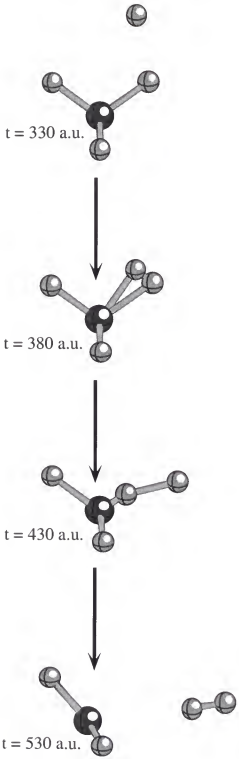

Figure 7.25: This is the END trajectory in the xz-plane with target orientation Edge II and impact parameter 1.30 a.u. The hydrogen H_2 breaks its bond with the carbon and together with the incoming proton (H_6) forms a hydrogen molecule that leaves slowly. This is part of channel F.

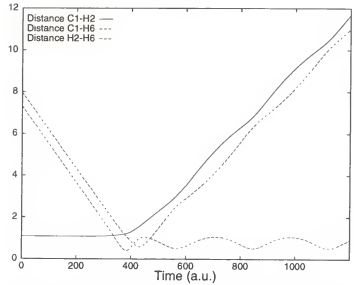

Figure 7.26: The time evolution of the relevant *C-H* and *H-H* distances is shown.

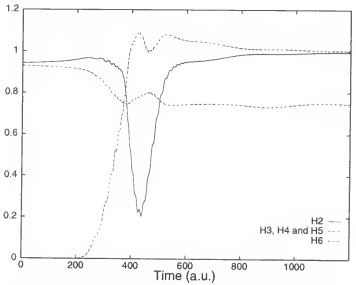

Figure 7.27: The electron charge evolution is shown in terms of the Mulliken populations on the hydrogen H_2 originally bonded to the carbon and on H_6, which is the incoming proton forming the product hydrogen molecule with H_2. The hydrogens of the remaining CH_3^+ fragment lose some electronic charge.

This can have several possible reasons. From the present calculations, it can be concludes that the hydrogen product molecule has very small translational energy. The formation of H_2^+ seems negligible and virtually all F trajectories result in molecular hydrogen with two electrons, leaving behind an essentially planar CH_3^+ fragment. From

the phenomenological formula of Nakai *et al.* [172] based on various experimental results, an estimate of the CT integral cross section can be obtained at 30 eV to be about 4–5 Å^2. This value is quite approximate since it results from an extrapolation of the experimental data at higher energies. The ICS are again calculated by (cf. eq. 94)

$$\sigma(E_{\rm lab}) = 2\pi \int_0^\infty b P_k^{\rm CT}(b; E_{\rm lab}) db \tag{23}$$

by numerical integration, where $P_k^{\rm CT}$ is the charge transfer probability for a given collision energy as a function of impact parameter and orientation k of the target. This probability is obtained for each trajectory by projecting the evolved state onto the appropriate final state. Averaging over the orientations of the target molecule is done by starting from the six basic target orientations (H1, H2, F1, F2, E1, and E2) of figure 7.21. The high symmetry of the target means that actually 132 different orientations are generated from these basic orientations. Any function, such as a cross section, obtained for the basic six orientations, is then represented by its values in 132 grid points on the parameter space of the group SO(3). The scheme used for integration over the Euler angles α, β, and γ on the intervals $[0, 2\pi]$, $[0, \pi]$, and $[0, 2\pi]$, respectively is described in the appendix E.

It is assumed that the E, D2 and D3 channels are included in the experimental data and the product channel are labeled by the nature of the fastest outgoing particle. Since the impact parameter resolution could be made finer, where the product channels undergo drastic changes, our integration is only approximate. The value of 2.7 Å^2 must be considered in satisfactory agreement with experiment. The results in table 7.5 show that $\sigma_k(E_{\rm lab})$ is larger for the most reactive orientations and that the E, D2, and D3 channels represent non-negligible percentages of the total. The F channel has the integral cross section 0.26 Å^2. There are no experimental data to which it can be compared.

Table 7.5: Charge transfer integral cross sections and percentage of integral cross section coming from the D2, D3, E, and FD2 channels for the different target orientations.

	Head I	Head II	Face I	Face II	Edge I	Edge II	Mean	Exp.
$\sigma(E_{lab} = 30eV)A^2$	0.41	6.22	3.51	0.74	5.31	2.77	3.3	4-5
Reactive channels ratio %	16	51	38	0	40	31		

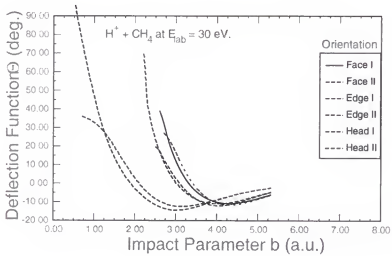

Figure 7.28: The deflection function versus impact parameter corresponding to the NT and CT channels is shown for the six different target orientations of Figure 1b. The classical primary rainbow is around 12 degrees. A glory angle is observed in all cases for impact parameter between 1.80 and 3.50 Bohr

The scattering angle θ_{lab} is by a variant of eq. 32 (cf. eq. 13)

$$\sin\theta_{Lab} = \frac{(p_x^2 + p_y^2)^{1/2}}{(p_x^2 + p_y^2 + p_z^2)^{1/2}} , \tag{24}$$

in terms of the components of the asymptotic momentum of the particle reaching the detector. The classical deflection function $\Theta(b)$. eq. 50, is in this system the scattering

angle with a positive sign in the repulsive case and a negative sign for the attractive case,

$$\theta_{Lab} = \pm[\Theta(b) - 2\pi n];\ n = 0 \tag{25}$$

Figure 7.28 displays this classical deflection function as a function of the impact parameter for the six distinct orientations. Only the CT and NT channels are present at these impact parameters. The classical primary rainbow angle corresponds to the maximum attractive part of the interaction between the projectile and target and is thus at the minimum of the deflection function which occurs at $3.00 \leq b_{\text{rainbow}} \leq 4.30$ Bohr. Our mean value for the classical primary rainbow is 12 degrees. The scattering angle of 0 degrees, the glory angle, can also be identified in Figure 4 and corresponds to smaller impact parameters, $1.80 \leq b_{\text{glory}} \leq 3.50$ Bohr. Similarly to the experiment there is no secondary rainbow for any of the orientations. Table 7.6 details the results for each of the six distinct target orientations.

Table 7.6: Classical and semiclassical rainbow angle (degrees) per orientation in the laboratory frame. The corresponding impact parameter in Bohr is also listed.

	Head I	Head II	Face I	Face II	Edge I	Edge II	Mean	Exp.
Classical θ_{rainbow}	12.4	11.7	10.9	14.4	12.1	11.0	12.0	
Semiclassical θ_{rainbow}	10.5	9.6	9.0	12.4	10.0	9.1	10.0	~ 10
b_{rainbow}	3.1	3.5	3.3	1.8	3.0	3.1	2.8	

For the almost spherical methane molecule the classical DCS per target orientation may be expressed as (cf. eq. 83 and 84, chapter 6)

$$\frac{\mathrm{d}\sigma(\theta_{Lab}, k)}{\mathrm{d}\Omega} = \sum_i \frac{b_i P_{ik}(b_i)}{\sin\theta_{Lab} |\partial\theta_{Lab}/\partial b|_{b_i;k}}. \tag{26}$$

where P_{ik} is the probability of a given process and the sum runs over all the contributing branches to the scattering angle θ_{Lab}. As before, this classical DCS calculated in this way

displays the already discussed singularities at the rainbow and glory angles as well as a too large primary rainbow angle. In this case. the uniform SC corrections for the END theory, eq. 85 through 88, is applied. The averaged semiclassically corrected rainbow, θ_r^{SC}, eq. 89 angle is 10.0 degrees in excellent agreement with the experimental value [151] of 10 degrees.

Non transfer (NT) and transfer (CT) DCS averaged over all the orientations are depicted along with the experimental values in figures 7.29 and 7.30, respectively. For the purpose of comparison the unnormalized experimental values have been normalized to the END results by matching the values of the DCSs at the rainbow angle. There are no error bars reported by the experiment. Even so, the agreement in the non transfer case must be judged to be satisfactory. Some disagreement occurs at very low scattering angles, where the blast through proton beam may also obscure some of the experimental results[151]. The agreement with the experiment is not good in the transfer case although the rainbow angle is predicted correctly. Indeed, the END value predicts a lower transfer probability than experiment at small scattering angles and a higher probability at large angles. The END DCS is flatter and more structured than the experimental one at small scattering angles. In general, the shape of the transfer END DCS resembles the END non-transfer one. This is probably a manifestation of the dominance of the non transfer process and the inability in the END dynamics at the present level of approximation to completely separate it from the charge transfer one. The capability to split the nuclear wave packet (see chapter 3) when added to the ENDyne code could improve the results Both END results exhibit oscillations due to the SC phase despite the averaging over target orientations. The addition of more orientations will result in less pronounced oscillatory behavior, but even so we must conclude that the END results for the charge transfer differential cross section are inadequate at this level. It should be noted that the

experimental [151] detection efficiency of hydrogen atoms is only 3%, making also the experimental transfer cross section less accurate than the non-transfer one.

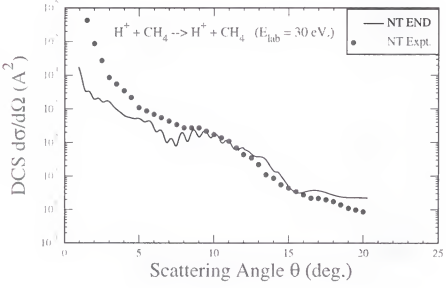

Figure 7.29: Semiclassical correction of END total differential cross section for the NT channel compared to experiment.

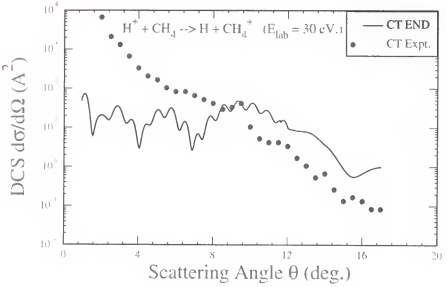

Figure 7.30: Semiclassical correction of END total differential cross section for the CT channel compared to experiment.

The experiments by the Toennies group[151] also seek to analyze the energy transfer between the proton and the methane. An END reproduction of the time-of-flight spectra would require many more trajectories in order to obtain statistically relevant relative intensities of each energy loss value. However, the evolution of the average energy transfer for the NT channel as a function of the scattering angle can be obtained with the present trajectories according to eq. 5. In this case, that expression can be rewritten as

$$\langle \Delta E_k(\theta) \rangle = \frac{\sum_i b_i P_{ik}^{\mathrm{NT}} |\partial b_i / \partial \theta| \Delta E_{ik}}{\sum_i b_i P_{ik}^{\mathrm{NT}} |\partial b_i / \partial \theta|}, \tag{27}$$

where ΔE_{ik} is the difference in kinetic energy between the incoming proton and the fastest outgoing particle, and P_{ik}^{NT} is the probability of no charge transfer to the fastest particle, both for target orientation *k*. The final value is also rotationally averaged. The results and their comparisons to the experimental data are displayed in fig.7.31. The above procedure underestimates the energy transfer, although the agreement with experiment is reasonable for the larger scattering angles. For small scattering angles the agreement is poorer and the experimental results appear to even have a different limiting form at zero scattering angle if one assumes a linear behavior. It seems reasonable to expect the energy transfer to tend to zero at small scattering angles since the average energy transfer is determined by the protons in the "blast through" beam not interacting with the target, *i.e.* coming in with large impact parameters. The assumption of a linear behavior may not be justified, but the experimental results for average energy transfer[151] at this energy has been fitted by a straight line.

In the experiments two independent ways to infer the relative abundances of the product fragments CH_4^+, CH_3^+, and CH_2^+ are used. On the one hand a mass spectrometry analysis of the heavy ion products was done, and on the other the energy loss spectra was obtained of the scattered hydrogen atoms for scattering angles up to 8 degrees. The

two methods give results that agree. The assumptions made in this analysis appear to be that (i) the mass spectrometer experiment sees all the heavy ions from all the possible processes, (ii) the energy loss spectrum remains the same for scattering angles greater than 8 degrees, (iii) the energy loss spectrum of the hydrogens separates into essentially non-overlapping regions, one for each of the three heavy ion species.

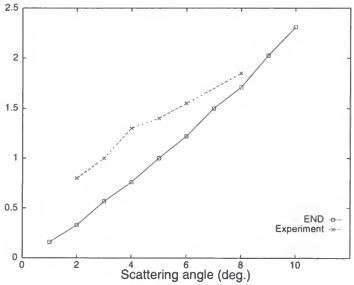

Figure 7.31: END and experimental[151] average kinetic energy loss of the proton versus scattering angle. The END results are averaged over target orientations.

In order to test these assumptions within the limitations of the present model, the following study, summarized in table 7.7, is performed. First, the ICS section formula, eq. (23) is used with the probability $P(b, E_{\rm lab})$ corresponding to the formation of each of the three cations, and simply compare the three $\sigma(E_{\rm lab})$ values obtained. By taking all processes into account we find a 50/50 CH_4^+/CH_3^+ ratio, very different from the experimental one. The great abundance of CH_3^+ might at first be surprising considering the rather small ranges of impact parameters of the trajectories that produce theCH_3^+ and CH_3 fragments (D2 and F of table 7.4) in comparison to those that produce CH_4^+ and CH_4. The deciding factor is the probabilities$P_{ik}(b_i, E_{\rm lab})$, which greatly favor

CH_3^+ over CH_3, and CH_4 over CH_4^+.

If instead of counting all processes the trajectories are restricted to those for which the fastest outgoing particle has a scattering angle smaller than or equal to 8 degrees, which is the same as in the hydrogen energy loss measurements, the agreement with experiment is quite satisfactory. Without a more precise knowledge of how the product ions were collected in the mass spectrometer it is difficult to comment further on this.

Table 7.7: Analysis of the fragmentation of methane.
Comparison between experiment and theory. All values in %.

	CH_4^+	CH_3^+	CH_2^+
Mass spectrometry analysis			
Experiment	74	22	4
END($\theta \leq$	67	30	3
8 degrees)			
END($\theta \leq$	83	16	1
15 degrees)			
END (All θ)	49	50	1
Hydrogen atom energy loss distribution			
Experiment	75	20	5
END($\theta \leq$	74	26	
8 degrees)			
END($\theta \leq$	76	24	
15 degrees)			
END	50	50	
($\theta \leq$ 30 degrees)			

A second study of END results was also carried out in order to compare with the second set of experimental results of the fragmentation ratios. The hydrogen energy loss spectra is harder to produce and the following procedure was adopted in order to obtain an estimate of the energy transferred to the target when an electron transfer happens. An upper limit to the energy loss can be estimated by taking the evolved final species (CH_4^+ or CH_3^+, treating it as a fully cationic particle at the evolved geometry, and performing a single point UHF STO-3G calculation. The difference between this energy and the energy of the geometrically optimized fragment with the same basis set is then added to the kinetic energy loss and provides an upper bound to the energy loss. The difference between the ionization potentials of the methane and the hydrogen atom is small in comparison to the approximations made. The trajectories that produce the CH_2 type fragments have been neglected in this analysis. The results are displayed in figures 7.32, 7.33 and 7.34 for scattering angels up to 8 degrees, which is the same as chosen in the experiment, 15 degrees, which is the highest measured scattering angle, and 30 degrees, respectively. Beyond 30 degrees successive trajectories give very different scattering angles and interpolation becomes less precise.

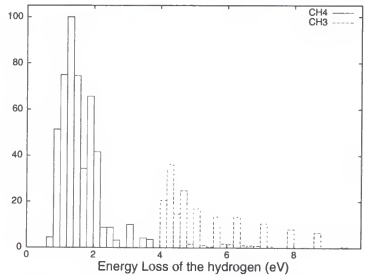

Figure 7.32: Calculated energy loss spectrum of hydrogen for scattering angles up to 8°

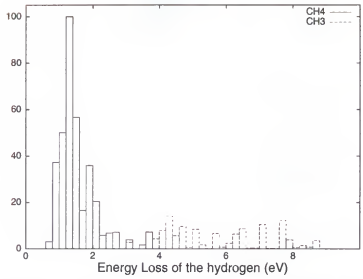

Figure 7.33: Calculated energy loss spectrum of hydrogen for scattering angles up to 15°

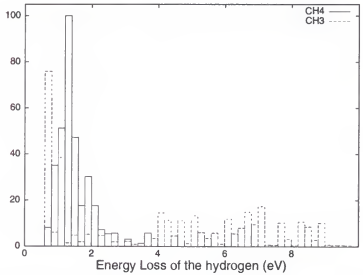

Figure 7.34: Calculated energy loss spectrum of hydrogen for scattering angles up to 15°

Note that the ≤ 8 degrees spectrum and that from ≤ 15 degrees are comparable and show a clear separation between trajectories leading to CH_4^+ and CH_3^+ type fragments. In contrast, the ≤ 30 degree spectrum shows that the amount of energy transferred to the carbon fragment is not systematically higher when CH_3^+ is formed. Thus, the assumption made in performing the experiment that the energy loss spectra for hydrogen should not change when all scattering angles are taken into account disagrees with our findings.

Actually, the large increase of CH_3^+ found when considering larger scattering angles is easily understood from the shape of the deflection function in figure 7.28. When the angle considered is greater than the rainbow angle the contributions of trajectories with large impact parameters,*i.e.* those that are dominant for small scattering angles, vanish, and only trajectories with small impact parameters contribute particles that reach the detector. At these greater angles the contributions from, say, the D2 channel becomes more important increasing the presence of CH_3^+ fragments.

The energy that separates the two parts of the ≤ 8 degrees spectrum is 4.0 eV on our scale. Now, it is interesting to note as a curious coincidence that if one simply integrates the two parts of the spectrum separated by a line at 4.0 eV, one finds the relative abundance of left/right, which is interpreted by the experimental presupposition as the ratio CH_4^+/CH_3^+, to be 72%/28%. This is quite different from the 50%/50% ratio found directly, which is due to the END results for the≤ 30 degrees spectrum (Figure 10) that shows a considerable amount ofCH_3^+ being formed with small hydrogen atom energy loss.

The net result of the above analysis is that the present theoretical analysis contradicts the experimental assumptions that the energy loss spectrum remains the same for scattering angles greater than 8 degrees, and that the energy loss spectrum of the hydrogens separates into essentially non-overlapping regions, one for each of the three heavy ion species at all scattering angles. The theoretical analysis of the fragmentation problem is of course approximate, but experience from other systems with this level of END theory gives us confidence in the qualitative correctness of the results. It also seems likely that the F channel actually exists and that very fact should introduce some difference between the two ways of estimating the fragmentation from the experiments, since the CH_3^+ will be accounted for in the mass spectrum, while theH_2 is not detected in the

energy loss spectrum.

The Proton-Water System

Initial Conditions and Final State Analysis

Finally, the QCSD END theory is applied to the proton-water system. This study is strategically very similar to the previous one so that it will be presented in a more concise from. A minimal STO-3G basis is used. Several trajectories are also calculated using a pVDZ basis [159], but no significant differences is observed with the results obtained with the smaller basis. The target water molecule is initially at rest in the laboratory frame in its electronic and vibrational ground state. The proton travels towards the water molecule with a momentum commensurate with the chosen collision energy and with an initial impact parameter b. For each trajectory, the scattering angle θ_{Lab}, the deflection function of the projectile, $\Theta(b)$ the probability, $P(b)$, for a certain process, such as charge transfer, to take place are calculated as in the previous system. The DCSs calculated again within the SC uniform approximation of the END theory, eq. 85 through 88.

With classical nuclei the initial orientation of the target needs specification. The rotation of the target is labeled by the Euler angles (α, β, γ) about the body-fixed axes. The reference orientation (0,0,0) is shown in figure 7.35. For this application a course rotational grid with 28 points is chosen generated from the ten target orientations given in table 7.8. Averaging over target orientations is then done by numerical quadrature over these grid points as in the case of proton and methane scattering.

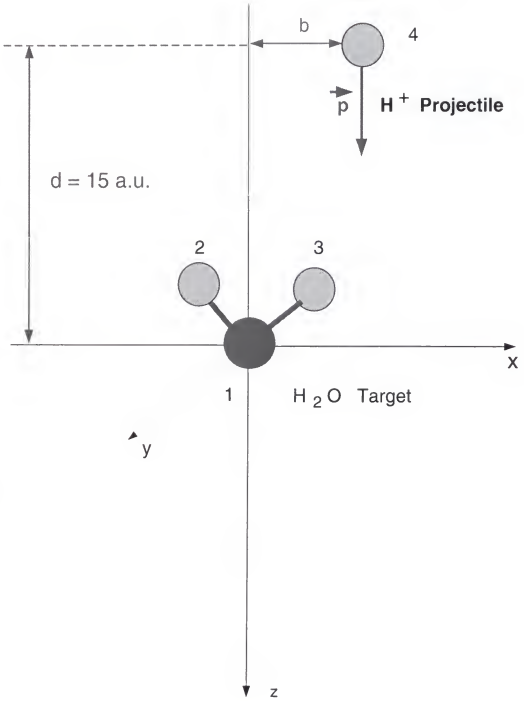

Figure 7.35: Reactant initial conditions for the $H^+ + H_2O$ system.

Table 7.8: Selected target orientation that create 36 grid points for rotational averaging

orientation	(α, β, γ)	θ_r	θ_r^{sc}
1	(0, 0, 0)	5.7	4.4
2	(0, 50, 0)	4.9	3.5
3	(0, 130, 0)	4.7	3.3
4	(0, 180, 0)	5.6	4.0
5	(180, 50, 0)	9.5	7.7
6	(180, 130, 0)	9.2	7.8
7	(0, 0, 90)	8.6	7.3
8	(0, 45, 90)	5.5	4.1
9	(0, 90, 90)	5.1	4.0
10	(0, 135, 90)	7.8	6.3
11	(0, 180, 90)	8.7	7.3
12	(180, 45, 90)	10.4	8.8
13	(180, 90, 90)	8.2	6.8
14	(180, 135, 90)	7.2	5.6

END Results.

The rotationally averaged non transfer DCS is shown together with the experimental values [152] in figure 7.36. The unnormalized experimental values have been matched with the theoretical ones at the 5° rainbow angle. The additional theoretical rainbow at 7.5° comes mainly from the scattering by the oxygen side of water and is not clearly discernible in the experimental cross section. This may be due to low signal to noise ratio [152]. The calculated values show pronounced rainbow oscillations at 4 degrees in close agreement with the experimental rainbow at 5 degrees. The theoretical results will also be much more smoothed out by taking into account more target orientations.

The vibrational energy transfer has also been analyzed in the TOF measurements for both inelastic and charge transfer collisions. Theoretical estimates are obtained by projecting the product water molecule state onto the electronic ground state and assuming

negligible rotational excitation (experiment estimates rotational excitation to be about 10% of energy loss of the protons). The results presented in figure 7.37 show slightly higher values and are in qualitative agreement with experiment up to 11 degrees.

The DCS for charge transfer are presented in figure 7.38. Again the experimental value at 5 degrees is normalized with the theoretical at 4 degrees. The similarities of the charge transfer and the inelastic cross sections in agreement with experiment are manifestations of the similarities between the respective deflection functions. END shows the charge transfer probability to be 1/10 of the inelastic one and the cross section is accordingly an order of magnitude less for the charge transfer case.

For this four atom system END gives good agreement with experiment for both inelastic and charge transfer scattering processes. This demonstrates the fact that even at the lowest level of approximation with nonadiabatic couplings taken into account the END wave function behaves satisfactorily.

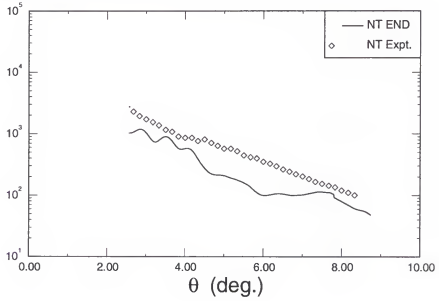

Figure 7.36: Non transfer total differential cross section for the $H^+ + H_2O$ collisions at 46 eV.

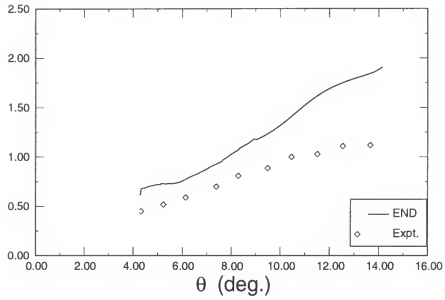

Figure 7.37: Vibrational energy transfer ΔE as a function of scattering angle.

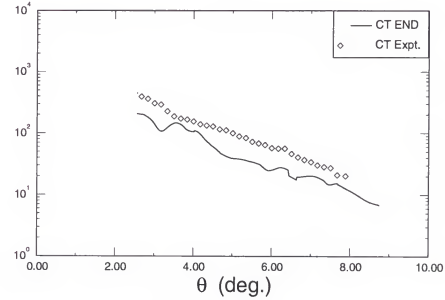

Figure 7.38: Charge transfer total differential cross section for the $H^+ + H_2O$ collisions at 46 eV.

CHAPTER 8
CONCLUSION AND FUTURE WORK

The present thesis work has set forth a quasi-classical and semiclassical formulation of the END theory in order to calculate scattering properties. The incorporation of the coherent state theory, to quasi-classically describe the rotational and vibrational nuclear degrees of freedom, and the adaptation of the some semiclassical techniques, to correct describe classical singularities, constitute the main theoretical achievement of this work. In the case of vibrational motions, the present formalism in terms of the canonical coherent state is the rigorous formulation of some crude methods developed in the past (*e.g.* the DECENT method by Giese and Gentry [173]). This theoretical effort also establishes a use of the canonical coherent state alternative to that proposed by Heller some twenty years ago [94–97]. In the case of the rotational motion, the introduction, study, and further formulation of a nearly quasi-classical rotational coherent state has no precedents in scattering theory, and constitutes an original aspect of the present method. The adaptation of the semiclassical techniques to treat classically originated effects sets forth in a more rigorous way some elementary semiclassical applications of the END theory made before [7]. A point of note in this matter is that the connection between those semiclassical techniques and the END wave function is explicitly shown in this work. On the whole, a quasi-classical and semiclassical wave packet formulation for scattering processes is obtained. This formulation is in some way the fulfillment of Heller's semiclassical wave packet dynamics for molecular processes even though many features of the END theory goes far beyond Heller's concepts. This formulation also sets up a feasible alternative to

Miller's S-matrix theory for the calculation of scattering properties.

All these theoretical developments have been coded into the program ECROSS. The final goal of this programming project is to incorporate the ECROSS code into the ENDyne program package to calculate dynamical properties automatically. The ECROSS program has been extensively used to evaluate the dynamical properties presented in chapter 7. The good results shown there prove the validity and accuracy of the END theory for the kind of systems proposed for study in this thesis. The fact that such a complex reactions system as $H^+ + CH_4$, a sixteen-body problem with many internal degrees of freedom, can be accurately treated without using predetermined PESs is a remarkable achievement of the END theory.

Future work along this lines of the quasi-classical and semiclassical END theory can bring out many aspects of the method. One possibility is the further application and of this model to systems similar to those discussed in this thesis. A study of the scattering system $H^+ + C_2H_2$, for which experimental results are available in Ref. [174], is under way at present. The testing of the rotational coherent state for scattering processes is still pending but it can be easily undertaken. There are in the literature many experimental and theoretical studies of rotationally resolved properties to test the accuracy of the proposed rotational model [37].

However, the more interesting research lies in the theoretical extensions of the present model and its subsequent applications to more complex systems. As has been indicated in chapter 7, a detailed studied of the vibrationally resolved differential cross sections for the charge-transfer channel in the $H^+ + H_2$ system has not been presented. In fact, that study was undertaken during this thesis research. That investigation was performed in a similar way as that for the nontransfer channel in the same system but taking into account the effect of the charge-transfer process on the nuclear dynamics. The vibrationally resolved

charge-transfer differential cross sections calculated in that way shown a poor agreement with the available experimental data in Ref. 157. The reason of these discrepancies were immediately understood. Since the semiclassical limit is applied to the nuclear degrees of freedom in the present END formulation, there is only one trajectory for the nuclear motion arising from a given set of initial conditions. During the evolution, the quantum mechanically described electrons are allowed to undergo quantum transitions, including charge-transfer processes. In fact, the good END charge-transfer integral cross sections shown in the previous chapter indicate that this quantum electronic evolution coupled with a classical nuclear dynamics is still very accurate. However, the classical nuclei evolving in the mean field made by the electronic states are forced to follow a unique trajectory. In the case of the $H^+ + H_2$ system, the charge-transfer probability is relatively low. This implies that the contribution of the excited electronic states to the electronic wave function is not very substantial. Therefore, the nuclear dynamics should be close to a nuclear dynamics on the ground electronic state. It is then very difficult to obtain an accurate charge-transfer nuclear evolution out of a non-transfer dominated nuclear dynamics. However, it is important to emphasize that this limitation is not inherent to the END theory itself but to the present realization of it. This limitation arises because the general END theory has been constrained in this formulation to its lowest possible level: that with one configuration for the electronic wave function and one configuration for the nuclear one. Therefore, a more advanced realization of the END theory has been discussed in chapter 3 in which a double configuration description for both nuclei and electrons have been prescribed. The double configuration nuclear wave function in the semiclassical limit is supposed to be flexible enough to generate two distinct nuclear trajectories: one for the nontransfer channels and the other for the charge-transfer ones. Each of these trajectories may properly reproduce the totally diverging dynamics of the

nontransfer and charge-transfer processes. Work on this fertile project is under way at present.

APPENDIX A
THE DIRAC DELTA FUNCTION

The Definition of The Delta Function

The Dirac delta function (or δ—function) belongs to the special category of the symbolic distributions functions [175], *i.e.* functions which only acquire meaning under some mathematical operations. Given the ordinary function $\phi(x)$, called the testing function, the symbolic definition of the one-dimensional delta function $\delta(x - x_0)$ is through

$$\int_{-\infty}^{\infty} dx\ \delta(x - x_0)\phi(x) = \phi(x_0) \tag{1}$$

i.e. the delta function "extracts" the specific function value $\phi(x_0)$ out of the integral. Like Ref. [175], but unlike [49], the condition $\delta(x - x_0) = 0, \quad x \neq x_0$ is not part of the definition. The testing functions $\phi(x)$ are supposed to be continuous and to have continuous derivatives of as many orders as needed. Additional properties required to these functions are examined in Ref. [175]. It should be emphasized that the above integral must be of Lebesgue or Stieljes type to exist, and not of Riemann type [175, 49]. However, such a subtle detail will be ignored henceforth since these integrals can be manipulated in the ordinary way. If the testing function is chosen as $\phi(x) = 1$ then it is immediate that

$$\int_{-\infty}^{\infty} dx\ \delta(x - x_0) = 1 \tag{2}$$

i.e. the delta function is normalized to one.

The previous definition of the delta function for the Cartesian coordinate x can be extended to a general coordinate $q = q(x)$, where this function is supposed to be monotonic to have a one-to-one correspondence. The new delta function $\delta(q - q_0)$ is defined through

$$\int_{q_1}^{q_2} dq\ \delta(q - q_0)\phi(q) = \phi(q_0) \tag{3}$$

where $q_0 = q(x_0)$, $q_1 = q(-\infty)$, and $q_2 = q(\infty)$. Since $dq = \left|q'(x)\right|dx$, where the absolute value is to keep both dx and dq positive, then

$$\begin{aligned} \phi(x_0) &= \phi[x(q_0)] \\ &= \int_{-\infty}^{\infty} dx\ \phi(x)\delta(x - x_0) \\ &= \int_{-\infty}^{\infty} dq\ \phi[x(q)]\delta[x(q) - x(q_0)]\left|q'(x)\right|^{-1} \end{aligned} \tag{4}$$

which implies that

$$\delta[q - q_0] = \frac{\delta(x - x_0)}{|q'(x)|} \tag{5}$$

If $q = -x$ then

$$\delta(x - x_0) = \delta(x_0 - x) \tag{6}$$

i.e. the delta function is even around the point x_0. Also, if $q = ax + b$ then

$$\delta[a(x - x_0)] = \left|a\right|^{-1}\delta(x_0 - x) \tag{7}$$

Additional properties of the delta function can be found in the cited literature.

The Delta Function As a Limit of Distribution Functions

In textbooks, it is customary to define the delta function by the value assignments

$$\delta(x - x_0) = \begin{cases} 0, & x \neq x_0 \\ 1, & x = x_0 \end{cases} \tag{8}$$

This definition is judged to be a nonsense in more rigorous contexts [175], being the proper definition that given before. However, the delta function can be related to some ordinary functions through a special limiting procedure. There exists some collection of distribution functions $\delta_c(x - x_0)$, where c is a natural or a real parameter, satisfying

$$\int_{-\infty}^{\infty} dx\ \delta_c(x - x_0) = 1 \tag{9}$$

for which it holds that

$$\lim_{c \to \infty} \int_{-\infty}^{\infty} dx\ \delta_c(x - x_0)\phi(x) = \phi(x_0) \tag{10}$$

These distribution functions are said to be approximations to the delta function. In the case of a natural c, the limiting procedure can be seen as a series sequence of increasingly more accurate approximating functions. Many distribution functions have been proposed to approximate the delta function, some of them are listed below [49]

$$\delta_c(x - x_0) = \left(\frac{c}{\pi}\right)^{\frac{1}{2}} \exp\left[-c(x - x_0)^2\right],\ c > 0 \tag{11}$$

$$\delta_c(x - x_0) = \frac{c}{\pi} \frac{1}{(1 + c^2 x^2)} \tag{12}$$

$$\delta_c(x - x_0) = \frac{\sin cx}{\pi x} = \frac{1}{2\pi} \int_{-c}^{c} dt\ \exp(ixt),\ c > 0 \tag{13}$$

and

$$\delta_c(x - x_0) = \begin{cases} 0, & (x - x_0) < -\frac{1}{2c} \\ c, & -\frac{1}{2c} < (x - x_0) < \frac{1}{2c},\ c > 0 \\ 0, & (x - x_0) > \frac{1}{2c} \end{cases} \tag{14}$$

Central to the END theory, it is the Gaussian distribution listed first (cf. eq. 19). The relationship of that distribution with the delta function can be proven straightforwardly. For instance, it is easy to see that [109]

$$\begin{aligned} \int_{-\infty}^{\infty} dx\ \delta_c(x - x_0) &= \left(\frac{c}{\pi}\right)^{\frac{1}{2}} \int_{-\infty}^{\infty} dx\ \exp\left[c(x - x_0)^2\right] \\ &= \left(\frac{c}{\pi}\right)^{\frac{1}{2}} \left(\frac{\pi}{c}\right)^{\frac{1}{2}} \\ &= 1 \end{aligned} \tag{15}$$

which holds even when $c \to \infty$. Also, if we expand a testing function $\phi(x)$ in a Taylor series around x_0

$$\phi(x) = \sum_{n=0}^{\infty} \frac{\phi^n(x_0)}{n!}(x - x_0)^n \tag{16}$$

then [109]

$$\begin{aligned} \int_{-\infty}^{\infty} \delta_c(x - x_0)\phi(x) = \left(\frac{c}{\pi}\right)^{\frac{1}{2}} \sum_{n=0}^{\infty} \frac{\phi^n(x_0)}{n!} \times \\ \int_{-\infty}^{\infty} dx\, (x - x_0)^n \exp\left[-c(x - x_0)^2\right] \\ = \sum_{n=0,\,2,\,4\ldots}^{\infty} \frac{\phi^n(x_0)}{n!} \left[\frac{(n-1)!!}{(2c)^{\frac{n}{2}}}\right] \end{aligned} \tag{17}$$

where, by symmetry, only the integrals with an even n are non vanishing. Therefore, it is immediate that

$$\lim_{c \to \infty} \int_{-\infty}^{\infty} dx\, \delta_c(x - x_0)\phi(x) = \phi(x_0) \tag{18}$$

This property also holds even when the testing function has only a first derivative which is continuous. In that case, the expansion in eq. 16 reduces to only two term including the rest (Lagrange mean value theorem). If this shorter expression is subjected to similar manipulations as those in eq. 17 then eq. 18 obtained once more. The same kind of proofs can be applied to the other distribution functions. Although all the properties of a delta function can be obtained by the shown limiting procedure, an assignment of the type $\delta(x - x_0) = \lim_{c \to \infty} \delta_c(x - x_0)$ for any x is not possible since those limits do not exist for any of the distribution functions.

The distribution functions are useful to prove additional properties of the delta function. For instance, although a delta function $\delta(x - x_a)$ is not a genuine testing function, it can still be proven that

$$\int_{-\infty}^{\infty} dx\, \delta(x - x_a)\delta(x - x_b) = \delta(x_a - x_b) \tag{19}$$

If two Gaussian distributions are used, it is easy to show that the product $\delta_c(x-x_a)\delta_c(x-x_b)$ is (cf. [176])

$$\delta_c(x-x_a)\delta_c(x-x_b) = \Big(\frac{c}{\pi}\Big)exp\Big[-\frac{c}{2}(x_a-x_b)^2\Big]\times \\ exp\Big[-2c[x-x_{ab}]^2\Big] \tag{20}$$

where

$$x_{ab} = \frac{x_a+x_b}{2} \tag{21}$$

Then, by integrating [109]

$$\int_{-\infty}^{\infty} dx\ \delta(x-x_a)\delta(x-x_b) = \Big(\frac{c}{\pi}\Big)exp\Big[-\frac{c}{2}(x_a-x_b)^2\Big]\times \\ \int_{-\infty}^{\infty} dx\ exp\Big[-2c(x-x_{ab})^2\Big] \\ = \Big(\frac{c}{2\pi}\Big)^{1/2} exp\Big[-\frac{c}{2}(x_a-x_b)^2\Big] \tag{22}$$

The last result is a Gaussian distribution $\delta_{\frac{c}{2}}(x_a-x_b)$ in either x_a or x_b, which is in turn an approximation to $\delta(x_a-x_b)$ when $\frac{c}{2}\to\infty$. Furthermore, by using Gaussian distributions and applying the Laplace's integration method [81] and related ideas, it can be proven that the following incomplete integrals are

$$\int_a^b dx\ \delta(x-x_0)\phi(x) \sim \phi(x_0),\ x_0\in[a,b] \tag{23}$$

and

$$\int_a^b dx\ \delta(x-x_0)\phi(x) \sim 0,\ x_0\notin[a,b] \tag{24}$$

within the approximation of the method.

The Delta Function in Multiple Dimensions

The generalization of the delta function to multiple dimensions is straightforward. For instance, for the three Cartesian coordinates the delta function $\delta(x-x_0, y-y_0, z-z_0)$

is defined as

$$\int dxdydz\ \delta(x-x_0,y-y_0,z-z_0)\phi(x,y,z)=\phi(x_0,y_0,z_0) \tag{25}$$

By using one-dimensional delta functions, it is easy to prove that

$$\delta(x-x_0,y-y_0,z-z_0)=\delta(x-x_0)\delta(y-y_0)\delta(z-z_0) \tag{26}$$

The transformation to a general delta function $\delta(q-q_0)$ of generalized coordinate q

$$q=q(x)=\{q_n\}=\{q_n(x_1,x_2,...\ x_N)\},\ n=1,2,...\ N \tag{27}$$

with $q_0=q(x_0)$, $q_1=q(-\infty)$, and $q_2=q(\infty)$, can be easily obtained by effecting that change of coordinates under the integration

$$\begin{aligned}\phi(x_0)&=\phi[x(q_0)]\\&=\int_{-\infty}^{\infty}dx\ \phi(x)\delta(x-x_0)\\&=\int_{q_1}^{q_2}dq\ \phi[x(q)]\delta[x(q)-x(q_0)]|\det(J)|^{-1}\end{aligned} \tag{28}$$

The Jacobian of the transformation $\det(J)$ is

$$\det(J)=\left|\frac{\partial(q_1,\ ....,\ q_N)}{\partial(x_1,\ ....,\ x_N)}\right| \tag{29}$$

From the previous integrals, it is immediate that

$$\delta(q-q_0)=\frac{\delta(x-x_0)}{|\det(J)|} \tag{30}$$

This expression is valid if the Jacobian is not singular and it is a generalization of the one-dimensional transformation given above. If the Jacobian is singular at some points then the transformation is not one-to-one. In such a case, there are, for instance, M different points $q_0^i,\ i=1,\ 2,\ ...\ ,\ M$ corresponding to the same $x_0=x\left(q_0^i\right),\ i=1,\ 2,\ ...\ ,\ M$. In the simple one-dimensional case, these points must be separated by $M-1$ points

s_i, $i = 1, 2, \ldots, M-1$ where the Jacobian is singular. Then, the full integration interval can be split into M subintervals, one for each root q_0^i. Then

$$\begin{aligned}\phi(x_0) &= \phi[x(q_0)] \\ &= \int_{-\infty}^{\infty} dx\ \phi(x)\delta(x - x_0) \\ &= \sum_{i=0}^{M} \int_{s_i}^{s_{i+1}} dq\ \phi[x(q)]\delta\left[x(q) - x\left(q_0^{i+1}\right)\right] |\det(J)|^{-1}\end{aligned} \tag{31}$$

where $s_0 = -\infty$ and $s_M = \infty$. Then, it holds that

$$\sum_{i=1}^{M} \delta\left(q - q_0^i\right) |\det(J)| = \delta(x - x_0) \tag{32}$$

where the incomplete delta function integrals given above have been used. The generalization to the multiple dimensions is straightforward. This properties has been used in the theory of classical DCS in chapter 5

APPENDIX B
THE $T^{\lambda}_{\mu\nu}$ TENSOR OPERATORS

In this appendix, the action of the operators $T^{\lambda}_{\mu\nu}$ (eq. 54 and 55, chapter 4) on the rotational states $|IMK\rangle$ will be investigated. Since these states form a complete set, we can always write

$$T^{\lambda}_{\mu\nu}|IMK\rangle = \sum_{I'M'K'} t^{I\ M\ K\ \lambda\mu\nu}_{I'M'K'}\ |I'M'K'\rangle \tag{1}$$

where the coefficients $t^{I\ M\ K\ \lambda\mu\nu}_{I'M'K'}$ are to be determined. By applying to $|IMK\rangle$ the commutation relationships of $T^{\lambda}_{\mu\nu}$ with both L_z and J_z eq. 54, it is obtained that

$$\begin{aligned} L_z\Big[T^{\lambda}_{\mu\nu}|IMK\rangle\Big] &= (K+\nu)\Big[T^{\lambda}_{\mu\nu}|IMK\rangle\Big] \\ J_z\Big[T^{\lambda}_{\mu\nu}|IMK\rangle\Big] &= (M+\mu)\Big[T^{\lambda}_{\mu\nu}|IMK\rangle\Big] \end{aligned} \tag{2}$$

This implies that the above linear combination must simplify to

$$\begin{aligned} T^{\lambda}_{\mu\nu}|IMK\rangle = \sum_{I'} t^{I\ \ M\ \ K\ \ \lambda\ \mu\ \nu}_{I'\ M+\mu\ K+\nu}\ |I'M+\mu\ K+\nu\rangle \\ \max\ (|M+\mu|,\ |K+\nu|) \le I' \le \infty \end{aligned} \tag{3}$$

To further determine the last sum, it is necessary to invoke the commutator relationships of $T^{\lambda}_{\mu\nu}$ with both $L_{\pm}$ and $J_{\pm}$, eq. 55. In the special case of the operators $T^{\lambda}_{\mu\pm\lambda}$ and $T^{\ \lambda}_{\pm\lambda\ \nu}$, they do commute with both $L_{\pm}$ and $J_{\pm}$. By applying the $\Big[L_{\pm}, T^{\lambda}_{\mu\pm\lambda}\Big] = 0$ relationships to the states $|I\ M \pm I\rangle$, it is obtained that

$$\begin{aligned} L_{\pm}T^{\lambda}_{\mu\pm\lambda}|I\ M \pm I\rangle &= T^{\lambda}_{\mu\pm\lambda}L_{\pm}|I\ M \pm I\rangle \\ &= 0 \end{aligned} \tag{4}$$

More explicitly, this last relationship implies that

$$
\begin{aligned}
L_{\pm}T^{\lambda}_{\mu\pm\lambda}|I\ M \pm I\rangle &= L_{\pm}\sum_{I'} t^{I\ M}_{I'\ M+\mu\ \pm I\pm\lambda}{}^{K\ \lambda\ \mu\ \pm\lambda}|I'\ M+\mu\ \pm I\pm\lambda\rangle \\
&= \sum_{I'}\left[I'\left(I'+1\right)-(\pm I\pm\lambda)(\pm I\pm\lambda\pm 1)\right]^{\frac{1}{2}}\times \\
&\qquad t^{I\ M}_{I'\ M+\mu\ \pm I\pm 1}{}^{K\ \lambda\,\mu\,\pm\lambda}|I'\ M+\mu\ \pm I\pm\lambda\pm 1\rangle \\
&= 0
\end{aligned}
\tag{5}
$$

To satisfy this requirement, all the $t^{I\ M}_{I'\ M+\mu\ \pm I\pm 1}{}^{K\ \lambda\,\mu\,\pm\lambda}$ must be zero except the one with $I' = I+\lambda$. Therefore,

$$
T^{\lambda}_{\mu\pm\lambda}|I\ M\ \pm I\rangle = |I+\lambda\ \ M+\mu\ \ \pm I\pm\lambda\rangle \tag{6}
$$

if $t^{I\ M}_{I+\lambda\ M+\mu\ \pm I\pm 1}{}^{K\ \lambda\,\mu\,\pm\lambda} = 1$ is set by normalization. Similarly, by applying $\left[J_{\pm}, T^{\lambda}_{\pm\lambda\nu}\right] = 0$ to $|I\pm IK\rangle$ it is obtained that

$$
T^{\lambda}_{\pm\lambda\nu}|I\ \pm I\ \ K\rangle = |I+\lambda\ \ \pm I\pm\lambda\ \ K+\nu\rangle \tag{7}
$$

To obtain the effect of these operators on the next states $|I\ M\ \pm I\mp 1\rangle$ and $|I\pm I\mp 1\ \ K\rangle$, a linear combination is again written as

$$
T^{\lambda}_{\mu\pm 1}|I\ M\ \pm I\mp 1\rangle = \sum_{I'} t^{I\ M}_{I'\ M+\mu\ \pm I\mp 1}{}^{K\ \lambda\,\mu\,\pm\lambda}|I'\ M+\mu\ \ \pm I\mp 1\rangle \tag{8}
$$

Then , by applying $L_{\pm}$ on both, it is obtained that

$$
\begin{aligned}
L_{\pm}T^{\lambda}_{\mu\pm\lambda}|IM\pm I\mp 1\rangle &= L_{\pm}\sum_{I'} t^{I\ M}_{I'\ M+\mu\ \pm I\mp 1}{}^{K\ \lambda\,\mu\,\pm\lambda}\times \\
&\qquad |I'\ M+\mu\ \ \pm I\mp 1\pm\lambda\rangle \\
&= \sum_{I'} t^{I\ M}_{I'\ M+\mu\ \pm I\mp 1}{}^{K\ \lambda\,\mu\,\pm\lambda}\times \\
&\qquad \left[I'\left(I'+1\right)-(\pm I\mp 1\pm\lambda)(\pm I\pm\lambda)\right]^{\frac{1}{2}}\times \\
&\qquad |I'M+\mu\pm I\pm\lambda\rangle
\end{aligned}
\tag{9}
$$

and, on the other side,

$$
\begin{aligned}
T^{\lambda}_{\mu\pm\lambda} L_{\pm} |I\ M\ \pm I \mp 1\rangle &= [I(I+1) - (\pm I \mp 1)(\pm I)]^{\frac{1}{2}} \times \\
& T^{\lambda}_{\mu\pm\lambda} |I\ M \pm I\rangle \\
&= [I(I+1) - (\pm I \mp 1)(\pm I)]^{\frac{1}{2}} \times \\
& |I+\lambda\ \ M+\mu\ \pm I \pm \lambda\rangle
\end{aligned}
\tag{10}
$$

Then,

$$
T^{\lambda}_{\mu\pm\lambda} |I\ M\ \ \pm I \mp 1\rangle = \left(\frac{I}{I+\lambda}\right)^{\frac{1}{2}} |I+\lambda\ \ M+\mu\ \ \pm I \mp 1 \pm \lambda\rangle \tag{11}
$$

Similarly,

$$
T^{\lambda}_{\pm\lambda\nu} |I\ \ \pm I \mp 1\ \ K\rangle = \left(\frac{I}{I+\lambda}\right)^{\frac{1}{2}} |I+\lambda\ \ \pm I \mp 1 \pm \lambda\ \ K+\nu\rangle \tag{12}
$$

Therfore, for the states $|IMK\rangle$ with $K = \pm I \mp k$ or $M = \pm I \mp m$ with $k\ (m) = 0,\ 1,\ 2,\ \ldots\ I$, the last procedures can be repeated by applying $k\ (m)$ times the $L_{\pm}\ (J_{\pm})$ operator to $T^{\lambda}_{\mu\pm\lambda}|IMK\rangle$ $(T^{\lambda}_{\pm\lambda\nu}|IMK\rangle)$. The final result is by induction

$$
\begin{aligned}
T^{\lambda}_{\mu\pm\lambda}|IMK\rangle &= \left\{\frac{[2(I+1)]!\ (I+K)!}{(2I)!\ (I+K+2\lambda)!}\right\}^{\frac{1}{2}} |I+\lambda\ \ M+\mu\ \ K \pm \lambda\rangle \\
T^{\lambda}_{\pm\lambda\nu}|IMK\rangle &= \left\{\frac{[2(I+1)]!\ (I+M)!}{(2I)!\ (I+M+2\lambda)!}\right\}^{\frac{1}{2}} |I+\lambda\ \ M \pm \lambda\ \ K+\nu\rangle
\end{aligned}
\tag{13}
$$

These expressions determine the four (all) $T^{\frac{1}{2}}_{\mu\nu}$ operators of Ref [123] and also all the $T^{1}_{\mu\nu}$ operators but one, $T^{\frac{1}{2}}_{00}$.

To determine this last operator, the general operators $T^{\lambda}_{\mu\ \pm\lambda\mp1}$ and $T^{\lambda}_{\pm\lambda\mp1\ \nu}$ with $\lambda \geq 1$ are taken into account. For them, the relationships

$$
\left[L_{\pm}, T^{\lambda}_{\mu\ \pm\lambda\mp1}\right] = (2\lambda)^{\frac{1}{2}} T^{\lambda}_{\mu\ \pm\lambda} \tag{14}
$$

and

$$
\left[J_{\pm}, T^{\lambda}_{\pm\lambda\mp1\ \nu}\right] = (2\lambda)^{\frac{1}{2}} T^{\lambda}_{\pm\lambda\mp1\ \nu} \tag{15}
$$

hold. Application of these properties to the states $|I\ M \pm I\rangle$, gives, for instance,

$$L_{\pm} T^{\lambda}_{\mu\ \pm\lambda\mp 1} |IM \pm I\rangle = (2\lambda)^{\frac{1}{2}}\ T_{\mu\pm\lambda} |IM \pm I\rangle \tag{16}$$

This kind of expressions relates the present type of operators with the previous ones. By introducing again the above linear expansion and successively treating all the states, a general expression can be obtained, as in the previous cases. The final results are

$$\begin{aligned} T^{\lambda}_{\pm\lambda\mp 1\ \nu} |IMK\rangle\ = & \left\{ \frac{2\lambda\ (I \mp M + 1)}{(I \pm M + 2\lambda)} \right\}^{-\frac{1}{2}} \times \\ & \left\{ \frac{(2I)!\ (I + M + 2\lambda)!}{(I + M)!\ [2(I+1)]!} \right\}^{-\frac{1}{2}} |I + \lambda\ \ M \pm \lambda\ \ K + \nu\rangle \end{aligned} \tag{17}$$

and

$$\begin{aligned} T^{\lambda}_{\mu\ \pm\lambda\mp 1} |IMK\rangle\ = & \left\{ \frac{2\lambda\ (I \mp K + 1)}{(I \pm K + 2\lambda)} \right\}^{-\frac{1}{2}} \times \\ & \left\{ \frac{(2I)!(I + K + 2\lambda)!}{(I + K)!\ [2(I+1)]!} \right\}^{-\frac{1}{2}} \times \\ & |I + \lambda\ \ M + \mu\ \ K \pm \lambda \mp 1\rangle \end{aligned} \tag{18}$$

From this expressions, the effect of the T^{1}_{00} operator is readily obtained.

APPENDIX C
THE ROTATIONAL COHERENT STATE MEASURE

In this appendix, it is shows by direct evaluation that the proposed signed measure for the rotational CS, eq. 67 is correct. The resolution of unity condition implies the expression

$$\int d\mu_{\pm}(x,y,z)|xyz\rangle\langle xyz| = \sum_{IMK}\sum_{I'M'K'} C\begin{smallmatrix} I' & M' & K' \\ I & M & K \end{smallmatrix} Int\begin{smallmatrix} I' & M' & K' \\ I & M & K \end{smallmatrix} \times |I'M'K'\rangle\langle IMK| \tag{1}$$

where the integrals $Int\begin{smallmatrix} I' & M' & K' \\ I & M & K \end{smallmatrix}$ are

$$Int\begin{smallmatrix} I' & M' & K' \\ I & M & K \end{smallmatrix} = \int d\mu(x,y.z)\ x^{I+M}x^{*I'+M'} \times z^{I+K}z^{*I+K'}y^{I}y^{*I'} \times \exp\left[-yy^{*}(1+xx^{*})^{2}(1+zz^{*})^{2}\right] \tag{2}$$

and the coefficients $C\begin{smallmatrix} I' & M' & K' \\ I & M & K \end{smallmatrix}$

$$C\begin{smallmatrix} I' & M' & K' \\ I & M & K \end{smallmatrix} = \left\{\frac{[(2I')!]^{2}}{I!\,(I'+M')!\,(I'-M')!\,(I'+K')!\,(I'-K')!}\right\}^{\frac{1}{2}} \times \left\{\frac{[(2I)!]^{2}}{I!\,(I+M)!\,(I-M)!\,(I+K)!\,(I-K)!}\right\}^{\frac{1}{2}} \tag{3}$$

By setting the proposed signed measured and by defining

$$b = b(x,x^{*},z,z^{*}) = (1+xx^{*})^{2}(1+zz^{*})^{2} \geq 1 \tag{4}$$

the integrals $Int\,{}_{I}^{I'}\,{}_{M}^{M'}\,{}_{K}^{K'}$ can be written as

$$Int\,{}_{I}^{I'}\,{}_{M}^{M'}\,{}_{K}^{K'} = \frac{1}{\pi^3}\int dxdz\;\; x^{I+M}x^{*I'+M'}z^{I+K}z^{*I'+K'}\,Int\,{}_{I}^{I'}(x,x^*,z,z^*) \tag{5}$$

where the new integrals $Int\,{}_{I}^{I'}(x,x^*,z,z^*)$ are explicitly

$$\begin{aligned} Int\,{}_{I}^{I'}(x,x^*,z,z^*) = \int_{-\infty}^{\infty}\int_{-\infty}^{\infty} dy_1dy_2\,(y_1+iy_2)^I(y_1-iy_2)^{I'}\times \\ \Big[4b^2\big(y_1^2+y_2^2\big)^2 - 8b\big(y_1^2+y_2^2\big)+1\Big]\times \\ \exp\Big[-b\big(y_1^2+y_2^2\big)\Big] \end{aligned} \tag{6}$$

with $y = y_1 + iy_2$. By changing into polar representation $y = r\exp(i\chi)$, the last integrals can be evaluated [109]

$$\begin{aligned} Int\,{}_{I}^{I'} &= \int_0^{\infty}\int_0^{2\pi} drd\chi\;\exp\big[i\big(I-I'\big)\chi\big]\;r^{I+I'+1}\times \\ &\qquad \Big[4b^2r^4 - 8br^2+1\Big]\exp\big[-br^2\big]\times \\ &= 2\pi\delta_{II'}\int_0^{\infty} dr\,\Big[4b^2r^{2I+5} - 8br^{2I+3} + r^{2I+1}\Big]\times \\ &\qquad \exp\big[-br^2\big] \\ &= 2\pi\delta_{II'}\left\{\frac{4(I+2)! - 8(I+1)! + I!}{2b^{I+1}}\right\} \\ &= \pi\delta_{II'}\frac{(2I+1)^2}{b^{I+1}}I! \end{aligned} \tag{7}$$

By setting this result into $Int\,{}_{I}^{I'}\,{}_{M}^{M'}\,{}_{K}^{K'}$ and by recalling the definition of b, eq. 4, it is obtained that

$$\begin{aligned} Int\,{}_{I}^{I'}\,{}_{M}^{M'}\,{}_{K}^{K'} = \delta_{II'}\frac{(2I+1)^2}{\pi^2}I!\times \\ Int\,{}_{M}^{M'}\,Int\,{}_{K}^{K'} \end{aligned} \tag{8}$$

where the integrals $Int\,{}_{M}^{M'}$ and $Int\,{}_{K}^{K'}$ are

$$\begin{aligned} Int\,{}_{M}^{M'} &= \int dx\;\frac{x^{I+M}x^{*I+M'}}{(1+xx^*)^{2I+2}} \\ Int\,{}_{K}^{K'} &= \int dz\;\frac{z^{I+K}z^{*I+K'}}{(1+zz^*)^{2I+2}} \end{aligned} \tag{9}$$

respectivley. Again, by changing to polar representation, $z = z_1 + iz_2 = p\exp(i\psi)$, the last integral can be written as [109]

$$
\begin{aligned}
Int\,{}^{K}_{K'} &= \int_{-\infty}^{\infty}\int_{-\infty}^{\infty} dz_1 dz_2\ \frac{(z_1+iz_2)^{I+K}\,(z_1-z_2)^{I+K'}}{[1+(z_1+iz_2)(z_1-iz_2)]^{2I+2}} \\
&= \int_0^{2\pi}\int_0^{\infty} d\psi dp\ \exp\left[i\big(K-K'\big)\psi\right]\ \frac{p^{2I+K+K'+1}}{(1+p^2)^{2I+2}} \\
&= 2\pi\delta_{KK'}\int_0^{\infty} dp\ \frac{p^{2I+2K+1}}{(1+p^2)^{2I+2}} = \\
&= 2\,\pi\delta_{KK'}\,\frac{(I+K)!(2I+2-I-K-2)!}{2\,(2I+2-1)!} \\
&= \pi\delta_{KK'}\,\frac{(I+K)!(I-K)!}{(2I+1)(2I)!}
\end{aligned}
\tag{10}
$$

By changing K for M in the last line, the expression for the integrals $Int\,{}^{M'}_{M}$ can be obtained. Therefore,

$$
Int\,{}^{I'\ M'\ K'}_{I\ \ M\ \ K} = \delta_{II'}\delta_{MM'}\delta_{KK'}\,\frac{(I!)^2\,(I+M)!\,(I+K)!\,(I-M)!\,(I-K)!}{[(2I)!]^2} \tag{11}
$$

and then

$$
\int d\mu_{\pm}(x,y,z)|xyz\rangle\langle xyz| \;=\; \sum_{IMK}|IMK\rangle\langle IMK| = 1 \tag{12}
$$

$$
(Q.\ E.\ D)
$$

.

APPENDIX D
AVERAGES IN THE ROTATIONAL COHERENT STATE

The evaluation of different operator averages in the rotational coherent state, eq. 63, involves a Poisson distribution in $r = yy^*(1+xx^*)^2(1+yy^*)^2$.,

$$P_0 = \exp(-r)\sum_{I=0}^{\infty}\frac{r^I}{I!} = 1 \ , \tag{1}$$

the power expansion of $(1+zz^*)^{2I}$

$$B_0^{2I}(zz^*) = (1+zz^*)^{2I} = \sum_{K=-I}^{I}\frac{(2I)!}{(I+K)!\,(I-K)!}(zz^*)^{I+K} \ , \tag{2}$$

the analogous power expansion of $(1+xx^*)^{2I}$, and their first and second moments shown explicitly below

$$\begin{aligned} P_1 &= \exp(-r)\sum_{I=0}^{\infty} I\frac{r^I}{I!} \\ &= r\exp(-r)\sum_{I=1}^{\infty}\frac{r^{I-1}}{(I-1)!} \\ &= r\exp(-r)\sum_{I'=0}^{\infty}\frac{r^{I'}}{I'!} \\ &= r \ , \end{aligned} \tag{3}$$

$$
\begin{aligned}
P_2 &= \exp(-r)\sum_{I=0}^{\infty} I^2 \frac{r^I}{I!} \\
&= r\exp(-r)\sum_{I=1}^{\infty} I \frac{r^{I-1}}{(I-1)!} \\
&= r\exp(-r)\sum_{I=1}^{\infty} (I-1)\frac{r^{I-1}}{(I-1)!} + \\
&\quad + r\exp(-r)\sum_{I=1}^{\infty} \frac{r^{I-1}}{(I-1)!} \qquad (4) \\
&= r\exp(-r)\sum_{I'=0}^{\infty} I' \frac{r^{I'}}{I'!} + \\
&\quad + \ r\exp(-r)\sum_{I'=0}^{\infty} \frac{r^{I'}}{I'!} \\
&= rP_1 + rP_0 \\
&= r^2 + r \ .
\end{aligned}
$$

$$
\begin{aligned}
B_1^{2I}(zz^*) &= \sum_{K=-I}^{I} K \frac{(2I)!\,(zz^*)^{(I+K)}}{(I+K)!\,(I-K)!} \\
&= \sum_{k=0}^{n=2I} k \frac{n!\,(zz^*)^k}{k!\,(n-k)!} - \\
&\quad - I\sum_{k=0}^{n=2I} \frac{n!\,(zz^*)^k}{k!\,(n-k)!} \\
&= \sum_{k=1}^{n=2I} \frac{n\,(n-1)!\,(zz^*)^k}{(k-1)!(n-1-k+1)!} - \qquad (5) \\
&\quad - IB_0^{2I}(zz^*) \\
&= 2Izz^* \sum_{k'=0}^{n'=2I-1} \frac{n'!(zz^*)^{k'}}{k'!(n'-k')!} - \\
&\quad - IB_0^{2I}(zz^*) \\
&= 2Izz^*(1+zz^*)^{2I-1} - I(1+zz^*)^{2I} \ .
\end{aligned}
$$

and (omitting some details)

$$
\begin{aligned}
B_2^{2I}(zz^*) &= \sum_{K=-I}^{I} K^2 \frac{(2I)!\,(zz^*)^{(I+K)}}{(I+K)!\,(I-K)!} \\
&= 2I(2I-1)(zz^*)^2(1+zz^*)^{2I-2} \\
&\quad + 2Izz^*(1+zz^*)^{2I-1} \\
&\quad - 4I^2 zz^*(1+zz^*)^{2I-1} + I^2(1+zz^*)^{2I} \ .
\end{aligned} \tag{6}
$$

The simplest averages evaluations involve the operators $\widehat{I}$ and $\widehat{I}^2$. They are

$$
\begin{aligned}
\langle xyz|\widehat{I}|xyz\rangle &= \exp\left[-yy^*(1+xx^*)^2(1+zz^*)^2\right]\times \\
&\qquad \sum_{I=0}^{\infty} I \frac{\left[yy^*(1+xx^*)^2(1+zz^*)^2\right]^I}{I!} \\
&= \exp(-r)\sum_{I=0}^{\infty} I\frac{r^I}{I!} \\
&= P_1 \\
&= r \ ,
\end{aligned} \tag{7}
$$

and

$$
\begin{aligned}
\langle xyz|\widehat{I}^2|xyz\rangle &= \exp\left[-yy^*(1+xx^*)^2(1+zz^*)^2\right] \\
&\qquad \sum_{I=0}^{\infty} I^2 \frac{\left[yy^*(1+xx^*)^2(1+zz^*)^2\right]^I}{I!} \\
&= \exp(-r)\sum_{I=0}^{\infty} I^2\frac{r^I}{I!} \\
&= P_2 \\
&= r^2 + r \ .
\end{aligned} \tag{8}
$$

The easiest first-order average to evaluate is obviously $\langle xyz|L_z|xyz\rangle$ which is

$$
\begin{aligned}
\langle xyz|L_z|xyz\rangle &= \exp(-r)\times \\
&\quad \sum_{I=0}^{\infty}\frac{(yy^*)^I}{I!}\sum_{M=-I}^{I}\frac{(2I)!\,(xx^*)^{(I+M)}}{(I+M)!\,(I-M)!}\times \\
&\quad \sum_{K=-I}^{I}\frac{(2I)!\,K(zz^*)^{(I+K)}}{(I+K)!\,(I-K)!} \\
&= \exp(-r)\sum_{I=0}^{\infty}\frac{(yy^*)^I}{I!}B_0^{2I}(xx^*)B_1^{2I}(zz^*)\times \\
&= \exp(-r)\sum_{I=0}^{\infty}\frac{(yy^*)^I(1+xx^*)^{2I}}{I!}\times \\
&\quad \left[2Izz^*(1+zz^*)^{2I-1}-I(1+zz^*)^{2I}\right] \qquad (9)\\
&= \frac{2zz^*}{(1+zz^*)}\exp(-r)\times \\
&\quad \left[\sum_{I=0}^{\infty}I\frac{(yy^*)^I(1+xx^*)^{2I}(1+zz^*)^{2I}}{I!}\right]-P_1 \\
&= \frac{2zz^*}{(1+zz^*)}P_1-P_1 \\
&= \left[\frac{2zz^*}{(1+zz^*)}-1\right]\langle xyz|\widehat{I}|xyz\rangle \\
&= \left(\frac{zz^*-1}{1+zz^*}\right)\langle xyz|\widehat{I}|xyz\rangle\ .
\end{aligned}
$$

In order to obtain the averages belonging to the operators L_x and L_y, the averages of L_+ and L_- are evaluated first. Beginning with $\langle xyz|L_+|xyz\rangle$

$$
\begin{aligned}
\langle xyz|L_+|xyz\rangle &= \exp(-r)\sum_{I=0}^{\infty}\frac{(yy^*)^I}{I!}(1+xx^*)^{2I}\times \\
&\quad \sum_{K=-I}^{I}\left[\frac{(2I)!^2}{(I+K+1)!\,(I-K-1)!\,(I+K)!\,(I-K)!}\right]^{\frac{1}{2}} \qquad (10)\\
&\quad [I(I+1)-K(K+1)]^{\frac{1}{2}}\,z^*(zz^*)^{(I+K)}\ .
\end{aligned}
$$

By setting the relationship

$$\begin{aligned} C_+ &= \frac{[I(I+1)-K(K+1)]}{(I+K+1)!\,(I-K-1)!} \\ &= \frac{(I-K)\left[I^2+I-K^2-K\right]}{(I+K)!\,(I-K)!\,(I+K+1)} \\ &= \frac{(I-K)^2\,(I+K+1)}{(I+K)!\,(I-K)!\,(I+K+1)} \\ &= \frac{(I-K)^2}{(I+K)!\,(I-K)!}\,. \end{aligned} \tag{11}$$

into the last average, it is obtained

$$\begin{aligned} \langle xyz|L_+|xyz\rangle = \exp(-r)\sum_{I=0}^{\infty}\frac{(yy^*)^I}{I!}(1+xx^*)^{2I}\times \\ z^*\sum_{K=-I}^{I}\frac{(2I)!}{(I+K)!\,(I-K)!}(I-K)(zz^*)^{(I+K)} \\ = z^*\exp(-r)\sum_{I=0}^{\infty}I\frac{r^I}{I!} - z^*\langle xyz|L_z|xyz\rangle \\ = z^*[\langle xyz|I|xyz\rangle - \langle xyz|L_z|xyz\rangle]\,. \end{aligned} \tag{12}$$

Since $L_- = L_+^\dagger$, it is easy to prove that

$$\begin{aligned} \langle xyz|L_-|xyz\rangle &= \langle xyz|L_+|xyz\rangle^* \\ &= z\,[\langle xyz|I|xyz\rangle - \langle xyz|L_z|xyz\rangle]\,. \end{aligned} \tag{13}$$

Finally,

$$\begin{aligned} \langle xyz|L_x|xyz\rangle &= \frac{1}{2}\langle xyz|L_+ + L_-|xyz\rangle \\ &= \frac{1}{2}(z^*+z)\langle xyz|I|xyz\rangle \\ &\quad + \frac{1}{2}(z^*+z)\langle xyz|L_z|xyz\rangle \\ &= \frac{z+z^*}{(1+zz^*)}\langle xyz|I|xyz\rangle\,. \end{aligned} \tag{14}$$

and

$$\begin{aligned} \langle xyz|L_y|xyz\rangle &= -\frac{i}{2}\langle xyz|L_+ - L_-|xyz\rangle \\ &= -\frac{i}{2}(z^*-z)\langle xyz|I|xyz\rangle \\ &\quad + \frac{i}{2}(z^*-z)\langle xyz|L_z|xyz\rangle \\ &= i\left(\frac{z-z^*}{1+zz^*}\right)\langle xyz|I|xyz\rangle\,. \end{aligned} \tag{15}$$

The evaluation of the second-order averages starts with $\langle xyz|L^2|xyz\rangle$ which is

$$\begin{aligned}\langle xyz|L^2|xyz\rangle &= \exp(-r)\sum_{I=0}^{\infty}[I(I+1)]\frac{r^I}{I!}\\ &= P_2 + P_1\\ &= r(r+2)\,.\end{aligned} \tag{16}$$

Next, $\langle xyz|L_z^2|xyz\rangle$ is

$$\begin{aligned}\langle xyz|L_z^2|xyz\rangle &= \exp(-r)\times\\ &\quad \sum_{I=0}^{\infty}\frac{(yy^*)^I}{I!}\sum_{M=-I}^{I}\frac{(2I)!\,(xx^*)^{(I+M)}}{(I+M)!\,(I-M)!}\times\\ &\quad \sum_{K=-I}^{I}\frac{(2I)!\,K^2(zz^*)^{(I+K)}}{(I+K)!\,(I-K)!}\\ &= \left[\frac{1-2zz^*}{1+zz^*}\right]^2 r^2 + \left[\frac{1+(zz^*)^2}{(1+zz^*)^2}\right]r\\ &= \langle xyz|L_z|xyz\rangle^2 + \left[\frac{1+(zz^*)^2}{(1+zz^*)^2}\right]\langle xyz|I|xyz\rangle\,.\end{aligned} \tag{17}$$

In order to obtain $\langle xyz|L_x^2|xyz\rangle$, $\langle xyz|L_y^2|xyz\rangle$, and $\langle xyz|L_xL_y + L_yLx|xyz\rangle$, $\langle xyz|L_+^2|xyz\rangle$, and $\langle xyz|L_-^2|xyz\rangle$ are evaluated first. $\langle xyz|L_+^2|xyz\rangle$ is

$$\begin{aligned}\langle xyz|L_+^2|xyz\rangle &= \exp(-r)\sum_{I=0}^{\infty}\frac{(yy^*)^I}{I!}(1+xx^*)^{2I}\times\\ &\quad \sum_{K=-I}^{I}\left[\frac{(2I)!}{(I+K+2)!\,(I-K-2)!}\,\frac{(2I)!}{(I+K)!\,(I-K)!}\right]^{\frac{1}{2}}\times\\ &\quad [I(I+1)-(K+1)(K+2)]^{\frac{1}{2}}\times\\ &\quad [I(I+1)-K(K+1)]^{\frac{1}{2}}\,z^{*2}(zz^*)^{(I+K)}\,.\end{aligned} \tag{18}$$

By setting the relationships

$$\begin{aligned}C_{++} &= \frac{[I(I+1)-(K+1)(K+2)][I(I+1)-K(K+1)]}{(I+K+2)!\,(I-K-2)!}\\ &= D_+C_+\,.\end{aligned} \tag{19}$$

with

$$
\begin{aligned}
D_+ &= \frac{(I-K-1)[I(I+1)-(K+1)(K+2)]}{(I+K+2)} \\
&= \frac{(I+K+2)(I-K-1)^2}{(I+K+2)} \\
&= (I-K-1)^2 \, .
\end{aligned} \tag{20}
$$

and C_+ given by eq. 11, into the last average, it is obtained that

$$
\begin{aligned}
\langle xyz|L_+^2|xyz\rangle = \exp(-r) \sum_{I=0}^{\infty} \frac{(yy^*)^I}{I!}(1+xx^*)^{2I} \times \\
\sum_{K=-I}^{I} \frac{(2I)!}{(I+K)!\,(I-K)!}(I-K) \times \\
(I-K-1)z^{*2}(zz^*)^{(I+K)} \\
= \frac{4z^{*2}}{(1+zz^*)^2}\langle xyz|I|xyz\rangle^2 \\
+ \frac{2z^{*2}}{(1+zz^*)^2}\langle xyz|I|xyz\rangle \, .
\end{aligned} \tag{21}
$$

Since $L_-^2 = L_+^{\dagger 2}$, it is easy to prove that

$$
\begin{aligned}
\langle xyz|L_-^2|xyz\rangle &= \langle xyz|L_+^{\dagger}|xyz\rangle^* \\
&= \frac{4z^2}{(1+zz^*)^2}\langle xyz|I|xyz\rangle^2 \\
&\quad + \frac{2z^2}{(1+zz^*)^2}\langle xyz|I|xyz\rangle \, .
\end{aligned} \tag{22}
$$

From the previous second order averages, it is obtained that

$$
\begin{aligned}
\langle xyz|L_x^2+L_y^2|xyz\rangle &= \langle xyz|L^2-L_z^2|xyz\rangle \\
&= \left[1-\left(\frac{1-zz^*}{1+zz^*}\right)^2\right]\langle xyz|I|xyz\rangle^2 \\
&\quad + \left[2-\frac{1+(zz^*)^2}{(1+zz^*)^2}\right]\langle xyz|I|xyz\rangle \\
&= \frac{4zz^*}{(1+zz^*)^2}\langle xyz|I|xyz\rangle^2 \\
&\quad + \frac{\left[1+4zz^*+(zz^*)^2\right]}{(1+zz^*)^2}\langle xyz|I|xyz\rangle \, .
\end{aligned} \tag{23}
$$

and

$$\begin{aligned}\langle xyz|L_x^2 - L_y^2|zyz\rangle &= \frac{1}{2}\langle xyz|L_+^2 + L_-^2|xyz\rangle \\ &= 2\frac{\left(z^2 + z^{*2}\right)}{\left(1+zz^*\right)^2}\langle xyz|I|xyz\rangle^2 \\ &\quad + \frac{\left(z^2 + z^{*2}\right)}{\left(1+zz^*\right)^2}\langle xyz|I|xyz\rangle\ .\end{aligned} \tag{24}$$

By combining the last two averages, it is immediate that

$$\begin{aligned}\langle xyz|L_x^2|xyz\rangle &= \langle xyz|L_x|xyz\rangle^2 \\ &\quad + \frac{\left[1 + 4zz^* + z^2 + z^{*2} + \left(zz^*\right)^2\right]}{2\left(1+zz^*\right)^2}\langle xyz|I|xyz\rangle\ ,\end{aligned} \tag{25}$$

and

$$\begin{aligned}\langle xyz|L_y^2|xyz\rangle &= \langle xyz|L_y|xyz\rangle^2 \\ &\quad + \frac{\left[1 + 4zz^* - z^2 - z^{*2} + \left(zz^*\right)^2\right]}{2\left(1+zz^*\right)^2}\langle xyz|I|xyz\rangle\ .\end{aligned} \tag{26}$$

In the same vein,

$$\begin{aligned}\langle xyz|[L_x,\ L_y]_+|zyz\rangle &= \frac{1}{2i}\langle xyz|L_+^2 - L_-^2|xyz\rangle \\ &= \frac{2\left(z^{*2} - z^2\right)}{i(1+zz^*)^2}\langle xyz|I|xyz\rangle^2 \\ &\quad + \frac{\left(z^{*2} - z^2\right)}{i(1+zz^*)^2}\langle xyz|I|xyz\rangle \\ &= \frac{2(z^* - z)(z^* + z)}{i(1+zz^*)^2}\langle xyz|I|xyz\rangle^2 \\ &\quad + \frac{(z^* - z)(z^* + z)}{i(1+zz^*)^2}\langle xyz|I|xyz\rangle\ .\end{aligned} \tag{27}$$

which can be finally written as

$$\begin{aligned}\langle xyz|[L_x,\ L_y]_+|zyz\rangle &= 2\langle xyz|L_x|xyz\rangle\langle xyz|L_y|xyz\rangle \\ &\quad + \frac{(z^* + z)}{(1+zz^*)}\langle xyz|L_y|xyz\rangle \\ &= 2\langle xyz|L_x|xyz\rangle\langle xyz|L_y|xyz\rangle \\ &\quad + \frac{(z^* - z)}{i(1+zz^*)}\langle xyz|L_x|xyz\rangle\ .\end{aligned} \tag{28}$$

Note that $\langle xyz|[L_x,\ L_y]_+|zyz\rangle = 0$ if $\langle xyz|I|xyz\rangle = 0$. When this last condition is not satisfied then it is possible to write more symmetrically

$$\langle xyz|[L_x,\ L_y]_+|zyz\rangle = 2\langle xyz|L_x|xyz\rangle\langle xyz|L_y|xyz\rangle + \frac{\langle xyz|L_x|xyz\rangle\langle xyz|L_y|xyz\rangle}{\langle xyz|I|xyz\rangle}\ , \qquad (29)$$
$$(\langle xyz|I|xyz\rangle \neq 0)\ .$$

To obtain the averages $\langle xyz|L_xL_z + L_zL_x|xyz\rangle$ and $\langle xyz|L_yL_z + L_zL_y|xyz\rangle$, it is necessary to evaluate first $\langle xyz|L_+L_z|xyz\rangle$ and $\langle xyz|L_-L_z|xyz\rangle$, and perform the proper combinations. These calculations are quite similar to the previous ones and their details are therefore omitted. The averages of the $\vec{J}$ components, their powers, and their combinations can be obtained in the same way as their $\vec{L}$ counterparts.

APPENDIX E
AVERAGE OVER INITIAL ANGULAR VARIABLES

In this appendix, the integration procedure used in the $H^+ + CH_4$ and the $H^+ + H_2O$ dynamics is explained in some detail. The following discussion refers to the first simple. In terms of the Euler angles the invariant measure of the SO(3) parameter space is $\mathrm{d}\alpha\mathrm{d}\gamma\sin\beta\mathrm{d}\beta$. The trapezoidal rule with a constant step length$h = 2\pi/n$ is used for the α and γ integrations, *i.e.*

$$\int_0^{2\pi} f(\alpha)\mathrm{d}\alpha = h\sum_{i=0}^{n-1} f_i, \tag{1}$$

where the fact that the first and last points are identical has been used.

The integral over β requires a bit more care. We choose to represent the integrand by the trapezoidal rule, but integrate the measure exactly,*i.e.*

$$\int_0^{\pi} f(\beta)\sin\beta\mathrm{d}\beta = \sum_{i=0}^{n-1}\int_{\beta_i}^{\beta_{i+1}} \tilde{f}_i(\beta)\sin\beta\mathrm{d}\beta, \tag{2}$$

with

$$\tilde{f}_i(\beta) = f_i + \frac{\beta-\beta_i}{\beta_{i+1}-\beta_i}(f_{i+1}-f_i). \tag{3}$$

Since

$$\begin{aligned}\int_{\beta_i}^{\beta_{i+1}} \tilde{f}(\beta)\sin\beta\mathrm{d}\beta = f_i[\cos\beta_i - h_i(\sin\beta_{i+1} - \sin\beta_i)] \\ - f_{i+1}[\cos\beta_{i+1} - h_i(\sin\beta_{i+1} - \sin\beta_i)]\end{aligned} \tag{4}$$

with $h_i = 1/(\beta_{i+1}-\beta_i)$ the quadrature becomes

$$\int_0^{\pi} f(\beta)\mathrm{d}\beta = \sum_{i=0}^{n} f_i w_i, \tag{5}$$

with the weights

$$w_0 = \cos\beta_0 - h_0(\sin\beta_1 - \sin\beta_0)$$
$$w_i = -h_i(\sin\beta_{i+1} - \sin\beta_i) + h_{i-1}(\sin\beta_i - \sin\beta_{i-1}) \quad (6)$$
$$w_n = -\cos\beta_n + h_{n-1}(\sin\beta_n - \sin\beta_{n-1}).$$

One advantage with this approximation is that the volume is obtained correctly regardless of how many grid points are used.

For the proton collisions with methane, with the HCH bond angle being $\theta = 109.47$ degrees we obtain the 132 grid points indicated in Table 7.3 in terms of the six basic target orientations. The overall weights for the function values at the six basic orientations are then for H1 and H2$\pi^2(2w_0 + w_2)$ and $\pi^2(2w_0' + w_2')$, respectively, for F1 and F2 $\pi^2(w_1 + 2w_3)$ and $\pi^2(w_1 + 2w_3')$, respectively, and for both E1 and E2$\pi^2(w_1' + w_2)$, where $\beta_0 = \beta_0' = 0,\ \beta_1 = \pi - \theta,\ \beta_1' = \theta/2, \beta_2' = \beta_2 = \theta,\ and\ \beta_3 = \beta_3' = \pi$. The averaging over orientations then means dividing the quadrature result by the total volume $8\pi^2$. It should be noted that the α integration has a step of $\pi/3$ for H1, H2, F1, and F2, and a step $\pi/2$ for E1 and E2

REFERENCES

1. E. Deumens, A. Diz, R. Longo, and Y. Öhrn, Rev. Mod. Phys **66**, 917 (1994).

2. E. Deumens et al., *ENDyne Software for Electron Nuclear Dynamics*, Quantum Theory Project, University of Florida, Gainesville FL 32611-8435, 1996.

3. M. Goldberger and K. Watson, *Collision Theory*, John Wiley and Sons, Inc., New York, 1st edition, 1964.

4. R. G. Newton, *Scattering Theory of Waves and Particles*, Springer-Verlag, New York, 1982.

5. J. R. Taylor, *Scattering Theory: The Quantum Theory of Nonrelatistic Collisions*, John Wiley and Sons, Inc., New York, 1972.

6. R. D. Levine and R. B. Bernstein, *Molecular Reaction Dynamics and Chemical Reactivity*, Oxford University, New York, 1987.

7. R. Longo, *Exploring a New Time-Dependent Method for Molecular Quantum Dynamics*, PhD thesis, University of Florida, Gainesville, FL, 1993.

8. W. Eastes, U. Ross, and J. P. Toennies, J. Chem. Phys. **70**, 1652 (1979).

9. J. R. Klauder, Beyond Conventional Quantization, Unpublished Book, 1997.

10. G. Schatz, J. Phys. Chem. **99**, 516 (1975).

11. J. R. Klauder and B.-S. Skagerstam, *Coherent States, Applications in Physics and Mathematical Physics*, World Scientific, Singapore, 1985.

12. M. D. Newton, Int. J. Quantum Chem.: Quant. Chem. Symp. **14**, 363 (1980).

13. M. S. Child, *Molecular Collision Theory*, Academic Press, London and New York, 1974.

14. F. T. Smith, Phys. Rev. **179**, 111 (1969).

15. D. R. Yarkony, Electronic structure aspects of nonadiabatic processes in polyatomic systems, 1995.

16. M. Baer, Quantum mechanical treatment of electronic transitions in atom-molecule collisions, in *Molecular collision dynamics*, edited by J. M. Bowman, pages 61–115, Springer-Verlag, Berlin, Heidelberg, New York, 1983.

17. M. Baer, The theory of electronic nonadiabatic transitions in chemical reactions, in *The Theory of Chemical Reaction Dynamics*, edited by M. Baer, volume I-IV, pages 219–280, CRC, Boca Raton, FL, 1985.

18. M. S. Child, Electronic excitation: Nonadiabatic transitions, in *Atom-Molecule Collision Theory, A Guide for the Experimentalist*, edited by R. B. Bernstein, pages 427–466, Plenum Press, New York and London, 1979.

19. G. Herzberg, *Molecular Spectra and Molecular Structure. I. Spectra of Diatomic Molecules*, D. Van Nostrand Co., New York, 2nd edition, 1950.

20. M. C. Zerner, Semiempirical molecular orbital methods, in *Reviews in Computational Chemistry*, edited by K. B. Lipkowitz and D. B. Boyd, volume 2, chapter 8, pages 313–365, VCH Publishers, New York, 1991.

21. M. J. Field, J. Chem. Phys. **96**, 4583 (1992).

22. F. O. Ellison, J. Am. Chem. Soc. **85**, 3540 (1963).

23. P. J. Kuntz, Interaction potentials II: Semiempirical atom-molecule potentials for collision theory, in *Atom-Molecule Collision Theory, A Guide for the Experimentalist*, edited by R. B. Bernstein, pages 79–110, Plenum Press, New York and London, 1979.

24. R. G. Parr and W. Yang, *Density-Funtional Theory of Atoms and Molecules*, International Series of Monographs on Chemistry, Oxford University Press, Clarendon Press, New York, Oxford, 1989.

25. R. Zare, *Angular Momentum*, John Wiley & Sons, New York, 1st edition, 1988.

26. N. F. Mott and H. S. W. Massey, *The Theory of Atomic Collisions*, Oxford University, Oxford, 1965.

27. M. Abramowitz and I. A. Stegun, *Handbook of Mathematical Functions*, National Bureau of Standards, U. S. Goverment Printing Office, Washington DC, 4th edition, 1964.

28. J. Jellinek and D. J. Kouri, Approximate treatments of reactive scattering: Infinite order sudden approximation, in *The Theory of Chemical Reaction Dynamics*, edited by M. Baer, volume I-IV, pages 219–280, CRC, Boca Raton, FL, 1985.

29. D. C. Clary, J. Chem. Phys. **95**, 7298 (1991).

30. D. C. Clary, J. Phys. Chem **98**, 10678 (1994).

31. Y. Öhrn and J. Linderberg, Mol. Phys. **49**, 53 (1983).

32. A. R. Kuppermann and P. G. Hippes, J. Chem. Phys. **84**, 5962 (1986).

33. D. J. Kouri, Rotational excitation II: Approximation methods, in *Atom-Molecule Collision Theory, A Guide for the Experimentalist*, edited by R. B. Bernstein, pages 301–358, Plenum Press, New York and London, 1979.

34. A. S. Dickinson and D. Richards, J. Phys. B **14**, 3663 (1980).

35. M. Baer and H. Nakamura, J. Chem. Phys. **87**, 4651 (1987).

36. M. Baer, G. Niedner-Schatteburg, and J. P. Toennies, J. Chem. Phys. **91**, 4169 (1989).

37. R. Schinke and J. M. Bowman, rotational rainbows in atom-diatom scattering, in *Molecular Collision Dynamics*, edited by J. M. Bowman, Topics in Current Physcis, pages 61–115, Springer-Verlag, Belin, Heidelberg, New York, 1983.

38. D. Secrest, Rotational Excitation I: The quantal treatment, in *Atom-Molecule Collision Theory, A Guide for the Experimentalist*, edited by R. B. Bernstein, pages 265–300, Plenum Press, New York and London, 1979.

39. H. Kröger, Phys. Rep. **210**, 45 (1992).

40. J. Broeckhove and L. Lathouwers, *Time Evolution of Electrons and Nuclei in Molecular Systems*, Plenum, New York, 1992.

41. D. Kosloff and R. Kosloff, J. Comput. Phys. **52**, 35 (1983).

42. M. D. Feit, J. A. Fleck, Jr., and A. Steiger, J. Comput. Phys. **47**, 412 (1982).

43. J. Alvarellos and H. Metiu, J. Chem. Phys. **88**, 4957 (1988).

44. V. Engel, J. Chem. Phys. **94**, 16 (1991).

45. S. Cheslowski, A. D. Bandrauk, and P. B. Corkum, Phys. Rev. Lett. **65**, 2355 (1990).

46. M. D. Feit and J. A. Fleck, Jr., J. Chem. Phys. **78**, 301 (1982).

47. M. D. Feit and J. A. Fleck, Jr., J. Chem. Phys. **80**, 2578 (1984).

48. H. Tal-Ezer and R. Kosloff, J. Chem. Phys. **81**, 3967 (1984).

49. G. Arfken, *Mathematical Methods For Physicists*, Academic Press Inc., Orlando, 1985.

50. J. Zhang, D. J. Kouri, K. Hang, D. W. Sckwenke, and D. G. Truhlar, J. Chem. Phys. **88**, 2492 (1988).

51. J. Park and J. Light, J. Chem. Phys. **85**, 5870 (1986).

52. U. Manthe and H. Köppel, J. Chem. Phys. **93**, 1658 (1990).

53. U. Manthe and H. Köppel, J. Chem. Phys. **93**, 345 (1990).

54. U. Manthe and H. Köppel, Chem. Phys. Lett. **178**, 36 (1990).

55. H. Köppel and U. Manthe, Femtosecond wave-packet dynamics on strongly coupled potential energy surfaces., in *Time Dependent Quantum Molecular Dynamics*, edited by J. Broeckhove and L. Lathouwers, pages 83–95, New York, 1992, Plenum Press.

56. R. H. Bisseling et al., J. Chem. Phys. **87**, 2760 (1987).

57. B. Vekhter, M. A. Ratner, and R. B. Gerber, J. Chem. Phys. **99**, 7916 (1993).

58. R. Alimi, R. B. Gerber, A. D. Hammerich, R. Kosloff, and M. A. Ratner, J. Chem. Phys **93**, 6484 (1990).

59. U. Manthe, H. Meyer, and L. S. Cederbaum, J. Chem. Phys. **97**, 9062 (1992).

60. R. Car and M. Parrinello, Phys. Rev. Lett. **55**, 2471 (1985).

61. H. Goldstein, *Classical Mechanics*, Addison-Wesley, Reading, MA, 2nd edition, 1980.

62. J. P. Ryckaert, G. Ciccotti, and H. Berendsen, J. Com. Phys. **23**, 327 (1977).

63. M. P. Allen and D. J. Tildesley, *Computer Simulation of Liquids*, Clarendon Press, Oxford, 1987.

64. H. Andersen, J. Com. Phys. **52**, 24 (1983).

65. M. Payne, M. P. Teter, D. Alla, T. A. Arias, and J. Joannopoulos, Rev. Mod. Phys. **64**, 1045 (1992).

66. D. K. Remler and P. A. Madden, Mol. Phys. **70**, 921 (1990).

67. K. C. Kulander, K. R. S. Devi, and S. E. Koonin, Phys. Rev. A **25**, 2968 (1982).

68. D. Tiszauer and K. C. Kulander, Phys. Rev. A **29**, 2909 (1984).

69. D. H. Tiszauer and K. C. Kulander, Comput. Phys. Commun. **63**, 351 (1991).

70. K. Runge, D. A. Micha, and E. Q. Feng, Int. J. Quantum Chem.: Quant. Chem. Symp. **24**, 781 (1990).

71. K. Runge, *A Time-Dependent Many-Electron Approach to Atomic and Molecular Interactions*, PhD thesis, Univeristy of Florida, Gainesville, FL, 1993.

72. D. A. Micha and K. Runge, Electronic energy and charge transfer in slow atomic collisions: A time-dependent molecular orbital approach, in *Time-Dependent Quantum Molecular Dynamics*, edited by J. Broeckhove and L. Lathouwers, pages 247–266, Plenum Press, New York, 1992.

73. K. V. Mikkelsen and M. Ratner, J. Phys. Chem. **93**, 1759 (1989).

74. D. R. Bates and R. McCarroll, Proc. R. Soc. London Ser. A **245**, 175 (1958).

75. J. B. Delos, Rev. Mod. Phys. **58**, 287 (1981).

76. W. Fritsch and C. D. Lin, Phys. Rep. **202**, 1 (1991).

77. A. Riera, Molecular model of fast atomic collisions, in *Time-Dependent Quantum Molecular Dynamics*, edited by J. Broeckhove and L. Lathouwers, pages 311–346, Plenum, New York, 1992.

78. D. A. Micha, Int. J. Quant. Chem. (1994), in print.

79. J. Theilhaber, Phys. Rev. B **46**, 12990 (1992).

80. M. Kimura and N. F. Lane, The low-energy, heavy-particle collisions - a close-coupling treatment, in *Advances in Atomic, Molecular and Optical Physics*, edited by D. Bates and B. Bederson, page 79, Academic, New York, 1990.

81. A. Erdelyi, *Asymptotic Expansions*, Dover Publications, Inc., New York, 1956.

82. M. S. Child, *Semiclassical Mechanics with Mollecular Applications*, Clarendon Press, Oxford, 1991.

83. N. Fröman, Semiclassical and Higher Orders Approximations: Properties. Solution of Connection Problems, in *Semiclassical Methods in Molecular Scattering and Spectroscopy*, edited by M. S. Child, Nato Advanced Study Institutes Series, Dordrecht, 1979, D. Reidel.

84. I. C. Percival, Adv. Chem. Phys. **36**, 1 (1977).

85. W. H. Miller, J. Phys. Chem. **53**, 1949 (1970).

86. W. H. Miller, Adv. Chem. Phys. **25**, 69 (1974).

87. D. W. Noid and R. A. Marcus, J. Chem Phys. **62**, 2119 (1975).

88. C. W. Eaker and G. C. Schatz, J. Phys. Chem. **89**, 2612 (1985).

89. R. A. Marcus, Chem. phys. Lett. **45**, 525 (1970).

90. R. P. Feyman and A. R. Hibbs, *Quantum Mechanics and Path Integrals*, McGraw-Hill, New York, 1965.

91. W. H. Miller, Adv. Chem. Phys. **30**, 77 (1975).

92. J. H. V. Vleck, Proc. Nat. Acad. Sci. **14**, 178 (1928).

93. J. D. Doll and W. H. Miller, J. Chem. Phys. **57**, 5019 (1972).

94. E. J. Heller, J. Chem. Phys. **62**, 1544 (1975).

95. E. J. Heller, Chem. Phys. Lett **34**, 321 (1975).

96. E. J. Heller, J. Chem. Phys. **65**, 4979 (1976).

97. E. J. Heller, J. Chem. Phys. **66**, 5777 (1977).

98. R. G. Littlejohn, Phys. Rep. **138**, 193 (1986).

99. P. Pechukas, Phys. Rev. **181**, 166 (1969).

100. P. Pechukas, Phys. Rev. **181**, 174 (1969).

101. L. D. Landau, Physik. Z. Sowjetunion U.S.S.R. **2**, 46 (1932).

102. C. Zener, Proc. Roy. Soc. **137**, 696 (1932).

103. Y. N. Demkov, Soviet Phys. JETP **18**, 138 (1964).

104. J. C. Tully and R. K. Preston, J. Chem. Phys. **55**, 562 (1971).

105. J. C. Tully, J. Chem. Phys. **93**, 1061 (1990).

106. P. Kramer and M. Saraceno, *Geometry of the Time-Dependent Variational Principle in Quantum Mechanics*, Springer, New York, 1981.

107. P. Ring and P. Schuck, *The Nuclear Many-Body Problem*, Springer-Verlag, New York,Heidelberg, Berlin, 1st edition, 1980.

108. E. Deumens and Y. Öhrn, J. Chem. Soc.,Faraday Trans. **93**, 919 (1997).

109. I. S. Gradshteyn and I. M. Ryzhik, *Table of Integrals, Series, and Products*, Academic Press Inc., Orlando, 4 edition, 1980.

110. D. J. Thouless, Nucl. Phys. **21**, 225 (1960).

111. D. J. Thouless, *The Quantum Mechanics of Many-Body System*, Academic Press, New York and London, 1961.

112. B. Mogensen, *A Novel Theoretical Description of Electron-Molecul e Reactions*, PhD thesis, University of Copenhagen, Department of Chemistry, Lab IV, Universitetsparken 5, Copenh agen O, DK2100, Denmark, 1997.

113. E. Deumens and Y. Öhrn, J. Mol. Struct. (THEOCHEM) **199**, 23 (1989).

114. J. A. Morales, E. Deumens, and Y. Öhrn, End Double Wave Packet Theory in the Nuclear Classical Limit, Unpublished Results, 1995.

115. J. A. Morales, E. Deumens, and Y. Öhrn, Semi and Quasi Classical Limits for Final Properties in the END Theory, Unpublished Results, 1995.

116. E. Deumens, Y. Öhrn, and B. Weiner, J. Math. Phys. **32**, 1166 (1991).

117. E. Schrödinger, Naturwissenschaften **14**, 664 (1926).

118. R. J. Glauber, Phys. Rev. Lett. **10**, 84 (1963).

119. C. Cohen-Tannoudji, B. Diu, and F. Laloë, *Quantum Mechanics*, volume 1, Wiley Interscience, New York, 1977.

120. J. M. Radcliffe, J. Phys. A **4**, 313 (1971).

121. A. M. Perelomov, Commun. Math. Phys. **26**, 222.

122. A. M. Perelomov, *Generalized Coherent States and Their Applications*, Springer, New York, 1986.

123. D. Janssen, Soviet Journal of Nuclear Physics **25**, 479 (1977).

124. L. Fonda, N. Mankoc, and M. Rosina, Phys. Rep. **158**, 160 (1988).

125. J. A. Morales, E. Deumens, and Y. Öhrn, Quasiclassical Rotational States: Reformulation of a Rotational Coherent State for Molecular Dynamics, In preparation for Phys. Rev. A, 1997.

126. A. M. Arthurs and A. Dalgarno, Proc. Roy. Soc. **A256**, 540 (1960).

127. B. A. B. R. E. Continetti and Y. Lee, J. Chem. Phys. **93**, 5719 (1990).

128. R. T. Pack, J. Chem. phys. **81**, 1841 (1984).

129. R. K. B. Helbing, J. Chem. Phys. **48**, 472 (1968).

130. F. A. Morse and R. B. Bernstein, J. Chem. Phys. **37**, 2019 (1962).

131. T. T. Warnock and R. B. Bernstein, J. Chem. Phys. **49**, 1878 (1968).

132. E. A. Gislason, Chem. Phys. Letters **42**, 315 (1976).

133. A. S. Dickinson, Correspondence-principle method for molecular collisions, in *Semiclassical Methods in Molecular Scattering and Spectroscopy*, edited by M. S. Child, NATO Advanced Study Institutes Series, pages 263–296, Dordrecht, 1979, D. Reidel.

134. A. S. Dickinson and D. Richards, Adv. Atom. Mol Phys. **18**, 165 (1982).

135. M. Karplus, R. Porter, and R. D. Sharma, J. Chem. Phys. **49**, 3259 (1965).

136. L. D. Thomas, Chem. Phys. Letters **51**, 35 (1977).

137. U. R. D. Beck and Schepper, Z. Phys. A **293**, 107 (1979).

138. U. R. D. Beck and Schepper, Z. Phys. A **299**, 97 (1980).

139. L. D. Thomas, Rainbow scattering in inelastic molecular collisions, in *Potential Energy Surfaces and Dynamics Calculations for Chemical Reactions and Molecular Energy Transfer*, edited by D. G. Truhlar, chapter 31, pages 737–758, Plenum Press, New York and London, 1981.

140. L. D. Thomas, J. Chem. Phys. **73**, 5905 (1980).

141. K. W. Ford and J. A. Wheeler, Ann. Phys. **7**, 259 (1959).

142. M. V. Berry, Proc. Phys. Soc. (London) **89**, 479 (1966).

143. J. N. L. Connor, Molec. Phys. **26**, 1217 (1973).

144. J. N. L. Connor, Molec. Phys. **27**, 853 (1974).

145. J. N. L. Connor, Semiclassical theory of elastic scattering, in *Semiclassical Methods in Molecular Scattering and Spectroscopy*, edited by M. S. Child, NATO Advanced Study Institutes Series, pages 45–108, Dordrecht, 1979, D. Reidel.

146. J. N. L. Connor and D. Farrelly, J. Chem. Phys **75**, 2831 (1981).

147. J. N. L. Connor and P. R. Curtis, J. Phys. A: Math. Gen. **15** (1982), 1179-1190.

148. T. P. I. Stewart, *Catastrophe Theory and its Applications*, Pitman, Boston, 1 edition, 1978.

149. M. V. Berry, J. Phys. B **2**, 381 (1969).

150. P. J. Brussaard and H. A. Tolhoek, Physica **23**, 955 (1957).

151. Y.-N. Chiu et al., J. Chem. Phys. **88**, 6814 (1988).

152. B. Friedrich, G. Niedner, M. Noll, and J. P. Toennies, J. Chem. Phys. **87**, 5256 (1987).

153. H. Udseth, C. F. Giese, and W. Gentry, Phys. Rev. A **8**, 2483 (1973).

154. J. R. Krenos, R. K. Preston, R. Wolfgang, and J. C. Tully, J. Chem. Phys. **60**, 1634 (1974).

155. K. Rudolph and J. P. Toennies, J. Chem. Phys. **65**, 4483 (1976).

156. V. Hermann, H. Schmidt, and F. Linder, J. Phys. B **11**, 493 (1978).

157. G. Niedner, M. Noll, J. Toennies, and C. Schlier, J. Chem. Phys. **87**, 2686 (1987).

158. A. Bjerre and E. E. Nikitin, Chem. Phys. Lett. **1**, 179 (1967).

159. T. H. Dunning, Jr., J. Chem. Phys. **90**, 1007 (1989).

160. C. Giese and W. R. Gentry, Phys. Rev. A **10**, 156 (1974).

161. H. Krüger and R. Schinke, J. Chem. Phys. **66**, 5087 (1977).

162. J. A. Morales, A. C. Diz, E. Deumens, and Y. Öhrn, Chem. Phys. Lett. **233**, 392 (1995).

163. J. N. L. Connor, D. Farrelly, and D. C. Mackay, J. Chem. Phys **74**, 3278 (1981).

164. A. Florescu, M. Sizun, and V. Sidis, J. Chem. Phys. **99**, 7277 (1993).

165. W. H. Cramer, J. Chem. Phys. **35**, 836 (1961).

166. A. V. Phelps, J. Phys. Chem. Ref. Data **19**, 653 (1990).

167. M. W. Gealy and B. V. Zyl, Phys. Rev. A **36**, 3091 (1987).

168. D. Koopman, Physical Review **154**, 154 (1966).

169. A. Diz, *Electron Nuclear Dynamics: A Theoretical Treatment Using Coherent States and the Time-Dependent Variational Principle*, PhD thesis, University of Florida, Gainesville, FL, 1992.

170. Y. Öhrn, J. Oreiro, and E. Deumens, Int. J. Quantum Chem. **58**, 583 (1996).

171. L. M. Raff, J. Chem. Phys. **60**, 2220 (1974).

172. Y. Nakai and T. Shirai, Atomic Data and Nuclear Data Tables **37**, 69 (1987).

173. C. F. Giese and W. R. Gentry, Phys. Rev. A **10**, 2156 (1974).

174. N. Aristov, G. Niedner-Schatteburg, J. P. Toennies, and Y.-N. Chiu, J. Chem. Phys. **95**, 7969 (1991).

175. B. Friedman, *Principles and Techniques of Applied Mathematics*, John Wiley & Sons, Inc., New York, 1 edition, 1965.

176. A. Szabo and N. S. Ostlund, *Modern Quantum Chemistry. Introduction to Advanced Electronic Structure Theory*, McGraw-Hill, New York, 1989.

BIOGRAPHICAL SKETCH

Jorge Alberto Morales was born to Martha Beatriz Samperio (b. 1931) and Jorge Alberto Morales (1930–1974) in Mar del Plata, Argentina, on July 4, 1963. His father was at the time of his birth a recently retired Navy officer working as a professor for navigation in Mar del Plata harbor. His mother was a retired elementary school teacher and a housewife. A sister, Maria Martha (b. 1966) completed his family circle. His relatives were mostly descendants of European immigrants who had arrived at Argentina by the end of the nineteenth century. Spaniards of undetermined origin, Italians from Como, and even British of undetermined origin were among his father's ancestors. Basques from Rentería, Spain, and Catalonians of undetermined origin were on his mother's side.

Jorge enjoyed a peaceful and comfortable childhood in a typical middle-class Argentinian family of the 1960s. He might now look back to that bygone era of a prosperous Argentina with a sense of nostalgia. He showed a penchant for intellectual activities at a very early age. For instance, he was very eager to enter school and learn how to read. This finally happened when he entered primary school first in the Instituto "San Alberto" and later in the Escuela N° 27 "Eduardo Peralta Ramos," both in Mar del Plata. He not only enjoyed reading but also history (classical andf Argentinian) and natural sciences. He did not like mathematics during his elementary studies and did not even discover its connection to physics and chemistry.

Although Jorge considered to become a historian, he finally decided to study chemistry following the example of the chemist Roberto C. Marcer, the father of his lifelong friend Fernando. With this goal in mind, he entered the Escuela Nacional de Educación

Técnica N°1 "Domingo F. Sarmiento" in Mar del Plata in 1976. In this technical school, he received an excellent education in chemistry, physics, and mathematics. He really discovered the beauty of mathematics at sixteen when studying calculus. His professor Fernando Suárez provided him with a an excellent education in analytical chemistry and a inclination to it. Although not encouraged in that technical environment, Jorge continued enjoying history and began to cultivate Spanish literature and western philosophy. He including met his favorite Argentinian writer, Jorge Luis Borges, in 1980. During the last part of his primary education and during all his secondary school, Jorge beheld the slowly and persistent decadence of his homeland.

By the end of 1981, Jorge earned his degree of Técnico Químico. At the beginning of 1983, he went for military service in the Argentinian Air Force. He served in the Policía Aeronáutica Nacional of the Mar del Plata Airport for fourteen months. Unlike some of his secondary school fellows, he was not sent to the front during the Islas Malvinas War in 1982.

After completing his military duties, Jorge entered the Universidad Nacional de Mar del Plata to study chemistry in 1983. He originally was interested in analytical chemistry but giving his interests in mathematics, he slowly shifted from that field first to physical chemistry and finally to quantum chemistry. His taste for philosophy, literature and now psychology paralleled his university activities. He earned his degree of Licenciado en Química by the end of 1989. He failed to obtain an industrial position in Mar del Plata and remained in the university as a chemistry and physics teacher until 1991. By then, he could sadly witness the deteriorated state of his country.

Encouraged by his friend Dr. Carlos Díaz and the theoretical chemist Dr. Francisco M. Fernández, at the Universidad Nacional de la Plata, he decided to become a scientist in quantum chemistry. With that goal in mind, he entered the University of Florida,

Gainesville, to earn a Ph. D. degree in quantum chemistry. After working with Dr. David A. Micha for one year and a half, he finally joined the research group of Dr. Yngve Öhrn and Dr. Erik Deumens. He learned a great deal of science there and transformed into a mature (or almost mature) scientist. Close to receiving his Ph. D. degree, Jorge is contemplating becoming a university professor and getting married. It is not clear which of these two ventures will be the most difficult.

I certify that I have read this study and that in my opinion it conforms to acceptable standards of scholarly presentation and is fully adequate, in scope and quality, as a dissertation for the degree of Doctor of Philosophy.

Yngve N. Ohrn, Chair
Professor of Chemistry

I certify that I have read this study and that in my opinion it conforms to acceptable standards of scholarly presentation and is fully adequate, in scope and quality, as a dissertation for the degree of Doctor of Philosophy.

Michael C. Zerner
Professor of Chemistry

I certify that I have read this study and that in my opinion it conforms to acceptable standards of scholarly presentation and is fully adequate, in scope and quality, as a dissertation for the degree of Doctor of Philosophy.

William Weltner, Jr.
Professor of Chemistry

I certify that I have read this study and that in my opinion it conforms to acceptable standards of scholarly presentation and is fully adequate, in scope and quality, as a dissertation for the degree of Doctor of Philosophy.

John R. Sabin
Professor of Physics

I certify that I have read this study and that in my opinion it conforms to acceptable standards of scholarly presentation and is fully adequate, in scope and quality, as a dissertation for the degree of Doctor of Philosophy.

James W. Dufty
Professor of Physics

This dissertation was submitted to the Graduate Faculty of the Department of Chemistry in the College of Liberal Arts and Sciences and to the Graduate School and was accepted as partial fulfillment of the requirements for the degree of Doctor of Philosophy.

December 1997

Dean, Graduate School